This dissertation is submitted to Informatics and Mathematical Modelling at the Technical University of Denmark in partial fulfillment of the requirements for the degree of Doctor of Philosophy.

The work has been supervised by Professor Hans True.

Kgs. Lyngby, July, 2002

Fujie Xia

Abstract

The present thesis is concerned with the modelling of the motion of the Three-Piece-Freight-Truck. Although the Three-Piece-Freight-Truck is very simple in its construction, the mathematical model is not simple at all. The model is definitely *nonlinear* resulting from the nonlinear kinematic and dynamical contact relations between wheels and rails, the nonlinear suspensions and the nonlinear dry friction damping. For low speeds of the truck the kinematic and dynamical nonlinearities might be linearized, but the very strongly nonlinear suspensions and the dry friction damping can not be linearized at all. The motion of the bolsters are at least two dimensional in the lateral and the vertical directions, so the friction on the surfaces of a wedge should be treated as *two-dimensional dry friction*, and the same is true for the dry friction on the surfaces of an adapter. For the motion with dry friction there exist two motion states: *stick motion* and *slip motion*, which leads to a discontinuity in the behaviour of the dynamical system and leads to a *collapse of the state space*, and consequently, change the degrees of freedom of the system repeatedly.

Due to the design clearances between the car body and the side supports on the bolsters the side supports must be modelled as nonlinear *dead-band springs*. The clearances in the assembly in the wedge damper systems give rise to a relative yaw motion of the bolster with respect to the side frame and a rotation around the truck center line and cause a *warping*. In addition the assembly clearances between the side frame and the adapter both in longitudinal and lateral directions produce another dead-band spring force.

The *tractive effort* on the car body in the longitudinal direction may be left out of consideration in the modelling of the passenger car, but the normal forces caused by it on the surfaces of the wedges will consequently produce friction forces in the Three-Piece-Freight Truck and should be considered. Therefore, the friction forces on the surfaces of wedges are asymmetrical for one pair of wedges as they should be.

The thesis is divided into 10 chapters. In the chapter 1, the research state-of-the art of the dynamics of the Three-Piece-Freight-Truck is reviewed. The framework of the model is introduced. Chapter 2 describes the concept of the *friction direction*

angle with which the *stick-slip motion* with *two-dimensional dry friction* can be numerically simulated. Its applications are illustrated in two simple systems. One is an oscillator with a Coulomb dry friction damper in chapter 2 and the other one is the wedge damper in chapter 3.

In the mechanical system it is possible that the degrees of freedom will vary with the different friction states. We give a detailed discussion of this type of *structure varying systems* in chapter 4.

For the performances of the vehicle on the track, the contact between a wheel and a rail plays a key role, where there are two types of contacts: One is kinematic and the other is dynamical. For the kinematic contact relation we trace the contact point of the wheel on its possible *trajectory* and the *on-line evaluation* of the kinematic contact parameters is introduced. The elastic contact assumption is used to determine the normal loads in the contact patch and then a fully nonlinear contact theory is used to obtain the creep forces. They are discussed in chapter 5.

The configuration of the Three-Piece-Freight-Truck and the corresponding positions of the elements, the velocities and some relations among the elements of the system will be described in chapter 6.

In chapter 7 the dynamic equations of the system are derived. Chapter 8 provides the numerical methods for the simulation of the system, the discussion focuses on the differential algebraic equations(DAEs) with discontinuous characteristics caused by the two-dimensional friction. In chapter 9 the numerical investigation is provided. The four general irregularities in tangent track are usually described in the form of a power spectrum density(PSD). We transform the PSD into the corresponding series in the time domain and then use the time series as excitations for the dynamical performances of the system. The *linear critical speed* and *nonlinear critical speed* and even the *chaotic motion* of the Three-Piece-Freight-Truck are discussed. Finally in chapter 10 certain conclusions are drawn, and some projects for further research are indicated.

Acknowledgments

The work presented in the thesis has been carried out at Informatics and Mathematical Modelling, the Technical University of Denmark under financial support by DSB(Danish State Railways), the Danish Research Agency and the Technical University of Denmark.

My sincere acknowledgment is extended to all who have a direct impact on this work or on my life in Denmark.

Special thanks go to my supervisor Prof. Hans True for his whole hearted support, interest, inspiration and numerous contributions. Moreover, he and his wife Mrs. Bonnie True made many efforts for me and my family to have a nice period in Denmark.

Many colleagues in IMM of DTU also helped me in my Ph.D. studies. It is certainly impossible to name all of them, however I would like to name Prof. P. Grove Thomsen, Prof. Henrik Madsen and Ms. Dorthe Thϕgersen.

I take this opportunity also to thank Professor W.M. Zhai and Professor W.H. Zhang who provided me with much help in many fields during my stay at the National Traction Power Key Laboratory and the Train and Track Research Institute in Southwest Jiaotong University in Chengdu of China for my visiting program.

Last but not least thanks to my wife Linhua Wu for her long time supports in many ways. Without her contribution, her patient and encouragement this work would never have been completed. During my Ph.D. program my son Wuxun Xia always made my spare time a lot of fun.

Contents

CHAPTER 1

Introduction

The *three-piece-freight-truck* has been running for about sixty years on the tracks of North America, South Africa, Australia, China and other countries. Without doubt, the significant advantages of the trucks are due to the very simple construction, safe and reliable operation, low price and maintenance costs, long service life and low energy consumption. Although a new radial truck has been developed for the freight vehicles and other types used in Europe, the family of three-piece-freight trucks still shares larger market in the world. That is not to say this type of railway vehicles has no disadvantages, on the contrary, its lower critical speed of the empty car on straight track, the high dynamic track loads, the performance depends on the weather condition and their state of contamination(dirt, oil) and the last but not the least the state of wear influences its dynamical performances.

The one obvious structural characteristic is that almost all contacting surfaces among the elements are direct contacts shown in Figure 1.1, in other words, the interconnections between the components are realized through *motion pairs* such as *sphere joints* and *slide pairs*. Comparing with the counterpart of a passenger car, the motion pairs are replaced by suspension elements and hydraulic or air dampers, such that the stability of the passenger car is improved greatly.

Additionally, while negotiating a curved track, the three-piece-freight-truck is loose enough to *warp*. The reason is that on the ends of the bolster simply sandwich the side frames via a pair of wedges with the unavoidable dimensional tolerance coming from manufacturing and the clearance in the assembly.

And more, if the vertical response of a bolster is large enough to separate the wedges then the friction damping will lose its function. In contrast if the relative velocity between the bolster and wedges goes toward zero then the stick motion will

consequently take place, which will cause unusual track loads.

Unfortunately, up to now, the dynamic performances of the three-piece-freight-truck have not been thoroughly understood by the dynamical experts. The main reason is that the simple construction leads to a not so simple mathematical model!

The model is definitely nonlinear resulting from the nonlinear kinematic and dynamical constraints between the wheels and the rails, the nonlinear suspensions and the nonlinear dry friction damping. For low running speed of the truck the nonlinearities of the kinematic and dynamical constraints could be linearized, but the very strong nonlinear suspensions and the dry friction damping can not be linearized at all. The motion of the bolsters are at least two dimensional in the lateral and the vertical directions, so the friction on the surfaces of a wedge should be treated as *two-dimensional dry friction*, and the same holds for the dry friction on the surfaces of an adapter. For the motion with dry friction there exist two motion states: *Stick motion* and *slip motion*, which lead to a discontinuity in the dynamical system and cause the collapse of state space. Consequently, it changes the degrees of freedom of the system. Because the design clearances between the car body and the side

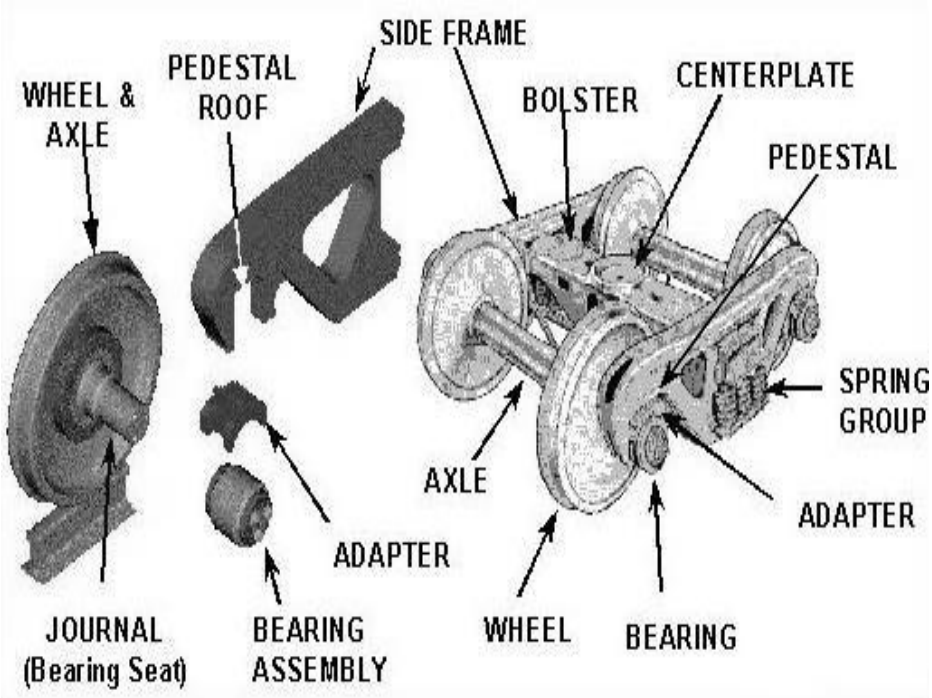

Figure 1.1: *The construction of the three-piece-freight-truck.*

supports on the bolsters are necessary such that leads to the side supports acting

as dead-band springs. The clearance in the assembly of the wedge damper systems cause the relative yaw motion of the bolster with respect to the side frame to rotate about the truck center line and to assume a state of *warping*. Also the assembly clearances between the side frame and the adapter both in longitudinal and lateral directions produce another dead-band spring force.

The *tractive effort* on the car body in the longitudinal direction may be left out of consideration in the modelling of the passenger train, but the normal forces caused by it on the surfaces of the wedges will consequently produce friction forces in the three-piece-freight truck and the normal forces should therefore be considered. Therefore, the friction forces on the surfaces of wedges are asymmetrical for one pair of wedges as they should be.

1.1 The review of the state of the arts of research

1.1.1 Two-dimensional dry friction

The story of the friction has a long history as it has been a topic of technological attention for a long time, and it is still a hot topic in scientific and engineering research today. Friction can easily been found in our daily life as well as in various engineering applications. In railway engineering nothing can be done without friction, because the friction between the wheels and the rails provides the traction force, and the friction on the wedge dampers provides the damping force to damp out the vibrations. It poses great challenges to researchers in the dynamic performance of the three-piece-freight-truck. First of all, friction is difficult to model, because the underlying mechanism is not entirely understood. Additionally, friction models are usually discontinuous, especially for the two or higher dimensional relative motion with friction. The theory used in most of the dynamical systems for smooth systems is not directly suitable to the systems with friction. Thus, the topic of the wedge dampers with friction is the current focus of several researchers in the world today.

In order to simulate the motion of a friction oscillator with a two-dimensional dry friction constraint, there are two unavoidable matters we must deal with. One is the hysteresis induced by the dry friction coefficients of static and kinetic friction and the other is the discontinuity induced by the stick-slip motion. It is not difficult to determine the components of the kinetic friction force vector and the static friction force vector individually, but no widely accepted way to treat the stick-slip motion exists, especially not for complicated mechanical systems. C-H Meng *et al.*[Meng, 1991] use a massless friction damper with two linear springs of finite stiffness to obtain the components of the friction force vector. However, when the stick-slip motion takes place the formulation was not provided rigorously. The method provided in their paper is not convenient for handling the two-dimensional dry friction in complicated mechanical systems.

For some special cases, the excitations are sinusoidal with the same frequency and with different amplitudes or phases and the orbits of responses will be reduced to straight line segments or to circular or elliptic shapes. In these cases the harmonic-

balance method is widely used to give an analytical approximate solution[Meng, 1991][Saw,1986][Sanlitark,1996][Yang,1998,2000]. However, for complicated excitations, e.g. sinusoidal excitations with different frequencies in two orthogonal directions or even time series, the orbit of the response will become a complex self-intersecting planar curve, and in this case the harmonic-balance method fails.

For dynamic systems with dry friction, Den Hartog[Den Hartog, 1931] presented a closed-form solution as early as in 1931 for the steady state zero-stop response of a harmonically excited oscillator with Coulomb friction. Since then one-stop, two-stops and multiple-stops per cycle have been reported[Hong,2000]. Responses with bifurcations and chaos have also been found in many fields[Feen,1992,1996], but most of the research efforts have focused on one-dimensional dry friction models, which means that the motion is along a straight line.

Recently, W. Sextro[Sextro,2002] provided a three-dimensional point contact element to treat the elastic contact with dry friction. The theory and methods can be used to the sliding contact and as well as the rolling contact. But it can not treat the stick-slip motion.

1.1.2 The stick-slip motion

The stick-slip motion is a phenomenon occurring in the systems with dry friction. It is important for us to understand the complete motion of the mechanical systems. Examples of the stick-slip motion of frictional systems include robot joints, braking systems, automotive squeak, rail-wheel contacts, micromechanics, machine-tool processes, earth-quake faults, space structures, turbine blades and wedge dampers. Please refer to a detailed description in the paper by Ibrahim [Ibrahim,1992]. From the point of view of vehicle systems dynamics, stick-slip motion may be one reason that causes unusual track loads. During a stick, there is a collapse in the dimension of the state space[Shaw,1986][Eich-Soellner,1998], which can be visualized in the state space by imaging that one of the states, the velocity, is directly constrained during stick. For a one forced one-degree-of-freedom oscillation, this produces an underlying one-map[Shaw, 1986][Feeny, 1992][Popp, 1992]. The slip state is the one where the relative velocity is different from zero.

The description of the stick-slip motion of the system with two-dimensional friction will be more difficult. For one, both the input forces on the system are needed to be known statically and kinematically and the components of the friction force vector in the orthogonal directions must be completely determined. Only then the stick or slip state can be distinguished. Additionally, the switch conditions for the collapse of the state space become complicated, especially, if one body has more than one surface in contact with others. The dynamics of railway vehicles with two-dimensional dry friction and stick-slip action at the surface elements in contact has not been reported before.

1.1.3 The friction coefficient

The friction coefficient plays a significant role for the motion of a system with friction. According to the characteristics of its application here we distinguish between four types.

- *Coulomb law*:
  The static and kinematic friction coefficients are the same constant, i.e.

$$\mu(V_r) = \mu \tag{1.1}$$

where V_r denotes the relative velocity. This simplest model has been used by many investigators for providing a variety of steady-state responses, including periodic, quasi-periodic, and even chaotic responses [Feen, 1992, 1993,1994] [Saw, 1986].

- *Static-dynamic friction model*:
  The static and kinetic friction coefficients are different constants, but the static friction coefficient is always larger than that of the kinetic friction coefficient, i.e.

$$\mu(V_r) = \begin{cases} \mu_k, & V_r \neq 0, \\ \mu_s, & V_r = 0. \end{cases} \tag{1.2}$$

where μ_s denotes the static friction coefficient and μ_k stands for the kinetic friction coefficient[Popp, 1992, 1996].

- *Relative velocity-dependent friction model*:
  The friction coefficient varies with the relative velocity. There are two ways to describe the friction model. One is to let the static friction coefficient be constant and only the kinetic friction coefficient changes with the relative velocity[Popp,1992,1996]

$$\mu(V_r) = \frac{\mu_s}{1 + c_1|V_r|} + c_2 + c_3 V_r^2 \tag{1.3}$$

where c_1, c_2, c_3 are constant parameters. The values of them provided by Pop [Pop, 1996] are 1.42, 0.1 and 0.01 respectively. The kinetic friction coefficient will be larger than the static friction coefficient for a certain large relative velocity.

The formula provided by Poiré and Bochet is [Kragelski,1971][Periard,1998]

$$\mu(V_r) = \mu_s \frac{1}{1 + 0.03|V_r|}. \tag{1.4}$$

and by Galton reads

$$\mu(V_r) = \mu_s \frac{1 + 0.018|V_r|}{1 + 0.097|V_r|}. \tag{1.5}$$

where the static friction coefficient is always larger than the kinetic friction coefficient.

In order to use one formula to replace all the laws above in this thesis[True 1999-2002] [Xia, 2001a] we provide an approximate relation using the hyperbolic secant function to describe the velocity-dependent friction coefficient as

$$\mu(V_r) = \mu_s sech(\alpha|V_r|) + \mu_k(1 - sech(\alpha|V_r|)). \tag{1.6}$$

By the selection of different values of the parameter α the formula yields different steepness of the continuous curve that describes the change from the static to the kinematic friction coefficient.

• *Anisotropic friction model*:

The above three types of friction models are all *isotropic friction* models since the value of the friction coefficient is the same in any motion direction. In other words, the friction force vector is always opposite the relative velocity. For the anisotropic friction model the friction coefficient can be represented by a friction coefficient tensor[Zmitrowicz, 1981a,b] and the friction force vector is along the line that deflects a certain angle from the line of the relative velocity.

1.1.4 The wedge dampers

In 1935, Standard Car Truck Company introduced friction damping to the freight car truck. Since then the freight trucks of the 1940's generally had the column friction wedge similar to designs popular today. The friction wedge is used in all three-piece-freight-trucks such as the conventional three-piece-freight-truck, the three-piece self-steering truck and the Y25 truck, to provide vertical and lateral damping in the secondary suspension, as well as lozenging stiffness between the side frame and the bolster[Fröhling, 1996, 1997, 1998].

The friction surfaces of the wedge are able to move relatively to one another in two orthogonal directions, that is laterally and vertically. Therefore the dynamic behaviors in both directions have to be taken into account when modelling the stick-slip motion. Some measurements and theoretical investigations were done by R.D. Fröhling [Fröhling, 1996, 1997, 2000], C. Cole[Colin,2001] and N. Bosso[Bosso *et al.*, 2000]. The hysteresis-loops of the forces vs the deflections were provided. But the dynamical results for simultaneously excitations in both vertical and lateral directions are not provided. Furthermore the effect of the friction between the side frame and adapter was neglected in their models.

Up to now, few reports on the response of wedge dampers with two-dimensional dry friction have been published [Fröhling, 1996, 1997, 2000][True,1999]. In order to understand the dynamical performances of the wedge dampers, we should first understand the responses of a two-dimensional dry friction oscillator and implement a basic numerical method. The non-linear discontinuous dynamic system with complicate excitations along orthogonal directions, is so complicated that analytical solutions to the problem can not be found, so we must use a numerical method.

1.1.5 Variable degrees of freedom system

We know that the stick-slip motion will cause a collapse of the state space, in other words, the degrees of the freedom of the system will vary with time. That brings at least two troubles for the modelling of the system. One is the discontinuity that will violate the continuous assumption of the existing numerical integral algorithms. The other is that if you neglect the fact of the discontinuity caused by the stick motion the time steps in the integration procedure will become very small and the problem behaves like a stiff one. For treating this problem there is no simple way except finding all the switch conditions[Eich-Soellner, 1998]and the corresponding acting friction forces and making the system piece-wise differentiable.

1.1.6 The dynamics of railway vehicles

The dynamics of the railway vehicle systems are closely related to the topic of stability. Stability of running of vehicles is one of the important design criteria of railway vehicles. As early as 1883 Klingel[Klingel,1883] analyzed the hunting motion of a single wheelset on a straight track by a purely kinematical method. The wavelength L of the hunting motion of a single wheelset was determined by

$$L = 2\pi\sqrt{\frac{rb}{\lambda}} \tag{1.7}$$

where r denotes the rolling radius, b is half the wheel distance and λ is the conicity.

For a loaded wheelset a purely kinematic motion is no longer possible. The theory of rolling contact mechanics in needed to investigate the stability. Carter[Carter, 1915] provided a model of a two-axled bogie including the tangential forces with a qualitatively correct linear law to calculate the creep forces. The wavelength of the hunting motion of the bogie is

$$L = 2\pi\sqrt{\frac{rb}{\lambda}(1 + \frac{a_w^2}{b^2})} \tag{1.8}$$

where a_w denotes half the axle distance in the bogie.

The main result of Carter is that a two-axled bogie with rigid suspension in longitudinal and horizontal directions and with a rigid frame never runs stably.

The main contribution of Matsudaira[Matsu, 1952] in this field was his distinction between forced vibrations and self-excited vibrations a first in railway vehicle dynamics; and he also introduced the concept of the *primary hunting motion* and the *secondary hunting motion*. The primary hunting motion occurred at lower vehicle speeds and was connected with large lateral car body motions. The secondary hunting motion occurred for high vehicle speeds and the wheelset motion was more dominating.

Wickens[Wickens,1965] derived a refined model of a two-axled bogie including the effect of the gravitational stiffness, which is important for worn profiles, and damping.

The results showed that it is possible to choose parameters in such a way that car body instability can be avoided.

However, the above stability is a linear stability. The linear stability theory of railway vehicles is more often than not yields a too high critical speed of the vehicle bogie. From the beginning of the 1960's much research effort has been invested in the nonlinear stability of the vehicles. De Pater[De Pater,1961] was probably the first one who introduced the method of *Krylow and Bogoljubov* into the investigation of nonlinear hunting motions. The quasi-linearization technique with sinusoidal input introduced by Cooperider, Hedrick, Law and Malstrom[Cooperrider,1975] is roughly the same as the *harmonic balance method* or the method of *Krylow and Bogoljubov*. Their results can not explain the existence of the nonlinear periodic limit cycle.

Still the nonlinear periodic limit cycle analysis is not sufficient to describe the behaviors of railway vehicles and bogies. One reason is that it cannot be proved that the periodic oscillation always exists. The first bifurcation analysis of the free running wheelset was performed by Huilgol [Huilgol,1978] and revealed a Hopf bifurcation from the steady state. The first observation of chaotic oscillations in models of railway vehicles was by Hans True and Kaas Petersen[Hans True,1983][Kaas,1986]. Further work demonstrating chaotic motion of railway wheelsets and vehicles include Hans True[True, 1993,1999,2001] and his colleagues, Meijaard and De Pater[Meijaard and De Pater 1989]. For further references the reader is refered to the paper presented by Knothe[Knothe, 1999].

The nonlinear stability of the motions of railway wagons was investigated by Pascal[Pascal,1993]. The effect of the rolling contact between the wheels and the rails was emphasized, but the effect of the friction damping in the model is not described. It is true that the forces between the wheels and the rails play a significant role for the motion of the vehicle systems. However, in the complete and strongly nonlinear system, the response of the vehicle is not a simple sum of the effects of the subsystems. It is therefore very difficult to relate a special kind of behavior to a special subsystem.

Hans True[True, 2002] has derived a strongly simplified model to investigate the dynamic performance of a freight bogie with dry friction and found that chaotic motion occurs in that model. The model considers only one dimensional dry friction but the stick motion is included.

1.2 The problem to be investigated in the present thesis

The main objective of the thesis is focussed on the understanding of the dynamical performance of the three-piece-freight-truck including the following features:

- The mass of the wedges is included.
- Both the lateral and the vertical motions of the bolster are included.
- The two-dimensional friction on the surfaces of the wedges and the surfaces of the

adapters is included.
• The effect of the tractive effort on the action of the wedge dampers is included.
• A velocity-dependent friction function is introduced.
• The three-dimensional kinematic constraint between a wheel and a rail is used.
• The full nonlinear dynamical constraints between the wheel and the rail are used.
• The structure varying systems caused by stick-slip motion are discussed in detail.
• The linear critical speeds and the nonlinear critical speed are calculated and even chaotic motion are investigated.
• A description of how the Power Spectral Density(PSD) is transformed into a time series.
• The dynamical responses of the three-piece-freight-truck to an irregular track are simulated.

We start with the fundamental topics such as the two-dimensional dry friction, stick-slip motion, structure varying systems, separated-coupled motion and the contact between a wheel and a rail. Through the investigation of these basic models we can better relate the dynamical phenomena to the corresponding problems in the three-piece-freight-truck. Finally we combine the basic models into the complete three-piece-freight-truck model with the kinematic and dynamical contact relations between the wheels and the rails.

In the thesis, a refined model of the three-piece-freight-truck is provided. It incorporates the mass of the wedges, the two-dimensional dry friction, the velocity-dependent friction coefficient, the stick-slip motion, the dead-band springs, the anti-warp stiffness, the effect of the tractive effort, the on-line evaluation of the kinematic contact parameters and the elastic dynamical contact relations between the wheelsets and the rails. Moreover, the applied numerical methods are discussed.

1.2.1 Two-dimensional dry friction

To describe a friction force vector on a plane, the modulus and the argument of the force should be known. Instead of the harmonic balance method used by most investigators[Cheng,1995][Saw,1986], we provide a numerical approach to describe the system with two-dimensional dry friction. The concept of the *friction direction angle* is introduced to determine the orthogonal components of the static and kinetic friction force vector. The *friction direction angle* is determined by either relative velocities or input forces. With this method the switch conditions for stick state, slip state and stick-slip state can be easily derived.

In the case of anisotropic friction the friction direction angle can be used to determine the equivalent friction coefficient and the deflection friction angle[Zmitrowcz, 1981a,b].

1.2.2 The coupling-separation motion of the wedge damper system

When the three-piece-freight-truck runs on the track, the excitations on the bolster in vertical direction may be so large, that the bolster will separate from the wedge and perform a free vibration only restrained by the coil springs in the suspension.

When separation takes place and if the displacement of the bolster in the vertical direction is smaller than its initial value, then a friction force exists on the surface of the wedge contacting the side frame because the displacement along the longitudinal direction differs from zero. During the separated motion if the displacement of the wedge in the vertical direction is larger than its initial value, then a free vibration of the wedge will occur. The bolster will perform a forced vibration without any friction damping. The detailed discussion will be focussed on the wedge dampers model.

1.2.3 The discontinuity with stick-slip motion

If the dynamic systems include the dry friction, structure varying systems, impact phenomena and hysteresis then the right-hand sides of the differential equations express the discontinuities of the forces, the jumps in the velocities and the number of the changing degrees of freedom. The discontinuity of the system might cause wrong error estimates and erroneous choice of step sizes in the numerical integration algorithm. In the model of the three-piece-freight-truck the discontinuities of the dry friction, impact and the hysteresis will appear.

Standard integration methods for treating the discontinuity may lead to an inefficient behavior or even to a failure of the integration caused by an order reduction of the method and wrong error estimates[Eich, 1998]. The way to handle the problem is to extend integration methods to be able to localize the roots of the so-called switching functions in order to permit a re-initialization at the points of discontinuity. Since the complete three-piece-freight-truck is a very complex system we will first discuss the dynamics of sub-systems of the three-piece-freight-truck and then combine them into the complete system.

1.2.4 The variable degrees of freedom system

The structure varying systems in the three-piece-freight-truck can be found in the sub-systems of the bolster-wedge-frames and the bolster-frame-wheelsets. In this thesis we will discuss the switch conditions and the corresponding acting friction forces and the transformation of the discontinuous system into a piece-wise differentiable system.

In Figure 1.2 we show the system of the bolster-wedges-frames. When the relative velocities $V_{rbf1} = V_b - V_{f1} = 0$ and $V_{rbf2} = V_b - V_{f2} = 0$ at same time with $V_b \neq 0$ then the bolster and the two side frames will have the same lateral velocity and move as one body. It means that the degrees of freedom of the system is reduced by 1. How about the friction forces on the surfaces between the bolster and side frames in the lateral and vertical directions? They are definitely not zero unless all the input forces

are zero. The other structure varying system is shown in Figure 1.3 which is the

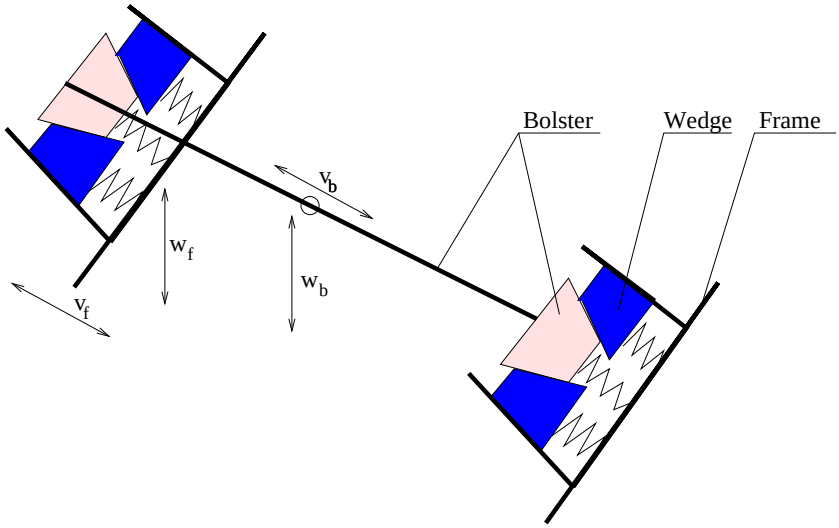

Figure 1.2: *The structure varying system of the bolster-wedge-frames.*

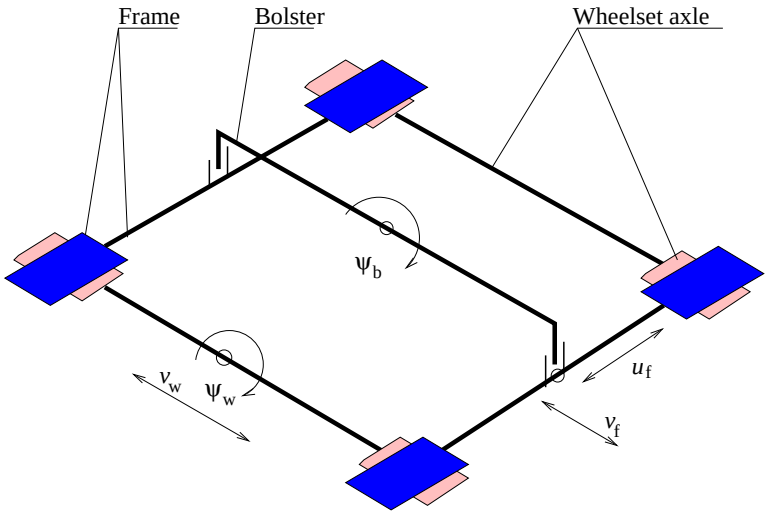

Figure 1.3: *The structure varying system of the bolster-frame-wheelsets.*

sub-system of the bolster-frame-wheelsets. The problem is: How can we determine

the friction forces on the contact surfaces between the frame and the wheelsets both in the longitudinal and lateral directions in the stick motion with non-zero input forces? In this thesis we will answer these questions.

1.2.5 The interaction between a wheel and a rail

For the kinematic constraints between a wheelset and rails a two dimensional model to calculate the kinematical constraint parameters is widely used. In that way the kinematic constraint parameters only depend on the lateral displacement and the effect of the yaw of the wheelset is neglected. In the present thesis we use a three dimensional contact model to determine the kinematic constraint parameters in two ways: One way is the geometrical method by means of the trajectory of the wheel tread and the other one is the analytical method through solving of a set of nonlinear algebraic equations. We furthermore extend the evaluation of the three dimensional contact parameters to include the determination of the dimension of the contact patch and the penetration between the wheel and rail.

For the dynamical constraints we use the *quasi-elastic* method to determine the normal loads and the full nonlinear formulations to calculate the tangential contact forces including table-looking[Xia, 1996][Kalker, 1996], SHE theory[Shen, 1983] and Polach's method[Polach, 1999].

1.2.6 Stability of the three-piece-freight truck

The only limitation of the model to perform the nonlinear analysis is the computation efficiency. Especially for the investigation of the critical speed, the verification of the chaotic motion by checking up the Poincaŕe map or the first return map, or the calculation of Lyapunov exponents is very time consuming.

1.2.7 The responses of the three-piece-freight-truck to the irregular tracks

An interesting objective is to find the responses of the complete freight vehicle under various excitations. We calculate the hysteresis loops of the normal forces on the surfaces of the wedges, and the friction forces on the surfaces of the wedges in lateral and vertical direction.

We use the power spectral density(PSD) provided by FRA(Federal Railroad Administration) to describe the irregularities of the track (class 1 to 6). Because of the strong nonlinearity of the system, the PSD can not be directly used as an excitation. We use the inverse Fourier transformation to transform the PSD into a corresponding time series and then use them as the excitations to obtain the final responses.

1.3 The outline of the thesis

The thesis is divided into 10 chapters. In the chapter 1, the state-of-the art of the research of the dynamics of the Three-Piece-Freight-Truck is reviewed. The framework of the model is introduced. Chapter 2 describes the concept of the friction direction angle with which the *stick-slip motion* with *two-dimensional dry friction* can be numerically simulated. Its applications are illustrated in two simple systems. One is an oscillator with a Coulomb dry friction damper in chapter 2 and the other one is the wedge damper in chapter 3.

In the mechanical system it is possible that the degrees of freedom will vary with the different friction states. We give a detailed discussion of this type of systems in chapter 4.

For the performances of the vehicle on the track, the contact between a wheel and a rail play a key role, where there are two types of contacts: One is kinematic and the other is dynamical. For the kinematic contact relation we trace the contact point of the wheel on its possible *contact trajectory* and the *on-line evaluation* of the kinematic contact parameters is introduced. The elastic contact assumption is used to determine the normal loads in the contact patch and then a fully nonlinear contact theory is used to obtain the creep forces. They are discussed in chapter 5.

The configuration of the Three-Piece-Freight-Truck and the corresponding positions of the elements, the velocities and some relations among the elements of the system will be described in chapter 6.

In chapter 7 the dynamic equations of the system are derived. Chapter 8 provides the numerical methods for the simulation of the system, the discussion focuses on the differential algebraic equations(DAEs) with discontinuous characteristics caused by the two-dimensional friction. In chapter 9 the numerical investigation is provided. The four general irregularities in a tangent track are usually described in the form of a power spectrum density(PSD). We transform the PSD into the corresponding series in the time domain and then use the time series as excitations for the dynamical performances of the system. The *linear critical speed* and *nonlinear critical speed* and even the *chaotic motion* of the Three-Piece-Freight-Truck are discussed. Finally in chapter 10 certain conclusions are drawn, and some projects for further research are indicated.

Chapter 2

Mechanical systems with two-dimensional dry friction

In this chapter we provide a mechanical model for investigating the stick-slip motion of a two-dimensional oscillator with dry friction exposed to excitations of any arbitrary shape. In contrast to the harmonic balance method used by most investigators[Meng, 1991][Sanliturk, 1996], we provide a numerical approach to investigate the system. The concept of a *friction direction angle*[Xia,2002] is introduced to determine the components of the static and kinetic friction force vectors and the hyperbolic secant function is introduced to deal with the transition of the friction force from static to kinetic state. The *friction direction angle* is determined by either relative velocities or input forces. With this method the switch conditions for stick state, slip state and stick-slip state can be easily derived. The orbits of the responses, which are straight line segments, circular or elliptic are obtained. In the general case, the orbit of the response is a complex planar curve. Zero-stop, two-stops and more than two-stops per cycle are also found.

One can also find other ways, a way is described in chapter 10 for example, to deal with the one oscillator with dry friction with one and two-dimensions. But as we will see in the next chapter and chapter 4 the friction direction angle will play a decisive role in a complex structure varying system. The concept is also useful in anisotropic friction.

2.1 Introduction

In order to simulate the motion of a friction oscillator with two-dimensional dry friction constraint, there are two unavoidable matters we must deal with. One is the hysteresis induced by the dry friction coefficients of static and kinetic friction and the other is the discontinuity induced by the stick-slip motion. It is not difficult to determine the components of the kinetic friction force vector and the static friction force vector individually, but no widely accepted way to treat the stick-slip motion exists, especially not for complicated mechanical systems. C-H Meng *et al.*[Meng, 1991] use a massless friction damper with two linear springs of finite stiffness to obtain the components of the friction force vector. However, when the stick-slip motion takes place the formulation was not provided rigorously. The method provided in their paper is not convenient for handling the two-dimensional dry friction in complicated mechanical systems.

For some special cases, the excitations are sinusoidal with the same frequency and with different amplitudes or phases and the orbits of responses will be reduced to straight line segments or to circular or elliptic shaps. In these cases the harmonic-balance method is widely used to give an analytical approximate solution[Meng, 1991][Sanliturk, 1996][Yang, 1998a,b,2000]. However, for complicated excitations, e.g. sinusoidal excitations with different frequencies in two orthogonal directions or even time series, the orbit of the response will become a complex self-intersecting planar curve, and in this case the harmonic-balance method fails.

For dynamic systems with dry friction, Den Hartog[Den Hartog, 1931] presented a closed-form solution as early as in 1931 for the steady state zero-stop response of a harmonically excited oscillator with Coulomb friction. Since then one-stop, two-stops and multiple-stops per cycle have been reported[Hong, 2000]. Responses with bifurcations and chaos have also been found in many fields[Saw, 1986][Feen, 1992][Popp, 1996][True, 1999], but most of the research efforts have focused on one-dimensional dry friction models, which means that the motion is along a straight line.

The two-dimensional Coulomb friction oscillator has wide applications in the fields of the freight-bogies on railways, turbo-machinery, earth quake theory and robot-walking mechanisms. Here we mainly shall turn our attention towards applications to the so-called wedge dampers in the three-piece-freight-bogie and dry friction dampers in the bogie Y25. In both cases they are used to dissipate the vibration energy produced by the interaction between wheels and rails[Gardner, 1997][Fröhling, 1998][Evans, 1998]. Up to now, only a few reports on the response of wedge dampers with two-dimensional dry friction have been published. In order to understand the dynamical performances of the wedge damper, which basically is a two-dimensional dry friction oscillator, we should first understand the responses of a two-dimensional dry friction oscillator and implement a basic numerical method. For the non-linear discontinuous dynamic systems with complex excitations in orthogonal directions, an analytical solution cannot be found, so we must use numerical methods.

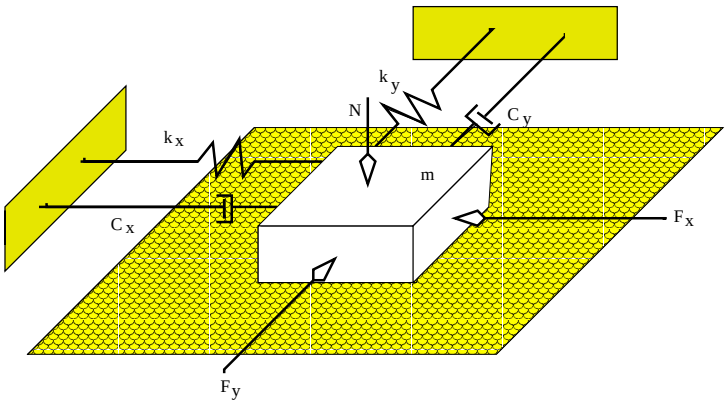

Figure 2.1: *A two-dimensional friction oscillator*

2.2 Description of a two dimensional friction oscillator

Consider the two-dimensional friction oscillator shown in Figure 1. The mass m is in contact with a plane surface and it is connected to fixed walls by two linear springs and two linear viscous dampers along the x and y directions respectively. Newton's second law applies, and the equations of motion of the system can easily be written as

$$m\ddot{x} + c_x\dot{x} + k_x x + F_{x\mu} = F_x \tag{2.1}$$

$$m\ddot{y} + c_y\dot{y} + k_y y + F_{y\mu} = F_y; \tag{2.2}$$

where the components of the friction forces $F_{x\mu}$ and $F_{y\mu}$ must satisfy the relation

$$F_\mu = \sqrt{F_{x\mu}^2 + F_{y\mu}^2} \leq \mu N. \tag{2.3}$$

N is the normal force on the mass, which in general is a state-dependent variable, for the sake of simplicity we assume that it is constant. μ is the friction coefficient, which has two states: A static coefficient of friction μ_s, and a kinetic coefficient of friction μ_k. We can therefore write the friction force as $F_\mu = -Nf(V)$, where $f(V)$ is determined by the relation[Feen, 1992]

$$f(V) = \begin{cases} \mu_k & \text{if } V > 0 \\ -\mu_s \leq f(V) \leq \mu_s & \text{if } V = 0 \\ -\mu_k & \text{if } V < 0 \end{cases} \tag{2.4}$$

The velocity V of the mass has the components $\dot{x}$ and $\dot{y}$, which determine the direction of the kinematic friction force. We have

$$|V| = \sqrt{\dot{y}^2 + \dot{x}^2}. \tag{2.5}$$

The derivatives of x and y are with respect to the time τ. The friction direction angle between $\dot{x}$ and $\dot{y}$ is defined by

$$\theta = \begin{cases} \tan^{-1}(\frac{\dot{y}}{\dot{x}}), & (\dot{x} \geq 0, \quad \dot{y} \neq 0) \\ \pi - \tan^{-1}(\frac{\dot{y}}{\dot{x}}), & (\dot{x} < 0, \quad \dot{y} \geq 0) \\ \pi + \tan^{-1}(\frac{\dot{y}}{\dot{x}}), & (\dot{x} < 0, \quad \dot{y} < 0) \end{cases} \tag{2.6}$$

Hence the components of the friction forces can be expressed in the following way:

$$F_{x\mu} = F_\mu \cos\theta, \quad F_{y\mu} = F_\mu \sin\theta \tag{2.7}$$

The driving forces F_x and F_y are arbitrary but in the present paper we assume that they are simple harmonic functions with driving (angular) frequencies ω_{xd} and ω_{yd} respectively:

$$F_x = f_{x0}\cos(\omega_{xd}\tau + \phi_x), \quad F_y = f_{y0}\cos(\omega_{yd}\tau + \phi_y) \tag{2.8}$$

where f_{x0} and f_{y0} are the amplitudes and ϕ_x and ϕ_y are the phases.

In the case of $k_x = k_y = k$ and $c_x = c_y = c$, we may rescale the time and the displacements:

$$x_s = \frac{kx}{N}, \quad y_s = \frac{ky}{N}, \quad t = \tau\sqrt{k/m}, \quad \omega_{xd} = \Omega_x\sqrt{m/k}, \quad \omega_{yd} = \Omega_y\sqrt{m/k}. \tag{2.9}$$

The equations (2.1) and (2.2) can then be written on dimensionless form:

$$\ddot{x_s} + \xi\dot{x_s} + x_s + f(\mu)\cos\theta = \beta_x\cos(\Omega_x t + \phi_x) \tag{2.10}$$

$$\ddot{y_s} + \xi\dot{y_s} + y_s + f(\mu)\sin\theta = \beta_y\cos(\Omega_y t + \phi_y) \tag{2.11}$$

where

$$\beta_x = f_{x0}/N, \quad \beta_y = f_{y0}/N, \quad \xi = c/\sqrt{km} \tag{2.12}$$

and the friction direction angle θ remains on the same form as (2.6) except that $\dot{x}$ and $\dot{y}$ are replaced by $\dot{x}_s$ and $\dot{y}_s$.

2.3 The friction direction angle and the friction force components

In order to define a friction force vector on a plane, its modulus and argument must be known. The modulus of the friction force vector is determined by (2.3) and (2.4), and its argument is given by the angle θ shown in Figure 2.2. Then the x and y components of the friction force can be determined. We call the angle θ the *friction direction angle*. The dry friction is assumed to be isotropic.

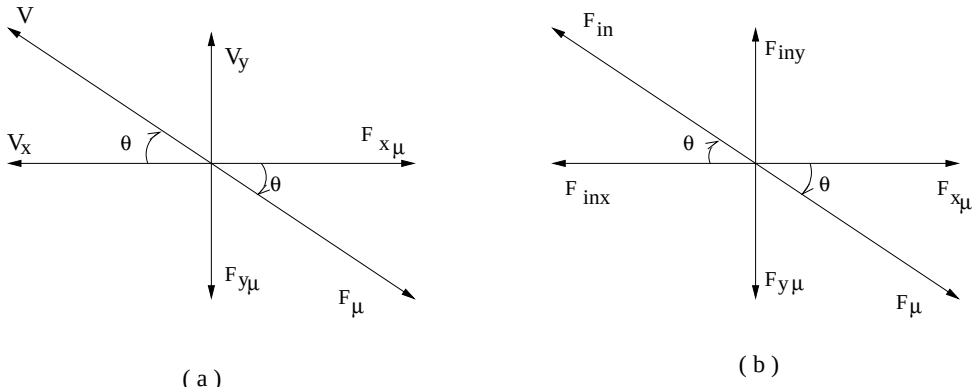

Figure 2.2: *The friction direction angle in a two-dimensional friction oscillator*

If the velocity components $V_x = \dot{x}$ and $V_y = \dot{y}$ of the mass are different from(0,0) then the friction direction angle is determined by the angle between the velocity V_x and the resultant velocity v. The modulus of the friction force vector is then equal to the normal force times the kinetic friction coefficient, viz. $F_\mu = N\mu_k$. The direction of the friction force is opposite to the resultant velocity V as shown in Figure 2.2(a) due to the isotropy. The friction direction angle is given by the velocities $V_x = \dot{x}$ and $V_y = \dot{y}$ in equations (2.6), and then the components of the friction force vector are given by equation (2.7).

If (V_x, V_y) equals (0, 0) then the maximum value of the friction force is equal to the normal force times the static friction coefficient, viz. $F_\mu = N\mu_s$, and the corresponding components of the friction force are equal to the corresponding input forces, viz. $F_{x\mu} = F_{inx}, F_{y\mu} = F_{iny}$. Although the mass is in rest, the friction force is not zero. We call this state a *nonzero static friction force equilibrium state*, and the friction force vector is equal and opposite to the input force, which is shown in Figure 2.2(b). The effect of the torque caused by the input force and friction force is neglected in the present paper. In other words, we can use the input forces F_{inx} and F_{iny} to determine the friction direction angle alternatively, viz.

$$\theta = \begin{cases} \tan^{-1}(\frac{F_{iny}}{F_{inx}}), & (F_{inx} \geq 0, \quad F_{iny} \neq 0) \\ \pi - \tan^{-1}(\frac{F_{iny}}{F_{inx}}), & (F_{inx} < 0, \quad F_{iny} \geq 0) \\ \pi + \tan^{-1}(\frac{F_{iny}}{F_{inx}}), & (F_{inx} < 0, \quad F_{iny} < 0) \end{cases} \tag{2.13}$$

When both the velocities and the input forces of the mass are equal to zero, then the friction force is zero and the system is also in equilibrium. We call this state a *zero friction force equilibrium state*. In this case the friction direction angle is undetermined.

We now extend the definition of the friction direction angle, θ to include the two

cases in (2.6) and (2.13). It is determined in the following way

$$\theta = \begin{cases} \chi(\dot{x_s}, \dot{y_s}), & (\dot{x_s} \bigvee \dot{y_s} \neq 0) \\ \psi(F_{inx}, F_{iny}), & (\dot{x_s} \bigwedge \dot{y_s} = 0, F_{inx} \bigvee F_{iny} \neq 0) \\ \emptyset, & (\dot{x_s} \bigwedge \dot{y_s} \bigwedge F_{inx} \bigwedge F_{iny} = 0) \end{cases} \tag{2.14}$$

where $\chi(\dot{x_s}, \dot{y_s})$ denotes the representation of θ by (2.6); $\psi(F_{inx}, F_{iny})$ stands for the representation of θ by (2.13) and $\emptyset$ is the empty set of θ. The symbol $\bigvee$ means disjunction and the $\bigwedge$ denotes conjunction. As a consequence, the components of the friction force vector in the two orthogonal directions can be determined by the following formulae:

$$\left.\begin{array}{l} F_{x\mu k} = F_\mu \cos\theta \\ F_{y\mu k} = F_\mu \sin\theta \end{array}\right\}, \quad (\dot{x}_s \vee \dot{y}_s \neq 0) \quad | \quad (\dot{x}_s \wedge \dot{y}_s = 0, \\ |F_{inx}| \geq |F_{x\mu s}|, |F_{iny}| \geq |F_{y\mu s}|) \tag{2.15}$$

$$\left.\begin{array}{l} F_{x\mu t} = F_{inx} \\ F_{y\mu t} = F_{iny} \end{array}\right\}, \quad (\dot{x}_s \wedge \dot{y}_s = 0, |F_{inx}| < |F_{x\mu s}|, |F_{iny}| < |F_{y\mu s}|) \tag{2.16}$$

Note that the components of the maximum friction force vector in the x and y directions, $F_{x\mu s}, F_{y\mu s}$ that are used in the conditions are determined by

$$\left.\begin{array}{l} F_{x\mu s} = \Re(\theta) N \mu_s \cos\theta \\ F_{y\mu s} = \Re(\theta) N \mu_s \sin\theta. \end{array}\right\} \tag{2.17}$$

where the function $\Re(\theta)$ is defined as

$$\Re(\theta) = \begin{cases} 1, & \theta \in \Theta \\ 0, & \theta \notin \Theta \end{cases} \tag{2.18}$$

in which the symbol Θ stands for a non-empty set of θ. (2.18) is used to determine the stick-slip switch conditions as we shall see in the coming sections.

It should be pointed out that if the stick motion takes place between two moving bodies then the (2.16) can not be directly used to determine the acting friction force components. In that case the switch conditions are needed to determine both the acting friction force components and the stick-slip states, which will be discussed in the following chapters.

In the case of a one-dimensional friction oscillator, the friction direction angle reduces to 0 or π (motion in x-direction) or $\pi/2$ or $3\pi/2$ (motion in y-direction). Therefore the friction direction angle can be used to instead of the sign function.

If the dry friction depends on the friction direction angle as a result of roughness anisotropy of the contact surfaces then the dry friction is called anisotropic friction[Zmitrowcz,1981a,b]. In that case the friction direction angle can be used to determine the deflection angle, β as shown in Figure 2.3. In that case the friction coefficient is then determined by

$$\mu_\theta = \sqrt{(\mu_{11}\cos\theta + \mu_{12}\sin\theta)^2 + (\mu_{21}\cos\theta + \mu_{22}\sin\theta)^2} \tag{2.19}$$

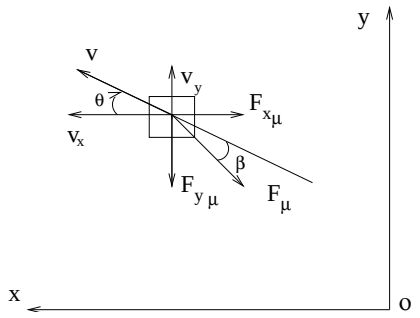

Figure 2.3: *Components of anisotropic friction forces*

and the deflection angle is determined by

$$\beta = \frac{(\mu_{22} - \mu_{11})\sin\theta - \mu_{12}\sin^2\theta + \mu_{21}\cos^2\theta}{\mu_{11}\cos^2\theta + \mu_{22}\sin^2\theta + (\mu_{12} + \mu_{21}\sin\theta\cos\theta)}. \tag{2.20}$$

The friction coefficients μ_{ij} may be found by sliding the mass along the axes of the orthogonal reference system (xoy). In any isotropic friction case $\mu_{ij} = \mu$ for $i = j$ and $\mu_{ij} = 0$ for $i \neq j$.

The components of the friction forces in the x and y directions are then determined by

$$\left.\begin{array}{l} F_{x\mu} = F_\mu \cos(\theta + \beta) \\ F_{y\mu} = F_\mu \sin(\theta + \beta) \end{array}\right\}, \quad (\dot{x}_s \vee \dot{y}_s \neq 0) \quad | \quad (\dot{x}_s \wedge \dot{y}_s = 0, \; |F_{inx}| \geq |F_{x\mu s}|, |F_{iny}| \geq |F_{y\mu s}|) \tag{2.21}$$

and

$$\left.\begin{array}{l} F_{x\mu s} = \Re(\theta) N \mu_s \cos(\theta + \beta) \\ F_{y\mu s} = \Re(\theta) N \mu_s \sin(\theta + \beta) \end{array}\right\} \tag{2.22}$$

In the same way the friction forces in other motion states can also be written out.

2.3.1 The external force and input force

When the resultant velocity of the mass is equal to zero, we say that the system is in the stick-phase. In this case the friction coefficient attains its maximum value μ_s and the associated friction force may reach its maximum value, which is the same as the definition of the maximum static friction force. If the acting force (input force) is less than the static friction force there is no motion occurring, because the static friction force will balance the input force. If the input force is larger than the static friction force, the balance will break and the mass will move under the action of the input force and the friction force with the kinetic friction coefficient μ_k. The

resulting motion is a consequence of the stick-slip action of the friction force. In order to deal with the stick-slip motion, we can use the friction direction angle and the determination of the related components of the friction force vector, which have just been discussed in the previous section.

In the case of a moving mass, which is called the slip-phase, we have the resultant forces:

$$F_{xh} = F_{inx} - F_{x\mu k} \tag{2.23}$$

$$F_{yh} = F_{iny} - F_{y\mu k} \tag{2.24}$$

and if the mass comes to rest, which is called the stick-phase, the resultant forces are:

$$F_{xl} = F_{inx} - F_{x\mu} \tag{2.25}$$

$$F_{yl} = F_{iny} - F_{y\mu} \tag{2.26}$$

where $F_{x\mu}, F_{y\mu}$ denote the acting friction forces. They are equal to $F_{x\mu k}, F_{y\mu k}$ for the slip-phase and $F_{x\mu t}, F_{y\mu t}$ for the stick-phase respectively. The friction forces $F_{x\mu k}, F_{y\mu k}$, $F_{x\mu t}, F_{y\mu t}$ are determined by (2.15) and (2.16). The input forces are defined by.

$$F_{inx} = F_x - c_x\dot{x} - k_x x, \quad F_{iny} = F_y - c_y\dot{y} - k_y y, \tag{2.27}$$

which may be used to find the friction direction angle.

The dependence of the friction coefficient on the relative velocity, was determined in three ways in[Popp, 1996]. Here we use a fourth approximate description[True, 2002][Xia, 2001a] that seems more appropriate for dry friction between two plane surfaces of steel or cast iron.

In order to obtain a continuous transition of the friction forces from zero to non-zero speeds we introduce as a weight function, the hyperbolic secant function

$$sech(\eta) = \frac{2}{e^{-\eta} + e^{\eta}} \tag{2.28}$$

To this end, we define the resulting forces acting on the mass at arbitrary speeds as

$$F_{rx} = F_{xl} sech(\dot{x_s}\alpha) + F_{xh}(1 - sech(\dot{x_s}\alpha)) \tag{2.29}$$

$$F_{ry} = F_{yl} sech(\dot{y_s}\alpha) + F_{yh}(1 - sech(\dot{y_s}\alpha)) \tag{2.30}$$

where α is a parameter that is related to the gradient of the change between μ_s and μ_k. A specified value of α provides the corresponding approximate friction characteristics. This model is well suited for the numerical implementation since the user remains in control of the numerical process during the switch from stick to slip. Figure 2.4 shows the curves of friction force as a function of the speed for various values of the parameter α.

Finally, the dynamical equation reads:

$$\begin{bmatrix} m & 0 \\ 0 & m \end{bmatrix} \begin{bmatrix} \ddot{x_s} \\ \ddot{y_s} \end{bmatrix} = \begin{bmatrix} F_{rx} \\ F_{ry} \end{bmatrix} \tag{2.31}$$

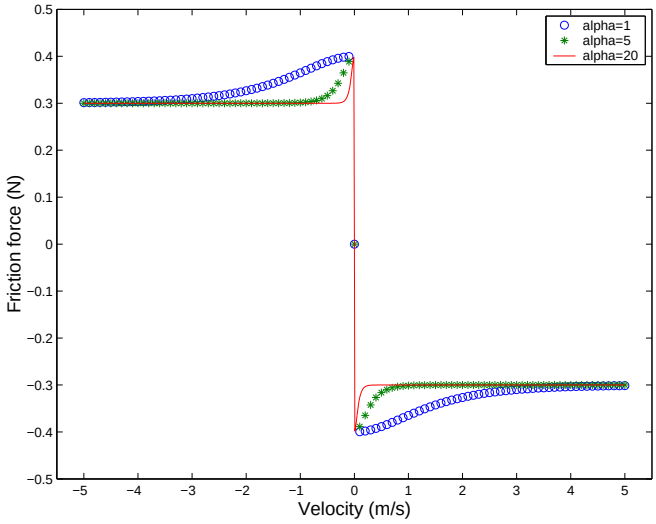

Figure 2.4: *The friction force with unit normal force as a function of the velocity for different parameter values* α.

2.3.2 Conditions for stick-slip motions

If the input forces satisfy the condition

$$|F_{inx}| > |F_{x\mu s}| \quad \bigvee \quad |F_{iny}| > |F_{y\mu s}| \tag{2.32}$$

or(valid only for the isotropic friction)

$$\sqrt{F_{inx}^2 + F_{iny}^2} > |F_\mu| \tag{2.33}$$

then the mass will change from the stick phase, to the slip phase.

When the system is in the slip phase, if it changes to the stick phase the input forces must satisfy the following conditions

$$|F_{inx}| < |N\mu_s \cos\theta sech(\alpha \dot{x_s}) + N\mu_k \cos\theta(1 - sech(\alpha \dot{x_s}))|, \tag{2.34}$$
$$|F_{iny}| < |N\mu_s \sin\theta sech(\alpha \dot{y_s}) + N\mu_k \sin\theta(1 - sech(\alpha \dot{y_s}))|. \tag{2.35}$$

During the slip-phase changing to stick-phase the velocity will change continuously. When the motion into the stick phase the components of the friction force vector are determined by the equation(2.16).

2.4 Characteristics of the two-dimensional friction oscillator

2.4.1 Special cases of the system

If the external force in equations (2.10) and (2.11) along the y(or x) direction is zero, it means that the mass only moves along the x(or y) direction. In this case the problem reduces to a one-dimensional friction oscillator, which has been investigated by many researchers[Meng, 1991][Den Hartog, 1931][Hong, 2000][Saw, 1986][Feen, 1992][Popp, 1996]. With the method introduced above, the friction direction angle θ then is either 0 or π, so the sign function can be replaced by the friction direction angle.

If two excitation forces share the relations $\Omega_x = \Omega_y$ and $\phi_x = \phi_y$, then

$$\frac{\beta_x \cos(\Omega_x t + \phi_x)}{\beta_y \cos(\Omega_y t + \phi_y)} = Constant. \tag{2.36}$$

Then there is a linear relation between the two friction force components, and the equations (2.10)(2.11) can be reduced to a one dimensional dynamic system:

$$\ddot{z} + c\dot{z} + z + \mu\theta_0 = \beta_z \cos(\Omega_z t + \phi) \tag{2.37}$$

where the θ_0 takes the values of 0 or π and the orbit of the response is a straight line segment.

In order to show this, we choose the parameter values: μ_s=$\mu_k = 0.4$, $\beta_x = 0.4$, $\beta_y = 0.2$ and $\Omega_x = \Omega_y = 0.7$, $\xi_x = \xi_y = 0.5$, $\phi_x = \phi_y = 0$. The simulation results are shown in Figure 2.5, in which the four left plots show the displacements and the phase diagram; and the right four plots show the friction force(in the figure the limit friction force overlaps the acting friction force) and the friction direction angle.

For $c_x = c_y$, $k_x = k_y$, i.e., a symmetric system, the response will have a circular orbit when the mass is excited by a sinusoidal excitation where the x and y components differ in phase by $\pi/2$[Meng, 1991]. The results are shown in Figure 2.6 for comparison with the results in[Meng,1991]. In the figure, the left four plots show the displacements, the phase diagram, the velocities and the exciting forces. If the amplitudes of the exciting forces are large enough then the acting friction force is identical to the limiting locus of the friction force. In the case where the amplitudes of the exciting forces are small as shown in the right four plots of Figure 2.6, then the acting friction force is less than the limiting locus of the friction force and obviously the system is in rest. In the figure, the dotted circle denotes the limiting locus of the friction force and the solid circle shows the acting friction force.

The orbit of the response will be elliptic under the excitations

$$\Omega_x = \Omega_y, \quad \phi_x \neq \phi_y \tag{2.38}$$

and the difference in phase differs from $\pi/2$. Letting the parameters $\beta_x = \beta_y = 0.5$, $\Omega_x = \Omega_y = 0.2$, $k_x = k_y = 1$, $\xi_x = \xi_y = 1$, $\phi_x = 0$, $\phi_y = \pi/4$ and $\mu_k = \mu_s = 0.4$.

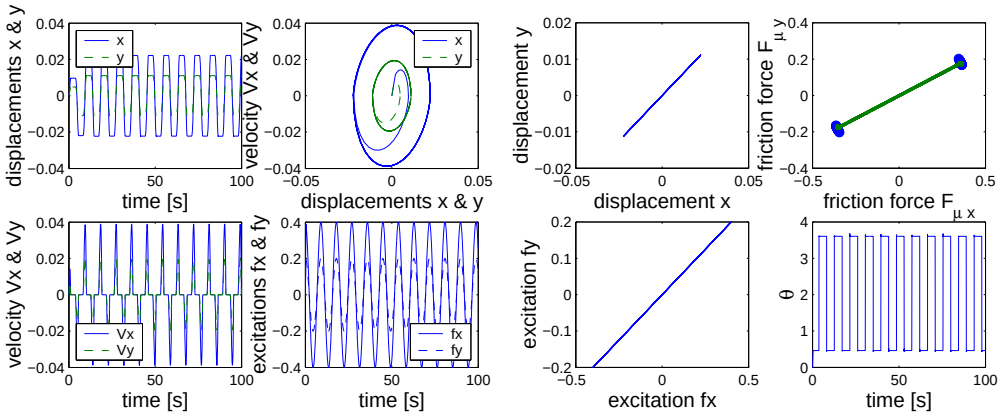

Figure 2.5: *The straight line segment orbit of the response to different amplitudes and the same frequencies of excitations. Left fours: responses and phase diagrams; Right fours: friction forces and friction direction angles*

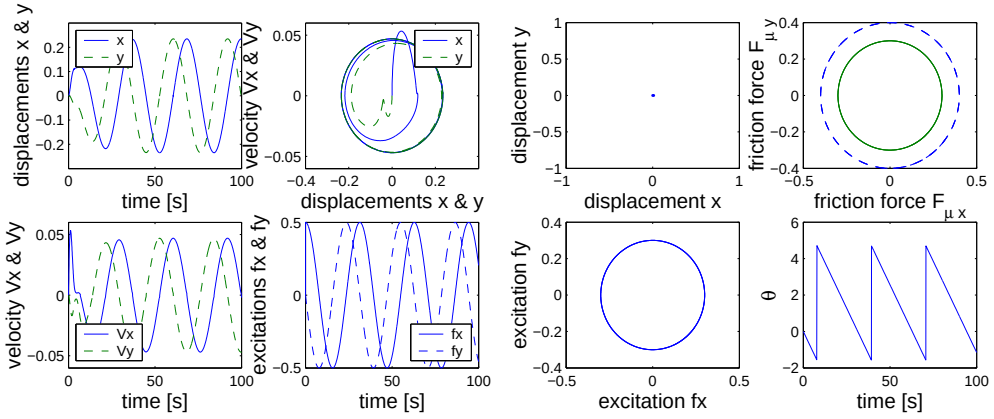

Figure 2.6: *Left: responses to sinusoidal excitations differing in phase by* $\pi/2$*;* $\mu_s = \mu_k = 0.4$ $\beta_x = \beta_y = 0.5$, $k_x = k_y = 1$, $\xi_x = \xi_y = 1$, $\phi_x = 0$, $\phi_y = \pi/2$. *Right: the trajectory, the friction forces and the friction direction angle with the parameters are same as the left except* $\beta_x = \beta_y = 0.3$

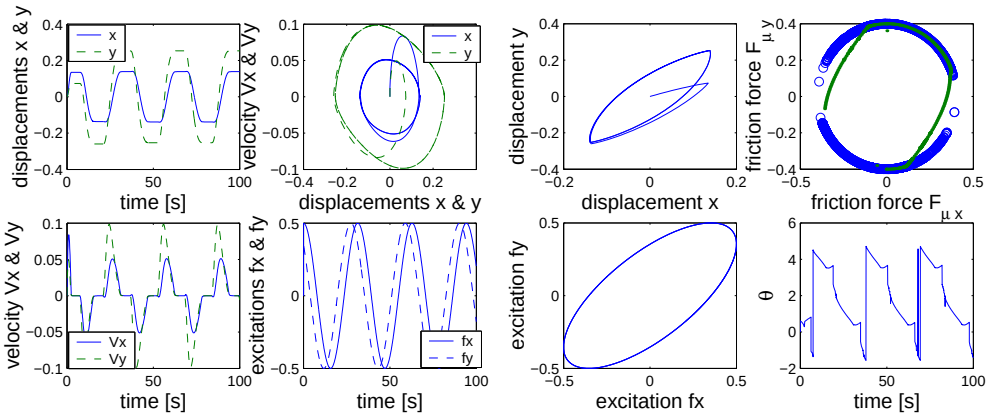

Figure 2.7: *Responses of the stick-slip state in which the orbit is elliptic:* $\beta_x = \beta_y = 0.5$, $\Omega_x = \Omega_y = 0.2$, $k_x = k_y = 1$, $\xi_x = \xi_y = 1$, $\phi_x = 0$, $\phi_y = \pi/4$.

The displacements, the phase diagram, the orbit of the response, the friction forces and the friction direction angles are shown in Figure 2.7. It is easy to see that there exist two stops per cycle. Correspondingly, in the plot of the acting friction force $F_{\mu y}$ versus $F_{\mu x}$ the circle is seen to be divided into two segments with a gap around $F_{\mu y} = 0$. Therefore the acting friction force is inside or on the limiting locus of the friction force. This means that there are two stick states per cycle. When the static coefficient of friction equals the kinematic coefficient of friction that is the case here, then the curve of the limiting locus of the friction force on the two-dimensional plane is a circle.

2.4.2 Multiple stops per cycle

In the case of one-dimensional friction, there are many types of steady-state behaviour: permanent sticking, zero stop per cycle(i.e., non-sticking oscillation), one-stop, two-stops, four-stops, six-stops per cycle, and so on[Hong, 2000]. As an example, only two stops and four stops per cycle are shown here. However, the three stops per cycle are also found for the two-dimensional friction case. The results are shown in Figure 2.8.

2.4.3 General responses of the system

In general case, the orbit of the response to arbitrary amplitudes and frequencies both in x and y directions is a plane curve. As an example, let the initial phases be zero. Figure 2.9 shows the steady state of the displacements and the phase diagram in the left four plots of the figure. The orbit of the response and the corresponding friction direction angle are shown in the right four plots of the figure. The figure

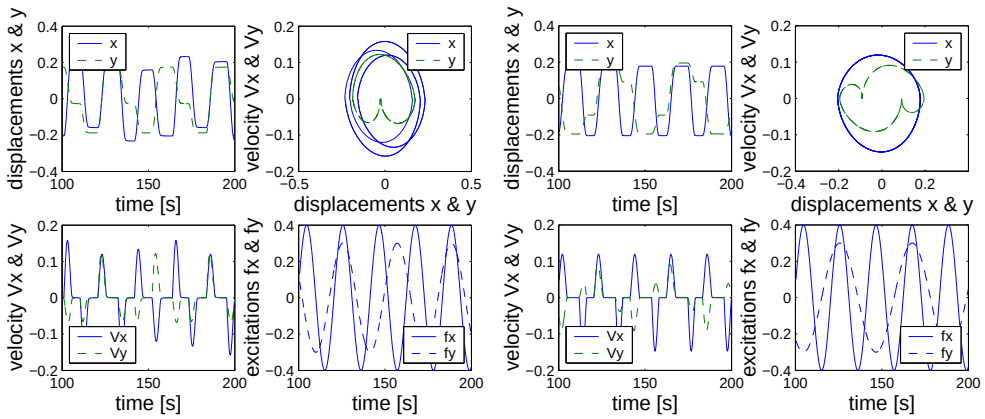

Figure 2.8: *Left: two and three-stops per cycle:* $\beta_x = 0.4$, $\beta_y = 0.3$, $\Omega_x = 0.3$ *and* $\Omega_y = 0.2$, $c_x = c_y = 0.5$*; Right: two and four-stops per cycle along x and y directions respectively: the parameters are same as the left except for the* $\Omega_y = 0.15$

clearly shows that the orbit of the response is not a simple circle or an ellipse but a rather complex planar curve.

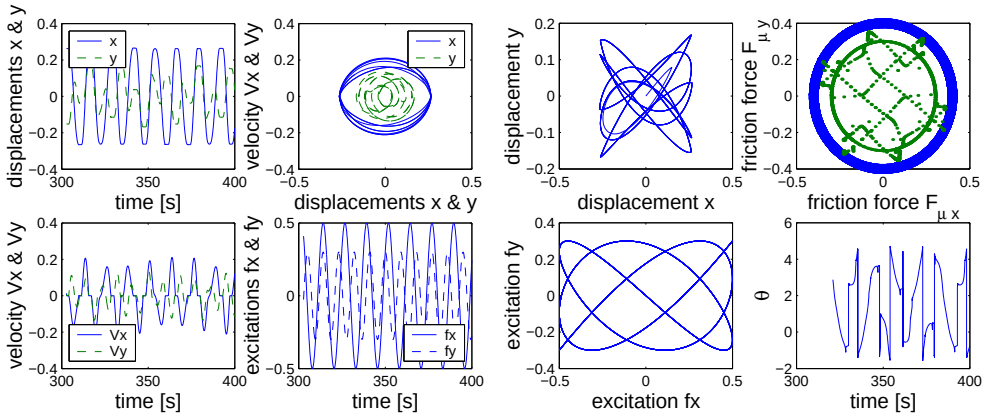

Figure 2.9: *Response to sinusoidal excitations with different amplitudes and frequencies:* $\mu_s = 0.4$, $\mu_k = 0.3$, $c_x = c_y = 1$, $\beta_x = 0.5$, $\beta_y = 0.3$, $\Omega_x = 0.5$, $\Omega_y = 0.7$*; Left fours: responses and phase diagrams; Right fours: the orbit of the response and the friction direction angle*

In this chapter, we have provided a method to simulate the stick-slip motion of a two-dimensional dry friction oscillator under complex excitations. The friction direction angle has been defined and successfully used to replace the sign function that is widely used in the one-dimensional friction oscillator. With the friction direction

angle both the module and the argument of the friction force vector can be determined for the stick state as well as for the slip state. By the switch-condition we can simulate the stick-slip motion numerically under various excitations.

The two-dimensional coupled oscillator can be uncoupled under certain conditions. The orbit of the responses of a two-dimensional friction oscillator will be a straight line segment, a circle or an ellipse depending on the details of the sinusoidal excitations. In the general case, the response is a complex planar curve. For various levels of excitations, the zero-stop, one-stop, two-stops and multiple stops per cycle will appear.

The cases involving a velocity-dependent friction coefficient, a collapse of the state space of the system caused by stick-slip motion and a variable normal force, especially, if the normal force is a state-dependent variable, the problem will be discussed in connection with our investigation of the model of wedge dampers in the three-piece-freight-bogie on railways in the next chapter.

Chapter 3

Modelling of wedge dampers with two-dimensional dry friction

A model of the wedge dampers of the Three-Piece-Freight-Truck in the presence of two-dimensional dry friction will be discussed in detail in this chapter. The model presented involves the three-dimensional motion of wedge dampers under external excitations both in the lateral and vertical directions, with the velocity-dependent friction coefficients. The lateral and vertical components of the dry friction force vectors on the surfaces of a wedge can be exactly calculated using the concept of friction direction angles introduced in chapter 2 and the switch conditions for the system in the cases of stick state and slip state. The responses of a wedge and a bolster to exciting forces on the bolster along the lateral, vertical or inclined directions are obtained. The results show that the vertical and lateral dynamic performances of the wedge dampers are coupled through the friction direction angles. One interesting phenomenon is that if the exciting force on the bolster is purely lateral then it will anyway cause both lateral as well as vertical vibrations of the wedge and the bolster. A switch condition for a coupling-separating motion between a wedge and a bolster is provided, and the coupling-separating motion is simulated with a numerical method. The structure of the natural frequency of the wedge dampers with two-dimensional dry friction is discussed in detail and some numerical results are provided.

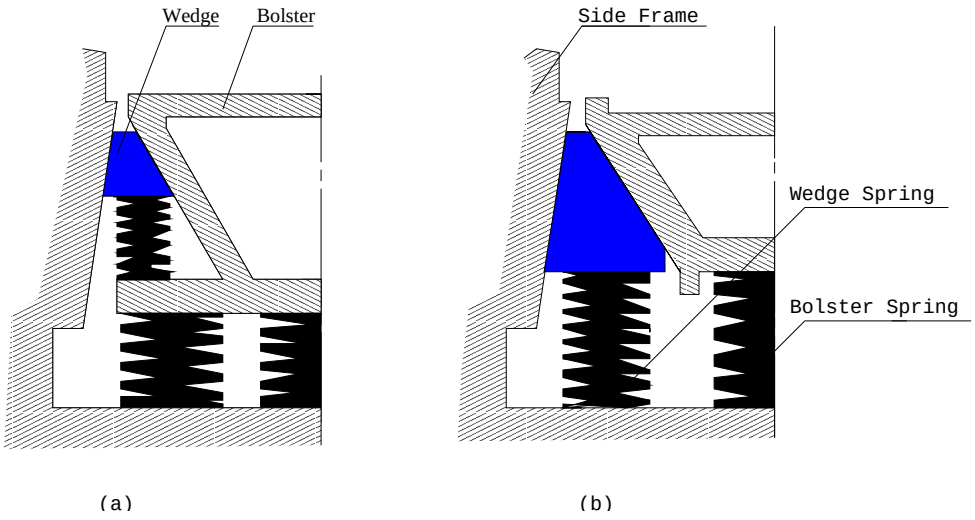

Figure 3.1: *Secondary suspension configurations for (a) constant and (b) variable damping*

3.1 Description of the wedge damper system

For the current three-piece-freight-truck, two main types of friction wedge suspensions are widely used. They differ by the method in which the wedges are spring loaded. The constant-damping suspension incorporates preloaded control springs that hold the wedges in place through a constant force which is shown in Figure 3.1(a), it is called *constant damping* or *ride control*. The variable-damping suspensions are characterized by a set of independent support springs that supply the wedge compression forces as a function of the displacement between the bolster and side frame is shown in Figure 3.1(b), which is often called *variable damping* or *ride master*. In the present thesis, we mainly focus the research efforts on the variable-damping suspensions. The methods can also be used to the constant-damping suspensions because it is simple from a mathematical point of view. As Figure 3.2 shows the wedges are spring-loaded into an approximately conformal space between the bolster and the side frames. Usually a friction plate is added between the surfaces of a wedge and the side frame, which easily can be changed with a new one when it is worn. In this chapter we consider the case that the wedge, the bolster and the side frame can move relatively to each other in the longitudinal, lateral and vertical directions. In order to study the performances of a wedge and a bolster relative to a side frame, the side frames are considered fixed. In this way the longitudinal motion of a bolster can be neglected since the symmetry of the action of the two wedges is preserved. Many investigators have focused on this problem in different ways. However, up to now, as to our knowledge, few models or theories considered

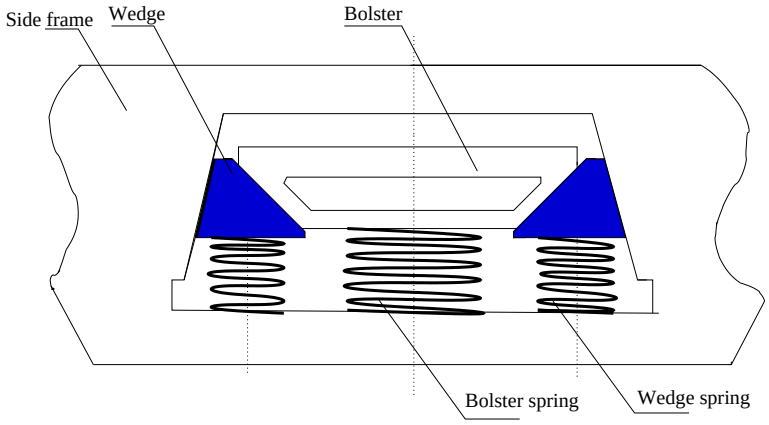

Figure 3.2: *Schematic cross-section of wedge dampers in Three-Piece-Freight-Truck*

the problem of wedge dampers with two-dimensional dry friction. The present existing models of the Three-Piece-Freight-Truck have at least one of five shortcomings:

- The mass of the wedge is neglected;
- Only the static or the kinetic dry friction coefficient is considered;
- Only one-dimensional dry friction is included;
- The determination of the lateral and vertical components of friction force vectors on the surfaces of a wedge are made with a constant normal force times the friction coefficient, $N_b\mu$.
- The stick-slip motion is neglected.

In this chapter we restrict the investigation to three directions of motion of the wedge and the bolster, i.e. in longitudinal, lateral and vertical direction. The mass of the bolster in the model includes also the mass of the loaded or empty car body. Using the symmetries in the construction only one eighth of the total enters the equations.

The normal stresses are replaced by single normal forces on both surfaces of the friction wedge. In order to understand the effects of dry friction on the responses of the wedge dampers, only dry friction damping without the effects of possible viscous damping is considered. The free bodies in the simple model are one of the friction wedges, one-fourth bolster, one-eighth of the car body and half of a spring group on either side of the truck, in addition the lumped masses of a bolster and a wedge are used. Figure 3.3 shows the free bodies and the forces on them. Letting the dry friction coefficients on the two surfaces of a wedge be μ_d, μ_b which have static and kinetic states and are defined by the friction function in chapter 1. With Eq. (2.3) we have

$$f_{\mu 1} = \sqrt{f_{\mu y1}^2 + f_{\mu z1}^2} \leq \mu_d S_d \tag{3.1}$$

and

$$f_{\mu 2} = \sqrt{f_{\mu y2}^2 + f_{\mu z2}^2} \leq \mu_b N_b \tag{3.2}$$

where $f_{\mu y1,2}, f_{\mu z1,2}$ stand for the components of the friction forces on the two surfaces of a wedge in the lateral and vertical directions respectively, and the index 1 denotes the surface of the wedge contacting on the side frame and the index 2 the surface of the wedge contacting the bolster; $f_{\mu 1}$ and $f_{\mu 2}$ denote the resultant Coulomb dry friction forces, which can be determined by eqns.(2.3) and (2.4). The notations on Figure 3.3 are used.

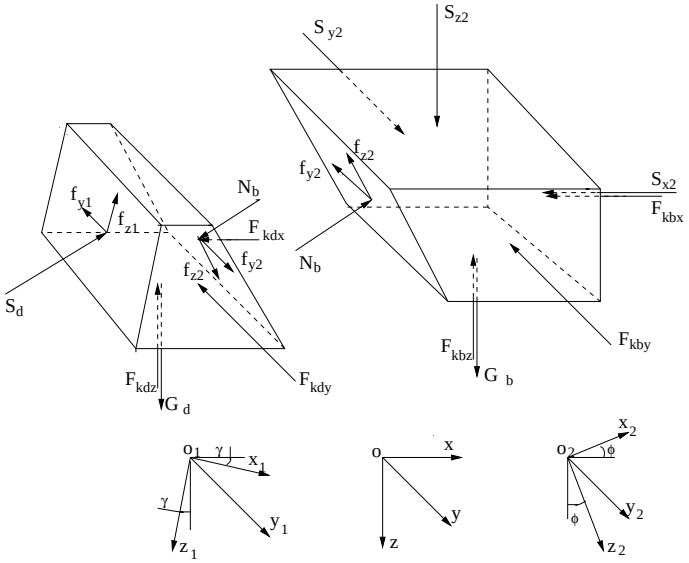

Figure 3.3: *The free bodies of a wedge and a bolster and the reaction forces on them*

Furthermore, due to the fact that $\dot{x}_{1,2}$=0 on the contacting surfaces, the velocities of a wedge and a bolster V_1 and V_2 , which determine the directions of the corresponding friction forces, are given by

$$V_{1,2} = \sqrt{\dot{z}_{1,2}^2 + \dot{y}_{1,2}^2} \tag{3.3}$$

in which the derivatives of $z_{1,2}$ and $y_{1,2}$ are respect with to time.

We use the fact that in eqns. (3.1)-(3.3) all terms correspond to the surface-fixed coordinates of the wedge, so that the relations between the surface-fixed coordinates and the general coordinates can be found as:

$$\begin{pmatrix} x_1 \\ y_1 \\ z_1 \end{pmatrix} = \begin{pmatrix} \cos\gamma & 0 & \sin\gamma \\ 0 & 1 & 0 \\ -\sin\gamma & 0 & \cos\gamma \end{pmatrix} \begin{pmatrix} x_d \\ y_d \\ z_d \end{pmatrix} \tag{3.4}$$

and

$$\begin{pmatrix} x_2 \\ y_2 \\ z_2 \end{pmatrix} = \begin{pmatrix} \cos\phi & 0 & -\sin\phi \\ 0 & 1 & 0 \\ \sin\phi & 0 & \cos\phi \end{pmatrix} \begin{pmatrix} x_{d,b} \\ y_{d,b} \\ z_{d,b} \end{pmatrix} \tag{3.5}$$

where γ is the angle between the left side surface of a wedge and its vertical surface and ϕ is the angle between the right side surface of a wedge and its vertical surface.

By Newton's second law the equations of motion of the system are:

$$m_d \begin{pmatrix} \ddot{x}_d \\ \ddot{y}_d \\ \ddot{z}_d \end{pmatrix} = \begin{pmatrix} S_d\cos\gamma - N_b\cos\phi - F_{kdx} + f_{\mu z1}\sin\gamma + f_{\mu z2}\sin\phi \\ f_{\mu y2} - f_{\mu y1} - F_{kdy} \\ N_b\sin\phi + S_d\sin\gamma - F_{kdz} + f_{\mu z2}\cos\phi - f_{\mu z1}\cos\gamma + G_d \end{pmatrix} \tag{3.6}$$

and

$$m_b \begin{pmatrix} \ddot{x}_b \\ \ddot{y}_b \\ \ddot{z}_b \end{pmatrix} = \begin{pmatrix} N_b\cos\phi - f_{\mu z2}\sin\phi - S_{x2} - F_{kbx} \\ -f_{\mu y2} - F_{kby} + S_{y2} \\ S_{z2} - N_b\sin\phi - F_{kbz} - f_{\mu z2}\cos\phi + G_b \end{pmatrix} \tag{3.7}$$

where

$$F_{kdx} = k_{dx}x_d, \quad F_{kdy} = k_{dy}y_d, \quad F_{kdz} = k_{dz}z_d, \tag{3.8}$$

$$F_{kbx} = k_{bx}x_b, \quad F_{kby} = k_{by}y_b, \quad F_{kbz} = k_{bz}z_b. \tag{3.9}$$

m_d is the mass of a wedge and m_b the mass of a fourth of a bolster; S_d denotes the normal force between a wedge and a side frame and N_b the normal force between a wedge and a bolster; $F_{k..}$ denotes the spring force of a wedge or a bolster spring with indices dx, dy, dz, bx, by, bz that denote the spring forces of the wedge and the bolster in the longitudinal, lateral or vertical direction respectively; S_{x2} is the internal force coming from the symmetry in the problem; S_{y2} and S_{z2} are external exciting forces on the bolster along the lateral and vertical directions; G_d, G_b the weights of the wedge and the bolster respectively.

We use the definition of the friction direction angle in chapter 2 to calculate the components of the friction forces on the surfaces of the wedge along the lateral and vertical directions. The friction direction angles read

$$\theta_1 = \begin{cases} \chi_1(\dot{y}_1, \dot{z}_1), & (\dot{y}_1 \bigvee \dot{z}_1 \neq 0) \\ \psi_1(F_{iny1}, F_{inz1}), & (\dot{y}_1 \bigwedge \dot{z}_1 = 0, F_{iny1} \bigvee F_{inz1} \neq 0), \\ \emptyset, & (\dot{y}_1 \bigwedge \dot{z}_1 \bigwedge F_{iny1} \bigwedge F_{inz1} = 0) \end{cases} \tag{3.10}$$

$$\theta_2 = \begin{cases} \chi_2(\dot{y}_{21}, \dot{z}_{21}), & (\dot{y}_{21} \bigvee \dot{z}_{21} \neq 0) \\ \psi_2(F^*_{inybd}, F_{inz2}), & (\dot{y}_{21} \bigwedge \dot{z}_{21} = 0, F^*_{inybd} \bigvee F_{inz2} \neq 0) \\ \emptyset, & (\dot{y}_{21} \bigwedge \dot{z}_{21} \bigwedge F^*_{inybd} \bigwedge F_{inz2} = 0) \end{cases} \tag{3.11}$$

where θ_1 is the friction direction angle of the friction force on the surface of the wedge contacting with side frame and θ_2 the friction direction angle of the friction force on

the surface of the wedge contacting with the bolster; the symbol $\vee$ means disjunction and the $\wedge$ denotes conjunction. Relative velocities $\dot{y}_{21}, \dot{z}_{21}$ are defined by

$$\dot{y}_{21} = \dot{y}_b - \dot{y}_d, \quad \dot{z}_{21} = (\dot{z}_b - \dot{z}_d)/\cos\phi \tag{3.12}$$

and $\dot{y}_d, \dot{y}_b, \dot{z}_d, \dot{z}_b$ are the velocities of the wedge and the bolster along lateral and vertical directions respectively; $F_{iny1}, F_{inybd^*}, F_{inz1}, F_{inz2}$ denote the input forces, which will be discussed in detail in section 3.2. The input forces described in the surface-fixed coordinate and in the general coordinate systems have the relations

$$F_{iny1} = F_{inyd}, \quad F_{inz1} = F_{inzd}/\cos\gamma, \quad F_{iny2} = F^*_{inybd}, \quad F_{inz2} = F_{inzb}/\cos\phi. \tag{3.13}$$

By use of the friction direction angles $\theta_{1,2}$, the components of the kinetic friction forces along lateral and vertical directions can be determined by the following formulae.

$$\left.\begin{array}{l} f_{y1\mu k} = f_{\mu 1}\cos\theta_1 \\ f_{z1\mu k} = f_{\mu 1}\sin\theta_1 \end{array}\right\}, (\dot{y}_1 \vee \dot{z}_1 \neq 0) \quad | \quad (\dot{y}_1 \wedge \dot{z}_1 = 0, \\ |F_{iny1}| \geq |f_{yd\mu s}| \vee |F_{inzd}| \geq |f_{zd\mu s}|) \tag{3.14}$$

$$\left.\begin{array}{l} f_{y1\mu t} = F_{iny1} \\ f_{z1\mu t} = F_{inz1} \end{array}\right\}, (\dot{y}_1 \wedge \dot{z}_1 = 0, |F_{iny1}| < |f_{yd\mu s}| \wedge |F_{inzd}| < |f_{zd\mu s}|), \tag{3.15}$$

$$\left.\begin{array}{l} f_{y2\mu k} = f_{\mu 2}\cos\theta_2 \\ f_{z2\mu k} = f_{\mu 2}\sin\theta_2 \end{array}\right\}, (\dot{y}_{21} \vee \dot{z}_{21} \neq 0) \quad | \quad (\dot{y}_{21} \wedge \dot{z}_{21} = 0, \\ |F^*_{inybd}| \geq |f_{yb\mu s}| \vee |F_{inzb}| \geq |f_{zb\mu s}|), \tag{3.16}$$

$$\left.\begin{array}{l} f_{y2\mu t} = F^*_{inybd} \\ f_{z2\mu t} = F_{inz2} \end{array}\right\}, \quad (\dot{y}_{21} \wedge \dot{z}_{21} = 0, |F^*_{inybd}| < |f_{\mu ybs}| \wedge |F_{inzb}| < |f_{zb\mu 2}|). \tag{3.17}$$

For the analysis of the stick motion between the wedge and the bolster and the wedge and the frame the components of the static friction force vector must be determined. They are used to set up the switch conditions.

$$f_{yd\mu s} = \Re(\theta_1) S_d \mu_{sd} \cos\theta_1, \tag{3.18}$$

$$f_{zd\mu s} = \Re(\theta_1) S_d \mu_{sd} \sin\theta_1 \cos\gamma, \tag{3.19}$$

$$f_{yb\mu s} = \Re(\theta_2) N_b \mu_{sb} \cos\theta_2, \tag{3.20}$$

$$f_{zb\mu s} = \Re(\theta_2) N_b \mu_{sb} \sin\theta_2 \cos\phi \tag{3.21}$$

where the function $\Re(\theta)$ is defined by (2.18). We suppose that no separation between a wedge and a bolster and the wedge and a side frame take place. With $\dot{x}_1 = 0$ and then calculating of the relative velocities between the surfaces of the wedge and the

bolster by equation (3.5) and letting the relative velocity along local x_2-axis be zero we can derive the following kinematic constraints of the system

$$\dot{x}_d = -\frac{\sin\gamma\sin\phi}{\sin(\gamma+\phi)}\dot{z}_b, \quad \dot{z}_d = \frac{\cos\gamma\sin\phi}{\sin(\gamma+\phi)}\dot{z}_b, \quad \dot{x}_b = 0 \tag{3.22}$$

Thus we have three independent variables y_d, y_b and z_b in our system.

Note that in eqns. (3.11), (3.16) and (3.17) we use F^*_{inybd} to represent the input force in the lateral direction. The reason is that the stick motion will take place between the two moving components of the wedge and bolster. When the wedge and the bolster are locked in the lateral direction we can write the acting friction force $f_{yb\mu t}$ as

$$F^*_{inybd} = \frac{1}{m_d+m_b}(F_{inyb}m_d - F_{inyd}m_b), \quad f_{yb\mu t} = F^*_{inybd} \tag{3.23}$$

and the switch conditions are

$$f_{yb\mu t} < f_{yb\mu s}, \quad \dot{y}_{21} \wedge \dot{z}_{21} = 0. \tag{3.24}$$

The acting friction forces on the surfaces of wedges for the stick state in the vertical direction, $f_{z1\mu t}$ and $f_{z2\mu t}$ can be determined by the equations (3.15) and (3.17) in a simple way.

3.2 The stick-slip motion of the wedge dampers

When the relative velocity between a wedge and a bolster is zero, we say that the wedge, the bolster or the system is in the stick-mode. When the relative speed of the wedge and the bolster is different from zero, we call the state the slip-motion. According to chapter 2 in the slip state the resultant external forces can be written as

$$F_{xdresh} = F_{inxdh} - F_{\mu xdh}, \tag{3.25}$$
$$F_{ydresh} = F_{inydh} - F_{\mu ydh}, \tag{3.26}$$
$$F_{zdresh} = F_{inzdh} - F_{\mu zdh}, \tag{3.27}$$
$$F_{ybresh} = F_{inybh} - F_{\mu ybh}, \tag{3.28}$$
$$F_{zbresh} = F_{inzbh} - F_{\mu zbh}. \tag{3.29}$$

Here the input forces and the friction forces are

$$F_{inxdh} = S_d\cos\gamma - N_b\cos\phi - F_{kdx} + N_b\mu_{kd}\sin\theta_2\sin\phi, \tag{3.30}$$

$$F_{\mu xdh} = -S_d\mu_{kd}\sin\theta_1\sin\gamma, \tag{3.31}$$

$$F_{inydh} = N_b\mu_{kb}\cos\theta_2 - F_{kdy}, \tag{3.32}$$

$$F_{\mu ydh} = S_d \mu_{kd} \cos\theta_1, \tag{3.33}$$

$$F_{inzdh} = N_b \sin\phi + S_d \sin\gamma - F_{kdz} + N_b \mu_{kb} \sin\theta_2 \cos\phi + G_d, -F_{kdy}, \tag{3.34}$$

$$F_{\mu zdh} = S_d \mu_{kd} \sin\theta_1 \cos\gamma, \tag{3.35}$$

$$F_{inybh} = S_{y2} - F_{kby}, \tag{3.36}$$

$$F_{\mu ybh} = N_b \mu_{kb} \cos\theta_2, \tag{3.37}$$

$$F_{inzbh} = S_{z2} - N_b \sin\phi - F_{kbz} + G_b, \tag{3.38}$$

$$F_{\mu zbh} = N_b \mu_{kb} \sin\theta_2 \cos\phi \tag{3.39}$$

where μ_{kd}, μ_{kb} denote the kinetic friction coefficients on the two surfaces of a wedge respectively.

In the stick-mode, the resultant external forces read

$$F_{xdresl} = F_{inxdl} - F_{\mu xdl}, \tag{3.40}$$

$$F_{ydresl} = F_{inydl} - F_{\mu ydl}, \tag{3.41}$$

$$F_{zdresl} = F_{inzdl} - F_{\mu zdl} \tag{3.42}$$

and

$$F_{ybresl} = F_{inybl} - F_{\mu ybl}, \tag{3.43}$$

$$F_{zbresl} = F_{inzbl} - F_{\mu zbl} \tag{3.44}$$

where the input forces and the friction forces in the longitudinal, lateral and vertical directions are defined by:

$$F_{inxdl} = S_d \cos\gamma - N_b \cos\phi - F_{kdx}, \tag{3.45}$$

$$F_{\mu xdl} = f_{z2\mu} \sin\phi - f_{z1\mu} \sin\gamma, \tag{3.46}$$

$$F_{inydl} = -F_{kdy} \tag{3.47}$$

$$F_{\mu ydl} = F_{iny1} + F^*_{\mu ybd}, \tag{3.48}$$

$$F_{inzdl} = N_b \sin\phi + S_d \sin\gamma - F_{kdz} + G_d, \tag{3.49}$$

$$F_{\mu zdl} = f_{z2\mu} \cos\phi + f_{z1\mu} \cos\gamma, \tag{3.50}$$

$$F_{inybl} = S_{y2} - F_{kby}, \tag{3.51}$$

$$F_{\mu ybl} = F^*_{\mu ybd}, \tag{3.52}$$

$$F_{inzbl} = S_{z2} - F_{kbz} - N_b \sin\phi + G_b, \tag{3.53}$$

$$F_{\mu zbl} = f_{z2\mu} \cos\phi \tag{3.54}$$

where $f_{z1\mu}, f_{z2\mu}$ denote the acting friction forces on the two surfaces of a wedge respectively, they are determined by

$$f_{z1\mu} = \begin{cases} f_{z1\mu k}, & F_{inzd} \geq f_{zd\mu s} \\ f_{z1\mu t}, & F_{inzd} < f_{zd\mu s} \end{cases}, \tag{3.55}$$

$$f_{z2\mu} = \begin{cases} f_{z2\mu k}, & F_{inzb} \geq f_{zb\mu s} \\ f_{z2\mu t}, & F_{inzb} < f_{zb\mu s} \end{cases} \tag{3.56}$$

The acting friction forces between the wedge and the bolster in the lateral direction for the stick-mode can be determined by (3.23) and the switch conditions can be written as

$$f_{y2\mu t} = F^*_{inybd} < f_{yb\mu s}, \quad \dot{y}_{21} = 0 \tag{3.57}$$

with (3.24).

Here we use the same method discussed in chapter 2. Thus the friction force characteristics depending on the relative velocity are approximately described by the hyperbolic secant function(2.27). We define the resulting forces acting on the wedge and the bolster at arbitrary speeds as[Xia, 2001a][True, 2002]

$$F_{rxd} = F_{xdresl} sech(\dot{x}_d \alpha) + F_{xdresh}(1 - sech(\dot{x}_d \alpha)), \tag{3.58}$$

$$F_{ryd} = F_{ydresl} sech(\dot{y}_d \alpha) + F_{ydresh}(1 - sech(\dot{y}_d \alpha)), \tag{3.59}$$

$$F_{rzd} = F_{zdresl} sech(\dot{z}_d \alpha) + F_{zdresh}(1 - sech(\dot{z}_d \alpha)), \tag{3.60}$$

$$F_{ryb} = F_{ybresl} sech(\dot{y}_b \alpha) + F_{ybresh}(1 - sech(\dot{y}_b \alpha)), \tag{3.61}$$

$$F_{rzb} = F_{zbresl} sech(\dot{z}_b \alpha) + F_{zbresh}(1 - sech(\dot{z}_b \alpha)) \tag{3.62}$$

where α is a parameter that determines the shape of the curve. Its value is chosen and depends on the magnitude of the relative velocity. For a higher speed a lower value is selected, and vice versa.

Finally, the equations of motion of our system are

$$m_d \begin{pmatrix} \ddot{x}_d \\ \ddot{y}_d \\ \ddot{z}_d \end{pmatrix} = \begin{pmatrix} F_{rx1} \\ F_{ry1} \\ F_{rz1} \end{pmatrix}, \qquad m_b \begin{pmatrix} \ddot{y}_b \\ \ddot{z}_b \end{pmatrix} = \begin{pmatrix} F_{ry2} \\ F_{rz2} \end{pmatrix}. \tag{3.63}$$

3.3 Numerical analysis

In the system the normal contact forces S_d and N_b usually are state-dependent quantities. For the simple system they can be expressed explicit but generally it may be impossible. They must be calculated numerically in dependence on time as all the other state variables.

In the system (3.63) there are three independent variables y_d, y_b and z_b; and we calculate reaction forces S_d and N_b explicitly in the equations. In this way we can reduce the system to five equations in the lateral accelerations of a wedge and a bolster, the vertical acceleration of the bolster, the side frame normal force and the bolster normal force. Taking matrix form, the equations read

$$\mathbf{A_s Y_s} = \mathbf{F_s}, \tag{3.64}$$

where

$$\mathbf{Y_s} = [S_d \quad N_b \quad \ddot{y}_d \quad \ddot{y}_b \quad \ddot{z}_b]^T \tag{3.65}$$

$$\mathbf{F_s} = \left\{ \begin{array}{l} \left\{ \begin{array}{l} -F_{kdx} \\ -F_{kdz} + G_d \\ -F_{kdy} \\ S_{y2} - F_{kby} \\ S_{z2} + G_b - F_{kbz} \end{array} \right\}, \quad \begin{array}{c} (\dot{y}_b \vee \dot{z}_b \neq 0) | (\dot{y}_b \wedge \dot{z}_b = 0, \\ |F^*_{inybd}| \geq |f_{yb\mu s}| \wedge |F_{inzb}| \geq |f_{zb\mu s}|) \end{array} \\ \left\{ \begin{array}{l} -F_{kdx} + f_{z1\mu t} \sin\gamma + f_{z2\mu t} \sin\phi \\ -F_{kdz} + G_d + f_{z2\mu t} \cos\phi - f_{z1\mu t} \cos\gamma \\ -F_{kdy} - F^*_{inybd} \\ S_{y2} - F_{kby} - F^*_{inybd} \\ S_{z2} + G_b - F_{kbz} - f_{z2\mu t} \cos\phi \end{array} \right\}, \quad \begin{array}{c} (\dot{y}_b \wedge \dot{z}_b = 0) \wedge \\ (|F_{inzb}| < |f_{zb\mu s}|) \wedge \\ (|F_{inybd}|^* < |f_{yb\mu s}|), \end{array} \\ \left\{ \begin{array}{l} S_{dold} \\ N_{bold} \\ 0 \\ 0 \\ 0 \end{array} \right\}, \quad \Re(\theta_1) = 0, \Re(\theta_2) = 0 \end{array} \right. \tag{3.66}$$

where S_{dold}, N_{bold} denote the values of S_d and N_b in the previous integral step.

$$\mathbf{A}_s = \left\{ \begin{array}{l} \left\{ \begin{array}{ccccc} a_{11} & a_{12} & 0 & 0 & m_d \frac{\sin\phi \sin\gamma}{\sin(\phi+\gamma)} \\ a_{21} & a_{22} & 0 & 0 & -m_d \frac{\sin\phi \cos\gamma}{\sin(\phi+\gamma)} \\ a_{31} & a_{32} & -m_d & 0 & 0 \\ 0 & a_{42} & 0 & -m_b & 0 \\ 0 & a_{52} & 0 & 0 & -m_b \end{array} \right\}, \quad \begin{array}{c} (\dot{y}_b \vee \dot{z}_b \neq 0) | \\ (\dot{y}_b \wedge \dot{z}_b = 0, \\ |F^*_{inybd}| \geq |f_{yb\mu s}| \wedge \\ |F_{inzb}| \geq |f_{zb\mu s}|) \end{array} \\ \left\{ \begin{array}{ccccc} C\gamma & -C\phi & 0 & 0 & a_{15} \\ S\gamma & S\phi & 0 & 0 & a_{25} \\ a_{31} & 0 & -m_d & 0 & 0 \\ 0 & 0 & 0 & -m_b & 0 \\ 0 & -S\phi & 0 & 0 & -m_b \end{array} \right\}, \quad \begin{array}{c} (\dot{y}_b \wedge \dot{z}_b = 0) \wedge \\ (|F_{inzb}| < |f_{zb\mu s}|) \wedge \\ (|F^*_{inybd}| < |f_{yb\mu s}|) \end{array}, \\ \left\{ \begin{array}{ccccc} 1 & 0 & 0 & 0 & 0 \\ 0 & 1 & 0 & 0 & 0 \\ 0 & 0 & 1 & 0 & 0 \\ 0 & 0 & 0 & 1 & 0 \\ 0 & 0 & 0 & 0 & 1 \end{array} \right\}, \quad \Re(\theta_1) = 0, \Re(\theta_2) = 0 \end{array} \right. \tag{3.67}$$

in which the a_{15}, a_{25} are defined by

$$a_{15} = m_d \frac{\sin\phi \sin\gamma}{\sin(\phi+\gamma)}, \quad a_{25} = -m_d \frac{\sin\phi \cos\gamma}{\sin(\phi+\gamma)}. \tag{3.68}$$

The other elements of $\mathbf{A_s}$ can be found in appendix A.

Letting $\dot{y}_d = q_1$, $\dot{y}_b = q_2$, $\dot{z}_b = q_3$, $y_d = q_4$, $y_b = q_5$, $z_b = q_6$, we can rewrite the second order differential equations in the form of a system of Differential-Algebraic Equation (DAE) [Hairer, 1991][Brenan, 1989]

$$\dot{\mathbf{q}} = \mathbf{f}(\mathbf{q}, \mathbf{z}), \tag{3.69}$$

$$\mathbf{0} = \mathbf{g}(\mathbf{q}, \mathbf{z}) \tag{3.70}$$

where

$$\mathbf{f} = \begin{bmatrix} z_1 & z_2 & z_3 & q_1 & q_2 & q_3 \end{bmatrix}^T, \tag{3.71}$$

$$\mathbf{g}(\mathbf{q}, \mathbf{z}) = \mathbf{F_s} - \mathbf{A_s}\mathbf{n}, \tag{3.72}$$

$$\mathbf{n} = \begin{bmatrix} S_d & N_b & z_1 & z_2 & z_3 \end{bmatrix}^T. \tag{3.73}$$

The system described by eqns. (3.69) and (3.70) is a piece-wise differentiable system so numerical integral method can be used to simulate the system[Hairer, 1991].

3.4 The motion of the wedge dampers under sinusoidal excitations when they are in contact with the bolster

As an example, consider the typical parameters of the wedge dampers in [Yan, 1993] [Cheng, 2000] as shown in Table 3.1.

Table 3.1: *Parameters of the system*

γ	2.5^0	k_{dx}(N/m)	0.8e6	k_{by}(N/m)	1.9e6	μ_{sb}	0.45
ϕ	45^0	k_{dy}(N/m)	0.8e6	k_{bz}(N/m)	2.69e6	μ_{kb}	0.35
m_d(Kg)	8	k_{dz}(N/m)	1.0e6	μ_{sd}	0.4		
m_b(Kg)	1906/10000	k_{bx}(N/m)	1.5e7	μ_{kd}	0.3		

Figure 3.4 shows the response of the wedge and the bolster along lateral and vertical directions on only lateral exciting force on the bolster. The amplitude of the exciting force is 5000N with the frequency 8π. In all figures in this section, the dotted line denotes the lateral excitation and the solid line the vertical excitation.

In this case the lateral vibrations of the wedge and the bolster look like bounded periodic responses and the amplitude of the vibration of the wedge is always less or equal to that of the response of the bolster. If the exciting force is less than the minimum of static friction forces on the surfaces of a wedge, the system will be motionless. The stick state can be found when the displacement reach its maximum values corresponding to the zero relative velocities[Hong, 2000]. Because the friction

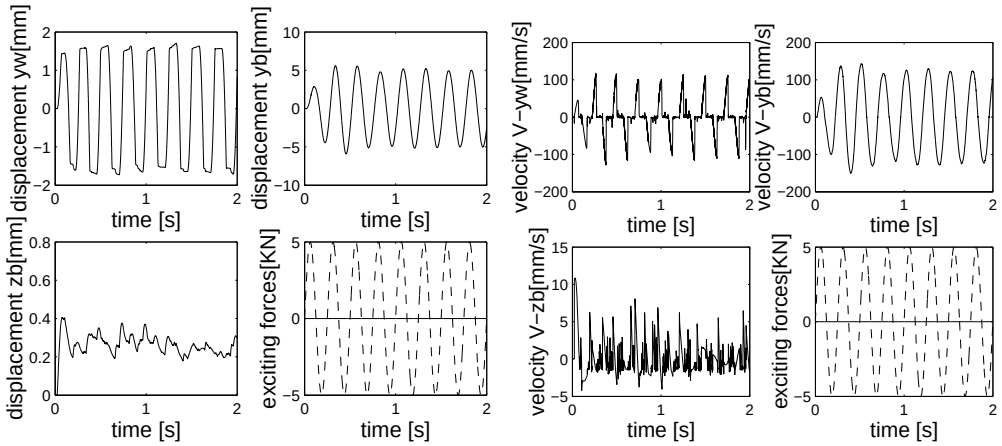

Figure 3.4: *Lateral responses of a wedge and a bolster to lateral exciting force on the bolster for an empty.*

damping, the vibration will reach its steady state with the same frequency as that of the exciting force.

The results show that although only a lateral exciting force acts on the bolster, it also induces the vertical movements of the bolster and the wedge. The reason can be explained as follows: Before the exciting force acts, the friction force on the surface between the wedge and the bolster acts only along vertical direction, that means that the friction direction angle equals to $\pi/2$, and the lateral component of the friction force is equal to zero. When the lateral exciting force acts, the friction direction angle changes from $\pi/2$, which means that the lateral component of the friction force increases from zero and subsequently the resultant input force may be bigger than the total static friction force and slip occurs. Immediately the vertical component of the friction force will drop to its kinematic value and the bolster will move vertically as well as laterally. The characteristics of the vibration are controlled by the levels of the excitations and the system parameters.

Figure 3.5 shows the responses of a wedge and a bolster under combined lateral and vertical exciting forces on the bolster. The amplitude of the lateral exciting force is 20000N and the frequency is 2π rad/s; the amplitude of the vertical exciting force is 10000N and the frequency is 4π rad/s. In this case the phase trajectory in its steady state is not circular, but a plan closed curve. The motions of the wedge and the bolster are complicated because they influence each other. The results show that the vertical motion of the bolster also effects the lateral responses of the wedge and the bolster. The responses of the wedge and the bolster are characterized by both the amplitudes and frequencies of the excitations. If the exciting force on the bolster is purely vertical, the amplitude of the vertical vibration of the bolster is smaller than that of the vibration under combination of the vertical and the lateral excitation.

Note that if the maximum amplitude of the vertical excitation in the case of an

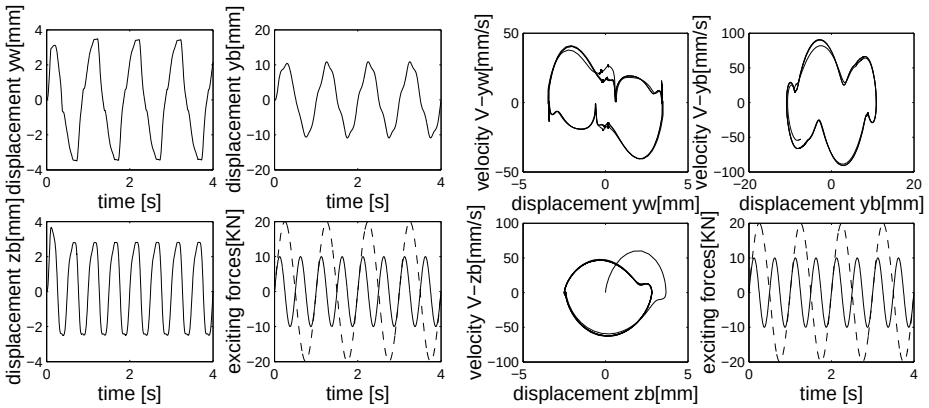

Figure 3.5: *Lateral and vertical responses of a bolster to both lateral and vertical exciting forces for an empty car; the dotted line denotes the lateral exciting force and the solid line the vertical exciting force*

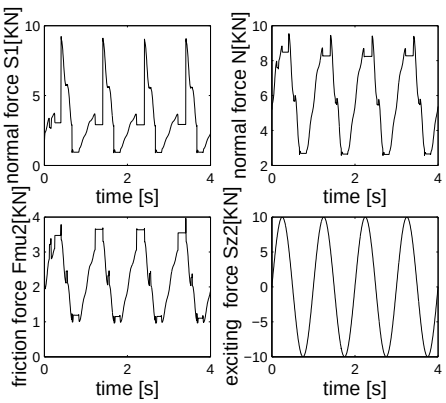

Figure 3.6: *Normal forces on the surfaces of a wedge to a large vertical exciting force with the amplitude 10000N and the frequency 2π.*

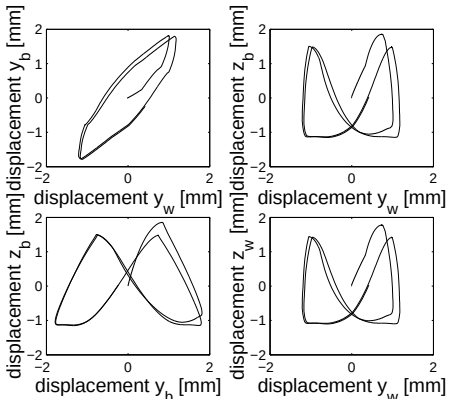

Figure 3.7: *The trajectories of a wedge and a bolster under the combination of lateral and vertical excitations with the frequencies* 2π *and* 4π *and the amplitudes* $3500N$ *and* $5000N$

empty car exceeds the weight of the car body, when the force direction is upward, then the friction force will be zero because the normal forces on the contacting surface become zero. Then the wedge and the bolster will separate and the present dynamical system can not deal with it, because the kinetic constraint relations are broken. That problem will be discussed in the next section.

If only a vertical exciting force acts on the bolster of either an empty or a loaded car, a steady motion of the system with intermediate stops per cycle will appear. In other words, a stick-phase develops, in which the input forces are less or equal to the maximal static friction force. In a large range of vertical exciting forces, the stick-slip motion will arise for both the empty and the loaded car far away from resonance, this is different from the case where only a lateral exciting force or both the lateral and vertical act on the bolster. These results can be found in Figure 3.6. Figure 3.6 shows the normal forces on the surfaces of the wedge. We can find an interesting phenomenon: The changing trends of the normal force are completely different when under the small levels of the excitation from the large ones. When the amplitude of the exciting force is large enough, the normal forces are larger for the downward motion of the bolster than for the upward motion. The result is the same as the static results reported by Fröhling [Fröhling, 1998].

Under the combination of the lateral and vertical excitations the trajectories of the wedge and the bolster are characterized by the frequency combinations of the excitations, which are shown in the right four curves of Figure 3.7. It can give an explanation of the observed shapes of wear on the surfaces of a wedge and a side frame from a three-piece-freight-truck.

3.5 The motion of the system under separation

When the three-piece-freight-truck runs on the track, the exciting force on the bolster in the vertical direction may be so large, that the bolster will separate from the wedge and perform a vibration without any contact with the wedge.

When separation takes place, and if the displacement of the wedge in the vertical direction is smaller than its initial value, then a friction force exists on the surface of the wedge contacting the side frame because the displacement in the longitudinal direction differs from zero. If the displacement of the wedge along the vertical direction is larger than its initial value, then a free vibration of the wedge will take place. The bolster will perform a forced vibration without any friction damping. Hence for the bolster, we have the following dynamic equation:

$$m_b \begin{pmatrix} \ddot{x}_b \\ \ddot{y}_b \\ \ddot{z}_b \end{pmatrix} = \begin{pmatrix} -S_{x2} - F_{kbx} \\ -F_{kby} + S_{y2} \\ S_{z2} - F_{kbz} \end{pmatrix}. \tag{3.74}$$

In this case the motion of the bolster in the longitudinal direction can not be neglected. The system(3.7) can be rewritten as

$$\ddot{x}_b + \frac{k_{bx}}{m_b} x_b = \frac{S_{x2}}{m_b}, \qquad \ddot{y}_b + \frac{k_{by}}{m_b} y_b = \frac{S_{y2}}{m_b}, \qquad \ddot{z}_b + \frac{k_{bz}}{m_b} z_b = \frac{S_{z2}}{m_b} \tag{3.75}$$

where S_{x2}, S_{y2} and S_{z2} are simply selected as harmonic excitations of the forms

$$S_{x2} = A_{fxb} \sin(\omega_{fxb} t + \phi_{xb0}), \tag{3.76}$$

$$S_{y2} = A_{fyb} \sin(\omega_{fyb} t + \phi_{yb0}), \tag{3.77}$$

$$S_{z2} = A_{fzb} \sin(\omega_{fzb} t + \phi_{zb0}) \tag{3.78}$$

where A_{fxb}, A_{fyb} and A_{fzb} stand for the amplitudes of the excitations, ω_{fxb}, ω_{fyb} and ω_{fzb} for the frequencies; and ϕ_{xb0}, ϕ_{yb0} and ϕ_{zb0} are the phases.

With the initial conditions at the time $t = 0$ when the separation of the wedge and bolster begins, the initial phases are not zeros in the general case, so the exact solutions of above equations are[Timoshenko, 1974]

$$x_b = C_{1x} \cos(\omega_{xb} t + \frac{\omega_{xb}\phi_{xb0}}{\omega_{fxb}}) + C_{2x} \sin(\omega_{xb} t + \frac{\omega_{xb}\phi_{xb0}}{\omega_{fxb}}) + C_{3x} \sin(\omega_{fxb} t + \phi_{xb0}), \tag{3.79}$$

$$y_b = C_{1y} \cos(\omega_{yb} t + \frac{\omega_{yb}\phi_{yb0}}{\omega_{fyb}}) + C_{2y} \sin(\omega_{yb} t + \frac{\omega_{yb}\phi_{yb0}}{\omega_{fyb}}) + C_{3y} \sin(\omega_{fyb} t + \phi_{yb0}), \tag{3.80}$$

$$z_b = C_{1z} \cos(\omega_{zb} t + \frac{\omega_{zb}\phi_{zb0}}{\omega_{fzb}}) + C_{2z} \sin(\omega_{zb} t + \frac{\omega_{zb}\phi_{zb0}}{\omega_{fzb}}) + C_{3z} \sin(\omega_{fzb} t + \phi_{zb0}) \tag{3.81}$$

where

$$C_{1x} = D_{1x} \cos(\frac{\omega_{xb}\phi_{xb0}}{\omega_{fxb}}) - \frac{D_{2x}}{\omega_{fxb}} \sin(\frac{\omega_{xb}\phi_{xb0}}{\omega_{fxb}}), \tag{3.82}$$

$$C_{2x} = \frac{D_{2x}}{\omega_{fxb}} \cos(\frac{\omega_{xb}\phi_{xb0}}{\omega_{fxb}}) + D_{1x} \sin(\frac{\omega_{xb}\phi_{xb0}}{\omega_{fxb}}), \tag{3.83}$$

$$C_{3x} = \frac{A_{fxb}}{k_{xb}[1 - (\frac{\omega_{fxb}}{\omega_{xb}})^2]}, \tag{3.84}$$

$$C_{1y} = D_{1y} \cos(\frac{\omega_{yb}\phi_{yb0}}{\omega_{fyb}}) - \frac{D_{2y}}{\omega_{fyb}} \sin(\frac{\omega_{yb}\phi_{yb0}}{\omega_{fyb}}), \tag{3.85}$$

$$C_{2y} = \frac{D_{2y}}{\omega_{fyb}} \cos(\frac{\omega_{yb}\phi_{yb0}}{\omega_{fyb}}) + D_{1y} \sin(\frac{\omega_{yb}\phi_{yb0}}{\omega_{fyb}}), \tag{3.86}$$

$$C_{3y} = \frac{A_{fyb}}{k_{yb}[1 - (\frac{\omega_{fyb}}{\omega_{yb}})^2]}, \tag{3.87}$$

$$C_{1z} = D_{1z} \cos(\frac{\omega_{zb}\phi_{zb0}}{\omega_{fzb}}) - \frac{D_{2z}}{\omega_{fzb}} \sin(\frac{\omega_{zb}\phi_{zb0}}{\omega_{fzb}}), \tag{3.88}$$

$$C_{2z} = \frac{D_{2z}}{\omega_{fzb}} \cos(\frac{\omega_{zb}\phi_{zb0}}{\omega_{fzb}}) + D_{1z} \sin(\frac{\omega_{zb}\phi_{zb0}}{\omega_{fzb}}), \tag{3.89}$$

$$C_{3z} = \frac{A_{fzb}}{k_{zb}[1 - (\frac{\omega_{fzb}}{\omega_{zb}})^2]}, \tag{3.90}$$

$$D_{1x} = x_{b0} - \frac{A_{fxb} \sin\phi_{xb0}}{k_{xb}[1 - (\frac{\omega_{fxb}}{\omega_{xb}})^2]}, \quad D_{2x} = \dot{x_{b0}} - \frac{A_{fxb} \cos\phi_{xb0}}{k_{xb}[1 - (\frac{\omega_{fxb}}{\omega_{xb}})^2]}, \tag{3.91}$$

$$D_{1y} = y_{b0} - \frac{A_{fyb} \sin\phi_{yb0}}{k_{yb}[1 - (\frac{\omega_{fyb}}{\omega_{yb}})^2]}, \quad D_{2y} = \dot{y_{b0}} - \frac{A_{fyb} \cos\phi_{yb0}}{k_{yb}[1 - (\frac{\omega_{fyb}}{\omega_{yb}})^2]}, \tag{3.92}$$

$$D_{1z} = z_{b0} - \frac{A_{fzb} \sin\phi_{zb0}}{k_{zb}[1 - (\frac{\omega_{fzb}}{\omega_{zb}})^2]}, \quad D_{2z} = \dot{z_{b0}} - \frac{A_{fzb} \cos\phi_{zb0}}{k_{zb}[1 - (\frac{\omega_{fzb}}{\omega_{zb}})^2]} \tag{3.93}$$

and

$$\omega_{xb}^2 = \frac{k_{xb}}{m_2}, \qquad \omega_{yb}^2 = \frac{k_{yb}}{m_2}, \qquad \omega_{zb}^2 = \frac{k_{zb}}{m_2}, \tag{3.94}$$

and ω_{fxb}, ω_{fyb} and ω_{fzb} are frequencies of excited forces. Obviously, the motions of the bolster are forced vibrations. For arbitrary exciting forces on the bolster in the lateral and vertical directions, the solutions can be obtained in the way shown in[Timoshenko, 1974], where the initial displacements and the velocities as well as the initial phases are not zero.

For the wedge, two cases should be considered: One is that the displacement of the wedge in the vertical direction is smaller than its initial value. In this case the friction force on the surface of the wedge in contact with the side frame should be included and the equations of motion(3.6) become

$$m_d \begin{pmatrix} -\ddot{z}_d \tan\gamma \\ \ddot{y}_d \\ \ddot{z}_d \end{pmatrix} = \begin{pmatrix} S_d \cos\gamma - F_{kdx} + S_d\mu_{kd} \sin\theta_1 \sin\gamma \\ -S_d\mu_{kd} \cos\theta_1 - F_{kdy} \\ S_d \sin\gamma - F_{kdz} - S_d\mu_{kd} \sin\theta_1 \cos\gamma \end{pmatrix}. \tag{3.95}$$

The solutions of the above equation are

$$y_d = a_{yd}\cos(\omega_{yd}t - \beta_{yd}), \tag{3.96}$$

$$z_d = a_{zd}\cos(\omega_{zd}t - \beta_{zd}), \tag{3.97}$$

$$x_d = -z_{zd}\tan\gamma \tag{3.98}$$

where

$$a_{yd} = \sqrt{y_{d0}^2 + (\frac{\dot{y}_{d0}}{\omega_{yd}})^2}, \quad \beta_{yd} = \tan^{-1}(\frac{\dot{y}_{d0}}{y_{d0}\omega_{yd}}), \quad \omega_{yws}^2 = \frac{k_{yd}}{m_d}, \tag{3.99}$$

$$a_{zd} = \sqrt{z_{d0}^2 + (\frac{\dot{z}_{d0}}{\omega_{zd}})^2}, \quad \beta_{zd} = \tan^{-1}(\frac{\dot{z}_{d0}}{z_{d0}\omega_{zd}}), \quad \omega_{zds}^2 = p_{ap} \tag{3.100}$$

and

$$p_{ap} = [k_{dz} - \sin\gamma(k_{dz} - k_{dx})(\sin\gamma - \mu_{kd}\sin\theta_1\cos\gamma)]/m_d. \tag{3.101}$$

The other case happens when the displacement of the wedge along the vertical direction is larger than its initial value. In this case the wedge performs free vibrations and the equations of motion can be written as

$$m_d \begin{pmatrix} \ddot{x}_d \\ \ddot{y}_d \\ \ddot{z}_d \end{pmatrix} = \begin{pmatrix} -F_{kdx} \\ -F_{kdy} \\ -F_{kdz} \end{pmatrix}. \tag{3.102}$$

The corresponding solutions read

$$x_d = a_{xd}\cos(\omega_{xd}t - \beta_{xd}), y_d = a_{yd}\cos(\omega_{yd}t - \beta_{yd}), z_d = a_{zd}\cos(\omega_{zd}t - \beta_{zd}) \tag{3.103}$$

where

$$a_{xd} = \sqrt{x_{d0}^2 + (\frac{\dot{x}_{d0}}{\omega_{xd}})^2}, \quad \beta_{xd} = \tan^{-1}(\frac{\dot{x}_{d0}}{x_{d0}\omega_{xd}}), \quad \omega_{xd}^2 = \frac{k_{xd}}{m_d}, \tag{3.104}$$

$$a_{yd} = \sqrt{y_{d0}^2 + (\frac{\dot{y}_{d0}}{\omega_{yd}})^2}, \quad \beta_{yd} = \tan^{-1}(\frac{\dot{y}_{d0}}{y_{d0}\omega_{yd}}), \quad \omega_{yd}^2 = \frac{k_{yd}}{m_d} \tag{3.105}$$

$$a_{zd} = \sqrt{z_{d0}^2 + (\frac{\dot{z}_{d0}}{\omega_{zd}})^2}, \quad \beta_{zd} = \tan^{-1}(\frac{\dot{z}_{d0}}{z_{d0}\omega_{zd}}), \quad \omega_{zd}^2 = \frac{k_{zd}}{m_d}. \tag{3.106}$$

For a certain large amplitude or a frequency near the resonant frequency of the excitation along the vertical direction, the response will change from a coupled into a separated motion. Figure 3.8 shows the vertical response of the bolster to a vertically exciting force. The filled area on the external force denotes that in that area the separation motion appear.

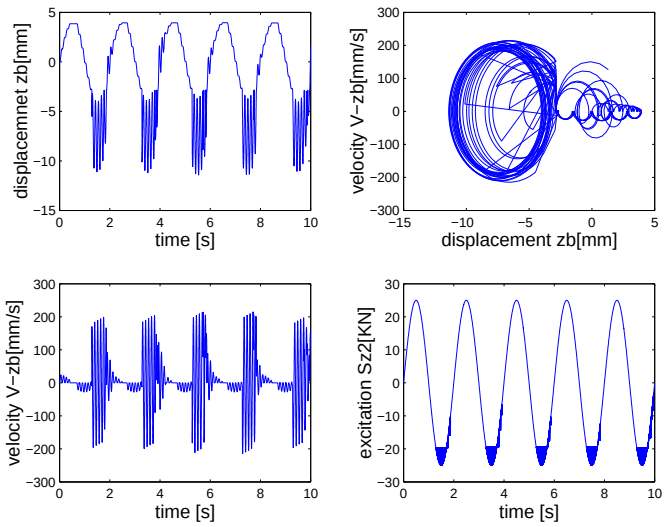

Figure 3.8: *Vertical responses of a bolster to a large exciting force on the bolster. The amplitude of the force is 23000N and the frequency is π(rad/s).* The shades on the curve denote the force corresponding to the separated motion

3.6 The contact switch-condition for the coupling-separating motion of the system

For the two motion states of the system, the motions are governed by two different sets of equations. The switch condition necessary to connect the two different movements must be set up so that a complete response of the system can be simulated. The separation begins when either of the normal forces on the surfaces of the wedge is equal to or smaller than zero. After then, the responses of the system belong to the separating state. If the surfaces of the bolster and the wedge meet, the coupled motion start. If the following condition

$$\mid z_b - z_d \mid \leq 0 \tag{3.107}$$

is true, then the coupled motion will start. The contact forces(impact forces) can be simply evaluated by the impulse law

$$N_b = \frac{m_b V_{bn} - m_d V_{wn}}{\Delta t}, \qquad S_d = \frac{N_b \cos\phi}{\cos\gamma} \tag{3.108}$$

where V_{bn} and V_{wn} stand for the approaching speeds along the normal directions of the surfaces of the wedge and Δt is the impact time.

In these cases there are two states of responses to certain large vertically exciting forces on the bolster: A coupled state and a separated state. In the first case,

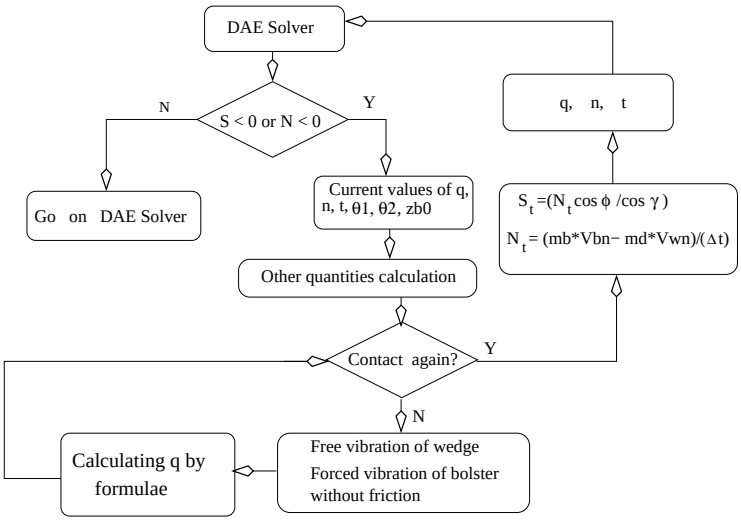

Figure 3.9: *The flow chart for the algorithm of the coupled-separated motion analysis*

the analytical solution is very difficult or impossible to find, so that a numerical method should be developed. In the second case the exact solution can be obtained. Combining the two cases a complete response of the wedge dampers to any levels of excitations can be simulated. The flow chart for the algorithm of the coupled-separated motion analysis is shown in Figure 3.9.

Figure 3.10 shows the complete response of the system with coupled-separated motion to a large exciting force. In the coupled state, the trends of the two curves are identical because there the kinematical constraints between the wedge and the bolster exist. In the case of the separated state, the wedge undergoes a free vibration with a higher frequency, and the response of the bolster is a forced vibration with a lower frequency. The motion of the system has two different frequencies. One of them is the same as that of the exciting force and the other is the free vibration frequency, so the trajectories of the two motions are different. When the contact switch-condition is fulfilled, a coupling takes place again.

3.7 The frequency response of the system

To understand the effect of dry friction damping on the response of the system, we calculate its frequency response. First, the natural frequencies of the wedge and the bolster are analyzed as following.

From the equations (3.6) and (3.7), we know that the motions of the wedge and the bolster are inertially coupled. Because of the effect of the dry friction, it is difficult to evaluate the frequency. However, we can analyze some special cases to

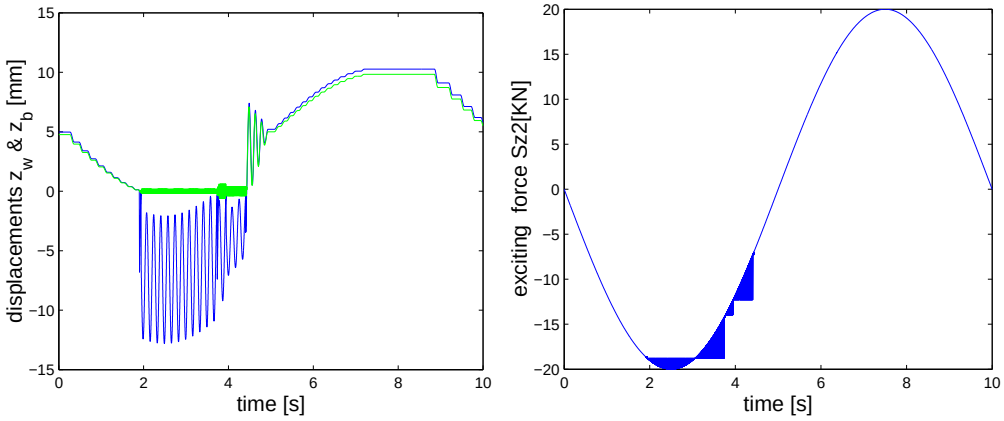

Figure 3.10: *The coupled-separated motions of the system to a vertical periodically varying force on the bolster: Amplitude: -20000N; frequency: 0.2π(rad/s). Left: Response. Right: Exciting force. The shades on the curve denote the force corresponding to the separated motion. The heavy color line denotes the motion of the bolster and the light color line denotes the motion of the wedge*

check the range of the frequencies of the system and the discussion in this section is limited in the range of slip motion of the system.

From equations (3.6), (3.7) and (3.10)-(3.17), we have

$$m_b\ddot{y}_b = -N_b\mu_{kb}\cos\theta_2 - k_{by}y_b + S_{y2}, \tag{3.109}$$

$$m_b\ddot{z}_b = -N_b\sin\phi - N_b\mu_{kb}\sin\theta_2\cos\phi - k_{bz}z_b + S_{z2}, \tag{3.110}$$

$$m_d\ddot{x}_d = S_d\cos\gamma + S_d\mu_{kd}\sin\theta_1\sin\gamma - N_b\cos\phi + N_b\mu_{kb}\sin\theta_2\sin\phi - k_{dx}x_d, \tag{3.111}$$

$$m_d\ddot{y}_d = N_b\mu_{kb}\cos\theta_2 - S_d\mu_{kd}\cos\theta_1 - k_{dy}y_d, \tag{3.112}$$

$$m_d\ddot{z}_d = N_b\sin\phi + N_b\mu_{kb}sin\theta_2\cos\phi + S_d\sin\gamma - S_d\mu_{kd}\sin\theta_1\cos\gamma - k_{dz}z_d. \tag{3.113}$$

For the separating motions, the frequencies of the wedge and the bolster can be easily found from (3.94) and (3.104) as

$$\omega_{yds} = \sqrt{\frac{k_{dy}}{m_d}}, \qquad \omega_{ybs} = \sqrt{\frac{k_{by}}{m_b}}, \qquad \omega_{zbs} = \sqrt{\frac{k_{zb}}{m_b}} \tag{3.114}$$

and ω_{zds} is given by (3.106). In the case of a coupling motion, the normal forces on the surfaces of the wedge depend on the state variables and the friction direction angle.

From(3.110) the normal force N_b can be found and with (3.113) the normal force S_d can be determined too. Substituting them into (3.109), (3.111) and (3.112), yield

$$\begin{aligned} m_d\ddot{y}_d + k_{dy}y_d = \\ \ddot{z}_b[\frac{m_b\mu_{kb}\cos\theta_2}{\sin\phi+\mu_{kb}\sin\theta_2\cos\phi} + \frac{\mu_{kd}\cos\theta_1}{\sin\gamma-\mu_{kd}\sin\theta_1\cos\gamma}(m_b+Bm_d)] \\ +z_b[\frac{k_{bz}\mu_{kb}\cos\theta_2}{\sin\phi+\mu_{kb}\sin\theta_2\cos\phi} + \frac{\mu_{kd}\cos\theta_1}{\sin\gamma-\mu_{kd}\sin\theta_1\cos\gamma}(k_{bz}+Bk_{dz})] \\ +\frac{\mu_{kd}\cos\theta_1}{\sin\gamma-\mu_{kd}\sin\theta_1\cos\gamma}S_{z2}, \end{aligned} \tag{3.115}$$

$$m_b\ddot{y}_b + k_{by}y_b = \frac{\mu_{kd}\cos\theta_2}{\sin\phi+\mu_{kb}\sin\theta_2\cos\phi}(m_b\ddot{z}_b + z_bk_{bz}) + S_{y2}, \tag{3.116}$$

$$\begin{aligned} \ddot{z}_b[(m_dB+m_b)\frac{\cos\gamma+\mu_{kd}\sin\theta_1\sin\gamma}{\sin\gamma-\mu_{kd}\sin\theta_1\cos\gamma} + m_b\frac{\cos\phi-\mu_{kb}\sin\theta_2\sin\phi}{\sin\phi+\mu_{kb}\sin\theta_2\cos\phi} - Am_d] \\ +z_b[(k_{bz}+Bk_{dz})\frac{\cos\gamma+\mu_{kd}\sin\theta_1\sin\gamma}{\sin\gamma-\mu_{kd}\sin\theta_1\cos\gamma} + \frac{\cos\phi-\mu_{kb}\sin\phi}{\sin\phi+\mu_{kb}\cos\phi}k_{bz} - Bk_{dz}] \\ = (\frac{\cos\gamma+\mu_{kd}\sin\theta_1\sin\gamma}{\sin\gamma-\mu_{kd}\sin\theta_1\cos\gamma} + \frac{\cos\phi-\mu_{kb}\sin\theta_2\sin\phi}{\sin\phi+\mu_{kb}\sin\theta_2\cos\phi})S_{z2} \end{aligned} \tag{3.117}$$

where

$$A = -\frac{\sin\gamma\sin\phi}{\sin(\gamma+\phi)}, \qquad B = \frac{\cos\gamma\sin\phi}{\sin(\gamma+\phi)} \tag{3.118}$$

Letting

$$k_{dzb} = (k_{bz}+Bk_{dz})\frac{\cos\gamma+\mu_{kd}\sin\theta_1\sin\gamma}{\sin\gamma-\mu_{kd}\sin\theta_1\cos\gamma}+\frac{\cos\phi-\mu_{kb}\sin\theta_2\sin\phi}{\sin\phi+\mu_{kb}\sin\theta_2\cos\phi}k_{bz}-Bk_{dz}, \tag{3.119}$$

$$m_{dzb} = (m_dB+m_b)\frac{\cos\gamma+\mu_{kd}\sin\theta_1\sin\gamma}{\sin\gamma-\mu_{kd}\sin\theta_1\cos\gamma}+m_b\frac{\cos\phi-\mu_{kb}\sin\theta_2\sin\phi}{\sin\phi+\mu_{kb}\sin\theta_2\cos\phi}-Am_d \tag{3.120}$$

we get the following cases.

Case 1. Without consideration of the friction.

In this case, the system is kinematically coupled, so that we have

$$\omega_{yw0} = \sqrt{\frac{k_{dy}}{m_d}}, \qquad \omega_{yb0} = \sqrt{\frac{k_{by}}{m_b}}, \qquad \omega_{zb0} = \sqrt{\frac{k_{dzb0}}{m_{dzb0}}} \tag{3.121}$$

where

$$k_{dzb0} = (k_{bz}+Bk_{dz})\frac{\cos\gamma}{\sin\gamma} + \frac{\cos\phi}{\sin\phi}k_{bz} - Bk_{dz} \tag{3.122}$$

and

$$m_{dzb0} = (m_dB+m_b)\frac{\cos\gamma}{\sin\gamma} + m_b\frac{\cos\phi}{\sin\phi} - Am_d. \tag{3.123}$$

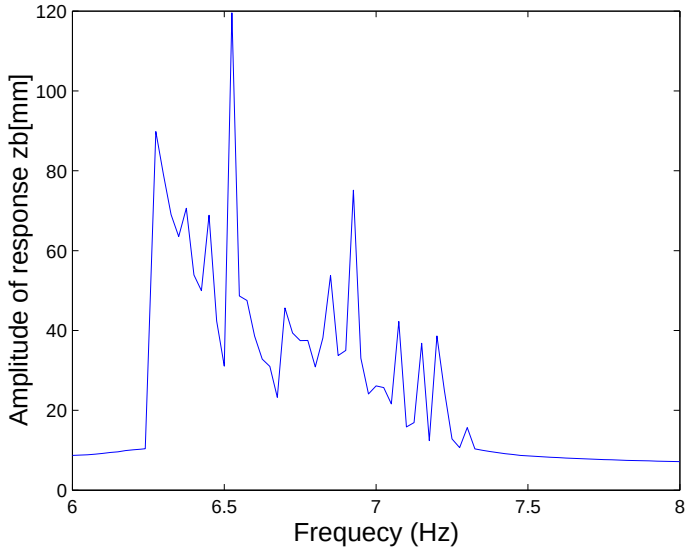

Figure 3.11: *Frequency response of the system for the only a vertically exciting force on the bolster with the amplitude 3000N.*

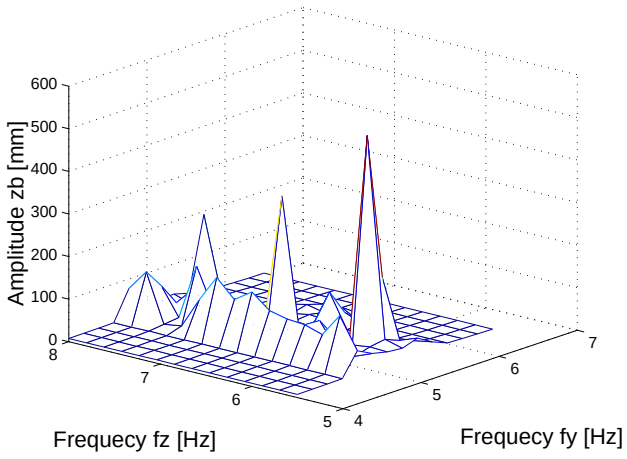

Figure 3.12: *Frequency response of the system for both the vertically and laterally exciting forces on the bolster with the amplitudes 3000N*

Case 2. The friction angles $\theta_1 = \theta_2 = \pi/2$ or $3\pi/2$.

In this case, the motions of the system reduce to a one dimensional vibration along the vertical direction. From (3.115), we can get

$$\omega_{zb1,2} = \sqrt{\frac{k_{dzb1,2}}{m_{dzb1,2}}} \tag{3.124}$$

where, for $\theta_1 = \pi/2$

$$k_{dzb1} = (k_{bz} + Bk_{dz})\frac{\cos\gamma + \mu_{kd}\sin\gamma}{\sin\gamma - \mu_{kd}\cos\gamma} + \frac{\cos\phi - \mu_{kb}\sin\phi}{\sin\phi + \mu_{kb}\cos\phi}k_{bz} - Bk_{dz} \tag{3.125}$$

and

$$m_{dzb1} = (m_d B + m_b)\frac{\cos\gamma + \mu_{kd}\sin\gamma}{\sin\gamma - \mu_{kd}\cos\gamma} + m_b\frac{\cos\phi - \mu_{kb}\sin\phi}{\sin\phi + \mu_{kb}\cos\phi} - Am_d \tag{3.126}$$

for $\theta_2 = 3\pi/2$

$$k_{dzb2} = (k_{bz} + Bk_{dz})\frac{\cos\gamma - \mu_{kd}\sin\gamma}{\sin\gamma + \mu_{kd}\cos\gamma} + \frac{\cos\phi + \mu_{kb}\sin\phi}{\sin\phi - \mu_{kb}\cos\phi}k_{bz} - Bk_{dz} \tag{3.127}$$

and

$$m_{dzb2} = (m_d B + m_b)\frac{\cos\gamma - \mu_{kd}\sin\gamma}{\sin\gamma + \mu_{kd}\cos\gamma} + m_b\frac{\cos\phi + \mu_{kb}\sin\phi}{\sin\phi - \mu_{kb}\cos\phi} - Am_d. \tag{3.128}$$

Case 3. The friction angles $\theta_1 = \theta_2 = 0$ or π.

In this case, the frequencies of the wedge and the bolster are determined by the formula (3.121).

Case 4. The friction angles are in the ranges (0, $\pi/2$), ($\pi/2$, π), (π, $3\pi/2$), ($3\pi/2$, 2π).

This is a general case, where the three equations of motion are dynamically coupled. The frequencies of the responses of the system will be distributed in a certain range. For the vertical response of the bolster, the frequency ω_{zb} is in the range $\omega_{zbs} < \omega_{zb} < \omega_{zb1}$.

According to the above analysis, the natural frequencies of the wedge and the bolster are influenced by the friction direction angles and friction coefficients. In some special cases, they can be calculated and the results are shown in Table 3.2. Figure 3.11 shows the response to an external force only in the vertical direction. Figure 3.12 shows the response to external forces both in the lateral and vertical directions. We find that the frequency response of the bolster is chaotic in nature[True, 1999-2002].

If the amplitude of the exciting force on the bolster in the vertical direction is smaller than 1800N, then there is no resonant response because the dry friction will damp out the vibration. The model shows that the dynamical system is a system of nonlinear Differential-Algebraic Equations characterized by discontinuous and multi-valued factors. The simulation results provide some information for us to understand the dynamical performances of wedge dampers.

Table 3.2: *Frequencies of the system*

$m_d(kg)$	$m_b(kg)$	μ_{kd}	μ_{kb}	$\theta_{1,2}$	$\omega_{yd}(Hz)$	$\omega_{yb}(Hz)$	$\omega_{zb}(Hz)$
8	1906	0	0	—	50.33	5.03	6.87
8	1906	0.3	0.35	$\pi/2$	50.33	5.03	7.32
8	1906	0.3	0.35	$3\pi/2$	50.33	5.03	6.57

The use of the concept of the friction direction angle makes it possible to calculate the components of the friction force vector in the cases of one-dimensional dry friction and two-dimensional dry friction as well for the stick state as for the slip state. The model also provides a successful application of the concept of friction direction angle.

From the numerical results we find that if the bolster is only forced to move along the lateral direction, not only lateral but also vertical vibrations of a wedge will arise; and more it will induce a vertical vibration of the bolster without any excitation in the vertical direction but the amplitude of the vertical response is small compared with the lateral one.

The stick-slip motion will appear in the motions of both a wedge and a bolster exposed to the lateral and the vertical excitations. The dry friction damping of a bolster is proportional to the normal forces on the wedge and the friction coefficients. The normal forces mainly depend on the mass of the car body including loads and exciting forces. In the case of an empty car, the normal forces on the surfaces of a wedge will become zero when the excitation amplitudes are large or frequency are near or equal to the vertical resonance frequency and the separated motions of the wedge and the bolster will appear.

In this chapter we consider the exciting forces S_{y2} and S_{z2} to be sinusoidal functions. It is not difficult to extend the model to deal with any other form of excitation. With the method in this chapter as a basic start, three-dimensional dry friction vibration in mechanical systems could be studied. Without doubt, how to introduce the model into the complete three-piece-freight-car remains a great challenge. We will discuss it in the following chapters.

The dynamical performance of the wedge dampers exposed to large and small excitations have been analyzed. For small amplitude excitations the motions of the wedge and the bolster are coupled. For certain large amplitudes of the exciting force or for excitation frequency in the range of the resonant frequency of the system the motions of the wedge and the bolster are separated.

In the case of coupled motion, the friction damping plays an important role to prevent resonant vibration of the bolster in vertical direction when it is exposed to a small amplitude exciting force with arbitrary frequency. If the amplitude of the exciting force becomes sufficiently large the dry friction can damp the level of the response of the system but can not damp out the resonant vibration of the system. The frequency response of the bolster in vertical direction is chaotic in nature.

Chapter 4

Variable degrees of freedom systems with two-dimensional dry friction

In the previous chapter we have found that it is complicated to model the system of the wedge dampers into a mathematical piece-wise continuous system because of the action of dry friction. We will further discuss this phenomenon in this chapter.

Among mechanical systems there exist systems in which the degrees of freedom vary with the different motion states of stick or slip caused by dry friction. It is very important to analyze this kind of system because it is widely used in the three-piece-freight-truck on railroads. Some investigators [Eich, 1998] have focussed on this problem only considering one-dimensional dry friction and alternatively refer it to *structural variant system*[Reithmeier, 1991] or *structure varying system*[Eich, 1998]. In this chapter we will extend the structural variant systems caused by stick-slip motion to two-dimensional dry friction. And more multi-point contact on the same body with two-dimensional dry friction are considered. The concept of *friction direction angle* is used to determine the friction force components both in the stick and slip motion states. The velocity-dependent dry friction coefficient is used. The *switch conditions* to control the motion states of systems and the corresponding acting friction forces are discussed in detail. The algorithm for the Differential-Algebraic-Equations (DAEs) of this kind system will be discussed.

4.1 Introduction

Among mechanical systems there exist some systems of which the degrees of the freedom will vary with the change of the acting dry friction force vector. In some literatures it is referred to as *structure varying system*[Eich,1998] or *structural variant system* [Reithmerier, 1991] where only one-dimensional friction and one contact point are included. In this chapter we will focus our effort on the multi-point contact on one body with two-dimensional dry friction. A typical application can be found in the railway vehicle with three-piece-freight-trucks.

In the investigation on the dynamics of the three-piece-freight-truck the two dimensional dry friction must be taken into account. First on the surfaces of the wedge contacting the side frame and the bolster in the lateral and vertical directions, and second is on the surfaces of the side frame contacting the top surfaces of the two adapters in the longitudinal and lateral directions. The former has been investigated without considering the movement of the side frame in chapter 3. The later differs from the former in that the motions between the frames and adapters are limited in longitudinal and lateral directions without any vertical relative motion. Since the relative velocity between a frame and a wheelset is equal to zero then they will share the same motion both in longitudinal and lateral directions. These structure varying systems caused by stick-slip motion can also be found in many fields of mechanical engineering.

4.2 The motion of a system with one-dimensional dry friction

First let us start with a rather simple varying degrees of freedom system as shown in Figure 4.1. A body on a plate, which is subjected to excitation force F_1. We here only consider the one dimensional dry friction on the contact surface between the bodies m_1 and m_2.

The equations of motion of the system can be written as

$$m_1\ddot{x}_1 = F_1 - F_\mu, \tag{4.1}$$
$$m_2\ddot{x}_2 = F_\mu - F_2. \tag{4.2}$$

If we use the following notation

$$F_\mu = \mu N sign(\dot{x}_1 - \dot{x}_2) \tag{4.3}$$

to define the acting friction force. Here μ is defined by the one of eqns.(1.1)-(1.6). If we then solve the eqns. (4.1) and (4.2) we find that in the stick motion state the friction force will equal zero. That is not true because the acting friction force in that case of the stick motion state is not zero unless $F_1 = F_2 = 0$! As a consequence, the numerical integral error will increase with the increase of $|\mu|$ and the steps increase

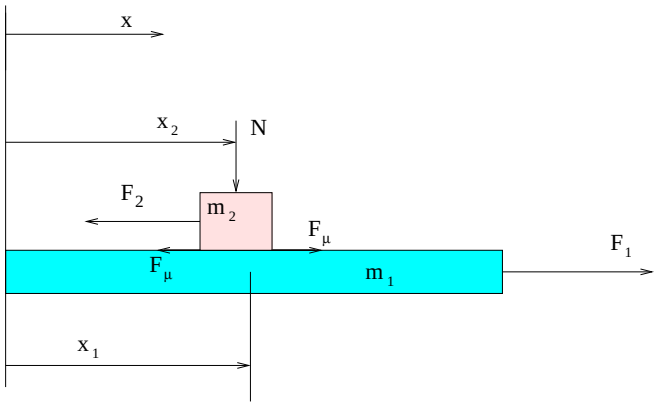

Figure 4.1: *A body on a plate which is subjected to excitation*

very much[Eich, 1998]. This behaviour is characteristic for stiff problems because of the high frequency vibration of the velocity. This way is not suitable for problems of this kind. Let us therefore consider the following method.

In the stick state the condition

$$x_1 - x_2 = 0 \tag{4.4}$$

holds. The derivative of equation (4.4) with respect to time to first and second second orders yields

$$\dot{x}_1 - \dot{x}_2 = 0, \tag{4.5}$$
$$\ddot{x}_1 - \ddot{x}_2 = 0. \tag{4.6}$$

When substitute the eqns. (4.1) and (4.2) into the Eq. (4.6) the switch condition for stick motion is yielded

$$\frac{F_1}{m_1} + \frac{F_2}{m_2} \leq \frac{F_{\mu s}}{m_1} + \frac{F_{\mu s}}{m_2} \tag{4.7}$$

together with condition (4.5). Here $F_{\mu s}$ denotes the static friction force. In this stick motion state the equation of motion of the system becomes

$$(m_1 + m_2)\ddot{x} = F_1 - F_2, \quad \ddot{x}_1 = \ddot{x}_2 = \ddot{x}, \tag{4.8}$$

which means that the degrees of freedom of the system reduces to one.

In which way can the two degrees of freedom of the system described by eqns.(4.1) and (4.2) automatically change into the one degree of freedom described by Eq.(4.8)? It can be easily verified that if the acting friction force for the stick-slip motion is

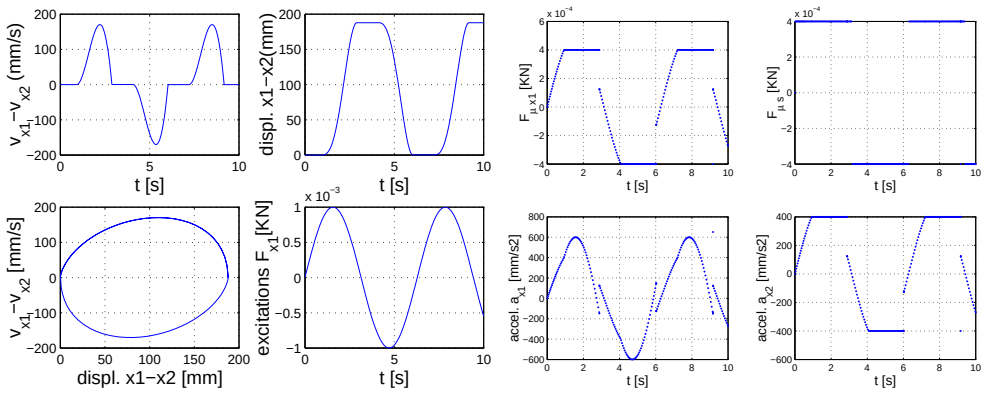

Figure 4.2: *Left: the relative velocity and displacement of the system Right: acting and limit friction forces on the system.* $m_1 = m_2 = 1$, $|N| = 1$, $F_1 = sin(t)$, $P = 0$, $\dot{x}_1(0) = \dot{x}_2(0) = 0$, $\mu_s = \mu_k = 0.4$

correctly determined then the system will vary its degrees of freedom from one to two. That can be done in the way below. From (4.7) set

$$\frac{F_1}{m_1} + \frac{F_2}{m_2} = \frac{F_{\mu t}}{m_1} + \frac{F_{\mu t}}{m_2} \tag{4.9}$$

then the acting friction force to the stick motion state can be determined by

$$F_{\mu t} = \frac{1}{m_1 + m_2}[m_2 F_1 + m_1 F_2]. \tag{4.10}$$

One can substitute the acting friction force obtained by (4.10) into the equations (4.1) and (4.2) and will find that the two eqns.(4.1) and (4.2) will become identical to Eq.(4.8).

If any one of the conditions (4.5) and (4.7) is not fulfilled then the acting friction force is determined by the kinematic friction coefficient multiplied by the normal force with Eq. (4.3). In this case the system returns to a two degrees of freedom system.

The numerical results are shown in Figure 4.2 where the same notation are used as [Eich,1998], and the Eq.(1.1) is used to determine the friction coefficient. The responses are completely identical with the results in[Eich, 1998] and in addition the friction force is also provided. If we use the different values of the static and kinetic friction coefficients of $\mu_s = 0.4$ and $\mu_k = 0.2$, we obtain the results shown in Figure 4.3. The figures show that the acting friction forces for the stick motion are not zero.

The example shows that systems like the above one can be successfully modelled using our definition of the variable degrees of freedom system. Next a more complex structural variant system with two-dimensional dry friction which can be used in the system as shown in Figure 1.3 will be discussed in detail.

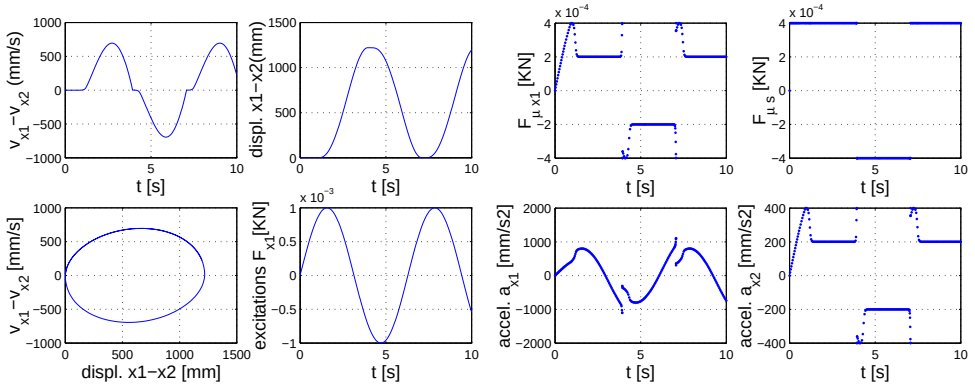

Figure 4.3: *Left: the relative velocity and displacement of the system Right: acting and limit friction forces on the system. The keys are same as Figure 4.2 except* μ_s *= 0.4 and* μ_k *=0.2 with friction function (1.2)*

4.3 The motion of a frame contacting two plates with two-dimensional dry friction

Figure 4.4 shows a mechanical system in which a frame on two plates which are subjected to excitations in both the x and y directions, where the friction forces act on the surfaces of the frame contacting two plates. The contacts between the plates and the ground are assumed completely smooth without any friction and the distance a as shown in Figure 4.4 is assumed as a constant without any change with the motion of the system.

$$m_1\ddot{x}_1 = F_{x1} - F_{kx1} - F_{x1\mu}, \tag{4.11}$$
$$m_1\ddot{y}_1 = F_{y1} - F_{ky1} - F_{y1\mu}, \tag{4.12}$$

$$m_2\ddot{x}_2 = F_{x2} - F_{kx2} - F_{x2\mu}, \tag{4.13}$$
$$m_2\ddot{y}_2 = F_{y2} - F_{ky2} - F_{y2\mu}, \tag{4.14}$$

$$m_3\ddot{x}_3 = F_{x1\mu} + F_{x2\mu} - F_{kx3} - F_{x3}, \tag{4.15}$$
$$m_3\ddot{y}_3 = F_{y1\mu} + F_{y2\mu} - F_{ky31} - F_{ky32} - F_{y31} - F_{y32}, \tag{4.16}$$
$$I_z\ddot{\psi} = a(F_{y1\mu} - F_{y2\mu}) - a(F_{y31} - F_{y32}) - a(F_{ky31} - F_{ky32}) \tag{4.17}$$

where

$$F_{kxi} = k_{xi}x_i, \quad F_{kyi} = k_{yi}y_i, \quad i = 1, 2, \tag{4.18}$$

$$F_{ky31} = k_{y31}(y_3 + a\psi), \quad F_{ky32} = k_{y32}(y_3 - a\psi). \tag{4.19}$$

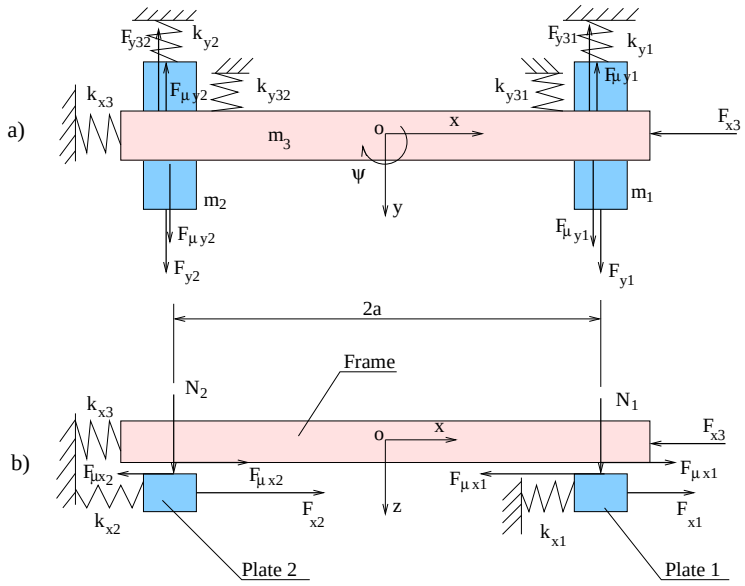

Figure 4.4: *A frame on two plates with two dimensional dry friction. a = 1 m.*

and a denotes the distance from the mass center of the frame to the frame/plate contact point.

4.3.1 The slip motion of the system

In the phase of the slip motion of the system the friction forces on the two contact surfaces can be determined by the method described in chapter 2 and [Xia, 2002].

$$\left.\begin{array}{l} F_{xi\mu} = N_i\mu\cos\theta_i \\ F_{yi\mu} = N_i\mu\sin\theta_i \end{array}\right\}, \quad (V_{xi3} \vee V_{yi3} \neq 0) \quad | \quad (V_{xi3} \wedge V_{yi3} = 0, \\ |F_{inxi}| \geq |F_{xi\mu s}|, |F_{inyi}| \geq |F_{yi\mu s}|), \tag{4.20}$$

$$\left.\begin{array}{l} F_{xi\mu} = F_{inxi} \\ F_{yi\mu} = F_{inyi} \end{array}\right\}, \quad (V_{xi3} \wedge V_{xi3} = 0, |F_{inxi}| < |F_{xi\mu s}|, |F_{inyi}| < |F_{yi\mu s}|) \tag{4.21}$$

where $i = 1, 2$; N_i stands for the normal force on the contact surfaces between frame and plate 1, 2 respectively; the friction direction angle θ_i is defined by

$$\theta_i = \left\{\begin{array}{ll} \chi(V_{xi3}, V_{yi3}), & (V_{xi3} \vee V_{yi3} \neq 0) \\ \psi(F_{inxi}, F_{inyi}), & (V_{xi3} \wedge V_{yi3} = 0, F_{inxi} \vee F_{inyi} \neq 0) \\ \emptyset, & (V_{xi3} \wedge V_{yi3} \wedge F_{inxi} \wedge F_{inyi} = 0) \end{array}\right. \tag{4.22}$$

where F_{inxi}, F_{inyi} stands for the input forces and $\emptyset$ is the empty set of θ_i. The relative velocities V_{xi3}, V_{yi3} will be determined in the next section 4.3.2.

Obviously the independent degrees of freedom of the system are seven for the slip motion state.

The static friction forces in the two orthogonal directions in the above formulae (4.20)-(4.21) can be determined by

$$\left.\begin{array}{l} F_{xi\mu s} = \Re(\theta_i) N_i \mu_s \cos\theta_i \\ F_{yi\mu s} = \Re(\theta_i) N_i \mu_s \sin\theta_i \end{array}\right\}, \quad i = 1, 2 \tag{4.23}$$

where $\Re(\theta_i)$ is defined by (2.18).

4.3.2 The stick motion of the system

First the switch conditions for the stick motion of the system will be derived and then corresponding acting friction forces be determined. It is known that in the stick motion state between the frame and the two plates the kinematic constraints

$$x_1 = x_3, \quad x_2 = x_3, \quad y_1 = y_3 + a\psi, \quad y_2 = y_3 - a\psi \tag{4.24}$$

hold at same time. If any one of the constraints is broken then the slip motion on the corresponding contact surface will immediately start.

It is also known that in the case of two-dimensional friction if the motion in one direction is slip motion then the state in the orthogonal direction must be a slip state because slip in any direction means that the corresponding relative velocity is different from zero. Similarly if the motion in the x direction is stick then the motion is stick too in the y direction, and vice versa.

Taking the second derivative of the constraints (4.24) with respect to time and combining the result with the eqns. (4.11)-(4.19) the switch conditions for the stick motion can be derived as following

From $\ddot{x}_1 = \ddot{x}_3$ and $\ddot{x}_2 = \ddot{x}_3$ we get

$$|\frac{F_{x1}}{m_1} - \frac{F_{kx1}}{m_1} + \frac{F_{x3}}{m_3} + \frac{F_{kx3}}{m_3}| \leq |F_{x1\mu s}(\frac{1}{m_1} + \frac{1}{m_3}) + \frac{F_{x2\mu s}}{m_3}| \tag{4.25}$$

$$|\frac{F_{x2}}{m_2} - \frac{F_{kx2}}{m_2} + \frac{F_{x3}}{m_3} + \frac{F_{kx3}}{m_3}| \leq |F_{x2\mu s}(\frac{1}{m_2} + \frac{1}{m_3}) + \frac{F_{x1\mu s}}{m_3}| \tag{4.26}$$

and from $\ddot{y}_1 = \ddot{y}_3 + a\ddot{\psi}$ and $\ddot{y}_2 = \ddot{y}_3 - a\ddot{\psi}$ other two relations are produced

$$\begin{aligned} |\frac{1}{m_1}(F_{y1} - F_{ky1}) + \frac{1}{m_3}(F_{ky31} + F_{ky32} + F_{y31} + F_{y32}) + \\ \frac{a^2}{I_z}(F_{y31} - F_{y32} + F_{ky31} - F_{ky32})| \leq \\ |\frac{F_{y1\mu s}}{m_1} + \frac{1}{m_3}(F_{y1\mu s} + F_{y2\mu s}) + \frac{a^2}{I_z}(F_{y1\mu s} - F_{y2\mu s})| \end{aligned} \tag{4.27}$$

and

$$|\frac{1}{m_2}(F_{y2}-F_{ky2})+\frac{1}{m_3}(F_{ky31}+F_{ky32}+F_{y31}+F_{y32})- \frac{a^2}{I_z}(F_{y31}-F_{y32}+F_{ky31}-F_{ky32})|\leq |\frac{F_{y2\mu s}}{m_2}+\frac{1}{m_3}(F_{y1\mu s}+F_{y2\mu s})-\frac{a^2}{I_z}(F_{y1\mu s}-F_{y2\mu s})| \tag{4.28}$$

with the kinematic conditions

$$V_{x13}=\dot{x}_1-\dot{x}_3=0,\quad V_{y13}=\dot{y}_1-\dot{y}_3-a\dot{\psi}=0, \tag{4.29}$$

$$V_{x23}=\dot{x}_2-\dot{x}_3=0,\quad V_{y23}=\dot{y}_2-\dot{y}_3+a\dot{\psi}=0. \tag{4.30}$$

The above conditions (4.25)-(4.30) are called the *switch conditions*. If all the conditions are fulfilled at same time, then the degrees of freedom of the system become three. If any one condition of the four conditions (4.25)-(4.28) or any one of the kinematic constraint (4.29) or (4.30) is broken then the motion between the frame and the plate 1 or 2 is slip motion. In that case the independent degrees of freedom of the system becomes five.

In the above switch conditions, $F_{x1\mu s}, F_{x2\mu s}, F_{y1\mu s}, F_{y2\mu s}$ denote the components of the static friction force vectors on contact the surfaces of the frame and the two plates in the x and y directions. They are determined by the normal force, static friction coefficient and friction direction angles.

We now consider three cases:

Case 1, stick everywhere. From eqns.(4.25)-(4.28) the acting friction forces, $F_{x1\mu}$, $F_{x2\mu}$, $F_{y1\mu}$, $F_{y2\mu}$ for the stick motion of the system, can be determined by solving the following equations

$$\begin{bmatrix} e_{11} & e_{12} & 0 & 0 \\ e_{21} & e_{22} & 0 & 0 \\ 0 & 0 & e_{33} & e_{34} \\ 0 & 0 & e_{43} & e_{44} \end{bmatrix} \begin{bmatrix} F_{x1\mu} \\ F_{x2\mu} \\ F_{y1\mu} \\ F_{y2\mu} \end{bmatrix} = \begin{bmatrix} F_{inx1} \\ F_{inx2} \\ F_{iny1} \\ F_{iny2} \end{bmatrix}, \quad \begin{array}{l} V_{x13}\wedge V_{y13}\wedge V_{x23}\wedge V_{y23}=0, \\ (F_{xi\mu}\leq F_{xi\mu s})\wedge \\ (F_{yi\mu}\leq F_{yi\mu s}),(i=1,2) \end{array} \tag{4.31}$$

where

$$e_{11}=\frac{1}{m_1}+\frac{1}{m_3},\quad e_{12}=\frac{1}{m_3},$$

$$e_{21}=\frac{1}{m_3},\quad e_{22}=\frac{1}{m_2}+\frac{1}{m_3},$$

$$e_{33}=\frac{1}{m_1}+\frac{1}{m_3}+\frac{a^2}{I_z},\quad e_{34}=\frac{1}{m_3}-\frac{a^2}{I_z},$$

$$e_{43} = \frac{1}{m_3} - \frac{a^2}{I_z}, \quad e_{44} = \frac{1}{m_2} + \frac{1}{m_3} + \frac{a^2}{I_z}$$

$$F_{inx1} = \frac{F_{x1}}{m_1} - \frac{F_{kx1}}{m_1} + \frac{F_{x3}}{m_3} + \frac{F_{kx3}}{m_3},$$

$$F_{inx2} = \frac{F_{x2}}{m_2} - \frac{F_{kx2}}{m_2} + \frac{F_{x3}}{m_3} + \frac{F_{kx3}}{m_3},$$

$$F_{iny1} = \frac{F_{y1} - F_{ky1}}{m_1} + \frac{F_{ky31} + F_{ky32} + F_{y31} + F_{y32}}{m_3} + \frac{a^2(F_{y31} - F_{y32} + F_{ky31} + F_{ky32})}{I_z},$$

$$F_{iny2} = \frac{F_{y2} - F_{ky2}}{m_2} + \frac{F_{ky31} + F_{ky32} + F_{y31} + F_{y32}}{m_3} - \frac{a^2(F_{y31} - F_{y32} + F_{ky31} - F_{ky32})}{I_z}.$$

Case 2: Stick between the frame and the plate 1

$$\begin{bmatrix} e_{11} & 0 \\ 0 & e_{33} \end{bmatrix} \begin{bmatrix} F_{x1\mu} \\ F_{y1\mu} \end{bmatrix} = \begin{bmatrix} F_{inx1} - \frac{F_{x2\mu}}{m_3} \\ F_{iny1} - \frac{F_{y2\mu}}{m_3} + \frac{a^2 F_{y2\mu}}{I_z} \end{bmatrix}, \begin{array}{l} (V_{x13} = 0) \wedge (V_{y13} = 0) \wedge \\ (V_{x23} \neq 0) \vee (V_{y23} \neq 0), \\ (F_{x1\mu} \leq F_{x1\mu s}) \wedge \\ (F_{y1\mu} \leq F_{y1\mu s}) \end{array} \tag{4.32}$$

with

$$F_{x2\mu} = N_2\mu(V_2)\cos\theta_2, \quad F_{y2\mu} = N_2\mu(V_2)\sin\theta_2 \tag{4.33}$$

and case 3: Stick between the frame and the plate 2

$$\begin{bmatrix} e_{21} & 0 \\ 0 & e_{43} \end{bmatrix} \begin{bmatrix} F_{x2\mu} \\ F_{y2\mu} \end{bmatrix} = \begin{bmatrix} F_{inx2} - \frac{F_{x1\mu}}{m_3} \\ F_{iny2} - \frac{F_{y1\mu}}{m_3} + \frac{a^2 F_{y1\mu}}{I_z} \end{bmatrix}, \begin{array}{l} (V_{x13} \neq 0) \vee (V_{y13} \neq 0) \wedge \\ (V_{x23} = 0) \wedge (V_{y23} = 0), \\ (F_{x2\mu} \leq F_{x2\mu s}) \wedge \\ (F_{y2\mu} \leq F_{y2\mu s}) \end{array} \tag{4.34}$$

with

$$F_{x1\mu} = N_1\mu(V_1)\cos\theta_1, \quad F_{y1\mu} = N_1\mu(V_1)\sin\theta_1 \tag{4.35}$$

where

$$V_i = \sqrt{V_{xi3}^2 + V_{yi3}^2}, \quad i = 1, 2. \tag{4.36}$$

In the above two cases the degrees of freedom are five. In order to calculate the friction direction angles, the input forces, F_{inxi}, F_{inyi} in the stick motion state are required. Actually they are equal to the acting friction forces but in opposite directions. With known input forces and known relative velocities the friction direction angles can now be determined both in the stick and slip motion states.

After the determination of the acting friction forces both for the stick and slip motion states the discontinuous system can be transformed into a piece-wise differentiable system. From a mathematical point of view general numerical integration schemes can be used for the dynamical system.

4.4 Numerical simulation

4.4.1 Numerical method

For the slip motion of the system the equation of motion of the system can be written in the first order ordinary differential equation in the general form as

$$\dot{\mathbf{q}} = \mathbf{f}(\mathbf{q}, \mathbf{z}), \tag{4.37}$$

$$\mathbf{z} = \mathbf{Const}. \tag{4.38}$$

where

$$q = [x_1 \quad y_1 \quad x_2 \quad y_2 \quad \psi \quad \dot{x}_1 \quad \dot{y}_1 \quad \dot{x}_2 \quad \dot{y}_2 \quad \dot{\psi}]^T \tag{4.39}$$

and $\mathbf{z}$ is related to the kinematic friction forces. When the motion of the system goes into stick motion, the independent degrees of freedom of the system is less than the degrees of freedom of the system with slip motion. In this case some kinematic constraints must be added. From a mathematical point of view, the ODEs system now becomes a DAEs system. In general form the DAEs can be written as

$$\dot{\mathbf{q}} = \mathbf{f}(\mathbf{q}, \mathbf{z}) \tag{4.40}$$

$$\mathbf{0} = \mathbf{g}(\mathbf{q}, \mathbf{z}) \tag{4.41}$$

where $\mathbf{z}$ is now a variable vector and is related to the acting friction forces.

In our system the constraint equation (4.24) is actually related only to the position variables

$$\mathbf{0} = \mathbf{g}(\mathbf{q}) \tag{4.42}$$

The system is called a DAE system with index-3 [Hairer, 1991][Brenan, 1989][Bendtsen, 1999]. In order to change the problem into an index-1 problem, we need to differentiate the algebraic equation(4.24) twice with respect to time as we have done in the section 4.3.1. Then the variable vector $\mathbf{z}$ can be found from

$$\mathbf{Az} = \mathbf{F} \tag{4.43}$$

where the entries of the matrix **A** and the elements of the vector **F** are determined by the eqns. (4.31)-(4.35). The DAEs with index-1 problem can be numerically solved with Runge-Kutta scheme but other solvers apply as well[Bendtsen, 1999]. The flow of the algorithm is shown in Figure 4.5.

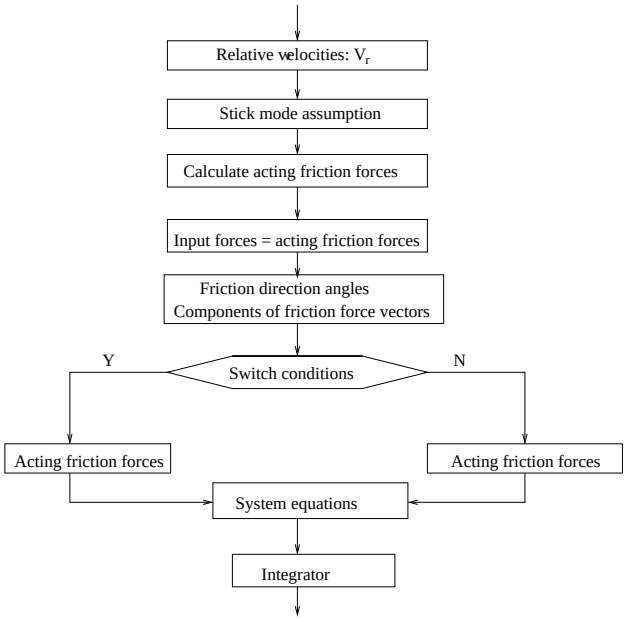

Figure 4.5: *The flow of the algorithm for the variable degrees of freedom system*

At the start of the algorithm it is recommendable to assume the motion of the system to be a stick motion.

4.4.2 Numerical studies

For the numerical studies the harmonic excitations are used as

$$F_{xi} = A_{xi} sin(q_{xi} t), \quad F_{yi} = A_{yi} sin(q_{yi} t), \quad i = 1, 2, 3, \tag{4.44}$$

$$F_{y3i} = A_{y3i} sin(q_{y3i} t), \quad i = 1, 2 \tag{4.45}$$

where $A_{x..}$ denotes the amplitude of the excitation and $q_{x..}$ stands for the frequency of the excitation. The gravity acceleration in the numerical studies here is set to be $1m/s^2$. The parameters of the system for the case studies are shown in Table 4.1.

Case 1

The left four curves of the Figure 4.6 show the relative motions between the plate 1

Table 4.1: *The parameters of the system for the case studies*

Parameter	Unit	Case 1	Case 2	Case 3	Case 4	Case 5	Case 6
A_{x1}	N	0.4	0.4	0.4	0.4-0.5	0.6	0.3
A_{y1}	N	0	0	0.4	0.4-0.5	0.45	0.3
A_{x2}	N	0	0.2	0	0.4-0.5	0.45	0.2
A_{y2}	N	0	0	0	0.4-0.5	0.45	-0.2
A_{x3}	N	0	0	0	0	0	0.5
A_{y31}	N	0	0	0	0	0	0.2
A_{y32}	N	0	0	0	0	0	-0.2
q_{x1}	rad/s	1	1	1	1	1	2
q_{y1}	rad/s	0	0	1	1	1	2
q_{x2}	rad/s	0	1	0	1	1	2
q_{y2}	rad/s	0	0	0	1	1	2
q_{x3}	rad/s	0	0	0	0	0	1
q_{y31}	rad/s	0	0	0	0	0	1
q_{y32}	rad/s	0	0	0	0	0	1
N_1	N	0.5	0.5	0.5	0.5	0.5	0.5
N_2	N	0.5	0.5	0.5	0.5	0.5	0.5
k_{x1}	rad/s	0	0	0	0	0	1
k_{y1}	rad/s	0	0	0	0	0	1
k_{x2}	rad/s	0	0	0	0	0	1
k_{y2}	rad/s	0	0	0	0	0	1
k_{x3}	rad/s	0	0	0	0	0	1
k_{y31}	rad/s	0	0	0	0	0	1
k_{y32}	rad/s	0	0	0	0	0	1
m_1	Kg	1	1	1	1	1	1
m_2	Kg	1	1	1	1	1	1
m_3	Kg	1	1	1	1	1	1
μ_k		0.3	0.3	0.3	0.3	0.3	0.3
μ_s		0.4	0.4	0.4	0.4	0.4	0.4
Friction function		(1.1)	(1.1) (1.3)	(1.3)	(1.3)	(1.3)	(1.3)

and the frame under the external force only in the x direction, where the difference of the displacements is equal to constant when the stick motions take place. The right four curves of the Figure 4.6 show the relative motions between the plate 2 and the frame in the x-direction. The motion between the plate 2 and the frame are a stick motion because the acting friction force components on the contact surface between the plate 2 and frame are always less than the corresponding static friction force components. Left four curves of Figure 7 show the motion of the plate 2. Right four curves of Figure 4.7 show the friction forces on the two contact surfaces. The modulus of the friction force on the surface between the plate 2 and frame is always equal to the half that of the friction force on the surface between the plate 1 and the frame when the motion between the plate 1 and the frame is in the slip motion state.

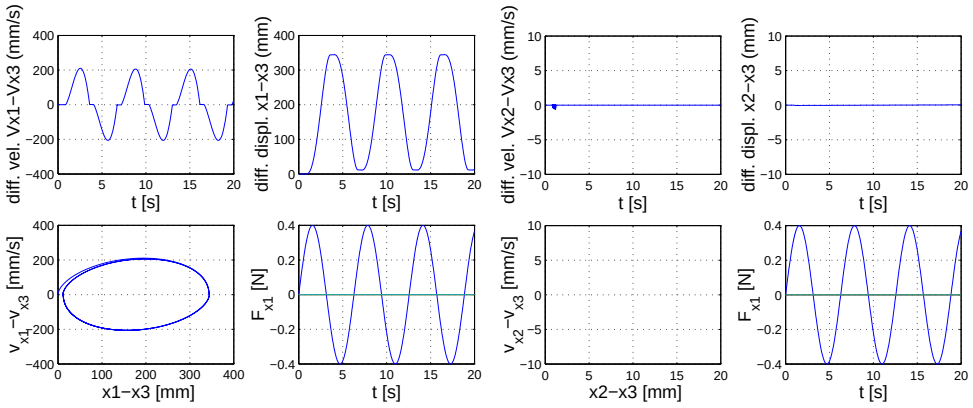

Figure 4.6: *Left: the relative velocity and the relative displacement between the plate 1 and the frame with friction function(1.2). Right: the response of the plate 2.*

Case 2

An interesting phenomenon is that if an external force acts on the plate 1 and only in the x-direction with an amplitude of 0.4 N and a frequency of $1rad/s$ and another external force acts on the plate 2-also in the x-direction-with an amplitude of $0.2N$ and a frequency of $1rad/s$ then all the relative motions are zero. In this case the motion of the system is complete stick motion and the acting friction forces on the surface between the plate 2 and the frame are zero.

Case 3

Next the two-dimensional motions of the system are considered. The parameters of the system for this case are shown in Table 4.1. The results are shown in Figure 4.8. In this case the yaw of the frame is different from zero as shown in Figure 4.9 and the motion between the plate 2 and the frame in the y direction is always stick with the frame because the acting friction force on the contact surface between the frame and plate 2 is always less than the corresponding static friction force. The friction forces are shown in the right four curves of the Figure 4.9.

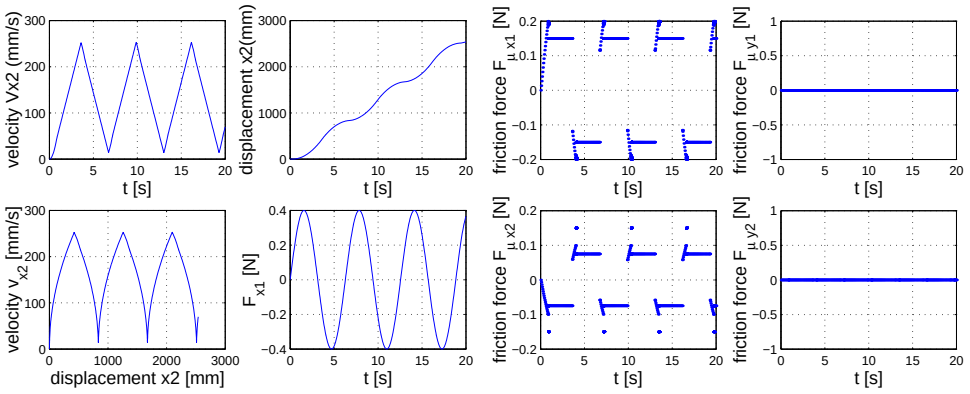

Figure 4.7: *Left: the response of the plate 2 with friction function(1.2). Right: the friction forces.*

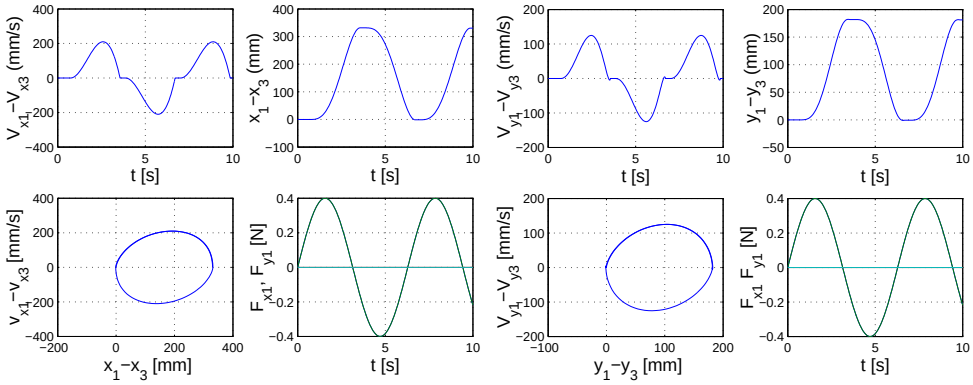

Figure 4.8: *Left: the relative velocity and the relative displacement between the plate 1 and the frame in the x direction with friction function (1.3). Right: the relative velocity and the relative displacement between the plate 1 and the frame in the y direction.*

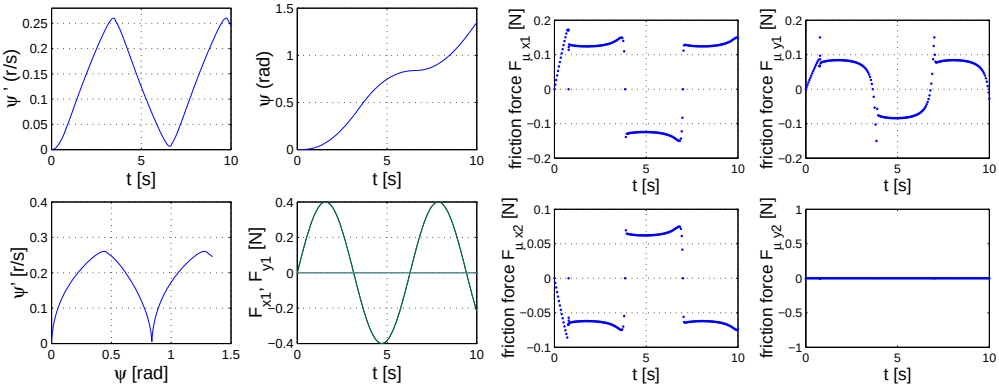

Figure 4.9: *Left: the yaw of the frame with friction function (1.3). Right: the friction forces.*

Case 4

As another example we start with the amplitudes of the external force being 0.4 N as shown in Table 1 on both the plate 1 and plate 2 both in x and y directions. In this case the motion of the system is definitely a stick motion. If the amplitudes of all the external forces are increased at same time then it is found that if the amplitudes are less than 0.42 N then all motions of the system are stick. Figure 4.10 shows the results when the amplitudes of the external forces are $0.5N$. In this case the yaw of the frame is zero as it should be.

Case 5

If the different amplitudes of the excitations on the two plates in the x or y directions are used then the yaw of the frame is obviously different from zero. As an example, we may use the the values of the excitations as shown in Table 1. This example shows that the difference amplitude of the excitations on the plate 1 and plate 2 is only in x direction. But we can find that the yaw of the frame still takes place. The results are shown in Figures 4.11-4.14. The reason that the yaw of the frame is different from zero is caused by the different components of the friction force vectors in the y direction on the two contact surfaces in the stick motion state although they are identical in the slip state.

Case 6

Finally we set the parameters of the system as shown in Table 1, then the resulting motions are shown in Figure 4.15 and Figure 4.16. We find that the distribution of the friction forces on the contact surfaces are complicated in the stick motion of the system. In the slip motion they are not on a circular orbit because the kinetic friction coefficient depends on the relative velocity.

From the above discussion it is known that the system of multi-point contacts on one body with two-dimensional dry friction can be modelled as a structural variant system characterized by the stick and slip motion.

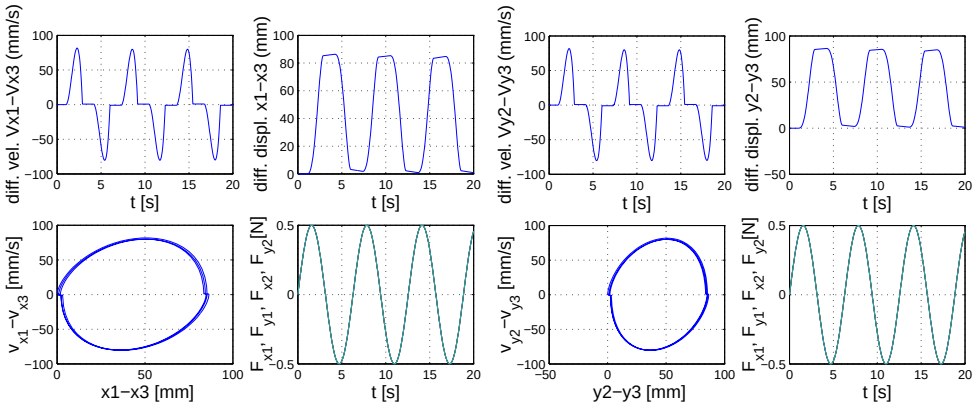

Figure 4.10: *Left: the relative velocity and the relative displacement between the plate 1 and the frame in the x direction with friction function(1.3). Right: the relative velocity and the relative displacement between the plate 2 and the frame in the y direction.*

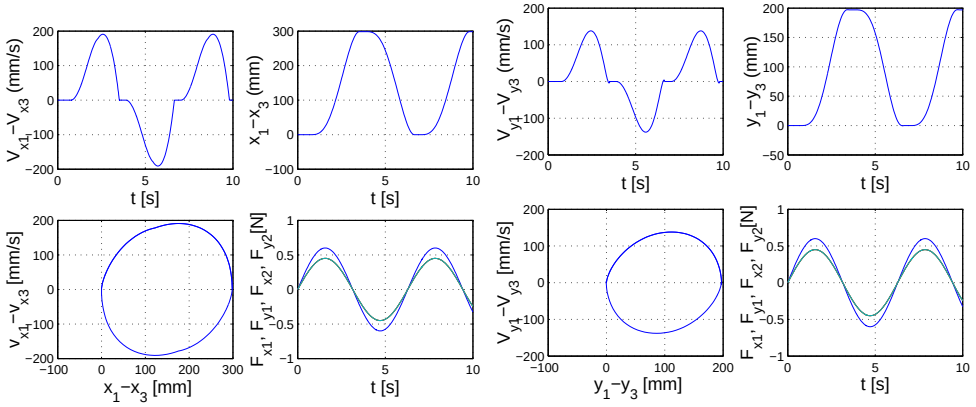

Figure 4.11: *Left: the relative velocity and the relative displacement between the plate 1 and the frame in the x direction with friction function (1.3). Right: the relative velocity and the relative displacement between the plate 1 and the frame in the y direction.*

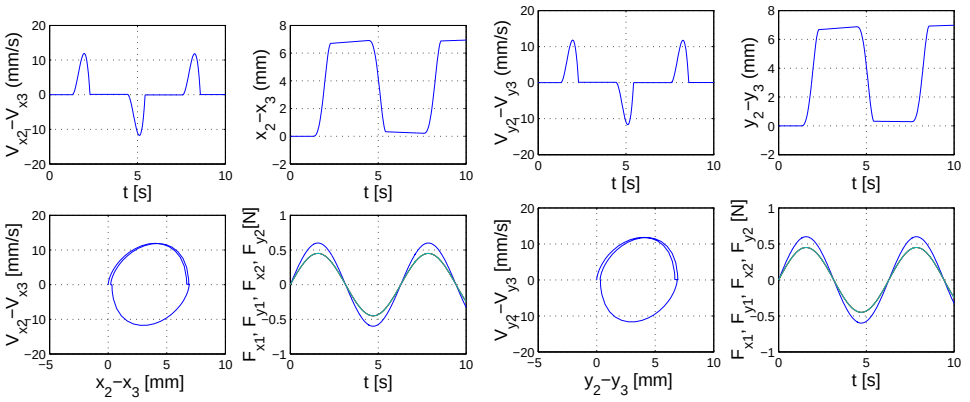

Figure 4.12: *Left: the relative velocity and the relative displacement between the plate 2 and the frame in the x direction with friction function (1.3). Right: the relative velocity and the relative displacement between the plate 2 and the frame in the y direction.*

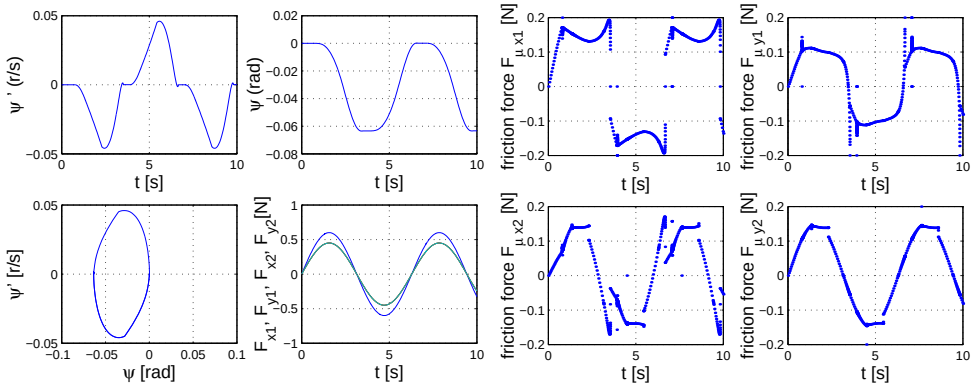

Figure 4.13: *Left: the yaw of the frame with friction function (1.3) Right: the friction forces.*

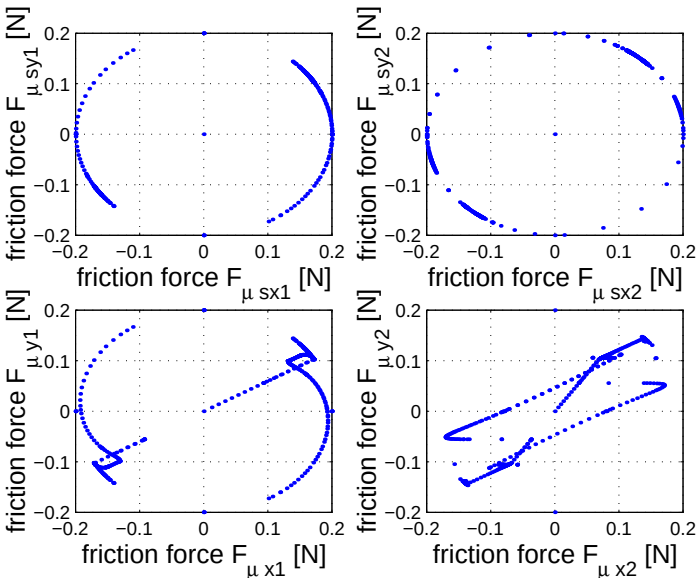

Figure 4.14: *The friction forces with friction function (1.3). Upper subplots: static friction forces; Lower subplots: acting friction forces.*

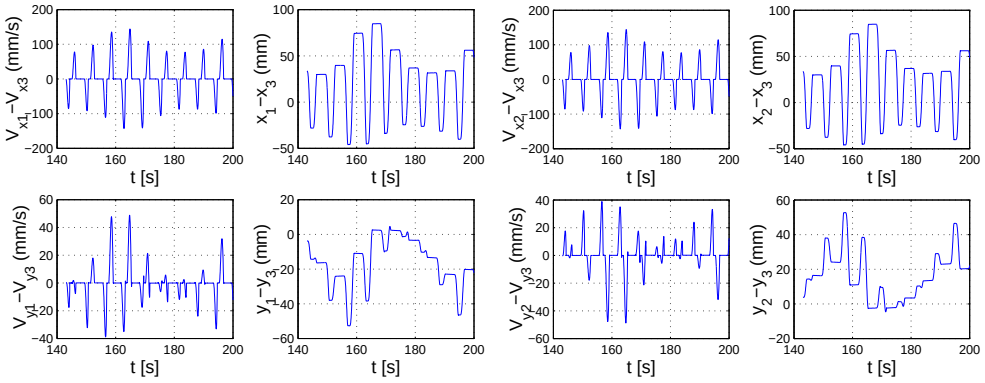

Figure 4.15: *Left: the relative velocity and the relative displacement between the plate 2 and the frame in the x direction with friction function (1.3). Right: the relative velocity and the relative displacement between the plate 2 and the frame in the y direction with friction function (1.3).*

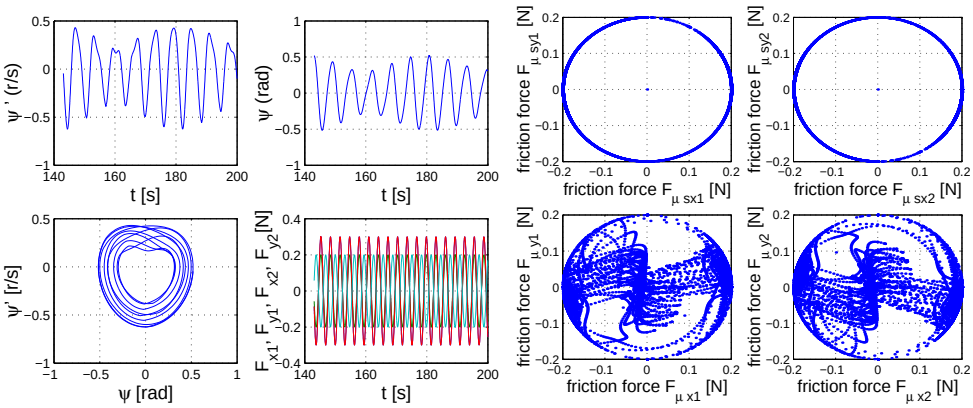

Figure 4.16: *Left: the yaw of the frame with friction function (1.3). Right: the friction forces with friction function (1.3).*

The independent degrees of freedom of the structure varying systems will vary according to the combinations of the stick-slip motions on the two surfaces in contact. The stick-slip motions are determined by the switch conditions and the corresponding acting friction forces.

If the acting friction forces are correctly evaluated with the corresponding switch conditions for the stick-slip motion then the degrees of freedom of the system will vary automatically. In other words, the discontinuous system will automatically becomes a piecewise differentiable system.

Chapter 5

Rolling contact between the wheels and the rails

The wheel and rail meet at a wheel/rail interface where the interaction between the steel wheel and the steel rail generates the necessary conditions for a railway vehicle to run stably on the track but it may also damage the rails and the wheels because of the high contact stresses. The stability of a moving railway vehicle depends on the linear or nonlinear critical operating speed, the lateral dynamic behavior, the adequate guidance and the ability of negotiating a curved track. The damage of the rails and the wheels involves wear of the rails and the wheels, corrugation, fatigue etc. An optimized railway system is one that satisfies high stability requirements and a low damage rate of the rails and the wheels. These aspects must be taken into account in the design of a bogie or a complete railway vehicle.

The contact is often described by as well the kinematical constraints(geometrical contacts) as dynamical constraints(physical contacts). For the kinematical constraints the rigid assumption of the wheelset and rails is usually used[De Pater, 1999, Kik, 1994]. The dynamical constraints based on the rigid assumption is used in the traditional method[De Pater, 1999]. In recent years based on the elastic contact is used[Pascal,1991]. Many investigators precalculate the kinematical constraint parameters and collect them in a table and then the dynamical calculation will use interpolated contact values based on the tabulated ones. We do it differently: The kinematical constraint parameters are evaluated on-line.

5.1 The kinematic constraints between the wheels and the rails

The effect of the kinematic constraints between a wheelset and a track goes back to Stephenson and later Klingel[Klingel,1883] who assumed a conical wheelset, which is roll on knife edge rails. Realistic wheel and rail profiles are often defined by segments of arcs of circles and polynomials. Wickens [Wickens,1965] improved the accuracy of Klingel's analysis for the case where the rail and wheel profiles are assumed to be circular arcs. The solution for the circular arc profiles is normally only valid for small lateral wheelset displacements. In the general case the wheel and rail profiles have other shapes due to wear and may be derived from profile measurements. It is not possible to obtain an analytic solution for the kinematic constraints with arbitrary wheel and rail profiles, so numerical methods are needed.

In the early numerical methods, the geometric contact between the track and the wheelset is considered to be two-dimensional[Cooperrider and Law, 1976], so that the effect of the yaw angle is ignored. More accurate theories for determining the geometric contact in three dimensions have been developed by Heumann [Heumann,1950-1953], De Pater[De Pater,1979, 1988, 1999], Duffek[Duffek,1982] and K. Wang[Wang,1984]. The effect of the track curves of the track in the horizontal and vertical directions has been analyzed and it was shown that the effect can be neglected by F. Xia[Xia, 2000].

The coordinate systems for the description of the wheelset, the rails and the contact geometry are shown in Figure 5.1.

It is necessary to know the geometrical relations between the profiles of the wheel and the rail for the central position of the wheelset, because they are the basic for the determination of the contact parameters. The contact parameters are strongly influenced by the combination of the profiles of the wheel and rail and the dimensions of the wheelset and track. Figure 5.2 shows the relation between the right hand side wheel and rail for the central position of the wheelset.

We can find from Figure 5.2 that the initial contact point (the wheelset in its central position) is characterized by the side gauge of the wheelset, the profiles and the inclination of the rail. In the general case the rolling radius on the initial contact point is not equal to the rolling radius that is measured at the vertical line 70 mm away from the inside gauge. In Europe the side gauge is usually 1360 mm but in China the value is 1353 mm.

The geometrical method first determines the same minimal distances between the two surfaces of the left hand and right hand side wheels and the corresponding rail profiles through adjusting the rolling angle of the wheelset for the given lateral displacement and yaw of the wheelset. After finding the contact point the corresponding geometrical contact parameters can be determined. This method for the two-dimensional contact problem has been used and implemented into a code RSGEO by Kik[Kik, 1994]. For the three-dimensional geometric contact problem, the two dimensional search on the surface of the wheel in the longitudinal and lateral directions are needed, so the computational time is high. This method is impossible to

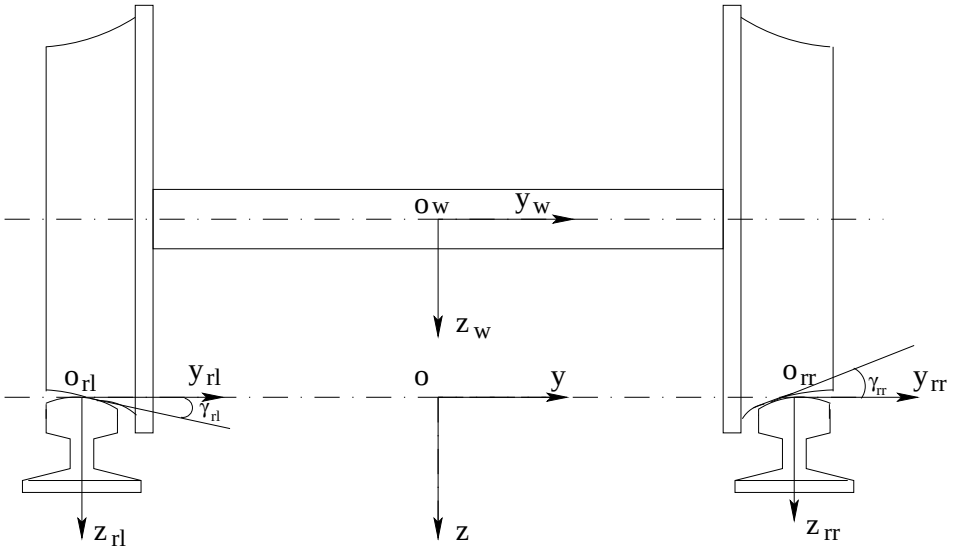

Figure 5.1: *The coordinate systems of the wheelset, track and the local contact points*

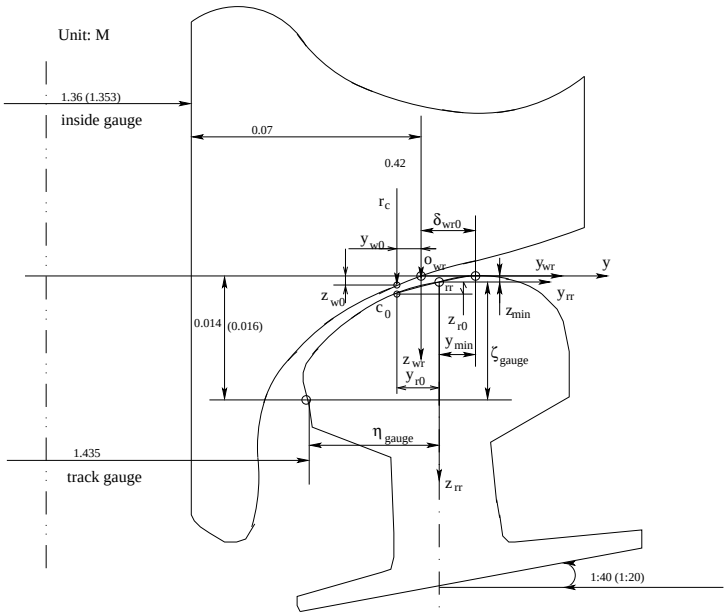

Figure 5.2: *The geometrical relation between a wheel profile and a rail profile*

apply for the on-line evaluation of the kinematic constraint parameters. In practice the pre-calculated parameter data are collected in a table once and for all. Another method replaces the surface of the wheel by the so-called trajectory on the tread of the wheel. The minimal distance comparison is processed between the trajectory and the profile of a rail[K. Wang, 1984], so the spatial curve surface is simplified to a spatial line. In this way the higher calculation efficiency makes it possible to perform the on-line evaluation of the kinematic constraint parameters.

The mathematical method is on a derivation of a set of algebraic equations. The set describes the contact relations for the contact between a wheel and a rail. Then it is solved numerically to get the contact parameters[De Pater, 1995, Xia 2000].

The kinematic constraint parameters enter the simulation of the vehicle dynamics on the track in two different ways. Either a table of the kinematic constraints for the entries of the lateral and yaw is made and then the parameters can be obtained by interpolation for the given lateral and yaw values of the wheelset. It is fast but the accuracy is not high. Another way is the so-called on-line evaluation. With this method the kinematic constraint parameters are calculated implicitly in the dynamical calculation. In this way the results are more accurate and easier to combine with the physical contact calculation.

5.1.1 The profiles of a wheel and a rail

The simplest contact model of rail/wheel contact is to assume the wheel to be cone and the rail to be a knife edge or an arc of a circle. This model can be used to calculate the linear critical speed[Wickens,1965]. The realistic profiles are often defined by segments of arcs of circles and cones. The new wheel and rail profiles are called theoretical profiles. The worn profiles can only bee defined by the measured data.

As well measured as theoretical profiles are used for the purpose of the simulation of the motion of the railway vehicles. For the theoretical profiles, it is easy to get the discrete data. However, for the measured profiles a little care has to be exercised in using a curve fitting method since not only are the smooth profiles needed but also their derivatives up to at least the second.

In general, the profiles of a wheel and a rail can be described by the functions

$$\zeta_r = f(\eta_r), \qquad \zeta_w = f(\eta_w) \tag{5.1}$$

where we introduce two new frames, one is $(C_r, \xi_r, \eta_r, \zeta_r)$. The origin C_r is located on the wheel/rail contact point on the rail for the central position of the wheelset; another is $(C_w, \xi_w, \eta_w, \zeta_w)$ which the origin C_w is on the wheel. The derivatives of the ζ_r and ζ_w with respect to the η_r and η_w respectively are associated with the contact angles γ_r and γ_w, which are defined as the angle between the contact plane at the wheel/rail contact point and the horizontal. They are expressed by:

$$\tan\gamma_r = \frac{d\zeta_r}{d\eta_r} = f'(\eta_r), \qquad \tan\gamma_w = \frac{d\zeta_w}{d\eta_w} = f'(\eta_w). \tag{5.2}$$

The radii of curvatures of the profiles in the contact point are

$$r_{yr} = (\frac{d^2\xi_r}{d\eta_r^2}\cos^3\gamma_r)^{-1}, \qquad r_{yw} = (\frac{d^2\xi_w}{d\eta_w^2}\cos^3\gamma_w)^{-1}. \tag{5.3}$$

The wheel tread profile we use in this thesis is called LM. It is widely used in the three-piece-freight-trucks on the Chinese railways. The profile of the rail is called 60 kg/m which is also the standard one used in China. Figures 5.3 and 5.4 show the theoretical profiles of LM and 60 kg/m. From the measured data of the profiles data-fitting methods are used to obtain the fitted profiles and the corresponding first and second derivatives as well. As formulae (5.2) and (5.3) shows, the first and secondary derivatives are used for the calculation of the contact angles and the curvatures at the contact points.

The B-spline curve fitting method applied by Kik[1994] in the code RSPROF, however the approximations must be done very carefully, especially if a profile is given by measured data[Slivsgaad, 1995].

The piece-wise curve fitting method was suggested by De Pater and implemented by Xia[Xia, 1998] where several polynomial segments which have smooth derivatives up to the fourth are used. The result is sensitive to the numbers of the segments and the flange curvature as well. Anyhow, for the simulation of the dynamics of the vehicles only part of the profiles are needed. From Figures 5.3 and 5.4 we know that the points on the profile of the wheel can be neglected for points less than 30 mm and larger than 120 mm in the lateral coordinate; For the rail profile, the points larger than 20 mm in the vertical coordinate can be neglected. In that way the piece-wise curve fitting method works well.

The measured data of the profile of LM and 60 kg/m were obtained by the tool $MiniProf^{TM}$. The fitted profiles with piece-wise curve fitting are shown in Figures 5.5 and 5.6. We use 8 polynomial segments to fit the profile of the wheel tread. For the profile of the left rail 19 polynomial segments are used.

Figure 5.3 shows the theoretical profile of the wheel LM and its first, secondary derivatives and the curvature. Figure 5.4 shows the theoretical profile of rail 60k/m.

The theoretical profiles are used to investigate the nonlinear characteristics on perfect tangent track. The measured profiles are used to simulate the dynamical responses of the vehicle on tangent track with irregularities.

5.1.2 On-line evaluation of the kinematic constraint parameters

A wheelset has six degrees of freedom, three displacements u_w, v_w, w_w and three rotations ϕ_w, θ_w and ψ_w. When it runs on two rigid rails two constraints are produced. Hence, the position of the wheelset can be described by four of the six coordinates u_w, v_w, w_w, ϕ_w, θ_w and ψ_w and we shall choose w_w and ϕ_w as dependent coordinates, which can be found as functions of v_w and ψ_w but other two independent variables u_w and θ_w have no effect on the dependent variables w_w and ϕ_w.

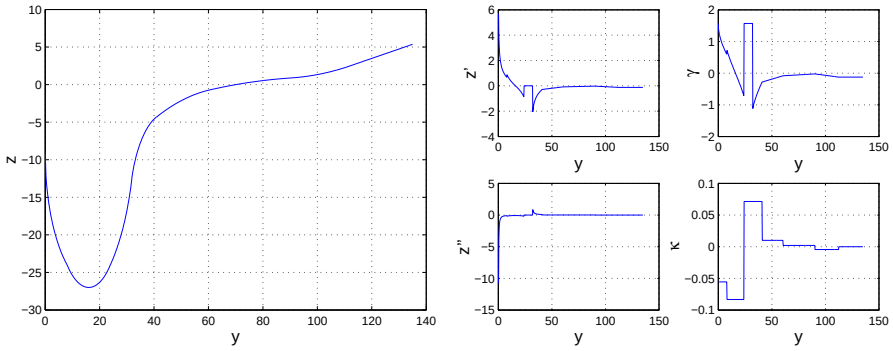

Figure 5.3: *The theoretical profile of wheel LM used in the three-piece-freight truck on Chinese railways*

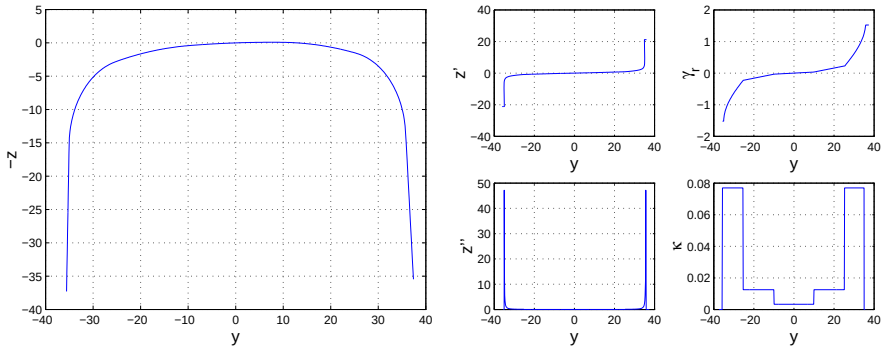

Figure 5.4: *The theoretical profile of rail 60k/m used in the main track in China*

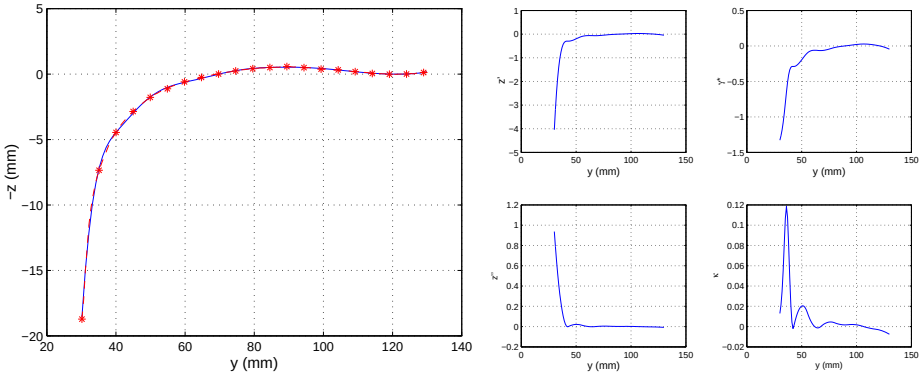

Figure 5.5: *The fitted profile with piece-wise curve fitting method for the measured data of the profile of wheel LM used in the three-piece-freight truck on Chinese railways.*

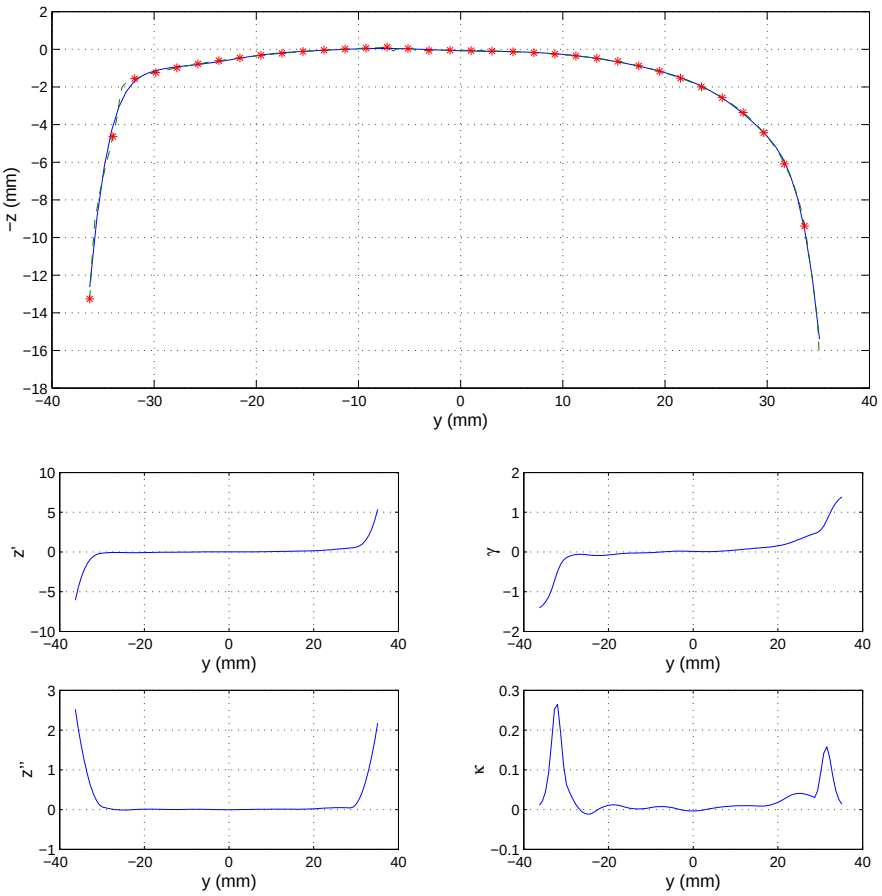

Figure 5.6: *The fitted profile with piece-wise curve fitting method for measured data of the profile of the left hand rail 60 kg/m used in the main track in China*

De Pater developed the mathematical method to determine the kinematic constraint parameters[De Pater 1995-1999]. His first order theory was introduced to get a simple method. By the first order theory, the kinematic constraint parameters of the contact angle, roll angle and the vertical displacement of a wheelset only depend on the lateral displacement of the wheelset, in other words, the effect of the yaw of the wheelset is neglected. G. Yang[Yang, 1993] extended the method to the case where the yaw of the wheelset is considered. F. Xia[Xia, 2000] analyzed a general case where not only the lateral and yaw of the wheelset are included but also the effects of the curvatures of the track in horizontal and vertical directions are considered. The results show that if the yaw is small and the vertical curvature is small then the difference between the exact theory and the first order theory is negligible.

In the case the contacting bodies are assumed to be rigid we use the two contact conditions: (1) the positions of the contact points of the wheel and rail should be identical in space; (2) at the contact point the unit normal vector of the surface coincides with the one of the corresponding wheel surface. Then the first order theory yields simplified kinematic constraint equations[Xia, 2000]:

$$\begin{aligned} & r\phi \mp (\eta_{rj} - \eta_{wj}) = v - v_{rj}, \\ & w \pm b\phi - (\zeta_{rj} - \zeta_{wj}) = w_{rj}, \quad (j = 1, 2), \\ & \pm\phi + \gamma_{rj} - \gamma_{wj} = \pm\phi_{rj} \end{aligned} \tag{5.4}$$

and

$$\xi_{rj} = u \mp b_j\psi, \tag{5.5}$$

$$\xi_{wj} = \pm r\psi \tan\gamma_{rj} \tag{5.6}$$

where r denotes the rolling radius; ϕ, ψ are the roll and yaw angles of the wheelset respectively; u, v, w denote the longitudinal, lateral and vertical displacements of the wheelset respectively; b is the half gauge; b_j denotes the distance from the mass center of the wheelset to the wheel/rail contact points. v_r, w_r, ϕ_r are the parameters that describe the irregularities of the track. ξ_r, ξ_w denote the longitudinal displacements of the contact point on the wheel tread and the rail. The index $j = 1$ denotes the right rail and $j = 2$ denotes the left rail; for $j = 1$ we use the upper sign of the $\mp$ or $\pm$ and for $j = 2$ we use the lower sign.

To solve the above nonlinear algebraic equations the Newton-Raphson's method is used but special attention should given to the points where double-point contact occur. In that case the prediction-correction method may provide a way to overcome the numerical problem[Seydel, 1988, Xia,1996].

Now we introduce another widely accepted geometrical method to determine the kinematical constraint parameters. For the reason of simplicity, the origin o of the reference coordinate system (o, x, y, z) is selected on the mass center of the wheelset. The lateral displacement and the yaw and roll rotations of the wheelset are v_w, ψ_w and ϕ_w respectively.

C denotes the contact point, C_0 is the lowest point of the rolling circle and O_1O_r denotes the common normal line through the point C(see Figure 5.7). For

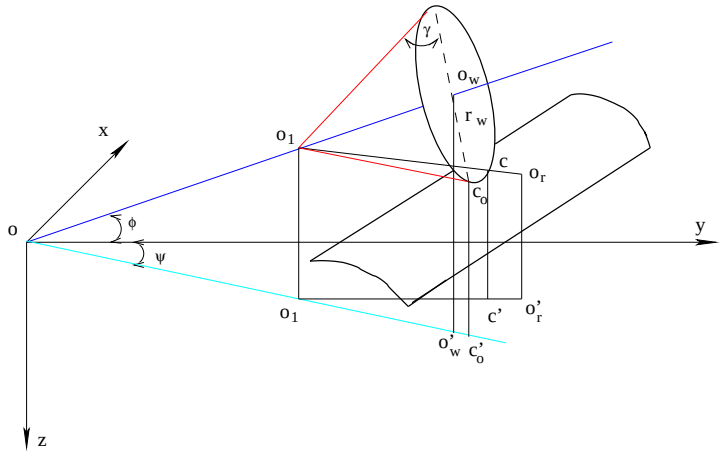

Figure 5.7: *The three-dimensional relation between a wheel and rail*

the known lateral displacement, the known yaw of the wheelset and the known track irregularities, the contact trajectory on the tread of the right wheel can be determined by the following formulae[Wang, 1984]

$$\begin{aligned} x &= x_{ow} + l_x r_w tg\gamma, \\ y &= y_{ow} - \frac{r_w}{1-l_x^2}(l_x^2 l_y tg\gamma + l_z m) + v_w, \\ z &= z_{ow} - \frac{r_w}{1-l_x^2}(l_x^2 l_z tg\gamma - l_y m) \end{aligned} \tag{5.7}$$

where $\gamma = \gamma_w - \phi_w$ denotes the contact angle and

$$l_x = -cos\phi_w sin\psi_w,$$

$$l_y = cos\phi_w cos\psi_w, \tag{5.8}$$

$$l_z = -sin\phi_w \tag{5.9}$$

denote the direction of the center line of the wheelset, and

$$x_{ow} = b_{wr} l_x,$$

$$y_{ow} = b_{wr} l_y, \tag{5.10}$$

$$z_{ow} = b_{wr} l_z \tag{5.11}$$

denote the coordinates of the center of the rolling circle in the reference coordinates (o, x, y, z) and b_{wr} is the distance between the mass center of the wheelset and the contact point. The parameter m is

$$m = \sqrt{1 - l_x(1 + tg^2\gamma)}. \tag{5.12}$$

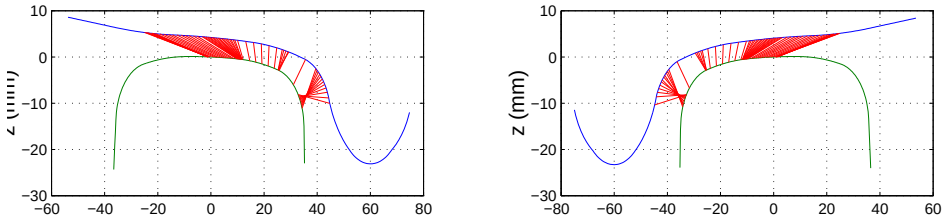

Figure 5.8: *The possible contact points between the theoretical wheel and rail profiles LM/60kg/m with inclination 1/40*

The trajectory for the left wheel/rail contact can be derived in the same way. After obtaining the trajectory then the contact points are determined by comparing the minimal distances between the contact trajectory and the profiles of two rails.

The effect of the four general irregularities in tangent track: The variation of the track gauge and the cross-level are incorporated in the determination of the contact position, and the lateral and vertical alignments are incorporated in the motion of the track reference frames.

5.1.3 Some results and a discussion of the contact point calculations

The computer program WRKIN has been developed to perform the calculations according to the theory outlined in section 5.1.2. The program is used to calculate the kinematic constraint parameters for the three dimensional wheel/rail contact and the dimensions of the contact area and the penetration between the wheel and the rail for the 1 N normal load. For the investigation of the kinematical constraints the profile of the LM wheel used in the three-piece-freight-truck in China and the profile of the rail 60kg/m also used in China are taken. The inclination is 1/20(40). The possible contact points between the wheel and the rail in dependence on the displacement of the wheelset indicate the domain of wear on the wheel and rail profiles. The distribution of the contact points not only depends on the combinations of the profiles of the wheel and the rail but also depends on the side gauge of the wheelset and the inclination of the rail. Figures 5.8 and 5.9 show the possible contact points for the combinations of the theoretical profiles of the wheel LM and the rail 60 kg/m and the combinations of the theoretical profiles of the wheel DSB97(Danish profile) and the rail UIC60, respectively. We have found that the contact interval of the combinations of the LM/60kg/m is less than the combinations of the DSB97/UIC60 for the rail inclination 1/40. Figure 5.10 shows the penetration of the wheel LM into the rail $60kg/m$ under $1N$ normal load. Figure 5.8 shows the possible contact points between the wheel and the rail in dependence on the lateral displacement of the wheelset. In order to display the effect of both the lateral displacement and the yaw of the wheelset

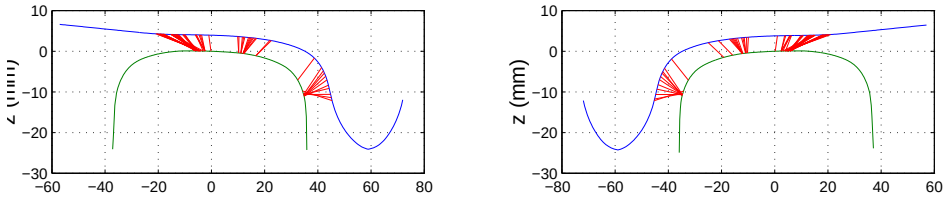

Figure 5.9: *The possible contact points between the theoretical profiles of the wheel DSB97 and the rail UIC60 with inclination 1/40*

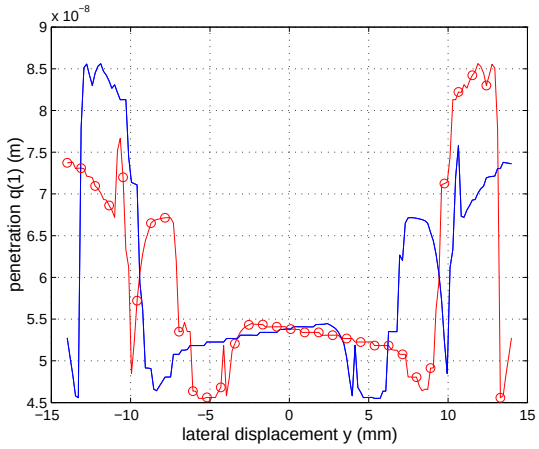

Figure 5.10: *The penetration* $q(1)$ *under the* $1N$ *normal force. The solid line denotes the right wheel/rail penetration and the solid line with 'o' on it denotes the left wheel/rail penetration.*

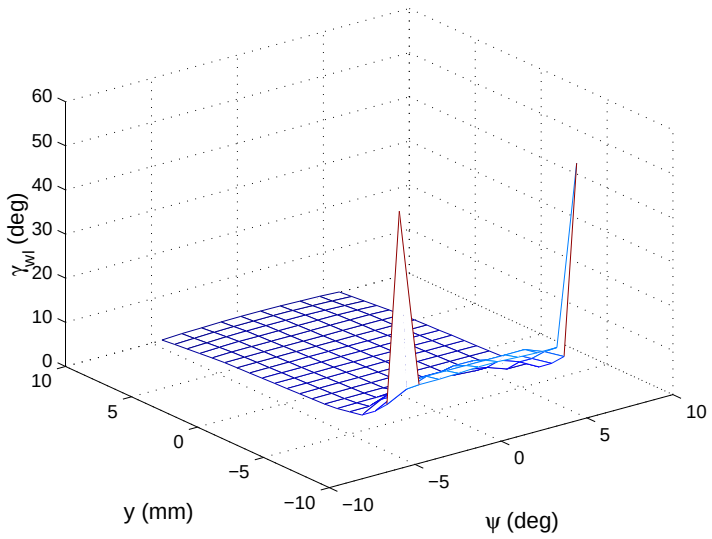

Figure 5.11: *The contact angle on the left side hand wheel*

on the kinematical constraint parameters the contact angles on the contact points, the roll angle of the wheelset and the vertical displacement of the wheelset are shown in the Figures 5.11, 5.12, 5.13 and 5.14.

Figures 5.15 and 5.16 show the effect of both the lateral displacement and the yaw of the wheelset on the semiaxes, a and b of the contact ellipse according to Hertz's theory and Figure 5.17 then shows the penetration influenced by both the lateral displacement and the yaw of the wheelset.

5.2 Dynamical constraints between a wheel and a rail

5.2.1 Determination of the normal loads

The normal loads in the contact area make the wheel/rail penetrate each other to form the contact patch. The dimension of the patch is used to determine the tangential forces between the wheel and the rail. The determination of the normal loads is not difficult if the dynamical contribution of the wheelset be left out of consideration. In that case, the solution for a static equilibrium of the wheelset on the two rails is needed. The problem will become more complicated for the case that the dynamical effect on the wheelset in the vertical direction and the roll rotation is included. The normal loads are the combination of the static and dynamical acting forces. A wheelset has six degrees of freedom in its free state. When it is put on the two rails

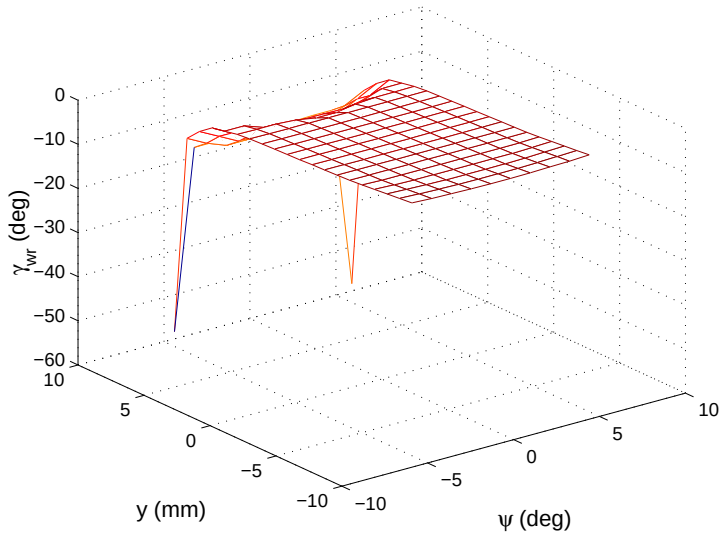

Figure 5.12: *The contact angle on the right side hand wheel*

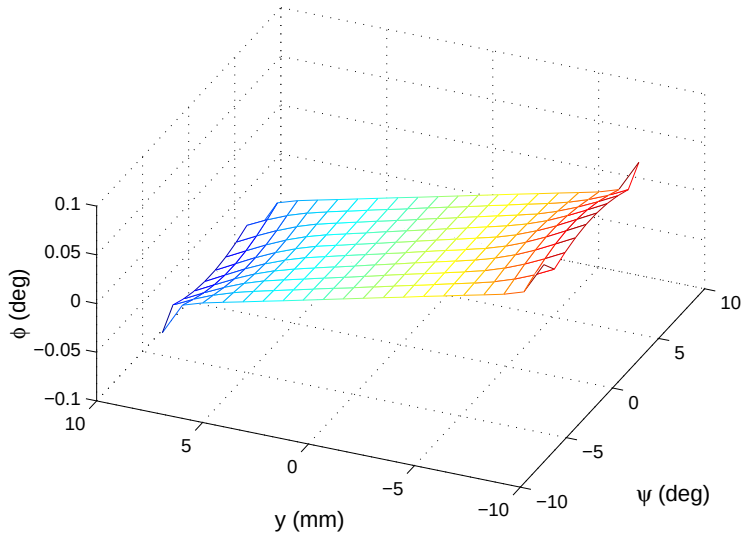

Figure 5.13: *The roll of the wheelset*

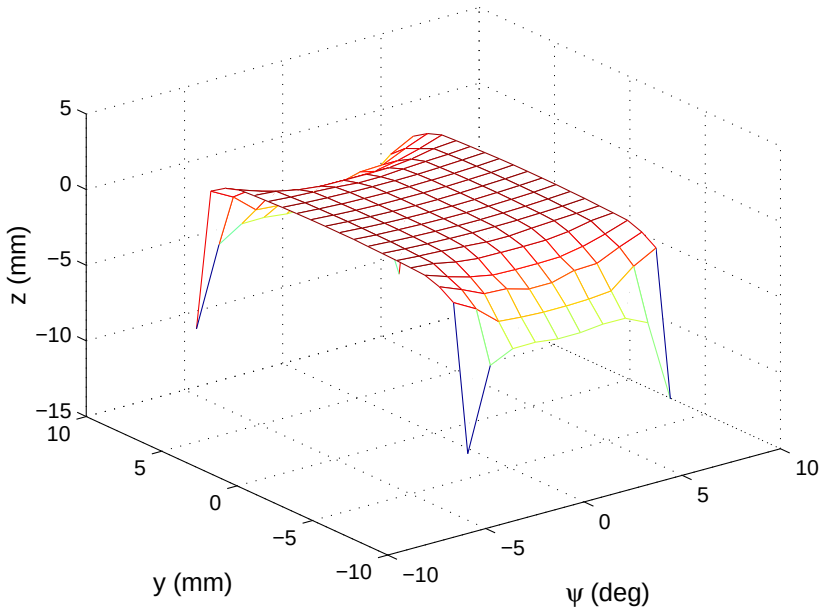

Figure 5.14: *The vertical displacement of the wheelset*

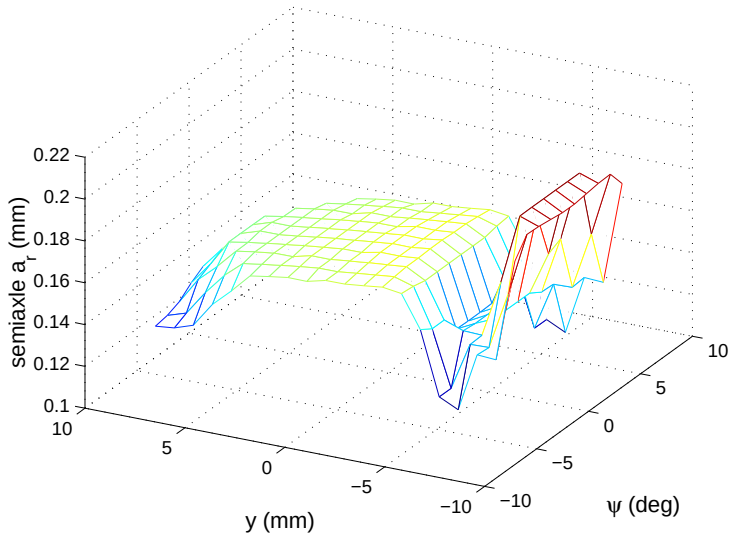

Figure 5.15: *The effect of both the lateral displacement and the yaw of the wheelset on the semi-axle a on the right-hand side contact point*

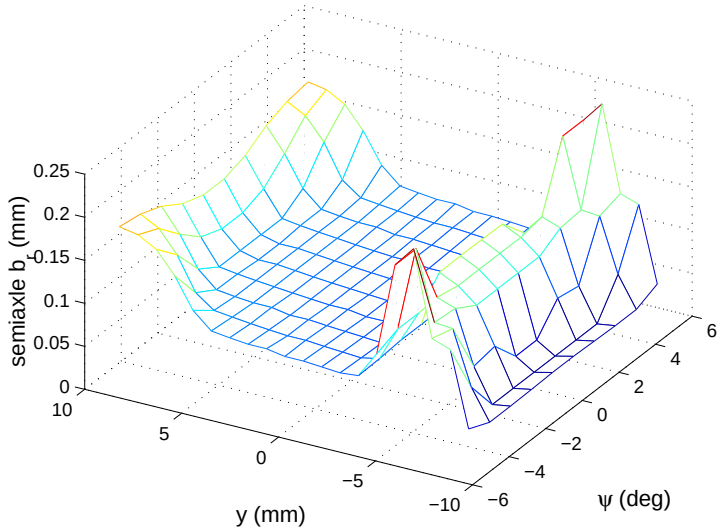

Figure 5.16: *The effect of both the lateral displacement and the yaw of the wheelset on the semi-axle b on the right-hand side contact point*

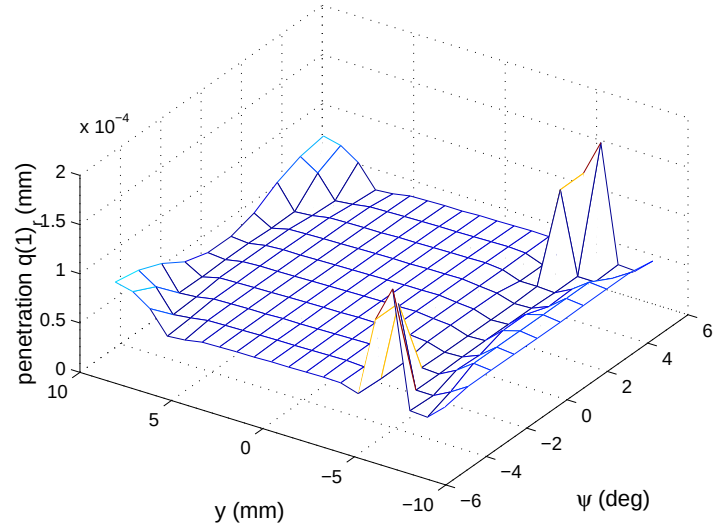

Figure 5.17: *The effect of both the lateral displacement and the yaw of the wheelset on the penetration $q(1)$ on the right-hand side contact point*

the two kinematic constraints are produced. If we assume that both the wheelset and the rails are rigid then we may derive four independent equations of motion of the wheelset together with two kinematic constraint equations. The normal forces can be found from the two kinematic constraint equations[Sauvage, 1990]. If the elastic assumption is used then the two kinematic constraint equations are free, in that case the Hertzian springs must be introduced as force connecting elements between the wheels and rails in order to keep the wheelset in contact with the track in the normal case.

Two methods are widely used to determine the normal force between a wheel and a rail[Sauvage, 1990]. One is called the rigid model. It considers the wheel and the rail as rigid bodies, where the two kinematical constraints exist among the six degrees of freedom of a wheelset on two rails. Then we can use the two dynamical equations of the vertical and the roll movements of the wheelset and the two kinematic constraints to determine the normal contact forces both on the left and right wheel/rail contact patches. A shortcoming of this method is that it can not yield the correct normal force when the wheel lifts the rail.

Another method to determine the normal force considers the elastic contact between the wheel and the rail. The key point in this method is to consider the penetration of the wheel into the rail[Slivsgaard, 1995][Sauvage, 1990]. In that case the six degrees of freedom of the wheelset are all independent. Pascal [Pascal, 1991] proposed a method where the penetration for the $1N$ normal forces are calculated first and collected into a table. When the penetration under the acting forces on the wheelset is determined from the dynamical simulation then the normal load is found from the relation

$$N_w = (\frac{q(N_w)}{q(1)})^{\frac{3}{2}} \tag{5.13}$$

where the penetration $q(1)$ will be discussed next.

The penetration $q(N_w)$ may be determined by the way shown in the paper [Sauvage,1990]. Anyhow the Hertzian stiffness is very high, about $10^9 N/m$, this method requires very small calculation steps–about one microsecond[Sauvage,1990]. The calculations of the strong nonlinear dynamic system will then be restricted by the calculational efficiency.

Here we shall use the static-dynamical method to calculate the normal force between a wheel and a rail. First the static normal loads are determined with the specified lateral displacement and the yaw rotation of the wheelset by means of the static equilibrium equations with an iteration algorithm. Then the penetration caused by the dynamical forces along the normal to the tangent contact plane is determined in the following way.

According to Kalker[Kalker,1990], the penetration q_n for the given semiaxes a and b of the contact patch is given by

$$q_n = (D_x + D_y)b^2 \frac{\mathbf{K}(k)}{\mathbf{E}(k)} \tag{5.14}$$

where D_x and D_y are the averaged radii of curvature in the directions(x, y). They are given by

$$D_x = \frac{1}{2}(\frac{1}{R_{xr}} + \frac{1}{R_{xw}}), \quad D_y = \frac{1}{2}(\frac{1}{R_{yr}} + \frac{1}{R_{yw}}). \tag{5.15}$$

$\mathbf{K}(k)$ and $\mathbf{E}(k)$ denote elliptical integrals. k depends on the ratio between the axes a and b which are given by[Garg, 1982]

$$a = m[3\pi N_w(K_1 + K_2)/4K_3]^{1/3}, \tag{5.16}$$
$$b = n[3\pi N_w(K_1 + K_2)/4K_3]^{1/3} \tag{5.17}$$

where N_w is the total normal force and

$$K_1 = \frac{1-\nu_w^2}{\pi G_w}, \quad K_2 = \frac{1-\nu_r^2}{\pi G_r}, \quad K_3 = D_x + D_y \tag{5.18}$$

G_w, G_r denote the shear modulus of elasticity of the wheel and rail materials, respectively; ν_w, ν_r stand for the Poisson's ratio for the wheel and rail materials, respectively.

By combination of the formulae (5.14), (5.16) and (5.17) we can find

$$q_n \propto N_w^{\frac{2}{3}}. \tag{5.19}$$

Under the assumption of elastic contact between the wheel and rail the Hertzian stiffness can be introduced to describe the elastic contact force. In this way, the normal load is determined by the Hertzian nonlinear theory from[Jenkins,1974]

$$q_n = G_{hertz} N_w^{2/3} \quad \Longleftrightarrow N_w = \frac{q_n^{3/2}}{G_{hertz}^{3/2}} \tag{5.20}$$

where the constant G_{hertz} depends on the elastic moduli and radii of curvature of the wheel and rail. For conical wheel profiles

$$G_{hertz} = 4.57 r^{-0.149} \times 10^{-8}, \quad (m/N^{2/3}), \tag{5.21}$$

and for worn profiles:

$$G_{hertz} = 3.86 r^{-0.115} \times 10^{-8}, \quad (m/N^{2/3}). \tag{5.22}$$

Here r denotes the rolling radius of the wheel. However by comparing the results between the traditional method and the new one we find that the value is small . The suitable value of the G_{hertz} for the profiles used in this thesis is about 10^{-6}. In fact, if we roughly evaluate the Hertzian stiffness with (5.20) by

$$K_h = 1/G_{hertz}^{3/2} \tag{5.23}$$

we can find that the Hertzian stiffness is about 10^{11} for the G_{hertz} in (5.21). Therefore the large G_{hertz} should be selected.

The dynamical penetration caused by the dynamical forces on the wheelset can be considered as a fluctuation around the static penetration. It may be described by

$$q_d = f(w_d, \phi_d, v, \psi, v_r, w_r) \tag{5.24}$$

with

$$w_d = w - w_s, \quad \phi_d = \phi - \phi_s \tag{5.25}$$

where w and ϕ denote the vertical displacement and roll rotation of the wheelset respectively; w_d and ϕ_d denote the dynamical displacements and roll rotation of the wheelset respectively, and w_s and ϕ_s denote the static displacements and roll rotation of the wheelset respectively. The static displacement and roll rotation, w_s and ϕ_s are determined by the evaluation of the kinematic constraints between the wheel and rail.

After determination of the dynamic penetration the total normal force is evaluated by

$$N_w = G_{hertz}(q_{ns} + q_d)^{1.5}. \tag{5.26}$$

With (5.20) the above relation can also be written as

$$N_w = N_{ws}(1 + \frac{q_d}{q_{ns}})^{1.5} \tag{5.27}$$

where q_{ns} denotes the penetration under the static normal load.

The comparison of the normal loads by the traditional method and the method in this thesis is shown in Figure 5.18.

5.2.2 Determination of the shape and the dimensions of the contact area

If the normal load N_w is determined then the formulae (5.16) and (5.17) can be used to determine the semiaxes a, b by looking up the values of the parameters of m, n in the precalculated table given by Hertz[Garg, 1982]. We also can use a direct way to determine the dimensions of the contact patch. Let c be the geometric mean of a and b:

$$c = \sqrt{ab} \tag{5.28}$$

the effective radius of curvature of the contacting surface is defined as

$$\rho = 2/(D_x + D_y) \tag{5.29}$$

In order to determine

$$\tau = \cos^{-1}(\frac{|D_x - D_y|}{D_x + D_y}) \tag{5.30}$$

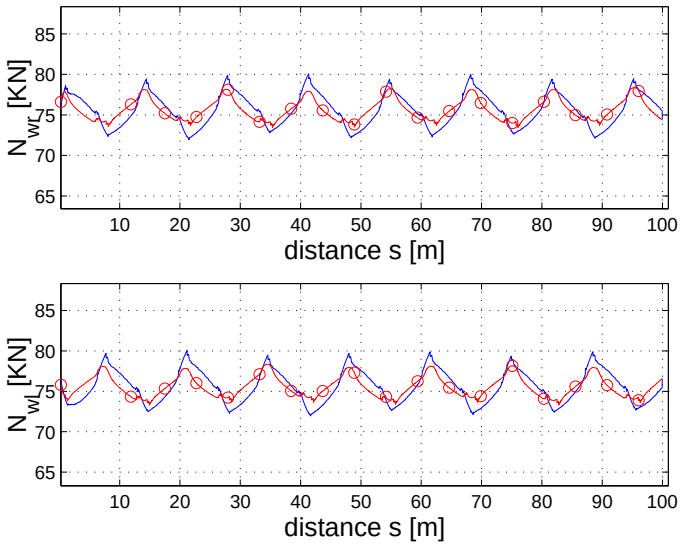

Figure 5.18: *The comparison of the normal forces. The solid line denotes the normal loads with the new method and the solid line with the o on it stands for the traditional method*

in such way that

$$0 \leq \tau \leq \pi/2 \tag{5.31}$$

and according to Hertzian theories from Kalker [Kalker,1967,1990] we can derive an equation for the quantity e^2 which determines the ratio between the semi-axes of the contact ellipse:

$$1 - 2\frac{1-e^2}{e^2}\frac{\mathbf{K}(e) - \mathbf{E}(e)}{\mathbf{E}(e)} = \cos\tau \tag{5.32}$$

where $\mathbf{K}(e)$ and $\mathbf{E}(e)$ are the following elliptic integrals,

$$\mathbf{K}(e) = \int_0^{\pi/2} \frac{d\phi}{\sqrt{1 - e^2 sin^2\phi}} \tag{5.33}$$

and

$$\mathbf{E}(e) = \int_0^{\pi/2} \sqrt{(1 - e^2 sin^2\phi)}d\phi \tag{5.34}$$

By the Taylor's expansion the elliptic integrals can be written as[De Pater, 1997] [Kreyszig, 1979]

$$\mathbf{K} = \frac{\pi}{2}[1 + \sum_{k=1}^{\infty} a_k e^{2k}], \quad \mathbf{E} = \frac{\pi}{2}[1 + \sum_{k=1}^{\infty} b_k e^{2k}] \tag{5.35}$$

where

$$\begin{aligned} a_1 &= \frac{1}{2^2}, \quad a_k = (\frac{2k-1}{2k})^2 a_{k-1} \qquad for \quad k = 2, 3, \cdots \\ b_1 &= \frac{1}{2^2}, \quad b_k = \frac{2k-3}{2k}\frac{2k-1}{2k} b_{k-1} \qquad for \quad k = 2, 3 \cdots \end{aligned} \tag{5.36}$$

so we have

$$(1 - e^2)\frac{\sum_{k=1}^{\infty} c_k e^{2(k-1)}}{1 - \sum_{k=1}^{\infty} b_k e^{2k}} = \frac{1}{2}(1 - \cos\tau) \tag{5.37}$$

where

$$c_1 = \frac{1}{2}, \quad c_k = \frac{(2k-3)(2k-1)}{(2k-2)2k} c_{k-1} \qquad for \quad k = 2, 3, \cdots \tag{5.38}$$

Thus for a given value of $\cos\tau$ from (5.30), e^2 can be found numerically from (5.37)[Xia, 1996].

The parameter e is connected with the ratio a/b

$$\begin{aligned} a/b &= \sqrt{1 - e^2} \qquad for \quad a \le b, \quad A \ge B, \\ a/b &= \frac{1}{\sqrt{1 - e^2}} \qquad for \quad a \ge b, \quad A \le B \end{aligned} \tag{5.39}$$

which is independent of the value of the normal force in the contact point.

For the normal force in the contact point c is determined by the relation

$$c = \sqrt[3]{\frac{3N_w(1-\nu)\rho\mathbf{E}}{4\pi G\sqrt{g}}} \tag{5.40}$$

where

$$g = \sqrt{1 - e^2}. \tag{5.41}$$

Thus the semiaxes a and b can be determined from(5.28) and (5.39). With the value b, the penetration q_n can also be determined by the relations (5.14) and (5.32)

$$q_n = (D_x + D_y)b^2[1 + \frac{e^2}{2(1 - e^2)}(1 - cos\tau)]. \tag{5.42}$$

5.2.3 Calculation of the creep forces

The first important contribution to the theory of rolling contact was due to Carter(1926), who was the first to propose the concept of *creepage*. Extensions of Carter's theory to the three-dimensional rolling contact was studied throughout the 60's. Vermeulen and Johnson(1964) generalized Carter's theory to three dimensions and established an approximate creep-force law. Since the middle of the 1960's, Kalker's theories on rolling contact mechanics have been the most widely used theories both in the simulation of railway vehicle dynamics and in the analysis of damage of the profiles of rails and wheels. For use in practical applications Shen, Hedrick and Elkins(1983) proposed an alternative creep-force law based on Kalker's creep coefficients and Johnson-Vermeulen's method.

The contact region between the wheel and the rail generally consists of a slip and an adhesion region. The slow sliding will take place in the contact region between the two bodies in rolling contact. The sliding phenomenon(or slip) is called the *creep* or the *creepage*.

There exist three different forms of creep: longitudinal, lateral and spin creep. The longitudinal creep, υ_x and the lateral creep, υ_y are the relative velocities between the wheel and the rail in the contact plane. The spin creep, ϕ_s is the relative angular velocity between the wheel and the rail about an axis normal to the contact plane.

According to Carter's definition, the creepages and the spin are

$$\upsilon_x = \frac{V_{wx} - V_{rx}}{V} = \frac{W_{tx}}{V}, \quad \upsilon_y = \frac{V_{wy} - V_{ry}}{V} = \frac{W_{ty}}{V}, \quad \phi_s = \frac{\Omega_{ws} - \Omega_{rs}}{V} = \frac{\Omega_n}{V} \tag{5.43}$$

where $V_{wx,y}$ denote the longitudinal and lateral velocities of the wheel; $V_{rx,y}$ denote the longitudinal and lateral velocities of the rail; Ω_{ws} and Ω_{rs} denote the angular velocity of the wheel and the rail about the vertical axis respectively. V is the actual velocity of the wheelset. The velocity differences W_{tx}, W_{ty} and Ω_n will be discussed in chapter 6.

Now the creepages are defined as:

$$\upsilon_{xij} = W_{txij}/V, \quad \upsilon_{yij} = W_{tyij}/V, \quad \phi_{sij} = \Omega_{nij}/V \tag{5.44}$$

where V is the longitudinal speed of the vehicle. In the case of small creepages, the relation between creep and creep forces is approximately linear. The linear rolling contact theory has been derived by Kalker and expressed as

$$\begin{bmatrix} T_x \\ T_y \\ M_z \end{bmatrix} = Gc^2 \begin{bmatrix} C_{11} & 0 & 0 \\ 0 & C_{22} & cC_{23} \\ 0 & -cC_{23} & c^2C_{33} \end{bmatrix} \begin{bmatrix} \upsilon_x \\ \upsilon_y \\ \phi_s \end{bmatrix} \tag{5.45}$$

where C_{11}, C_{22}, C_{23} and C_{33} denote the creep coefficients[Kalker,1967].

For large values of creepages, the nonlinear dependence of the creep force on the creep becomes important. Kalker has developed the exact rolling contact theory[Kalker, 1990] and implemented it in the program CONTACT. Unfortunately, it is virtually impossible to use the exact theory in the practical simulations of the

dynamics of a railway system due to the high computational time. For that reason, Kalker has developed another program FASTSIM. FASTSIM is much faster than CONTACT but the difference between the results of CONTACT and FASTSIM never exceed values of 10%-15%[De Pater, 1997].

For practical application, Shen-Hetrick-Elkins improved Kalker's linear theory on the basis of the Vermeulen-Johnson formulae [Shen, 1983]. Shen *et al* assume that the resultant tangential force T_R is determined by

$$T_R = \begin{cases} \mu N_w[(\frac{T_R^*}{\mu N_w}) - \frac{1}{3}(\frac{T_R^*}{\mu N_w})^2 + \frac{1}{27}(\frac{T_R^*}{\mu N_w})^3], & for \quad T_R^* \leq 3\mu N_w \\ \mu N_w, & for \quad T_R^* > 3\mu N_w \end{cases} \tag{5.46}$$

with

$$T_R^* = \sqrt{T_x^2 + T_y^2} \tag{5.47}$$

where T_x and T_y are calculated according to Kalker's linear theory. Introducing the reduction coefficient

$$\varepsilon = T_R / T_R^* \tag{5.48}$$

the creep forces are

$$f_x = \varepsilon T_x, \quad f_y = \varepsilon T_y \tag{5.49}$$

In order to improve the computation efficiency of FASTSIM, another practical method for finding the tangential forces consists in a collecting a sufficiently large number of values of the reduced creep forces, f_x f_y in a table, each with four entries and to interpolate linearly in these tables[De Pater, 1997, Xia, 1996, Kalker, 1997]. It should be pointed out that because of the limited data in the look-up table, differences from the exact theory will be found. Large tables are more exact, but the searching in such large tables consumes calculation time.

Recently, O. Polach has provided another way to determine the creep forces and he argued that it has a short calculation time and a smaller difference between the calculated values and the exact theory[Polach,1999], and is more correct than the theory of Shen, Hedrick and Elkins.

In the theory of Polach, as shown in Figure 5.19, the tangential stress is proportional to the total creepage υ and the distance from the leading edge with a proportionality constant C, which is a value characterizing the contact elasticity of the bodies(tangential contact stiffness). The tangential contact stiffneff can be obtained from Kalker's constants [Kalker, 1967]. The gradient of the tangential stress in the area of adhesion (see Figure 5.19) is

$$\varepsilon = \frac{2}{3}\frac{C\pi a^2 b}{N_w \mu}\upsilon. \tag{5.50}$$

The tangential force is then

$$\mathbf{F} = -\tau_0 \frac{4ab}{3}(\frac{\varepsilon}{1+\varepsilon^2} + \tan^{-1}\varepsilon) \tag{5.51}$$

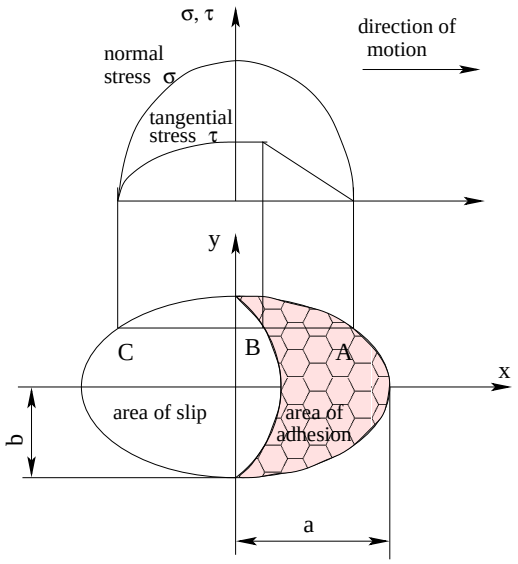

Figure 5.19: *A simplified distribution of normal and tangential stresses in the wheel-rail contact area*

According to the theory of Hertz

$$\tau_0 = \frac{3}{2}\frac{N_w \mu}{\pi ab} \tag{5.52}$$

which by substitution into (5.51) yields

$$\mathbf{F} = -\frac{2N_w \mu}{\pi}\left(\frac{\varepsilon}{1+\varepsilon^2} + \tan^{-1}\varepsilon\right), \tag{5.53}$$

$$\mathbf{F}_i = \mathbf{F}\frac{\upsilon_i}{\upsilon} \qquad (i = x, y). \tag{5.54}$$

According to Kalker's theory, we obtain the tangential contact stiffness C and the Eq. (5.50) then becomes

$$\varepsilon = \frac{1}{4}\frac{G\pi abc_{jj}}{N_w \mu}\upsilon \tag{5.55}$$

and

$$c_{jj} = \sqrt{(C_{11}\frac{\upsilon_x}{\upsilon})^2 + (C_{22}\frac{\upsilon_y}{\upsilon})^2}. \tag{5.56}$$

If we take the spin ϕ_s into account, the lateral tangential force can be written as

$$F_{yc} = F_y + F_{ys} \tag{5.57}$$

where F_{ys} is the increase of the tangential force caused by the spin, which is

$$F_{ys} = -\frac{9}{10} a N_w \mu K_m (1 + 6.3(1 - e^{-\frac{a}{b}})) \frac{\phi_s}{v_c} \tag{5.58}$$

where

$$K_m = |\varepsilon_s| (\frac{\delta^3}{3} - \frac{\delta^2}{2} + \frac{1}{6}) - \frac{1}{3}\sqrt{(1-\delta^2)^3}, \tag{5.59}$$

$$\delta = \frac{\varepsilon^2 - 1}{\varepsilon^2 + 1}, \tag{5.60}$$

$$\varepsilon_s = \frac{8}{3} \frac{G\pi b\sqrt{ab}}{N_w \mu} \frac{C_{23} v_{yc}}{1 + 6.3(1 - e^{-\frac{a}{b}})}, \tag{5.61}$$

$$v_c = \sqrt{v_x^2 + v_{yc}^2}. \tag{5.62}$$

Here v_{yc} is given as

$$\begin{aligned} v_{yc} &= v_y + \phi_s a \quad for \quad |v_y + \phi_s a| > |v_y|, \\ v_{yc} &= v_y \qquad for \quad |v_y + \phi_s a| \leq |v_y|. \end{aligned} \tag{5.63}$$

For the sake of comparison the theory of Shen, Hetrick and Elkins, the table looking method and the theory of Polach are all implemented in our model.

CHAPTER 6

The configuration and kinematics of the Three-Piece-Freight-Truck

In the previous chapters we have introduced some basic concepts of the friction direction angle, stick-slip motion, structure varying system, and kinematic constraints and dynamical constraints between wheels and rails. All of them will be combined into the modelling of the dynamics of the three-piece-freight-truck hereafter.

In order to derive the more realistic mathematical model the construction of the three-piece-freight-truck should first be understood thoroughly. The interconnections and the motion transfer mechanisms between the components need also to be known clearly. With the principle of the multibody system dynamics we must to find a suitable connection element to describe the interconnections correctly. In this chapter the coordinate systems which are used to describe the motions are introduced. The construction and the description of the model are then discussed. The kinematic constraints and the creepages between the wheels and the rails are analyzed.

6.1 Introduction of the three-piece-freight-truck

A hopper wagon and the three-piece-freight-truck are shown in Figure 6.1 and Figure 1.1. A car body is supported by two three-piece-freight-trucks(bogies) through two center plates on the two bolsters. A strong pivot through the center plate is used to prevent the separation of the car body from the bolsters during the motion. In order to obtain a good curve negotiation two side supports on either bolster are designed

Figure 6.1: *A hopper three-piece-freight-wagon*

to provide an additional support on the car body in the case of large roll rotations between the car body and the bolsters. A conventional three-piece-freight-truck, as shown in Figure 1.1, consists of two wheelsets, one side frame on each side of the wheelsets supported by the adapters. For one truck a bolster is supported by two groups of springs one on each side of the frame and four wedges are used to provide dry friction on the surfaces of the wedges contacting both the side frame and the bolster.

Because of the configuration characteristics of the three-piece-freight-truck they differ from the passenger truck in that there is no longitudinal motion between the bolster and the side frame at least for a truck during normal running, and the relative yaw motion of the bolster with respect to the side frames causes the side frames to rotate about the vertical truck center line and to assume a *parallelogram* configuration. This type of deformation, referred to as *warping*, is restricted by friction between the bolster and side frames and is limited by the contact of the bolster ends against the side frames. In truck assemblies there are clearances between the adapters and the side frames both in the longitudinal and lateral directions such that the wheelset can move longitudinally and laterally until the wheelset hits the stops.

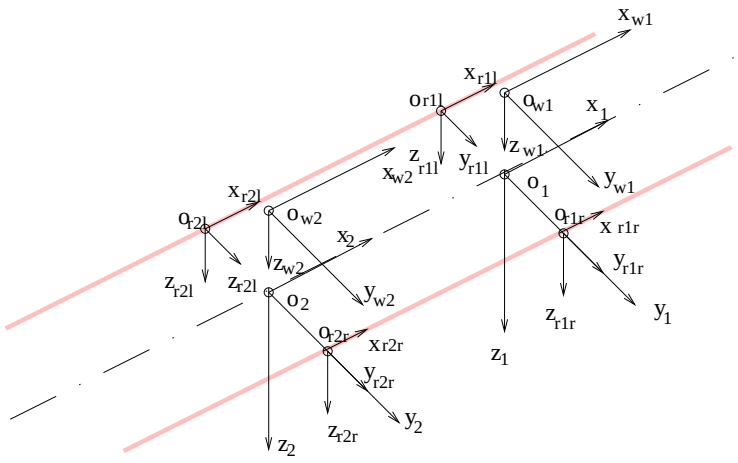

Figure 6.2: *The coordinate systems*

6.2 The coordinate systems and the degrees of freedom of the system

The description of the configuration and orientation of the railway vehicles on the track are related to the definition of coordinate systems. In order to describe the absolute motion of the three-piece-freight-truck on an arbitrary form of track three coordinate systems are needed: the inertial, transfer and relative coordinate systems. The absolute motion of the components of the three-piece-freight-truck is the vector sum of the transfer and the relative motions. However we are only interested in the *parasitic motion* for the dynamical performance analysis of the three-piece-freight-truck, i.e. the parasitic motions of the wheelsets and other components of the system are required. For the investigation of the behavior of the vehicle on a curved track, the motion of the transfer coordinate system will cause an additional force called the Gyroscopic force. Additionally spring forces caused by the bodies on the different position of the curve are needed to included. However, if we only consider the motion of the vehicle on the tangential track, then the coordinate systems and the relations among them will become rather simple. If the motion of the vehicle is at a constant speed along a straight track then we can choose the transfer coordinate system to be the inertial coordinate system. The coordinate systems are shown in Figure 6.2.

Figure 6.2 only shows the two sets of reference coordinate systems. One is used to describe the parasitic motion of the wheelset number 1 and the other is used to describe the wheelset number 2. The motion of the wheelsets are described with respect to the inertial reference coordinate systems. Other reference coordinate systems can be defined in a similar way.

The origin o_{wi} of the wheelset frame $(o_{wi}, x_{wi}, y_{wi}, z_{wi})$ is located in the mass

Table 6.1: *Degrees of freedom of the wagon with two three-piece-freight trucks*

Components	Long.	Lat.	Vert.	Roll	Pitch	Yaw
Front truck leading wheelset	u_1	v_1	w_1	ϕ_1	χ_1	ψ_1
Front truck trailing wheelset	u_2	v_2	w_2	ϕ_2	χ_2	ψ_2
Rear truck leading wheelset	u_3	v_3	w_3	ϕ_3	χ_3	ψ_3
Rear truck trailing wheelset	u_4	v_4	w_4	ϕ_4	χ_4	ψ_4
Front truck left side frame	u_{f1}	v_{f1}	w_{f1}	—	χ_{f1}	ψ_{f1}
Front truck right side frame	u_{f2}	v_{f2}	w_{f2}	—	χ_{f2}	ψ_{f2}
Rear truck left side frame	u_{f3}	v_{f3}	w_{f3}	—	χ_{f3}	ψ_{f3}
Rear truck right side frame	u_{f4}	v_{f4}	w_{f4}	—	χ_{f4}	ψ_{f4}
Front truck left wedges	u_{d1}	v_{d1}	w_{d1}	—	—	—
	u_{d2}	v_{d2}	w_{d2}	—	—	—
Front truck right wedges	u_{d3}	v_{d3}	w_{d3}	—	—	—
	u_{d4}	v_{d4}	w_{d4}	—	—	—
Rear truck left wedges	u_{d5}	v_{d5}	w_{d5}	—	—	—
	u_{d6}	v_{d6}	w_{d6}	—	—	—
Rear truck right wedges	u_{d7}	v_{d7}	w_{d7}	—	—	—
	u_{d8}	v_{d8}	w_{d8}	—	—	—
Front truck bolster	—	v_{b1}	w_{b1}	ϕ_{b1}	—	ψ_{b1}
Rear truck bolster	—	v_{b2}	w_{b2}	ϕ_{b1}	—	ψ_{b1}
Car body	—	v_o	w_o	ϕ_o	χ_o	ψ_o

center of the wheelset i with the positive direction to the right rail. The coordinate system(o_{wi}, x_{wi}, y_{wi}, z_{wi}) is not completely fixed to the wheelset because the wheelset can rotate about the axis $o_{wi}y_{wi}$. The position of the origin o_{wi} is (0, 0, -r) with respect to the inertial reference frame(o_i, x_i, y_i, z_i).

We see that the distance between the origins of the two inertial frames (o_1,o_2) is constant. The irregularities of the track can be described as displacements of the origins, (o_{r1l}, o_{r1r}) of the local frames of $(o_{r1l}, x_{r1l}, y_{r1l}, z_{r1l})$ and $(o_{r1r}, x_{r1r}, y_{r1r}, z_{r1r})$ in the lateral and vertical directions.

6.2.1 The degrees of freedom of the system

As Figure 6.3 shows, our model of the four-axle three-piece-freight-wagon has nineteen principal components. These are the car body, two truck bolsters, eight wedges, four side frames, and four wheelsets. The degrees of freedom of the system are given in Table 1, where the total degrees of freedom is 81. But we will see that not all the degrees of freedom are independent and there exist some relations due to the joint connections between the car body and the bolsters, the sliding contact between the bolsters and the wedges, and the side frames and the adapters(wheelsets).

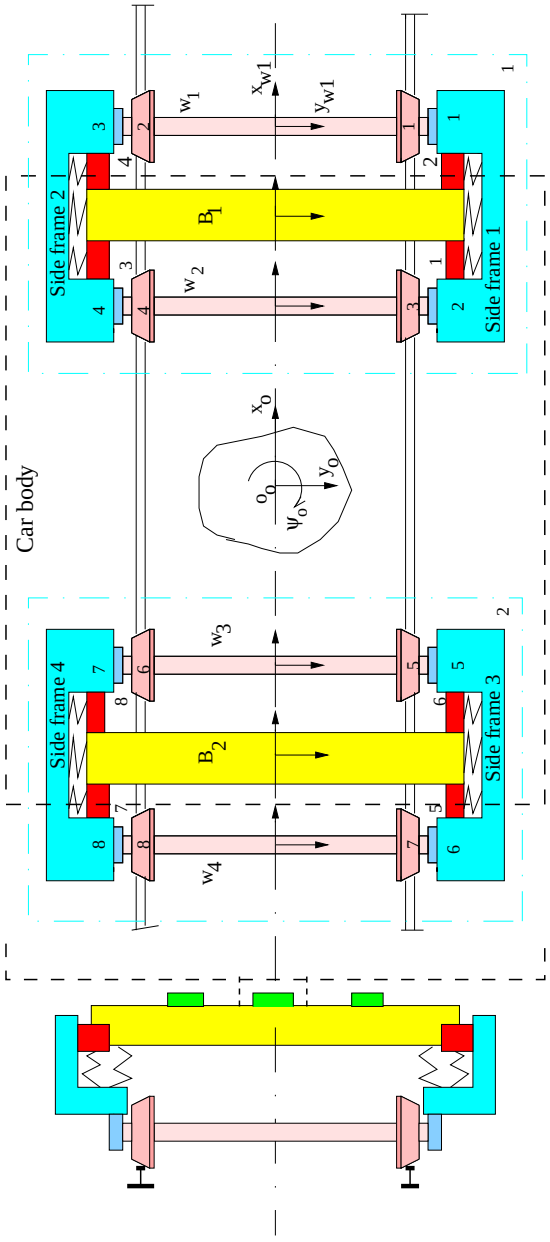

Figure 6.3: *The description of the model of the Three-Piece-Freight-Truck*

6.3 The interconnections between the components

The relations between the coordinate systems of the components of the three-piece-freight-car are shown in Figure 6.4.

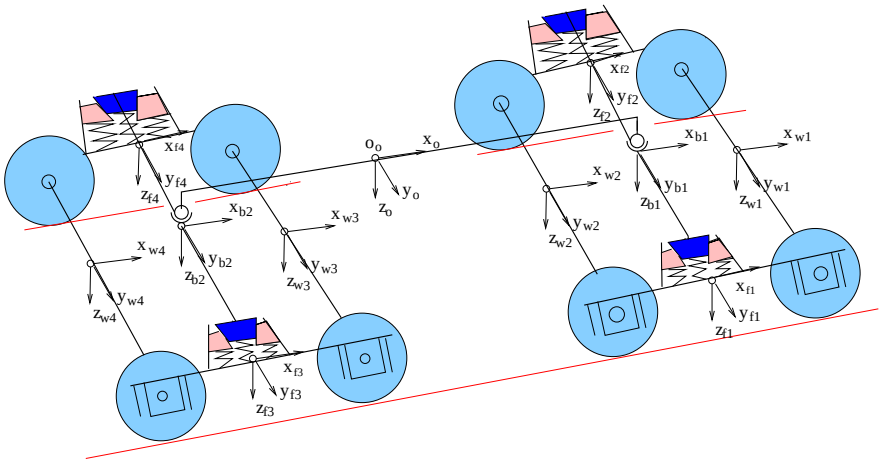

Figure 6.4: *The relations between the coordinate systems of the components of the three-piece-freight-car*

6.3.1 The relations between the car body and the bolsters

The vehicle body has six degrees of freedom. If we neglect parasitic motion along the longitudinal direction we choose the 2 displacements of the center of mass v_o, w_o in the lateral and vertical directions and the three rotations ϕ_o, χ_o, ψ_o with respect to the reference coordinates(o_o, x_o, y_o, z_o) around the axes $o_o x_o$, $o_o y_o$ and $o_o z_o$ as the five degrees of freedom. The center plates which are used to connect the car body and the bolsters can be modelled as sphere joints as shown in Figure 6.5 where all the translations between the car body and the two bolsters are blocked but all the relative rotations are free. The clearances between the car body and the side supports are modelled to be dead-band stop springs with the spring forces acting in the vertical direction and the friction on the surfaces of the side supports are integrated into the yaw friction moment on the car body and bolsters. The parasitic motions of the car

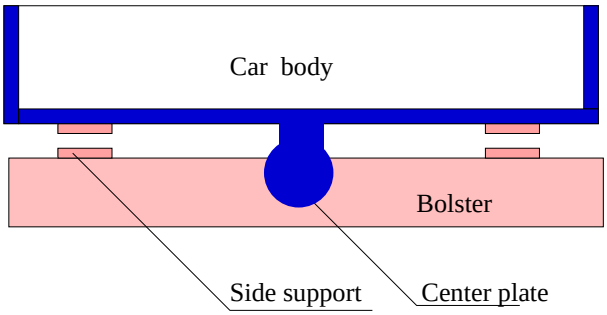

Figure 6.5: *The modelling of the center plate*

body can be described by the roll rotation ϕ_o and the relations below

lateral displacement,

$$v_o = \frac{v_{b1} + v_{b2}}{2} \tag{6.1}$$

vertical displacement,

$$w_o = \frac{w_{b1} + w_{b2}}{2} \tag{6.2}$$

pitch,

$$\chi_o = \frac{w_{b2} - w_{b1}}{2a^*_{oc}} \tag{6.3}$$

yaw,

$$\psi_o = \frac{v_{b1} - v_{b2}}{2a^*_{oc}} \tag{6.4}$$

where $2a^*_{oc}$ denotes the distance between the mass centers of the two bolsters. The positions of the secondary suspensions on the bolsters with respect to the reference coordinate system $(o_{bi}, x_{bi}, y_{bi}, z_{bi})$ are determined by

$$\begin{bmatrix} x_{bs2k} \\ y_{bs2k} \\ z_{bs2k} \end{bmatrix} = \begin{bmatrix} (-1)^k b^*_{bs2}\psi_{bi} \\ v_{bi} + (-1)^{k+1} b^*_{bs2} \\ w_{bi} + (-1)^{k+1} b^*_{bs2}\phi_{bi} - (r + h_b) \end{bmatrix} \tag{6.5}$$

where for $i = 1, k = 1, 2$; for $i = 2, k = 3, 4$. b^*_{bs2} denotes the distance between the mass center of the bolster and the secondary suspension. r denotes the radius of the wheel for the central position of the wheelset. h_b is the distance from the wheel axle to the center of the bolster in vertical direction.

6.3.2 The relations between the wedges and the bolsters

In the case of no separating motion between the wedge and the bolster it is required that a pair of wedges on either the left side or the right side of a bogie must be

used to retain the symmetrical construction of the bogie. For one pair of wedges, the relations

$$u_{di} = -u_{dk}, \quad w_{di} = w_{dk}, \quad (i = 1, 3, 5, 7; \quad k = 2, 4, 6, 8). \tag{6.6}$$

hold. In the case of a coupled motion with the bolster, the displacements of the wedges with respect to the reference coordinates $(o_{bi}, x_{bi}, y_{bi}, z_{bi})$ are controlled by the relations(See chapter 3)

$$u_{di} = \mp b^*_{bs2}\psi_{bj} + (-1)^i a_{bd} + (-1)^i \frac{\sin\gamma \sin\phi}{\sin(\gamma+\phi)}(w_{bj} \pm b^*_{bs2}\phi_{bj} - w_{fk}) \tag{6.7}$$

$$w_{di} = \frac{\cos\gamma \sin\phi}{\sin(\gamma+\phi)}(w_{bj} \pm b^*_{bs2}\phi_{bj} - w_{fk}) \tag{6.8}$$

where for $j = 1$, $i = 1, 2, 3, 4$, $k = 1, 2$; for $j = 2$, $i = 5, 6, 7, 8$, $k = 3, 4$. For $i = 1, 2, 5, 6$ we use the upper sign of $\pm$ or $\mp$ and for $i = 3, 4, 7, 8$ we use the lower sign of $\pm$ or $\mp$. But in the case of the separated state the relations described in (6.6), (6.7) and (6.8) are broken and u_{wi}, w_{wi} become independent quantities(See chapter 3). a_{bd} denotes the distance from the mass center of the wedge to the axis $o_{bi}y_{bi}$ of the reference coordinates $(o_{bi}, x_{bi}, y_{bi}, z_{bi})$.

6.3.3 The relations between the side frames and the other components

The side frame is connected to the bolster through the wedges, and to the wheelsets through adapters, where the adapter mass can be neglected. There is no relative translation between the ends of the bolster and the corresponding side frames in the longitudinal direction. The yaw of the bolster will cause a translation motion of the side frame in the longitudinal direction. The vertical motions of the wheelsets will force a corresponding vertical motion and a pitch rotation of the side frames because the interconnections between the side frames and the wheelsets(via adapters) can be modelled as slide pairs which are shown in Figure 6.6. The relations between the

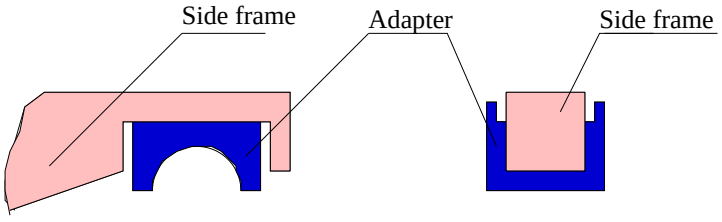

Figure 6.6: *The contact between the end of a frame and an adapter*

side frames and the bolsters and the wheelsets can be written as

$$u_{fi} = (-1)^i b^*_{bs2}\psi_{bj}, \quad (i = 1, 2, j = 1; i = 3, 4, j = 2), \tag{6.9}$$

$$w_{f1,2} = 0.5(w_{w1} + w_{w2} \pm b_{ws}(\varphi_{w1} + \varphi_{w2})), \tag{6.10}$$
$$w_{f3,4} = 0.5(w_{w3} + w_{w4} \pm b_{ws}(\varphi_{w3} + \varphi_{w4})), \tag{6.11}$$
$$\chi_{f1,2} = -0.5(w_{w1} \pm b_{ws}\varphi_{w1} - w_{w2} \mp b_{ws}\varphi_{w2})/a_{wb}, \tag{6.12}$$
$$\chi_{f3,4} = -0.5(w_{w3} \pm b_{ws}\varphi_{w3} - w_{w4} \mp b_{ws}\varphi_{w4})/a_{wb} \tag{6.13}$$

where b_{ws} denotes the distance between the mass center of a wheelset and the contact point with the adapter in lateral direction. a_{wb} denotes the distance from the wheel axle to the mass center of the side frame in longitudinal direction. For the index 1, 3 takes the upper sign of the $\pm$ or $\mp$ and for the index 2, 4 then takes the lower sign of the $\pm$ or $\mp$.

6.3.4 The positions of the points on the wheelsets

In order to determine the relative motions between the ends of the side frames and the wheelsets in the longitudinal and lateral directions we need to know the position of the adapter on the wheelset. For any point on wheelsets we have the relations

$$\begin{bmatrix} x_{wi} \\ y_{wi} \\ z_{wi} \end{bmatrix} = \begin{bmatrix} u_{wi} \\ v_{wi} \\ w_{wi} - r \end{bmatrix} + G_{wi} \begin{bmatrix} x^*_{wi} \\ y^*_{wi} \\ z^*_{wi} \end{bmatrix} \qquad (i = 1, 2, 3, 4) \tag{6.14}$$

where $(x^*_{wi}, y^*_{wi}, z^*_{wi})$ denote the point measured with respect to the wheelset coordinate system and

$$G_{wi} = \begin{bmatrix} 1 & -\psi_{wi} & 0 \\ \psi_{wi} & 1 & -\phi_{wi} \\ 0 & \phi_{wi} & 1 \end{bmatrix}. \tag{6.15}$$

So the position of the surfaces of the adapters contact with the wheelset with respect to the reference coordinate frame of the wheelset (o_i, x_i, y_i, z_i) are then

$$\begin{bmatrix} x_{ws1k} \\ y_{ws1k} \\ z_{ws1k} \end{bmatrix} = \begin{bmatrix} u_{wi} \\ v_{wi} \\ w_{wi} - r \end{bmatrix} + \begin{bmatrix} (-1)^k b_{wsi}\psi_{wi} \\ (-1)^{k+1} b_{wsi} \\ (-1)^{k+1} b_{wsi}\phi_{wi} \end{bmatrix}, \quad (k = 1, \cdots, 8, i = 1, \cdots, 4). \tag{6.16}$$

6.3.5 The extensions of the suspensions

The relative distances between the wheelsets and the side frames are determined by

$$\begin{bmatrix} u_{s1x} \\ u_{s1y} \\ u_{s1z} \end{bmatrix} = \begin{bmatrix} u_{fk} - u_{wi} + (-1)^{i+1} b^*_{ws2}\psi_{wj} \\ v_{fk} - v_{wj} + (-1)^{i+1}\psi_{fk} \\ 0 \end{bmatrix}, \quad \begin{array}{l}(i = 1, \cdots, 4, j = 1, 2, k = 1, 2; \\ i = 5, \cdots, 8, j = 3, 4, k = 3, 4)\end{array} \tag{6.17}$$

where the values can be used to determine the values of the dead-band stop spring forces between the wheelsets and the frames in the longitudinal and lateral directions.

The relative extensions of the secondary suspensions between the bolsters and side frames are

$$\begin{bmatrix} u_{s2xi} \\ u_{s2yi} \\ u_{s2zi} \end{bmatrix} = \begin{bmatrix} 0 \\ v_{bk} - v_{fi} \\ w_{bk} - w_{fi} \end{bmatrix} + (-1)^{i+1} b^*_{bs2} \begin{bmatrix} 0 \\ 0 \\ \phi_{bk} \end{bmatrix}, \quad (i = 1, \cdots, 4, k = 1, 2). \tag{6.18}$$

The extensions of the springs between wedges and side frames can be written as

$$\begin{bmatrix} u_{s3xi} \\ u_{s3yi} \\ u_{s3zi} \end{bmatrix} = \begin{bmatrix} (-1)^i \frac{\sin\gamma \sin\phi}{\sin(\gamma+\phi)} (w_{bj} \pm b^*_{bs2}\phi_{bj} - w_{fk}) \\ v_{di} - v_{fk} \\ \frac{\cos\gamma \sin\phi}{\sin(\gamma+\phi)} (w_{bj} \pm b^*_{bs2}\phi_{bj} - w_{fk}) \end{bmatrix}, \tag{6.19}$$
$$(i = 1, 2, j = 1, k = 1; i = 3, 4, j = 1, k = 2$$
$$i = 5, 6, j = 2, k = 3; i = 7, 8, j = 2, k = 4)$$

where for $i = 1, 2, 5, 6$ we use the upper sign of the " $\pm$ " and for $i = 3, 4, 7, 8$ we use the lower sign of the " $\pm$ ".

With the above eqns.(6.17), (6.18) and (6.19) the corresponding spring forces can be completely determined when the relative displacements are known.

6.4 Determination of the creeps between the wheels and the rails

The relative velocities in the wheel/rail contact points are used to determine the creepages between the wheels and rails. The creep contact forces depend on the creepages. When the relative motion of the wheelset is determined then the motion of the contact points on the wheel can be determined. The relative velocity and the angular velocity of the mass center of the wheelset are

$$\mathbf{v}_{wreli} = [\dot{u}_{wi} \quad \dot{v}_{wi} \quad \dot{w}_{wi}]^T, \tag{6.20}$$

$$\omega_{wreli} = \omega_{wsi} + G_{wi}\omega^*_{wi} \tag{6.21}$$

where ω_{wsi} is the angular velocity caused by the parasitic motion of the wheelset with respect to the reference system $(o_{wi}, x_{wi}, y_{wi}, z_{wi})$ and ω^*_{wi} is the angular velocity of the wheelset i about its axis of revolution with respect to the coordinate system $(o_{wi}, x_{wi}, y_{wi}, z_{wi})$. Thus we have

$$\omega_{wsi} = [\dot{\phi}_{wi} \quad 0 \quad \dot{\psi}_{wi}]^T, \qquad \omega^*_{wi} = [0 \quad -V/r \quad 0]^T \tag{6.22}$$

so together with (6.15) we have

$$\omega_{wreli} = [\dot{\phi}_{wi} + V\psi_{wi}/r \quad \dot{\chi}_{wi} - V/r \quad \dot{\psi}_{wi} - V\phi_{wi}/r]^T. \tag{6.23}$$

The transfer velocity of the wheelset is constant V and the transfer angular velocity is zero such that the total velocity of the wheelset and the total angular velocity of the wheelset i are

$$\mathbf{v}_{wi} = \begin{bmatrix} V + \dot{u}_{wi} \\ \dot{v}_{wi} \\ \dot{w}_{wi} \end{bmatrix}, \tag{6.24}$$

and

$$\omega_{wi} = \begin{bmatrix} \dot{\phi}_{wi} + V\psi_{wi}/r \\ \dot{\chi}_{wi} - V/r \\ \dot{\psi}_{wi} - V\phi_{wi}/r \end{bmatrix}. \tag{6.25}$$

For the investigation of the dynamical contact we must know the value of the wheelset velocity v_{cij} in the wheel/rail contact points, C_{wij}. We suppose the track to be rigid so the rail velocity is zero in the wheel/rail contact points. Then the velocities in the wheel/rail contact points are

$$\mathbf{v}_{cij} = \mathbf{v}_{wij} + \widetilde{\omega}_{reli}\mathbf{r}^*_{cij} \tag{6.26}$$

where the screw symmetrical matrix $\widetilde{\omega}_{reli}$ is

$$\widetilde{\omega}_{reli} = \begin{bmatrix} 0 & -(\dot{\psi}_{wi} - V\phi_{wi}/r) & \dot{\chi}_{wi} - V/r \\ \dot{\psi}_{wi} - V\phi_{wi}/r & 0 & -(\dot{\phi}_{wi} + V\psi_{wi}/r) \\ -(\dot{\chi}_{wi} - V/r) & \dot{\phi}_{wi} + V\psi_{wi}/r & 0 \end{bmatrix}, \tag{6.27}$$

and

$$\mathbf{r}^*_{cij} = \begin{bmatrix} \xi_{wij} \mp b\psi_{wi} \\ \pm(b - \eta_{wij}) - r\phi_{wi} \\ \pm b\phi_{wi} + r + \zeta_{wij} \end{bmatrix}. \tag{6.28}$$

The term to the second order in the displacement coordinates can be neglected and we find the resulting velocity vector

$$\mathbf{v}_{cij} = \begin{bmatrix} \dot{u}_{wi} + r\dot{\chi}_{wi} \mp b\dot{\psi}_{wi} - V\zeta_{wij}/r \\ \dot{v}_{wi} - r\dot{\phi}_{wi} - V\psi_{wi} \\ \dot{w}_{wi} \pm b\dot{\phi}_{wi} + V\xi_{wij}/r \pm bV\psi_{wi}/r \end{bmatrix} \tag{6.29}$$

where ξ_{wij} is defined by (5.6). The components of the $\mathbf{v}_{cij}$ projected onto the contact plane are

$$\mathbf{W}_{txynij} = \mathbf{H}_{tn}\mathbf{v}_{cij}, \quad \mathbf{\Omega}_{nij} = \mathbf{H}_{tn}\omega_{wi} \tag{6.30}$$

where $\mathbf{W}_{txynij}$ and $\mathbf{H}_{tn}$ are defined by

$$\mathbf{W}_{txynij} = [W_{txij} \quad W_{tyij} \quad W_{nij}]^T, \tag{6.31}$$

$$\mathbf{H}_{tn} = \begin{bmatrix} 1 & 0 & 0 \\ 0 & \cos\gamma_{ij} & \mp\sin\gamma_{ij} \\ 0 & \pm\sin\gamma_{ij} & \cos\gamma_{ij} \end{bmatrix}. \tag{6.32}$$

By the definition of the Eq.(5.44) the creep components are determined by

$$\upsilon_{xij} = (\dot{u}_{wi} + r\dot{\chi}_{wi} \mp b\dot{\psi}_{wi})/V - \zeta_{wij}/r, \tag{6.33}$$

$$\upsilon_{yij} = -\psi_{wi}\cos^{-1}\gamma_{ij} + (\dot{v}_{wi} - r\dot{\phi}_{wi})/V\cos\gamma_{ij} \tag{6.34}$$

and the spin is

$$\phi_{sij} = \mp r^{-1}\sin\gamma_{ij} + \dot{\psi}_{wi}\cos\gamma_{ij}/V. \tag{6.35}$$

Here in this section the index $i = 1, \cdots, 4$; $j = 1, 2$ and j =1 stands for the right rail and j =2 denotes the left rail seen in the direction of motion of the wagon. For j =1 take the upper sign of $\pm$ or $\mp$ and for j =2 take the lower sign of $\pm$ or $\mp$.

It should be pointed out that to obtain the relation (6.34) from (6.30) and (5.44) we use the fact that the relative velocity between the wheel and the rail in their common normal direction is equal to zero ($W_{nij} = 0$), i.e.

$$\dot{w}_{wi} \pm b\dot{\phi}_{wi} + V\xi_{wij}/r \pm bV\psi_{wi}/r = \mp\frac{\sin\gamma_{ij}}{\cos\gamma_{ij}}(\dot{v}_{wi} - r\dot{\phi}_{wi} - V\psi_{wi}). \tag{6.36}$$

CHAPTER 7

Dynamical equations of the Three-Piece-Freight-Truck

In this chapter a multibody-based method is applied to derive the dynamic equations of each component of the three-piece-freight-truck and then combine them with the kinematic constraints into the final dynamic system.

The model of a railway system can be divided into three parts: The vehicle subsystem, the rolling contact between the wheels and the rails and the substructure of the rails. The track can be modelled as a rigid or elastic body in different models. For the high speed passenger car the rigid or elastic assumption of the track yield clearly different results for the dynamic performance of the railway vehicle[W.Zhai,1996]. In the present thesis the track is assumed to be rigid because the speed of the three-piece-freight-truck is usually lower than $100KM/h$ so the elastic effect of the track may be neglected.

7.1 Introduction

Multibody system models have been used to investigate theoretically the dynamics of mechanical systems like vehicles, linkages and robots in an effective way. A short list of representative works, in which the reader can find a detailed presentation of the matter, is given by Haug[Haug, 1989], Sciehlen[Schiehlen,1986,1990] or Eich-Soellner[Eich-Soellner,1998].

Once the equations of motion have been set up and the inputs prepared the vehicle response can be simulated. Although various powerful computer softwares, such as ADAMAS/Rail, Simpack, NUCARS and MEDYNA, are now available to

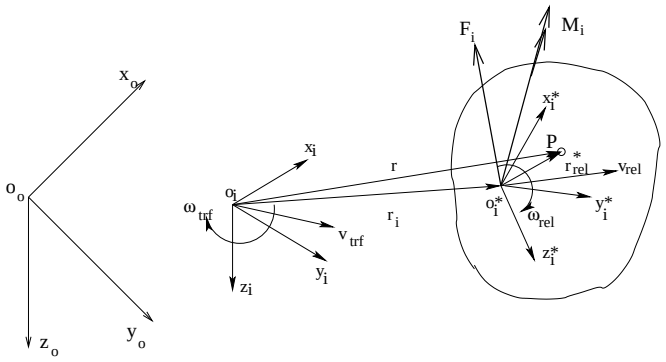

Figure 7.1: *The description of a moving body with respect to an non-inertial transfer coordinate reference system*

carry out these simulation, there still are some problems which can hardly be solved with these softwares. The stick-slip motion of the three-piece-freight-truck with two-dimensional dry friction for example and the nonlinear dynamical performances are two great challenges. The dynamics of the railway vehicles with dry friction damping have been investigated by many researchers. The dynamical performance of the three-piece-freight-truck with one dimensional dry friction was investigated by Harder [Harder, 2000], with ADAMS/Rail. The dynamic simulations of rail vehicles with friction damped Y25 bogies was provided by Evans and Rogers [Evans, 1998] using VAMPIRE and Bosso *at el.* [Bosso, 2000] with ADAMS/Rail. Detailed introduction of the development of the dynamics of the railway vehicle systems are given by Garg and Dukkipatti [Garg, 1982], Kalker [Kalker, 1990], Knothe [Knothe, 1999, 2001] and True [True, 1999].

The Newton-Euler equations of motion for the moving body i (the frame attached on the body be $(o_i^*, x_i^*, y_i^*, z_i^*)$ with respect to a transfer coordinate system (o_i, x_i, y_i, z_i) and the inertial reference frame (o_o, x_o, y_o, z_o), which are shown in Figure 7.1 are [De Pater,1999] [Schiehlen,1986]

$$m_i[\dot{\mathbf{v}}_{itrf} + \widetilde{\omega}_{itrf}\mathbf{v}_{itrf} + (\dot{\widetilde{\omega}}_{itrf} + \widetilde{\omega}^2_{itrf})\mathbf{r}_{irel} + 2\widetilde{\omega}_{itrf}\mathbf{v}_{irel} + \dot{\mathbf{v}}_{irel}] = \mathbf{f}_i, \tag{7.1}$$

$$\begin{aligned}\mathbf{I}_i\dot{\omega}_{itrf} + \widetilde{\omega}_{itrf}\mathbf{I}_i\omega_{itrf} + \widetilde{\omega}_{itrf}\omega_{itrf}(\mathbf{I}_{xi} + \mathbf{I}_{yi} + \mathbf{I}_{zi}) + \\ 2\widetilde{\omega}_{irel}\mathbf{I}_i\omega_{itrf} + \mathbf{I}_i\dot{\omega}_{irel} + \widetilde{\omega}_{irel}\mathbf{I}_i\omega_{irel} = \mathbf{m}_i.\end{aligned} \tag{7.2}$$

Here $\mathbf{f}_i$ is the total force which is applied at the body i and $\mathbf{m}_i$ is the moment of the forces applied at the body i, taken with respect to the mass center of that body.

The inertial tensor $\mathbf{I}_i$ is a variable quantity, which satisfies the relation

$$\mathbf{I}_i = G_i\mathbf{I}_i^*G_i^T \tag{7.3}$$

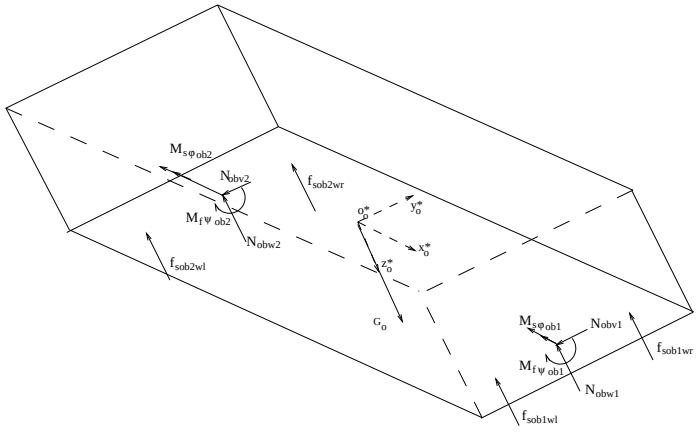

Figure 7.2: *The free body diagram of the car body*

where G_i stands for the rotation matrix of the coordinates attached to the body.

If the transfer reference coordinate system moves with a constant velocity along a straight line then the Newton-Euler equations of the motion reduce to a very simple form

$$m_i \dot{\mathbf{v}}_{irel} = \mathbf{f}_i, \tag{7.4}$$

$$\mathbf{I}_i \dot{\omega}_{irel} + \widetilde{\omega}_{irel} \mathbf{I}_i \omega_{irel} = \mathbf{m}_i. \tag{7.5}$$

When we apply equations (7.4) and (7.5) in our system to each component then the corresponding dynamic equations can be derived.

7.2 The dynamical equations of each component of the system

7.2.1 The car body

The car body is connected to the bolster via the center plates which can be modelled as a spherical joint. Because the radius of the spherical joint is small compared with the other dimensions of the car body, the effect of the friction produced by the spherical joint on the roll rotation of the car body and the bolster is neglected. But the effect of the friction torque on the yaw rotation is still considered. In other words, only one-dimensional friction is included for the friction on the surfaces of the center plates. And more the friction torque is small except on the side supports in contact with the car body through curved track, so we simply treat it as a Coulomb friction

function (1.1) with zero friction force for the strick motion state. The equations of motion of the car body can be written as

$$\mathbf{M}_o\ddot{\mathbf{q}}_o = \mathbf{f}_{sfo} + \mathbf{f}_{wo} + \mathbf{f}_{cto} \tag{7.6}$$

where the mass matrix $\mathbf{M}_o$ and the variable vector $\mathbf{q}_o$ are respectively

$$\mathbf{M}_o = \begin{bmatrix} m_o & 0 & 0 & 0 & 0 \\ 0 & m_o & 0 & 0 & 0 \\ 0 & 0 & I^*_{ox} & 0 & 0 \\ 0 & 0 & 0 & I^*_{oy} & 0 \\ 0 & 0 & 0 & 0 & I^*_{oz} \end{bmatrix}, \quad \mathbf{q}_o = \begin{bmatrix} v_o \\ w_o \\ \phi_o \\ \chi_o \\ \psi_o \end{bmatrix}. \tag{7.7}$$

The force vector $\mathbf{f}_{sfo}$ becomes

$$\mathbf{f}_{sfo} = [0 \quad f_{sfob} \quad -M_{s\phi ob1} - M_{s\phi ob2} \quad 0 \quad -M_{f\psi ob1} - M_{f\psi ob1}]^T \tag{7.8}$$

where

$$f_{sfob} = f_{sob1wl} + f_{sob1wr} + f_{sob2wl} + f_{sob2wr} \tag{7.9}$$

with

$$f_{sobiwl} = \begin{cases} k_{os}b_{os}(\phi_o - \phi_{bi}), & (\phi_o - \phi_{bi} < 0) \wedge (|b_{os}(\phi_o - \phi_{bi})| \geq \Delta_{ob})), \\ 0, & |b_{os}(\phi_o - \phi_{bi})| < \Delta_{ob}), \quad i = 1, 2 \end{cases}, \tag{7.10}$$

$$f_{sobiwr} = \begin{cases} -k_{os}b_{os}(\phi_o - \phi_{bi}), & (\phi_o - \phi_{bi} > 0) \wedge (|b_{os}(\phi_o - \phi_{bi})| \geq \Delta_{ob})), \\ 0, & |b_{os}(\phi_o - \phi_{bi})| < \Delta_{ob}), \quad i = 1, 2 \end{cases} \tag{7.11}$$

and the roll moments $M_{s\phi ob1}$ and $M_{s\phi ob2}$ which are caused by the contact between the car body and the side supports are determined by

$$M_{s\phi ob1} = \begin{cases} k_{os}b^2_{os}(\phi_o - \phi_{b1}), & |b_{os}(\phi_o - \phi_{b1})| \geq \Delta_{ob}), \\ 0, & |b_{os}(\phi_o - \phi_{b1})| < \Delta_{ob}) \end{cases}, \tag{7.12}$$

$$M_{s\phi ob2} = \begin{cases} k_{os}b^2_{os}(\phi_o - \phi_{b2}), & |b_{os}(\phi_o - \phi_{b2})| \geq \Delta_{ob}), \\ 0, & |b_{os}(\phi_o - \phi_{b2})| < \Delta_{ob}) \end{cases} \tag{7.13}$$

Here b_{os} is the distance from the center plate to the side support. k_{ob} denotes the stiffness of the side support in the vertical direction. Δ_{ob} denotes the display between the car body and the side support on the bolster. The yaw moments $M_{f\psi ob1}$ and $M_{f\psi ob2}$ caused by friction on the surfaces of the center plates and possibly on the surfaces of the side supports are

$$M_{f\psi obi} = \begin{cases} (N_{obwi}\rho_o + k_{os}b_{os}(\phi_o - \phi_{bi}))\mu_o sign(\dot{\psi}_o - \dot{\psi}_{bi}), & b_{os}|\phi_o - \phi_{bi}| \geq \Delta_{ob} \\ N_{obwi}\rho_o\mu_o sign(\dot{\psi}_o - \dot{\psi}_{bi}), & b_{os}|\phi_o - \phi_{bi}| < \Delta_{ob}, \quad i = 1, 2. \end{cases} \tag{7.14}$$

Here μ_o denotes the friction coefficient on the surfaces of the center plates and the side supports. ρ_o denotes the radius of the center plate. For the reason of simplicity we only consider the slip motion for the relative motions between the car body and the bolsters.

The weight of the car body is given by the vector $\mathbf{f}_{wo}$

$$\mathbf{f}_{wo} = [0 \quad G_o \quad 0 \quad 0 \quad 0]^T \tag{7.15}$$

and the contact force vector f_{cto} is determined by

$$\mathbf{f}_{cto} = -[N_{obv1}+N_{obv2} \quad N_{obw1}+N_{obw2} \quad 0 \quad (N_{obw2}-N_{obw1})a^*_{oc} \quad (N_{obv1}-N_{obv2})a^*_{oc}]^T. \tag{7.16}$$

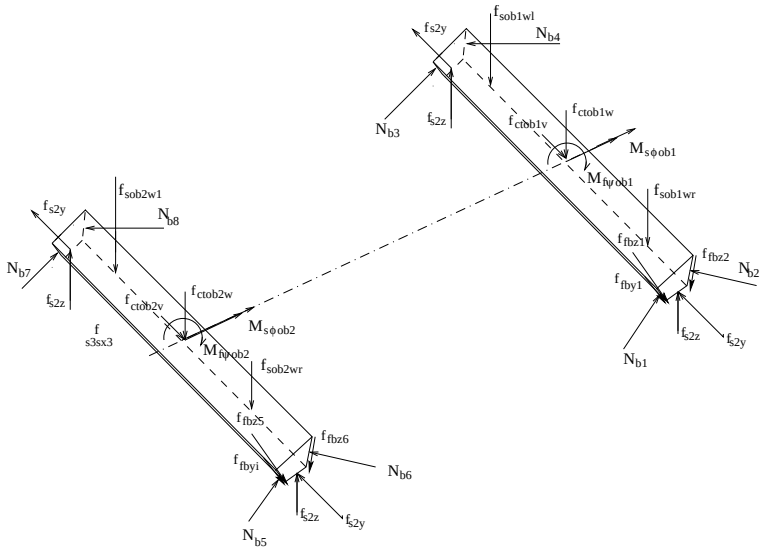

Figure 7.3: *The free body diagram of the bolsters and applied forces on them*

7.2.2 The bolsters

The equations of motion of the bolster i can be written as

$$\mathbf{M}_b\ddot{\mathbf{q}}_{bi} = \mathbf{f}_{sbi} + \mathbf{f}_{wbi} + \mathbf{f}_{ctbi} + \mathbf{f}_{fbi}, \quad i = 1, 2 \tag{7.17}$$

where the variable vector and the mass matrix are respectively

$$\ddot{\mathbf{q}}_{bi} = [\ddot{v}_{bi} \quad \ddot{w}_{bi} \quad \ddot{\phi}_{bi} \quad \ddot{\psi}_{bi}]^T, \tag{7.18}$$

$$\mathbf{M}_b = \begin{bmatrix} m_b & 0 & 0 & 0 \\ 0 & m_b & 0 & 0 \\ 0 & 0 & I_{bx} & 0 \\ 0 & 0 & 0 & I_{bz} \end{bmatrix}, \quad (i = 1, 2). \tag{7.19}$$

The spring forces and the contact forces on the bolster number 1 are determined respectively by

$$\mathbf{f}_{sb1} = - \begin{bmatrix} (k_{y2} + 2k_{y3})(v_{b1} - v_{f1}) + (k_{y2} + 2k_{y3})(v_{b1} - v_{f2}) \\ k_{z2}(w_{b1} - w_{f1}) + k_{z2}(w_{b1} - w_{f2}) + f_{sob1wl} + f_{sob1wr} \\ 2b_{bs2}^{*2} k_{z2}\phi_{b1} - M_{s\phi ob1} \\ k_{\psi bf}(\psi_{b1} - \psi_{f1}) + k_{\psi bf}(\psi_{b1} - \psi_{f2}) \end{bmatrix}, \tag{7.20}$$

$$\mathbf{f}_{ctb1} = \begin{bmatrix} 0 \\ -(N_{b1} + N_{b2} + N_{b3} + N_{b4}) \sin\phi \\ (-N_{b1} - N_{b2} + N_{b3} + N_{b4}) \sin\phi b_{bs2}^* \\ M_{ctbd1} \end{bmatrix} + \begin{bmatrix} N_{obv1} \\ N_{obw1} \\ N_{obv1} h_{bc}^* \\ 0 \end{bmatrix} \tag{7.21}$$

where the h_{bc}^* denotes the distance from the center plate to the line through the mass center of the bolster.

The spring forces and the contact forces on the bolster number 2 are

$$\mathbf{f}_{sb2} = - \begin{bmatrix} (k_{y2} + 2k_{y3})(v_{b2} - v_{f3}) + (k_{y2} + 2k_{y3})(v_{b2} - v_{f4}) \\ k_{z2}(w_{b2} - w_{f3}) + k_{z2}(w_{b2} - w_{f4}) + f_{sob2wl} + f_{sob2wr} \\ 2b_{bs2}^{*2} k_{z2}\phi_{b2} - M_{s\phi ob2} \\ k_{\psi bf}(\psi_{b2} - \psi_{f3}) + k_{\psi bf}(\psi_{b2} - \psi_{f4}) \end{bmatrix}, \tag{7.22}$$

$$\mathbf{f}_{ctb2} = \begin{bmatrix} 0 \\ -(N_{b5} + N_{b6} + N_{b7} + N_{b8}) \sin\phi \\ (-N_{b5} - N_{b6} + N_{b7} + N_{b8}) \sin\phi b_{bs2}^* \\ M_{ctbd2} \end{bmatrix} + \begin{bmatrix} N_{obv2} \\ N_{obw2} \\ N_{obv2} h_{bc}^* \\ 0 \end{bmatrix} \tag{7.23}$$

in which $k_{\psi bf}$ denotes the anti-warp stiffness (effective warp stiffness). The anti-warp stiffness is a state-dependent variable. For the sake of simplicity here we take it as a constant. M_{ctb1} denotes the torque produced by the contact force on the contact surface of the wedges in the longitudinal direction. We will see that it can be eliminated from the final dynamical system in the next section.

The friction forces on the bolster number 1 are determined by

$$\mathbf{f}_{fb1} = \begin{bmatrix} -\mu_d(S_{d1}\cos\theta_{d1} + S_{d2}\cos\theta_{d2} + S_{d3}\cos\theta_{d3} + S_{d4}\cos\theta_{d4}) \\ -\mu_b\cos\phi(N_{b1}\sin\theta_{b1} + N_{b2}\sin\theta_{b2} + N_{b3}\sin\theta_{b3} + N_{b4}\sin\theta_{b4}) \\ b_{bs2}^*\mu_b\cos\phi(-N_{b1}\sin\theta_{b1} - N_{b2}\sin\theta_{b2} + N_{b3}\sin\theta_{b3} + N_{b4}\sin\theta_{b4}) \\ M_{f\psi ob1} + M_{f\psi bd1} \end{bmatrix} \tag{7.24}$$

and on the bolster number 2 are calculated by

$$\mathbf{f}_{fb2} = \begin{bmatrix} -\mu_d(S_{d5}\cos\theta_{d5} + S_{d6}\cos\theta_{d6} + S_{d7}\cos\theta_{d7} + S_{d8}\cos\theta_{d8}) \\ -\mu_b\cos\phi(N_{b5}\sin\theta_{b5} + N_{b6}\sin\theta_{b6} + N_{b7}\sin\theta_{b7} + N_{b8}\sin\theta_{b8}) \\ b_{bs2}^*\mu_b\cos\phi(-N_{b5}\sin\theta_{b5} - N_{b6}\sin\theta_{b6} + N_{b7}\sin\theta_{b7} + N_{b8}\sin\theta_{b8}) \\ M_{f\psi ob2} + M_{f\psi bd2} \end{bmatrix} \tag{7.25}$$

where μ_d, μ_b stand for the friction coefficients on the surfaces of the wedge contacting the frame and bolster respectively. $M_{f\psi bd1,2}$ denotes the torque produced by the longitudinal friction force on the contact surface between the bolsters and wedges and it can be eliminated in the final dynamic system. In the present thesis the effect of the friction torque produced by the lateral friction force component on the surfaces of the wedges contacting the frames are neglected.

Finally the components of the weight of the bolsters are

$$\mathbf{f}_{wbi} = G_b \begin{bmatrix} 0 \\ \cos(z_g, y_{bi}) \\ \cos(z_g, z_{bi}) \\ 0 \\ 0 \end{bmatrix}, \quad (i = 1, 2) \tag{7.26}$$

where G_b denotes the weight of the bolster and z_g stands for the vertical line.

7.2.3 The wedges

In the analysis of the motions of the wedge the effect of the torque acting on it can be neglected. We consider here the motions in the longitudinal, lateral and vertical directions. The equations of motion for the wedge i is (see Figure 7.4)

$$m_d \begin{bmatrix} \ddot{u}_{di} \\ \ddot{v}_{di} \\ \ddot{w}_{di} \end{bmatrix} = \mathbf{f}_{sdi} + \mathbf{f}_{fdi} + \mathbf{f}_{ctdi} + \mathbf{f}_{wdi}, \quad (i = 1, \cdots, 8) \tag{7.27}$$

where the spring force vector related to the bolster number 1 is determined by

$$\mathbf{f}_{sdi} = - \begin{bmatrix} (-1)^i k_{x3} \frac{\sin\gamma \sin\phi}{\sin(\gamma+\phi)} (w_{b1} + b^*_{bs2}\phi_{b1} - w_{f1}) \\ k_{y3}(v_{di} - v_{f1}) \\ k_{z3} \frac{\cos\gamma \sin\phi}{\sin(\gamma+\phi)} (w_{b1} + b^*_{bs2}\phi_{b1} - w_{f1}) \end{bmatrix}, \quad (i = 1, 2), \tag{7.28}$$

$$\mathbf{f}_{sdj} = - \begin{bmatrix} (-1)^j k_{x3} \frac{\sin\gamma \sin\phi}{\sin(\gamma+\phi)} (w_{b1} - b^*_{bs2}\phi_{b1} - w_{f2}) \\ k_{y3}(v_{dj} - v_{f2}) \\ k_{z3} \frac{\cos\gamma \sin\phi}{\sin(\gamma+\phi)} (w_{b1} + b^*_{bs2}\phi_{b1} - w_{f2}) \end{bmatrix}, \quad (j = 3, 4) \tag{7.29}$$

and to the bolster number 2 is determined by

$$\mathbf{f}_{sdk} = - \begin{bmatrix} (-1)^k k_{x3} \frac{\sin\gamma \sin\phi}{\sin(\gamma+\phi)} (w_{b2} + b^*_{bs2}\phi_{b2} - w_{f3}) \\ k_{y3}(v_{dk} - v_{f3}) \\ k_{z3} \frac{\cos\gamma \sin\phi}{\sin(\gamma+\phi)} (w_{b2} + b^*_{bs2}\phi_{b2} - w_{f3}) \end{bmatrix}, \quad (k = 5, 6), \tag{7.30}$$

$$\mathbf{f}_{sdm} = - \begin{bmatrix} (-1)^m k_{x3} \frac{\sin\gamma \sin\phi}{\sin(\gamma+\phi)} (w_{b2} - b^*_{bs2}\phi_{b2} - w_{f4}) \\ k_{y3}(v_{dm} - v_{f4}) \\ k_{z3} \frac{\cos\gamma \sin\phi}{\sin(\gamma+\phi)} (w_{b2} - b^*_{bs2}\phi_{b2} - w_{f4}) \end{bmatrix}, \quad (m = 7, 8). \tag{7.31}$$

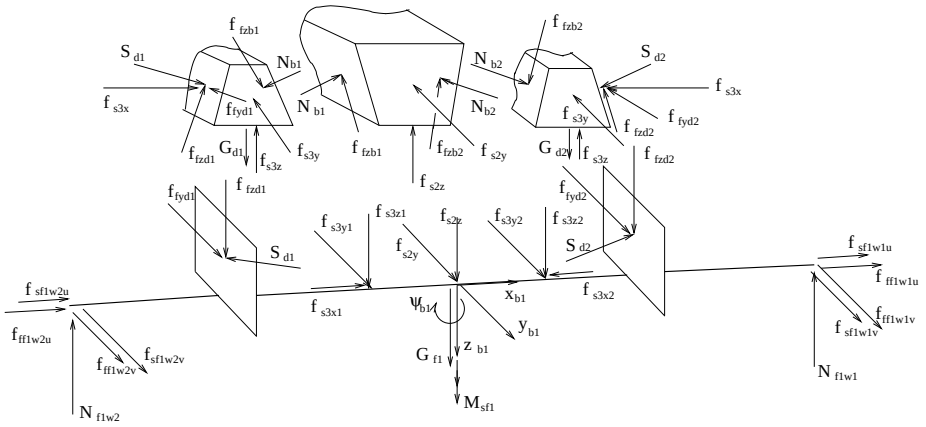

Figure 7.4: *The free body diagram of the wedges 1, 2 and the frame 1 and the reacting forces on them*

The components of the weight of the wedge are

$$\mathbf{f}_{wdi} = [0 \quad 0 \quad G_d]^T, \quad (1 = 1, 2, \cdots, 8) \tag{7.32}$$

where G_d denotes the weight of the wedge.

The contact force vector $\mathbf{f}_{ctdi}$ is determined by

$$\mathbf{f}_{ctdi} = \begin{bmatrix} (-1)^{i+1} S_{di} \cos\gamma + (-1)^i N_{bi} \cos\phi \\ 0 \\ S_{di} \sin\gamma + N_{bi} \sin\phi \end{bmatrix}, \quad (i = 1, \ldots, 8). \tag{7.33}$$

Finally, the friction forces are given by

$$\mathbf{f}_{fdi} = \begin{bmatrix} (-1)^{i+1} S_{di} \mu_d \sin\theta_{di} \sin\gamma + (-1)^{i+1} N_{di} \mu_b \sin\theta_{bi} \sin\phi \\ N_{di} \mu_b \cos\theta_{bi} - S_{di} \mu_d \cos\theta_{di} \\ N_{di} \mu_b \sin\theta_{bi} \cos\phi - S_{di} \mu_d \sin\theta_{di} \cos\gamma \end{bmatrix}, \quad (i = 1, \cdots, 8) \tag{7.34}$$

where the friction direction angles θ_{di} and θ_{bi} on the surfaces of the wedge can be determined in the way introduced in chapter 2 and 3.

7.2.4 The side frames

There are no primary suspensions between the side frames and the wheelsets so there exist only the state-dependent normal forces and the nonsmooth tangent dry friction forces on the contact surfaces between the side frames and the wheelsets. More if the clearances between the side frames and the wheelsets both in longitudinal and

lateral directions are taken up then a soft impact will take place. It means that the kinematic constraints between the side frames and the wheelsets are provided only by dry friction when the clearances are free. We use the dead-band stops to describe the clearances and the soft impacts. The dynamical equations for the side frame i can be written as

$$\mathbf{M}_f\ddot{\mathbf{q}}_{fi} = \mathbf{f}_{sfi} + \mathbf{f}_{wfi} + \mathbf{f}_{ffi} + \mathbf{f}_{ctfi} + \mathbf{f}_{ffwi}, \quad (i = 1, 2, 3, 4) \tag{7.35}$$

where the mass matrix and the variable vector are defined by

$$\mathbf{M}_f = \begin{bmatrix} m_f & 0 & 0 & 0 & 0 \\ 0 & m_f & 0 & 0 & 0 \\ 0 & 0 & m_f & 0 & 0 \\ 0 & 0 & 0 & I_{fy} & 0 \\ 0 & 0 & 0 & 0 & I_{fz} \end{bmatrix}, \quad \ddot{\mathbf{q}}_{fi} = \begin{bmatrix} \ddot{u}_{fi} \\ \ddot{v}_{fi} \\ \ddot{w}_{fi} \\ \ddot{\chi}_{fi} \\ \ddot{\psi}_{fi} \end{bmatrix}. \tag{7.36}$$

The spring forces on the side frames are determined by

$$\mathbf{f}_{sf1} = \begin{bmatrix} f_{sf1w1u} + f_{sf1w2u} \\ f_{sf1w1v} + f_{sf1w2v} + (k_{y2} + 2k_{y3})(v_{b1} - v_{f1}) \\ k_{z2}(w_{b1} + b^*_{bs2}\phi_{b1} - w_{f1}) + k_{z3}(w_{b1} + b^*_{bs2}\phi_{b1} - w_{f1})C\gamma S\phi \\ 0 \\ (f_{sf1w1v} - f_{sf1w2v})a_{wb} + k_{\psi bf}(\psi_{b1} - \psi_{f1}) \end{bmatrix}, \tag{7.37}$$

$$\mathbf{f}_{sf2} = \begin{bmatrix} f_{sf2w1u} + f_{sf2w2u} \\ f_{sf2w1v} + f_{sf2w2v} + (k_{y2} + 2k_{y3})(v_{b1} - v_{f2}) \\ k_{z2}(w_{b1} + b^*_{bs2}\phi_{b1} - w_{f2}) + k_{z3}(w_{b1} + b^*_{bs2}\phi_{b1} - w_{f2})C\gamma S\phi \\ 0 \\ (f_{sf2w1v} - f_{sf2w2v})a_{wb} + k_{\psi bf}(\psi_{b1} - \psi_{f2}) \end{bmatrix}, \tag{7.38}$$

$$\mathbf{f}_{sf3} = \begin{bmatrix} f_{sf3w3u} + f_{sf3w4u} \\ f_{sf3w3v} + f_{sf3w4v} + (k_{y2} + 2k_{y3})(v_{b2} - v_{f3}) \\ k_{z2}(w_{b2} + b^*_{bs2}\phi_{b2} - w_{f3}) + k_{z3}(w_{b2} + b^*_{bs2}\phi_{b2} - w_{f3})C\gamma S\phi \\ 0 \\ (f_{sf3w3v} - f_{sf3w4v})a_{wb} + k_{\psi bf}(\psi_{b2} - \psi_{f3}) \end{bmatrix}, \tag{7.39}$$

$$\mathbf{f}_{sf4} = \begin{bmatrix} f_{sf4w3u} + f_{sf4w4u} \\ f_{sf4w3v} + f_{sf4w4v} + (k_{y2} + 2k_{y3})(v_{b2} - v_{f4}) \\ k_{z2}(w_{b2} + b^*_{bs2}\phi_{b2} - w_{f4}) + k_{z3}(w_{b2} + b^*_{bs2}\phi_{b2} - w_{f4})C\gamma S\phi \\ 0 \\ (f_{sf4w3v} - f_{sf4w4v})a_{wb} + k(\psi_{b2} - \psi_{f4}) \end{bmatrix} \tag{7.40}$$

in which $C\gamma S\phi$ is the short expression of $\frac{cos\gamma sin\phi}{sin(\gamma+\phi)}$. The spring forces(impact forces) between the wheelsets and the side frames in longitudinal direction are determined by

$$f_{sfjwku} = \begin{cases} 0, & |\Delta u_{fwi}| \le \Delta x_f \\ k_{x1}(\Delta u_{fwi} - sign(\Delta u_{fwi})\Delta x_f), & |\Delta u_{fwi}| > \Delta x_f \end{cases} \tag{7.41}$$

where $(i = 1, \cdots, 8; \quad j, k = 1, \cdots, 4)$ and

$$\Delta u_{fw1} = -b^*_{bs2}\psi_{b1} + h_f\chi_{f1} - (u_{w1} - b_{ws}\psi_{w1}), \tag{7.42}$$

$$\Delta u_{fw2} = -b^*_{bs2}\psi_{b1} - h_f\chi_{f1} - (u_{w2} - b_{ws}\psi_{w2}), \tag{7.43}$$

$$\Delta u_{fw3} = b^*_{bs2}\psi_{b1} + h_f\chi_{f2} - (u_{w1} - b_{ws}\psi_{w1}), \tag{7.44}$$

$$\Delta u_{fw4} = b^*_{bs2}\psi_{b1} - h_f\chi_{f1} - (u_{w2} - b_{ws}\psi_{w2}), \tag{7.45}$$

$$\Delta u_{fw5} = -b^*_{bs2}\psi_{b2} + h_f\chi_{f3} - (u_{w3} - b_{ws}\psi_{w3}), \tag{7.46}$$

$$\Delta u_{fw6} = -b^*_{bs2}\psi_{b2} - h_f\chi_{f3} - (u_{w4} - b_{ws}\psi_{w4}), \tag{7.47}$$

$$\Delta u_{fw7} = b^*_{bs2}\psi_{b2} + h_f\chi_{f4} - (u_{w4} - b_{ws}\psi_{w3}), \tag{7.48}$$

$$\Delta u_{fw8} = b^*_{bs2}\psi_{b2} - h_f\chi_{f4} - (u_{w3} - b_{ws}\psi_{w4}) \tag{7.49}$$

where h_f denotes the distance from the mass center of the frame to the contact surface between the frame and the adapter in the vertical direction; Δx_f stands for the clearance between the frame and the adapter in the longitudinal direction. The spring forces (impact forces) between the wheelsets and the side frames in lateral direction are determined by

$$f_{sfjwkv} = \begin{cases} 0, & |\Delta v_{fwi}| \le \Delta y_f \\ k_{y1}(\Delta v_{fwi} - sign(\Delta v_{fwi})\Delta y_f), & |\Delta v_{fwi}| > \Delta y_f \end{cases} \tag{7.50}$$

where

$$\Delta v_{fw1} = v_{f1} + \psi_{f1}a_{wb} - v_{w1}, \tag{7.51}$$

$$\Delta v_{fw2} = v_{f1} - \psi_{f1}a_{wb} - v_{w2}, \tag{7.52}$$

$$\Delta v_{fw3} = v_{f2} + \psi_{f2}a_{wb} - v_{w1}, \tag{7.53}$$

$$\Delta v_{fw4} = v_{f2} - \psi_{f2}a_{wb} - v_{w2}, \tag{7.54}$$

$$\Delta v_{fw5} = v_{f3} + \psi_{f3}a_{wb} - v_{w3}, \tag{7.55}$$

$$\Delta v_{fw6} = v_{f3} - \psi_{f3}a_{wb} - v_{w4}, \tag{7.56}$$

$$\Delta v_{fw7} = v_{f4} + \psi_{f4}a_{wb} - v_{w4}, \tag{7.57}$$

$$\Delta v_{fw8} = v_{f4} - \psi_{f4}a_{wb} - v_{w4} \tag{7.58}$$

where Δy_f stands for the clearance between the frame and the adapter in the lateral direction.

The components of the weight of the side frames read

$$\mathbf{f}_{wfi} = [0 \qquad 0 \qquad G_f \qquad 0 \qquad 0]^T, \quad (i = 1, 2, 3, 4) \tag{7.59}$$

The contact forces and the friction forces on the surfaces of the wedges contacting the side frames are determined by

$$\mathbf{f}_{ctfi} = -\begin{bmatrix} N_{ctbdi} \\ 0 \\ S_{di}\sin\gamma + N_{fiw1} + N_{fiw2} \\ a_{wb}(N_{fiw2} - N_{fiw1}) \\ 0 \end{bmatrix}, (i = 1, 2), \tag{7.60}$$

$$\mathbf{f}_{ctfi} = -\begin{bmatrix} N_{ctbdi} \\ 0 \\ S_{di}\sin\gamma + N_{fiw3} + N_{fiw4} \\ a_{wb}(N_{fiw4} - N_{fiw3}) \\ 0 \end{bmatrix}, (i = 3, 4), \tag{7.61}$$

$$\mathbf{f}^*_{ffi} = \begin{bmatrix} N_{fbdj} \\ \mu_d(S_{di}\cos\theta_{di} + S_{dk}\cos\theta_{dk}) \\ \mu_d\cos\gamma(S_{di}\sin\theta_{di} + S_{dk}\sin\theta_{dk}) \\ 0 \\ a_d\mu_d(S_{di}\cos\theta_{di} - S_{dk}\cos\theta_{dk}) \end{bmatrix}, \quad j = 1, \cdots, 4 \tag{7.62}$$

where $i = 1, 3, 5, 7$; $k = i + 1$ and $\mathbf{f}_{ff1} = \mathbf{f}^*_{ff1}$, $\mathbf{f}_{ff2} = \mathbf{f}^*_{ff3}$, $\mathbf{f}_{ff3} = \mathbf{f}^*_{ff5}$, $\mathbf{f}_{ff4} = \mathbf{f}^*_{ff7}$. a_d denotes the distance from the mass center of the wedge to the mass center of the bolster in the longitudinal direction. We will see that the contact force N_{ctbdi} and the friction force N_{fbdi} can be eliminated in the final dynamic system.

And finally the friction on the top surfaces of the adapters are determined by

$$\mathbf{f}_{ffw1} = \begin{bmatrix} f_{fwu1} \\ f_{fwv1} \\ f_{fww1} \\ f_{fw\chi 1} \\ f_{fw\psi 1} \end{bmatrix} = \begin{bmatrix} \mu_f(N_{f1w1}C\theta_{f1} + N_{f1w2}C\theta_{f2}) \\ \mu_f(N_{f1w1}S\theta_{f1} + N_{f1w2}S\theta_{f2}) \\ 0 \\ 0 \\ a_{wb}\mu_f(N_{f1w1}S\theta_{f1} - N_{f1w2}S\theta_{f2}) \end{bmatrix}, \tag{7.63}$$

$$\mathbf{f}_{ffw2} = \begin{bmatrix} f_{fwu2} \\ f_{fwv2} \\ f_{fww2} \\ f_{fw\chi 2} \\ f_{fw\psi 2} \end{bmatrix} = \begin{bmatrix} \mu_f(N_{f2w1}C\theta_{f3} + N_{f2w2}C\theta_{f4}) \\ \mu_f(N_{f2w1}S\theta_{f3} + N_{f2w2}S\theta_{f4}) \\ 0 \\ 0 \\ a_{wb}\mu_f(N_{f2w1}S\theta_{f3} - N_{f2w2}S\theta_{f4}) \end{bmatrix}, \tag{7.64}$$

$$\mathbf{f}_{ffw3} = \begin{bmatrix} f_{fwu3} \\ f_{fwv3} \\ f_{fww3} \\ f_{fw\chi 3} \\ f_{fw\psi 3} \end{bmatrix} = \begin{bmatrix} \mu_f(N_{f3w3}C\theta_{f5} + N_{f3w4}C\theta_{f6}) \\ \mu_f(N_{f3w3}S\theta_{f5} + N_{f3w4}S\theta_{f6}) \\ 0 \\ 0 \\ a_{wb}\mu_f(N_{f3w3}S\theta_{f5} - N_{f3w4}S\theta_{f6}) \end{bmatrix} \tag{7.65}$$

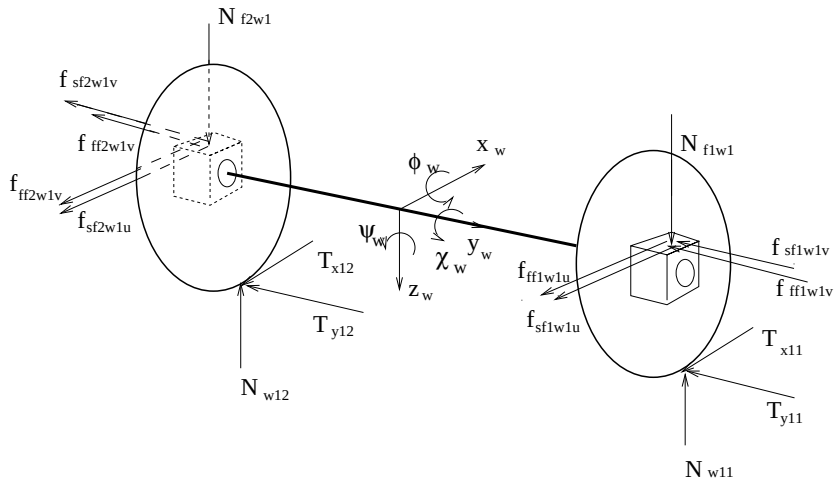

Figure 7.5: *The free body diagram of the wheelset number 1 and the reacting forces on it*

and

$$\mathbf{f}_{ffw4} = \begin{bmatrix} f_{fwu4} \\ f_{fwv4} \\ f_{fww4} \\ f_{fw\chi 4} \\ f_{fw\psi 4} \end{bmatrix} = \begin{bmatrix} \mu_f(N_{f4w3}C\theta_{f7} + N_{f4w4}C\theta_{f8}) \\ \mu_f(N_{f4w3}S\theta_{f7} + N_{f4w4}S\theta_{f8}) \\ 0 \\ 0 \\ a_{wb}\mu_f(N_{f4w3}S\theta_{f7} - N_{f4w4}S\theta_{f8}) \end{bmatrix} \tag{7.66}$$

where the friction direction angle θ_{fi} is determined in the way introduced in chapter 2 and 3. $S\theta$ and $C\theta$ are the short expressions of the $sin\theta$ and $cos\theta$ respectively.

7.2.5 The wheelsets

The wheelsets provide the supports for the entire vehicle and supply the contact forces that keep the vehicle system on the track. The interconnection between the wheelsets and the side frames are through the adapters. The adapters can be considered as bearings with very small mass therefore their effect on the motion of the system can be neglected. Furthermore the friction between the adapters and the wheelsets are neglected in our investigation. The inertial tensor of a wheelset with respect to its axle is

$$\mathbf{I}_w^* = \begin{bmatrix} I_{wx} & 0 & 0 \\ 0 & I_{wy} & 0 \\ 0 & 0 & I_{wz} \end{bmatrix}. \tag{7.67}$$

where $I_{wx} = I_{wz}$ due to the rotational symmetry. By means of the rotation matrix $\mathbf{G}_{wi}$ the inertial tensor can be transformed to[De Pater, 1997]

$$\mathbf{I}_w = \mathbf{I}_w^* + (I_{wx} - I_{wy}) \begin{bmatrix} 0 & \psi_{wi} & 0 \\ \psi_{wi} & 0 & -\phi_{wi} \\ 0 & -\phi_{wi} & 0 \end{bmatrix}. \tag{7.68}$$

The dynamical equations of the wheelset i reads

$$\mathbf{M}_w \ddot{\mathbf{q}}_{wi} = \mathbf{f}_{gwi} + \mathbf{f}_{swi} + \mathbf{f}_{nfwi} + \mathbf{f}_{wwi} + \mathbf{f}_{fwi} + \mathbf{f}_{twi} + \mathbf{f}_{ctwi} \tag{7.69}$$

where the mass matrix and the components of the variable vector are defined by

$$\mathbf{M}_w = \begin{bmatrix} m_w\mathbf{E} & \mathbf{0} \\ \mathbf{0} & \mathbf{I}_w^* \end{bmatrix}, \quad \ddot{\mathbf{q}}_{wi} = [\ddot{u}_{wi}, \quad \ddot{v}_{wi}, \quad \ddot{w}_{wi}, \quad \ddot{\phi}_{wi}, \quad \ddot{\chi}_{wi}, \quad \ddot{\psi}_{wi}]^T. \tag{7.70}$$

Here $\mathbf{E}$ is the 3×3 unit matrix and from (6.27) and (7.5) the gyroscopic force $\mathbf{f}_{gwi}$ is

$$\mathbf{f}_{gwi} = -\frac{I_{wy}V}{r} \begin{bmatrix} 0 \\ 0 \\ 0 \\ \dot{\psi}_{wi} \\ 0 \\ -\dot{\phi}_{wi} \end{bmatrix}, \quad (i = 1, 2, 3, 4). \tag{7.71}$$

$\mathbf{f}_{swi}$ are the dead-band stop spring force vectors (see (7.41) and (7.50)) applied at the wheelset i. They read

$$\mathbf{f}_{sw1} = - \begin{bmatrix} f_{sf1w1u} + f_{sf2w1u} \\ f_{sf1w1v} + f_{sf2w1v} \\ 0 \\ 0 \\ 0 \\ (f_{sf2w1u} - f_{sf1w1u})b_{ws} \end{bmatrix}, \mathbf{f}_{sw2} = - \begin{bmatrix} f_{sf1w2u} + f_{sf2w2u} \\ f_{sf1w2v} + f_{sf2w2v} \\ 0 \\ 0 \\ 0 \\ (f_{sf2w2u} - f_{sf1w2u})b_{ws} \end{bmatrix} \tag{7.72}$$

$$\mathbf{f}_{sw3} = - \begin{bmatrix} f_{sf3w3u} + f_{sf4w3u} \\ f_{sf3w3v} + f_{sf4w3v} \\ 0 \\ 0 \\ 0 \\ (f_{sf4w3u} - f_{sf3w3u})b_{ws} \end{bmatrix}, \mathbf{f}_{sw4} = - \begin{bmatrix} f_{sf3w4u} + f_{sf4w4u} \\ f_{sf3w4v} + f_{sf4w4v} \\ 0 \\ 0 \\ 0 \\ (f_{sf4w4u} - f_{sf3w4u})b_{ws} \end{bmatrix} \tag{7.73}$$

$\mathbf{f}_{fwi}$ are the kinetic friction force vectors applied at the wheelset i. They are

$$\mathbf{f}_{fw1} = - \begin{bmatrix} \mu_f(N_{f1w1}C\theta_{f1} + N_{f2w1}C\theta_{f3}) \\ \mu_f(N_{f1w1}S\theta_{f1} + N_{f2w1}S\theta_{f3}) \\ 0 \\ 0 \\ 0 \\ b_{ws}\mu_f(N_{f2w1}S\theta_{f3} - N_{f1w1}S\theta_{f1}) \end{bmatrix}, \tag{7.74}$$

$$\mathbf{f}_{fw2} = -\begin{bmatrix} \mu_f(N_{f1w2}C\theta_{f2} + N_{f2w2}C\theta_{f4}) \\ \mu_f(N_{f1w2}S\theta_{f2} + N_{f2w2}S\theta_{f4}) \\ 0 \\ 0 \\ 0 \\ b_{ws}\mu_f(N_{f2w2}S\theta_{f4} - N_{f1w2}S\theta_{f2}) \end{bmatrix}, \tag{7.75}$$

$$\mathbf{f}_{fw3} = -\begin{bmatrix} \mu_f(N_{f3w3}C\theta_{f5} + N_{f4w3}C\theta_{f7}) \\ \mu_f(N_{f3w3}S\theta_{f5} + N_{f4w3}S\theta_{f7}) \\ 0 \\ 0 \\ 0 \\ b_{ws}\mu_f(N_{f4w3}S\theta_{f7} - N_{f3w3}S\theta_{f5}) \end{bmatrix} \tag{7.76}$$

and

$$\mathbf{f}_{fw4} = -\begin{bmatrix} \mu_f(N_{f3w4}C\theta_{f6} + N_{f4w4}C\theta_{f8}) \\ \mu_f(N_{f3w4}S\theta_{f6} + N_{f4w4}S\theta_{f8}) \\ 0 \\ 0 \\ 0 \\ b_{ws}\mu_f(N_{f4w4}S\theta_{f8} - N_{f3w4}S\theta_{f6}) \end{bmatrix} \tag{7.77}$$

and the contact forces on the surfaces between the frames and the wheelsets are

$$\mathbf{f}_{nfw1} = \begin{bmatrix} 0 \\ 0 \\ N_{f1w1} + N_{f2w1} \\ b_{ws}(N_{f1w1} - N_{f2w1}) \\ 0 \\ 0 \end{bmatrix}, \quad \mathbf{f}_{nfw2} = \begin{bmatrix} 0 \\ 0 \\ N_{f1w2} + N_{f2w2} \\ b_{ws}(N_{f1w2} - N_{f2w2}) \\ 0 \\ 0 \end{bmatrix}, \tag{7.78}$$

$$\mathbf{f}_{nfw3} = \begin{bmatrix} 0 \\ 0 \\ N_{f3w3} + N_{f4w3} \\ b_{ws}(N_{f3w3} - N_{f4w3}) \\ 0 \\ 0 \end{bmatrix}, \quad \mathbf{f}_{nfw4} = \begin{bmatrix} 0 \\ 0 \\ N_{f3w4} + N_{f4w4} \\ b_{ws}(N_{f3w4} - N_{f4w4}) \\ 0 \\ 0 \end{bmatrix}. \tag{7.79}$$

The weights of the wheelsets are

$$\mathbf{f}_{wwi} = [0 \quad G_w cos(z_g, y_{wi}) \quad G_w cos(z_g, z_{wi}) \quad 0 \quad 0 \quad 0]^T. \tag{7.80}$$

The normal load of the wheelset on the rail, $\mathbf{f}_{ctwi}$ has already been determined in chapter 5. We can use the creepage between the wheels and rails to determine the tangent contact forces as we have done in chapter 5. The tangential contact forces

and the normal forces of the four wheelsets can be written in the matrix form

$$\mathbf{f}_{twi} = -\mathbf{H}_{ti} \begin{bmatrix} T_{xi1} \\ T_{yi1} \\ T_{xi2} \\ T_{yi2} \end{bmatrix}, \quad \mathbf{f}_{ctwi} = -\mathbf{H}_{ni} \begin{bmatrix} N_{wi1} \\ N_{wi2} \end{bmatrix}, \quad i = 1, \cdots, 4 \tag{7.81}$$

in which the coefficient matrices $\mathbf{H}_{ti}$ and $\mathbf{H}_{ni}$ are defined by

$$\mathbf{H}_{ti} = \begin{bmatrix} 1 & 0 & 1 & 0 \\ 0 & cos\gamma_{i1} & 0 & cos\gamma_{i2} \\ 0 & -sin\gamma_{i1} & 0 & -sin\gamma_{i2} \\ 0 & -r_{i1}cos\gamma_{i1} & 0 & -r_{i2}cos\gamma_{i2} \\ r_{i1} & 0 & r_{i2} & 0 \\ -b_{i1} & 0 & b_{i2} & 0 \end{bmatrix}, \quad i = 1, \cdots, 4, \tag{7.82}$$

$$\mathbf{H}_{ni} = \begin{bmatrix} 0 & 0 \\ -sin\gamma_{i1} & -sin\gamma_{i2} \\ cos\gamma_{i1} & cos\gamma_{i2} \\ b_{i1}cos\gamma_{i1} & -b_{i2}cos\gamma_{i2} \\ 0 & 0 \\ 0 & 0 \end{bmatrix}, \quad i = 1, \cdots, 4. \tag{7.83}$$

Here r_i denotes the rolling radius and b_i is the distance from the mass center to the wheel/rail contact point. The index 1 denotes the right-hand side rail and 2 stands for the left-hand side rail seen in the direction of motion of the vehicle.

7.2.6 The effect of the tractive effort on the contact forces on the surfaces of the wedges

Finally, we treat the tractive effort on the car body. We assume that the force is applied at the point on the line through the mass center of the car body. If it is not the case a torque should be added. As Figure 7.6 shows, the equations for the free body of half the bolster are

$$N_1 \sin\phi + N_1\mu_b \cos\phi + N_2 \sin\phi + N_2\mu_b \cos\phi = N_{ob1}, \tag{7.84}$$

$$N_2 \cos\phi + N_2\mu_b \sin\phi = N_1 \cos\phi + N_1\mu_b \sin\phi + L_{ob1} \tag{7.85}$$

where

$$L_{ob1} = F_{ffw1u} + F_{sfw1u}. \tag{7.86}$$

The solutions for N_1 and N_2 are

$$N_1 = \frac{N_{ob1}}{2(\sin\phi + \mu_b \cos\phi)} - \frac{L_{ob1}}{2(\cos\phi + \mu_b \sin\phi)}, \tag{7.87}$$

$$N_2 = \frac{N_{ob1}}{2(\sin\phi + \mu_b \cos\phi)} + \frac{L_{ob1}}{2(\cos\phi + \mu_b \sin\phi)}. \tag{7.88}$$

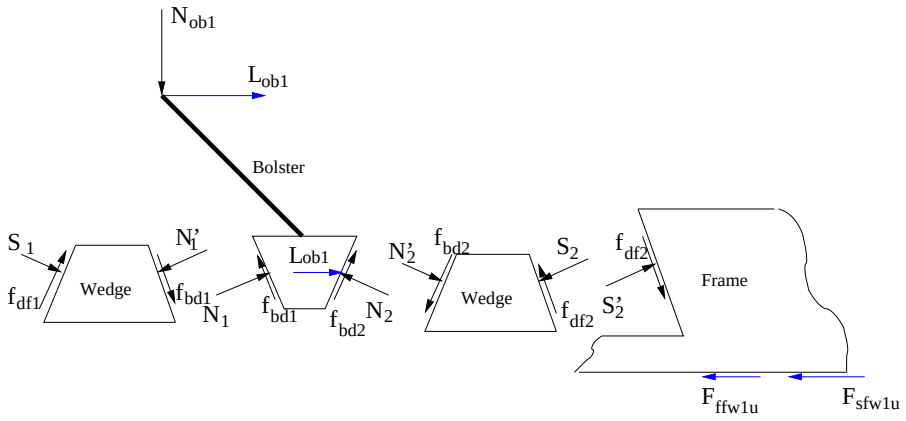

Figure 7.6: *The free body diagram of the bolster, the wedge and the frame. The* L_{ob1} *denotes the tractive effort on the bolster*

If the condition

$$L_{ob1} = N_{ob1}\frac{\cos\phi + \mu_b \sin\phi}{\sin\phi + \mu_b \cos\phi} \tag{7.89}$$

is fulfilled then the normal contact force N_1 will be zero. In consequence, for the motion of the bolster in the upwards vertical direction and if its displacement is less than its initial displacement then the normal forces on the surfaces of the wedge will also be zero and the numerical results will be provided in chapter 9. For the case of the $N_1 = 0$, then from eqns. (7.84) and (7.85)

$$N_2 = \frac{N_{ob1}}{\sin\phi + \mu_b \cos\phi} + \frac{L_{ob1}}{\cos\phi + \mu_b \sin\phi}. \tag{7.90}$$

By the equations

$$N_1' \cos\phi - N_1'\mu_b \sin\phi = S_1 \cos\gamma + S_1\mu_d \sin\gamma, \tag{7.91}$$
$$N_2' \cos\phi - N_2'\mu_b \sin\phi = S_2 \cos\gamma + S_2\mu_d \sin\gamma \tag{7.92}$$

and note $S_1' = S_1$, $S_2' = S_2$, $N_1' = N_1$ and $N_2' = N_2$ we have the solutions for the S_1 and S_2

$$S_1 = N_1\frac{\cos\phi - \mu_b \sin\phi}{\cos\gamma + \mu_d \sin\gamma}, \quad S_2 = N_2\frac{\cos\phi - \mu_b \sin\phi}{\cos\gamma + \mu_d \sin\gamma}. \tag{7.93}$$

The above results show that the normal contact forces on the surfaces of the wedges are asymmetrical, and so are the corresponding friction forces. For the case of the

force L_{ob1} in the opposite direction then in the same way we get

$$N_1 = \frac{N_{ob1}}{2(\sin\phi + \mu_b \cos\phi)} + \frac{L_{ob1}}{2(\cos\phi + \mu_b \sin\phi)}, \tag{7.94}$$

$$N_2 = \frac{N_{ob1}}{2(\sin\phi + \mu_b \cos\phi)} - \frac{L_{ob1}}{2(\cos\phi + \mu_b \sin\phi)}. \tag{7.95}$$

If the condition

$$L_{ob1} = N_{ob1} \frac{\cos\phi + \mu_b \sin\phi}{\sin\phi + \mu_b \cos\phi} \tag{7.96}$$

is fulfilled then

$$N_1 = \frac{N_{ob1}}{\sin\phi + \mu_b \cos\phi} + \frac{L_{ob1}}{\cos\phi + \mu_b \sin\phi}, \quad N_2 = 0. \tag{7.97}$$

Finally, the friction forces on the surfaces of wedges are included into the model for the complete system.

7.3 The kinematic constraints and the dynamical system

In the previous sections the dynamical equations of the each component of the three-piece-freight-truck have been described with the non-generalized coordinates. To form the complete three-piece-freight-truck model certain interconnections between the components are needed. The interconnections produce some kinematic constraints which include translations and rotations. For that reason the non-generalized coordinates used to describe the motions of the components are not all independent.

7.3.1 The independent and the dependent variables of the system

In chapter 6 we have shown that the number of the total degrees of the freedom of our system is 81. Because they are not all independent we need to select the independent variables and to obtain the dependent ones from the kinematic constraints.

The interconnections exist between the car body and the two bolsters via two center plates; the bolsters and the wedges, the wedges and the side frames and the side frames and the adapters through sliding contacts. The contacts between wheelsets and rails are considered as elastic rolling contacts so that the kinematic constraints can be replaced by dynamic relations. For the kinematic constraint of the center plate which is modelled as a sphere joint, the translation motions of the bolster and car body is identical in the longitudinal, lateral, vertical directions. In the pitch and yaw rotations they are controlled by kinematic constraints. For the wedge and the bolster, the relations (6.6), (6.7) and (6.8) hold, and the yaw of the bolster and the longitudinal translation of the side frame are not independent of each

other. The vertical displacement and the pitch of the frame are related to the motion of corresponding wheelsets.

There is no general way to select the optimal generalized coordinates for a complicated multibody system. We select the 41 independent variables as

$$\begin{aligned}\mathbf{x}_i = \quad & [\phi_o \quad v_{b1} \quad w_{b1} \quad \phi_{b1} \quad v_{b2} \quad w_{b2} \quad \phi_{b2} \quad \psi_{b1} \quad v_{f1} \quad \psi_{f1} \quad v_{f2} \\ & \psi_{f2} \quad u_{w1} \quad v_{w1} \quad \psi_{w1} \quad u_{w2} \quad v_{w2} \quad \psi_{w2} \quad \psi_{b2} \quad v_{f3} \quad \psi_{f3} \\ & v_{f4} \quad \psi_{f4} \quad u_{w3} \quad v_{w3} \quad \psi_{w3} \quad u_{w4} \quad v_{w4} \quad \psi_{w4} \quad w_{w1} \quad \phi_{w1} \\ & w_{w2} \quad \phi_{w2} \quad w_{w3} \quad \phi_{w3} \quad w_{w4} \quad \phi_{w4} \quad \chi_{w1} \quad \chi_{w2} \quad \chi_{w3} \quad \chi_{w4}]^T\end{aligned} \tag{7.98}$$

and the 40 dependent variables are

$$\begin{aligned}\mathbf{x}_d = \quad & [v_o \quad w_o \quad \chi_o \quad \psi_o \quad u_{d1} \quad v_{d1} \quad w_{d1} \quad u_{d2} \quad v_{d2} \quad w_{d2} \\ & u_{f1} \quad w_{f1} \quad \chi_{f1} \quad u_{d3} \quad v_{d3} \quad w_{d3} \quad u_{d4} \quad v_{d4} \quad w_{d4} \quad u_{f2} \\ & w_{f2} \quad \chi_{f2} \quad u_{d5} \quad v_{d5} \quad w_{d5} \quad u_{d6} \quad v_{d6} \quad w_{d6} \quad u_{f3} \quad w_{f3} \\ & \chi_{f3} \quad u_{d7} \quad v_{d7} \quad w_{d7} \quad u_{d8} \quad v_{d8} \quad w_{d8} \quad u_{f4} \quad w_{f4} \quad \chi_{f4}]^T.\end{aligned} \tag{7.99}$$

7.3.2 The kinematic constraints between the components of the system

The geometrical relations we have described in chapter 6 can be differentiated twice with respect to the time in order to obtain the kinematical constraints between the independent and dependent variables. The effects of the pitch and yaw rotations of the side frames on the vertical and lateral motions of the wedges are small and can be neglected.

The relations connecting the car body motions to the motions of the bolster are

$$\ddot{v}_o = \frac{\ddot{v}_{b1} + \ddot{v}_{b2}}{2}, \tag{7.100}$$

$$\ddot{w}_o = \frac{\ddot{w}_{b1} + \ddot{w}_{b2}}{2}, \tag{7.101}$$

$$\ddot{\chi}_o = \frac{\ddot{\chi}_{b2} - \ddot{\chi}_{b1}}{2a^*_{oc}}, \tag{7.102}$$

$$\ddot{\psi}_o = \frac{\ddot{v}_{b1} - \ddot{v}_{b2}}{2a^*_{oc}}. \tag{7.103}$$

The lateral motion of a wedge has been treated as an independent motion but then the full vehicle model will become too large for the numerical integration. We found that the lateral motion of the wedges are limited by the rimmed bolsters so it can be considered the same as the lateral motion of the bolsters. Therefore the kinematic relations between the bolster and the wedge are

$$\ddot{v}_{di} = \ddot{v}_{b1}, \qquad (i = 1, \cdots, 4), \quad \ddot{v}_{dj} = \ddot{v}_{b2}, \qquad (j = 5, \cdots, 8) \tag{7.104}$$

and in the longitudinal and vertical direction we obtain

$$\begin{array}{l}\ddot{u}_{di} = -S\gamma S\varphi(\ddot{w}_{b1} \pm b^*_{bs2}\ddot{\varphi}_{b1}), \quad (i = 1, \cdots, 4) \\ \ddot{w}_{di} = C\gamma S\varphi(\ddot{w}_{b1} \pm b^*_{bs2}\ddot{\varphi}_{b1}), \quad (' + ' \text{for} \quad i = 1, 2, \quad ' - ' \text{for} \quad i = 3, 4),\end{array} \tag{7.105}$$

$$\begin{array}{l}\ddot{u}_{dj} = -S\gamma S\varphi(\ddot{w}_{b2} \pm b^*_{bs2}\ddot{\varphi}_{b2}), \quad (j = 5, \cdots, 8) \\ \ddot{w}_{dj} = C\gamma S\varphi(\ddot{w}_{b2} \pm b^*_{bs2}\ddot{\varphi}_{b2}), \quad (' + ' \text{for} \quad j = 5, 6, \quad ' - ' \text{for} \quad j = 7, 8)\end{array} \tag{7.106}$$

where $S\gamma S\phi$ denotes the short expression of the term $\frac{sin\gamma sin\phi}{sin(\gamma+\phi)}$.

The kinematic constraints between the side frames and the bolsters and the wheelsets are

$$\ddot{u}_{fi} = (-1)^i b^*_{bs2}\ddot{\psi}_{bj}, \qquad (j = 1, i = 1, 2; j = 2, i = 3, 4), \tag{7.107}$$

$$\ddot{w}_{fi} = 0.5(\ddot{w}_{w1} + \ddot{w}_{w2} + (-1)^{i+1} b_{ws}(\ddot{\varphi}_{w1} + \ddot{\varphi}_{w2})), \quad (i = 1, 2), \tag{7.108}$$

$$\ddot{\chi}_{fi} = -0.5(\ddot{w}_{w1} + (-1)^{i+1} b_{ws}\ddot{\varphi}_{w1} - \ddot{w}_{w2} + (-1)^i b_{ws}\ddot{\varphi}_{w2})/a_{wb}, \quad (i = 1, 2), \tag{7.109}$$

$$\ddot{w}_{fi} = 0.5(\ddot{w}_{w3} + \ddot{w}_{w4} + (-1)^{i+1} b_{ws}(\ddot{\varphi}_{w3} + \ddot{\varphi}_{w4})), \quad (i = 3, 4), \tag{7.110}$$

$$\ddot{\chi}_{fi} = -0.5(\ddot{w}_{w3} + (-1)^{i+1} b_{ws}\ddot{\varphi}_{w3} - \ddot{w}_{w4} + (-1)^i b_{ws}\ddot{\varphi}_{w4})/a_{wb}, \quad (i = 3, 4). \tag{7.111}$$

7.3.3 The dynamical system

The are two types of kinematic constraints caused by the interconnections, one is no friction and it is called smooth constraints. The other one is related to the friction and is called non-smooth constraint. For the smooth constraints the contact forces on the contacting surfaces can be eliminated by the method provided by Haug[Haug,1989]. For the non-smooth constraints the contact forces can not be eliminated because the friction forces need to be included and they are of course related to the contact forces.

For the complete system with all variables and all applied forces on the components of the system the variational equation of motion of the system is formulated in a matrix form in the formulation of d'Alembert[Haug,1989] as

$$\delta\mathbf{x}^T[\mathbf{M}\ddot{\mathbf{x}} + \mathbf{F}_s - \mathbf{F}] = \mathbf{0} \tag{7.112}$$

where $\mathbf{F}_s$ denotes the spring force and $\mathbf{F}$ stands for the other applied forces including the normal contact forces on the contact surfaces between the two bodies.

The elements in $\delta\mathbf{x}^T$ usually are not independent, therefore the kinematic constraints must be introduced. Generally, the kinematic constraints can be expressed as

$$\mathbf{g}(\mathbf{x}, \mathbf{x}_i) = \mathbf{0} \tag{7.113}$$

where $\mathbf{x}_i$ denotes the vector of independent variables. In general the equation defines the relations between the independent and dependent variables implicitly, so Newton-Raphson method can be used to obtain a numerical solution.

In some cases the kinematic constraints can be expressed explicitly as

$$\mathbf{x} = \mathbf{J}(t)\mathbf{x}_i + \mathbf{G}(t) \tag{7.114}$$

where $\mathbf{J}(t)$ denotes the coefficient matrix which usually is time-dependent and $\mathbf{G}(t)$ stands for the other time-dependent terms.

In our system, as we have discussed in chapter 6 all entries of the matrix $\mathbf{J}(t)$ and $\mathbf{G}(t)$ are constant, such that we have

$$\dot{\mathbf{J}} = \ddot{\mathbf{J}} = \mathbf{0}, \quad \dot{\mathbf{G}} = \ddot{\mathbf{G}} = \mathbf{0}. \tag{7.115}$$

Then we have the relation

$$\ddot{\mathbf{x}} = \mathbf{J}\ddot{\mathbf{x}}_i. \tag{7.116}$$

Thus equation(7.112) with the independent variables can be rewritten as

$$\mathbf{J}^T \delta \mathbf{x}_i^T [\mathbf{M}\mathbf{J}\ddot{\mathbf{x}}_i + \mathbf{F}_s - \mathbf{F}] = \mathbf{0}. \tag{7.117}$$

Because the variation of $\mathbf{x_i}$ now is the independent variable vector, we finally get the dynamical equation

$$\mathbf{J}^T\mathbf{M}\mathbf{J}\ddot{\mathbf{x}}_i = \mathbf{J}^T(\mathbf{F} - \mathbf{F}_s). \tag{7.118}$$

It should be pointed out that the spring force vector $\mathbf{F}_s$ also depends on the dependent variables, however we have already determined the spring extensions of the suspensions in chapter 6, therefore the spring extensions are known quantities and so are the spring forces.

The force vector $\mathbf{F}$ includes the contact force vector $\mathbf{F}_{ct}$, the friction force vector $\mathbf{F}_f$, the weight $\mathbf{F}_w$ and the gyroscopic force $\mathbf{F}_g$ and tangential wheel/rail contacting forces $\mathbf{F}_{ctw}$ and $\mathbf{F}_{tw}$.

We rearrange the terms of the above equation as

$$\mathbf{J}^T\mathbf{M}\mathbf{J}\ddot{\mathbf{x}}_i - \mathbf{J}^T(\mathbf{F}_f + \mathbf{F}_{ct}) = \mathbf{J}^T(\mathbf{F}_w + \mathbf{F}_g - \mathbf{F}_s - F_{ctw} - \mathbf{F}_{tw}). \tag{7.119}$$

There are 41 independent variables to be solved for in the system. And the contact forces $\mathbf{F}_{ct}$ which have 28 components are also wanted. The 28 contact forces are: 4 contact forces, $\mathbf{N}_{ob}$ on the center plates; 8 contact forces, $\mathbf{S}_d$ on the surfaces of the wedges contacting the side frames; 8 contact forces, $\mathbf{N}_b$ on the surfaces of the wedges contacting the bolsters and 8 contact forces, $\mathbf{N}_{fwp}$ on the surfaces of the adapters. Hence we need in total 69 equations to determine the 69 unknown quantities. We have used 81 equations to describe the motion of each component in the system. For the relation(6.6) the number of the equations reduce to 73. In the following way the number of the equations can be further reduced to 69.

In equations (7.17) and (7.35) we have the following 6 equations

$$I_{bz}\ddot{\psi}_{b1} = -k_{\psi bf}(\psi_{b1} - \psi_{f1}) - k_{\psi bf}(\psi_{b1} - \psi_{f2}) + M_{ctb1} + M_{f\psi ob1} + M_{f\psi bd1}, \tag{7.120}$$

$$I_{bz}\ddot{\psi}_{b2} = -k_{\psi bf}(\psi_{b2}-\psi_{f3}) - k_{\psi bf}(\psi_{b2}-\psi_{f4}) + M_{ctb2} + M_{f\psi ob2} + M_{f\psi bd2}, \quad (7.121)$$

$$m_f \ddot{u}_{fi} = \mathbf{f}_{sfi}(1) + N_{ctbdi} + N_{fbdi} + \mathbf{f}_{ffwi}(1), \quad i = 1, \cdots, 4. \quad (7.122)$$

Using the relations (7.107) and by multiplying the sides of the above equation (7.122) by $(-1)^i b^*_{bs2}, (i = 1, \cdots, 4)$ and then add them to the equations (7.120) and (7.121) respectively, and next by means of the relations

$$b^*_{bs2}(N_{ctbd2} - N_{ctbd1}) = M_{ctbd1}, \quad b^*_{bs2}(N_{ctbd4} - N_{ctbd3}) = M_{ctbd2} \quad (7.123)$$

and

$$b^*_{bs2}(N_{fbd2} - N_{fbd1}) = M_{f\psi bd1}, \quad b^*_{bs2}(N_{fbd4} - N_{fbd3}) = M_{f\psi bd2}. \quad (7.124)$$

we can reduce the above 6 equations to the following 2 equations

$$\begin{aligned}(I^*_{bz} + 2m_f b^{*2}_{bs2})\ddot{\psi}_{b1} &= b^*_{bs2}[(f_{fwu3} + f_{fwu4})C\psi_{f2} - (f_{fwu1} + f_{fwu2})C\psi_{f1}] \\ &\quad + M_{f\psi ob1} + M_{sfw12} - M_{s\psi bf1} - M_{s\psi bf2}, \quad (7.125)\end{aligned}$$

$$\begin{aligned}(I^*_{bz} + 2m_f b^{*2}_{bs2})\ddot{\psi}_{b2} &= b^*_{bs2}[(f_{fwu7} + f_{fwu8})C\psi_{f4} - (f_{fwu5} + f_{fwu6})C\psi_{f3}] \\ &\quad M_{f\psi_{ob2}} + M_{sfw34} - M_{s\psi bf3} - M_{s\psi bf4} \quad (7.126)\end{aligned}$$

where

$$M_{s\psi bfi} = k_{\psi bf}(\psi_{bj} - \psi_{fi}), \quad i = 1, 2, \quad j = 1; \quad i = 3, 4, \quad j = 2, \quad (7.127)$$

$$M_{sfw12} = b^*_{bs2}[(f_{sf2w1u} + f_{sf2w2u})C\psi_{f2} - (f_{sf1w1u} + f_{sf1w2u})C\psi_{f1}], \quad (7.128)$$

$$M_{sfw34} = b^*_{bs2}[(f_{sf4w3u} + f_{sf4w4u})C\psi_{f4} - (f_{sf3w3u} + f_{sf3w4u})C\psi_{f3}] \quad (7.129)$$

and $C\psi$ denotes the short expression of $cos\psi$.

The relative motions between the bolster and the frame are motions in the lateral and vertical direction and the yaw rotation. Therefore we use the anti-warp stiffness and the corresponding spring torque to describe the restoring force against the warp motion.

Besides the contact forces $\mathbf{S}_{di}$ on the surfaces of the wedges contacting the side frames, we must also consider the additional contact forces on these surfaces applied by the side frame by the friction forces on the surfaces of the tops of the adapters. The magnitude of the force vector is equal to the value of the sum of the friction forces on the two top surfaces of the adapters contacting one side frame in the longitudinal direction. If the force vector is positive then the force vector acts only on the wedges numbered 1, 3, 5 and 7(see Figure 7.6); otherwise, it acts on the wedges numbered 2, 4, 6 and 8. Obviously, the additional contact force leads to the asymmetric friction forces on a pair of two wedges.

The contact forces on the center plates are

$$\mathbf{N}_{ob} = [N_{obv1} \quad N_{obw1} \quad N_{obv2} \quad N_{obw2}]^T. \quad (7.130)$$

The contact forces related to the friction on the surfaces of the wedges which contact the bolsters and side frames are

$$\begin{aligned}\mathbf{N}_{bd} = [&S_{d1} \quad N_{b1} \quad S_{d2} \quad N_{b2} \quad S_{d3} \quad N_{b3} \quad S_{d4} \quad N_{b4} \\ &S_{d5} \quad N_{b5} \quad S_{d6} \quad N_{b6} \quad S_{d7} \quad N_{b7} \quad S_{d8} \quad N_{b8}]^T\end{aligned} \tag{7.131}$$

and the contact forces on the surfaces of the adapters are

$$\mathbf{N}_{fwp} = [N_{f1w1} \quad N_{f1w2} \quad N_{f2w1} \quad N_{f2w2} \quad N_{f3w3} \quad N_{f3w4} \quad N_{f4w3} \quad N_{f4w4}]^T. \tag{7.132}$$

The contact force on the central plates $N_{obv1}, N_{obw1}, N_{obv2}, N_{obw2}$ are also needed because they act as a part of the input force on the bolster to determine the friction direction angle on the surfaces of the wedges.

Hence there are totally 28 unknown contact forces in the system needed to be determine in dependence on the 41 independent variables. Let

$$\mathbf{F}_{ev} = [\mathbf{N}_{ob} \quad \mathbf{N}_{bd} \quad \mathbf{N}_{fwp}]^T \tag{7.133}$$

then the system can be written as

$$\begin{bmatrix} \mathbf{A}_a & \mathbf{M}_{dep}\mathbf{J} \\ \mathbf{A}_b & \mathbf{M}_{ind} \end{bmatrix} \begin{bmatrix} \mathbf{F}_{ev} \\ \ddot{\mathbf{x}}_i \end{bmatrix} = \begin{bmatrix} \mathbf{F}_{dep} \\ \mathbf{F}_{ind} \end{bmatrix} \tag{7.134}$$

where $\mathbf{M}_{dep}$ is the mass matrix related to the dependent variables, and the $\mathbf{M}_{ind}$ denotes the mass matrix related to the independent variables. The entries of the matrix $\mathbf{J}$ in (7.134) are different from these of the matrix $\mathbf{J}$ in (7.114)-(7.119).

The matrices $\mathbf{A}_a$ and $\mathbf{A}_b$, where their entries are a function of the friction direction angles, friction coefficients and the construction parameters, can be written as

$$\mathbf{A}_{a,b} = f(\theta, \quad \mu_b, \quad \mu_d, \quad \mu_f, \quad p) \tag{7.135}$$

where p denotes the construction parameters.

If the purpose of the simulation is only focussed on the slip motion then the friction direction angle is uniquely determined by the corresponding relative velocities alone. In that case the entries of the matrices $\mathbf{A}_a$ and $\mathbf{A}_b$ are determined by the state space variables. However, if the stick-slip motion of the system is included then the matrices $\mathbf{A}_a$ and $\mathbf{A}_b$ become discontinuous. That problem will be discussed in detail in the next chapter.

CHAPTER 8

The numerical method

The normal integration methods such as Runge-Kutta explicit or implicit schemes or other formula can not be directly applied to the system (7.134) in the previous chapter. There are two reasons: One is that the entries of the matrices, $\mathbf{A}_a$ and $\mathbf{A}_b$ are discontinuous due to the stick-slip motion of the system; the other is that the independent variables of the system will change from stick-state to slip-state, i.e. a collapse of the space-state will occur as we have discussed in chapters 3 and 4. In this chapter the numerical method is discussed for the complete vehicle with three-piece-freight-trucks.

8.1 The slip state motion of the system

We have shown that there are 41 independent variables in our dynamical system and the 28 normal contact forces on the surfaces of the wedges and the adapters are needed to be determined together with the dependent variables.

In any case the perturbation motions of the wheelsets around their axes can be uncoupled because the applied torque on the wheelset around its axle is only provided by the tangential forces in the longitudinal direction. This is also true for the roll motion of the car body because the applied torque around the $(o_o x_o)$ is only provided by the side support forces when the clearances between the car body and the side supports are taken up.

Anyhow the independent variables can be divided into four groups that are uncoupled from each other(approximately), so the numerical algorithm becomes easier.

That means that the Eq.(7.134) can be further written as

$$\begin{bmatrix} \mathbf{A}_{o1} & \mathbf{M}_{o1}\mathbf{J}_{o1} & \mathbf{0} & \mathbf{0} & \mathbf{0} & \mathbf{0} & \mathbf{0} \\ \mathbf{A}_{d} & \mathbf{M}_{d}\mathbf{J}_{d} & \mathbf{0} & \mathbf{0} & \mathbf{0} & \mathbf{0} & \mathbf{0} \\ \mathbf{A}_{bvwr} & \mathbf{M}_{bvwr}\mathbf{J}_{bvwr} & \mathbf{0} & \mathbf{0} & \mathbf{0} & \mathbf{0} & \mathbf{0} \\ \mathbf{0} & \mathbf{0} & \mathbf{A}_{fwp} & \mathbf{M}_{fwp}\mathbf{J}_{fwp} & \mathbf{0} & \mathbf{0} & \mathbf{0} \\ \mathbf{0} & \mathbf{0} & \mathbf{A}_{wwr} & \mathbf{M}_{wwr} & \mathbf{0} & \mathbf{0} & \mathbf{0} \\ \mathbf{0} & \mathbf{0} & \mathbf{A}_{fvy} & \mathbf{0} & \mathbf{M}_{fvy} & \mathbf{0} & \mathbf{0} \\ \mathbf{0} & \mathbf{0} & \mathbf{A}_{wuvy} & \mathbf{0} & \mathbf{M}_{wuvy} & \mathbf{0} & \mathbf{0} \\ \mathbf{0} & \mathbf{0} & \mathbf{0} & \mathbf{0} & \mathbf{0} & \mathbf{M}_{wp} & \mathbf{0} \\ \mathbf{0} & \mathbf{0} & \mathbf{0} & \mathbf{0} & \mathbf{0} & \mathbf{0} & I_{ox} \end{bmatrix} \begin{bmatrix} \mathbf{N}_{obd} \\ \ddot{\mathbf{x}}_{odb} \\ \mathbf{N}_{fwp} \\ \ddot{\mathbf{x}}_{fwwr} \\ \ddot{\mathbf{x}}_{fvywuvy} \\ \ddot{\mathbf{x}}_{wp} \\ \ddot{\phi}_{o} \end{bmatrix}$$

$$= \begin{bmatrix} \mathbf{F}_{o1} \\ \mathbf{F}_{d} \\ \mathbf{F}_{bvwr} \\ \mathbf{F}_{fwp} \\ \mathbf{F}_{wwr} \\ \mathbf{F}_{fuvy} \\ \mathbf{F}_{wuvy} \\ \mathbf{F}_{wp} \\ \mathbf{F}_{or} \end{bmatrix} \tag{8.1}$$

where

$$\mathbf{x}_{odb} = [v_{b1} \quad w_{b1} \quad \phi_{b1} \quad v_{b2} \quad w_{b2} \quad \phi_{b2}]^T, \tag{8.2}$$

$$\mathbf{x}_{fwwr} = [w_{w1} \quad \phi_{w1} \quad w_{w2} \quad \phi_{w2} \quad w_{w3} \quad \phi_{w3} \quad w_{w4} \quad \phi_{w4}]^T, \tag{8.3}$$

$$\mathbf{x}_{fvywuvy} = [\mathbf{x}_{fwf} \quad \mathbf{x}_{fwr}]^T \tag{8.4}$$

with

$$\mathbf{x}_{fwf} = [\psi_{b1} \quad v_{f1} \quad \psi_{f1} \quad v_{f2} \quad \psi_{f2} \quad u_{w1} \quad v_{w1} \quad \psi_{w1} \quad u_{w2} \quad v_{w2} \quad \psi_{w2}]^T, \tag{8.5}$$

$$\mathbf{x}_{fwr} = [\psi_{b2} \quad v_{f3} \quad \psi_{f3} \quad v_{f4} \quad \psi_{f4} \quad u_{w3} \quad v_{w3} \quad \psi_{w3} \quad u_{w4} \quad v_{w4} \quad \psi_{w4}]^T, \tag{8.6}$$

and

$$\mathbf{x}_{wp} = [\psi_{w1} \quad \psi_{w2} \quad \psi_{w3} \quad \psi_{w4}]^T \tag{8.7}$$

The force vectors on the right hand side of the equation (8.1) are related to the external forces in the corresponding directions and have been determined in the chapter 7.

For the slip motion of all components of the system the above system is continuous and can be directly integrated numerically. The equation (8.1) can be written in the first order form in the following way (see chapters 2, 3 and 4). Let

$$\dot{\mathbf{x}}_i = [q_1 \quad q_2 \quad \cdots \quad q_{41}], \tag{8.8}$$

$$\mathbf{x}_i = [q_{42} \quad q_{41} \quad \cdots \quad q_{82}] \tag{8.9}$$

then the equation can be written as

$$\mathbf{q}' = \mathbf{f}(\mathbf{q}, \quad \mathbf{z}, \quad \mathbf{f}_{tw}, \quad \mathbf{f}_{ctw}), \tag{8.10}$$

$$\mathbf{0} = \mathbf{g}_v(\mathbf{q}, \mathbf{n}), \tag{8.11}$$

$$\mathbf{0} = \mathbf{g}_w(\mathbf{q}, \mathbf{f}_{tw}, \mathbf{f}_{ctw}) \tag{8.12}$$

where

$$\mathbf{f} = [z_1 \quad z_2 \quad \ldots \quad z_{41}; \quad q_1 \quad q_2 \ldots \quad q_{41}, \quad \mathbf{f}_{tw}, \quad \mathbf{f}_{ctw}]^T, \tag{8.13}$$

$$\mathbf{g}_v(\mathbf{q}, \mathbf{n}) = \mathbf{A}_c \mathbf{n}_v - \mathbf{F}_{ev}, \tag{8.14}$$

$$\mathbf{g}_w(\mathbf{q}, \mathbf{f}_{tw}, \mathbf{f}_{ctw}) = \mathbf{0}, \tag{8.15}$$

$$\mathbf{n} = [N_1 \quad N_2 \quad \cdots \quad N_{28} \quad z_1 \quad z_2 \quad \cdots \quad z_{41}]^T \tag{8.16}$$

Eq.(8.15) is actually the compact form of the Eq. (7.81). The term $\mathbf{A}_c\mathbf{n}_v$ stands for the left-hand side of the Eq. (7.134) and $\mathbf{F}_{ev}$ denotes the right-hand side of the Eq. (7.134). So the dynamic system of the three-piece-freight-truck is a DAEs system with the index 1.

In general some features of the system should be known before the numerical integration. If the system is discontinuous or non-smooth then the system must first be transformed to a piece-wise smooth system. It is very important but not easy to do for a complicated system like the three-piece-freight-truck with dry friction. Next if the system is stiff then a suitable integral algorithm should be selected. In practical, the fast explicit integral formula are first selected if they fail then we try other implicit methods.

There are many numerical integral methods that can be used for the solution of the DAEs with index 1. We use Runge-Kutta's method for our problem because it is effective and zero-stable.

From the theoretical point of view, the continuous Differential-Algebraic-Equations (DAEs) can be solved without great difficulty. We use the following algorithm to solve the system.

8.1.1 Numerical algorithm for solving the DAEs for the slip state

step 1
From the velocities and displacements obtained in the previous step, the kinematic constraint parameters between wheels and rails can be determined.
Step 2
Calculation of the normal loads and creep forces between wheels and rails.
Step 3

The uncoupled motions of the perturbation rotations of the wheelsets, ($\ddot{\chi}_{wi}, i = 1, \cdots, 4$) can be determined.

Step 4

Determination of the spring forces of the secondary suspensions, the dead-band stop forces, the anti-warp forces and others.

Step 5

With the friction forces on the surfaces of the wedges contacting the side frames that are obtained in the previous step the normal forces on the surfaces of the adapters can be determined.

Step 6

Determination of the friction direction angles for the friction on the surfaces of the wedges and the adapters.

Step 7

Solution of the Eq.(8.15).

Step 8

Calculation of the state space variables and repeat step 1 to step 7.

8.2 The stick-slip motion of the system

From the equation(8.1) we know that when some relative velocities equal zero the corresponding friction forces can not be directly calculated by the equations (2.16) or (3.15) and (3.17). In some cases they are evaluated by the equations (2.16) or (3.15) and (3.17) and in some cases they are determined by the way described in the chapter 4. That means that the stick-slip motion causes not only a discontinuity but also a collapse of the state space because the degrees of freedom of the system change. So the Eq.(8.1) can not be directly used to evaluate the integrated function in the stick motion.

8.2.1 The switch conditions for the sub-system of the wagon-bolster-wedges

From Eq. (8.1) the sub-system of the wagon-bolster-wedges can be written as following

$$\begin{bmatrix} \mathbf{A}_{o1} & \mathbf{M}_{o1}\mathbf{J}_{o1} \\ \mathbf{A}_{d} & \mathbf{M}_{d}\mathbf{J}_{d} \\ \mathbf{A}_{bvwr} & \mathbf{M}_{bvwr}\mathbf{J}_{bvwr} \end{bmatrix} \begin{bmatrix} \mathbf{N}_{obd} \\ \ddot{\mathbf{x}}_{odb} \end{bmatrix} = \begin{bmatrix} \mathbf{F}_{o1} \\ \mathbf{F}_{d} \\ \mathbf{F}_{b} \end{bmatrix} \tag{8.17}$$

where $\ddot{\mathbf{x}}_{odb}$ is defined by(8.2) and the other terms can be found in the appendix **B**.

In chapter 3 the improved model of the wedge dampers have been derived and their dynamical performances have been analyzed. In chapter 7 we have combined this model into the complete three-piece-freight-truck system. Thereby some new problems arise. One is that the side frame is fixed in the wedge dampers model, such that the friction force is equal to the input force on the wedge for the stick motion

between the wedge and the side frame. The second is that the motion of the wedge dampers are not influenced by the motion state of the other end of the bolster. Last, but not least, the effect of the roll rotation of the bolster should be included.

Here we will discuss these new problems and find a way to describe the stick-slip motion between the wedges, bolsters and side frames in the lateral and vertical directions.

Figure 1.2 shows the complete wedge damper system for one three-piece truck. It is made up of one bolster, four wedges and two side frames.

For the relative motions between the bolsters/wedges and side frames in the lateral direction the following relations are true while the stick motions take place

$$V_{b1f1} = \dot{v}_{b1} - \dot{v}_{f1} = 0, \quad V_{b1f2} = \dot{v}_{b1} - \dot{v}_{f2} = 0 \tag{8.18}$$

and

$$V_{b2f3} = \dot{v}_{b2} - \dot{v}_{f3} = 0, \quad V_{b2f4} = \dot{v}_{b2} - \dot{v}_{f4} = 0 \tag{8.19}$$

where v_{b1f1} denotes the relative velocity between the bolster 1 and frame 1 and so on.

The different possible stick motions are expressed by the following conditions:

- $V_{b1f1} = 0, V_{b1f2} = 0, \qquad V_{b2f3} = 0, V_{b2f4} = 0;$
- $V_{b1f1} = 0, V_{b1f2} \neq 0, \qquad V_{b2f3} = 0, V_{b2f4} \neq 0;$
- $V_{b1f1} \neq 0, V_{b1f2} = 0, \qquad V_{b2f3} \neq 0, V_{b2f4} = 0.$

In the same way we have used in chapter 4, the switch conditions and the corresponding friction forces can be derived as

$$f_{\mu f1dy} = |\frac{m_f m_b}{m_f + m_b}(\frac{F_{inb1y}}{m_b} - \frac{F_{inf1y}}{m_f})| \leq |f_{\mu sf1dy}|, (V_{b1f1} = 0, V_{b1f2} \neq 0), \tag{8.20}$$

$$f_{\mu f2dy} = |\frac{m_f m_b}{m_f + m_b}(\frac{F_{inb1y}}{m_b} - \frac{F_{inf2y}}{m_f})| \leq |f_{\mu sf2dy}|, (V_{b1f2} \neq 0, V_{b1f2} = 0), \tag{8.21}$$

$$f_{\mu f3dy} = |\frac{m_f m_b}{m_f + m_b}(\frac{F_{inb2y}}{m_b} - \frac{F_{inf3y}}{m_f})| \leq |f_{\mu sf3dy}|, (V_{b2f3} = 0, V_{b2f3} \neq 0), \tag{8.22}$$

$$f_{\mu f4dy} = |\frac{m_f m_b}{m_f + m_b}(\frac{F_{inb2y}}{m_b} - \frac{F_{inf4y}}{m_f})| \leq |f_{\mu sf4dy}|, (V_{b2f4} \neq 0, V_{b2f4} = 0), \tag{8.23}$$

$$\begin{aligned} f_{\mu f1dy} + f_{\mu f2dy} &= |\frac{1}{2m_f + m_b}[2F_{inb1y}m_f - m_b(F_{inf1y} + f_{inf2y})]| \\ &\leq |f_{\mu sf1dy} + f_{\mu sf2y}|, \qquad (V_{b1f1} = 0, V_{b1f2} = 0) \end{aligned} \tag{8.24}$$

and

$$\begin{aligned} f_{\mu f3dy} + f_{\mu f4dy} &= |\frac{1}{2m_f + m_b}[2F_{inb2y}m_f - m_b(F_{inf3y} + f_{inf4y})]| \\ &\leq |f_{\mu sf3dy} + f_{\mu sf4y}|, \qquad (V_{b2f3} = 0, V_{b2f4} = 0). \end{aligned} \tag{8.25}$$

where $f_{\mu f1dy}$ denotes the acting friction force in the lateral direction and similarly for the others. $f_{\mu sf1dy}$ and so on stands for the corresponding static friction force. F_{inb1y}, F_{inf1y} and so on are the input forces on the bolsters and frames in the lateral direction.

We know from chapter 2, 3 and 4 that in the simple system the input forces do not include the friction forces but for the multi-point contacts between one bolster and two side frames the kinematical friction forces must be included. That means if the relative motion on any one contact surface is different from zero then the kinematical friction force on that surface should be included in the corresponding input force.

After getting the acting friction forces in the stick states, the corresponding input forces which are used to calculate the corresponding friction direction angle on that contact surface are set to be equal to the corresponding acting friction forces. The friction direction angle is used to determine the static friction force components that are necessary in the switch conditions. The acting friction forces on the surfaces of the wedges in the vertical direction are determined in the following way:

We take the truck 1 to be an example. The stick motions will take place if the following conditions

$$V_{bd12z} = \dot{w}_{b1} + \dot{\phi}_{b1}b^*_{bs2} - \dot{w}_{d1} = 0, \tag{8.26}$$

$$V_{bd34z} = \dot{w}_{b1} - \dot{\phi}_{b1}b^*_{bs2} - \dot{w}_{d3} = 0 \tag{8.27}$$

are fulfilled. Here we assume $\dot{w}_{d1} = \dot{w}_{d2}$ and $\dot{w}_{d3} = \dot{w}_{d4}$.

For any possible stick motion we have the conditions below

$$V_{bd12z} = 0, V_{bd34z} = 0, \tag{8.28}$$

$$V_{bd12z} = 0, V_{bd34z} \neq 0, \tag{8.29}$$

$$V_{bd12z} \neq 0, V_{bd34z} = 0. \tag{8.30}$$

Here we use a simple way to describe the acting friction forces on the surfaces of the wedges in the vertical direction. The basic idea is that the input force on the bolster in the vertical direction is directly used to determine the acting friction forces. To the end we have

$$f_{\mu bd12zt}{=}F_{inbz} - f_{\mu bd34z}, \quad (V_{bd12z} = 0, V_{bd34z} \neq 0), (|f_{\mu bd12zt}| \leq |f_{\mu bd12zs}|)), \tag{8.31}$$

$$f_{\mu bd1zt}{=}0.5f_{\mu bd12zt}, \quad f_{\mu bd2zt} = 0.5f_{\mu bd12zt} \tag{8.32}$$

$$f_{\mu bd34zt}{=}F_{inbz} - f_{\mu bd12z}, \quad (V_{bd12z} \neq 0, V_{bd34z} = 0), (|f_{\mu bd34zt}| \leq |f_{\mu bd34zs}|)), \tag{8.33}$$

$$f_{\mu bd3zt}{=}0.5f_{\mu bd34zt}, \quad f_{\mu bd4zt} = 0.5f_{\mu bd34zt} \tag{8.34}$$

and

$$f_{bd12zt} = f_{\mu bd34zt} = \frac{F_{inbz}}{2}, \quad V_{bd12z} = 0, V_{bd34z} = 0, |F_{inbz}| \leq |f_{\mu bd12zs} + f_{\mu bd34zs}| \tag{8.35}$$

We know that the motions of the wedges in the longitudinal and vertical directions depend on the vertical motion of the bolster so for the stick motions the friction force on the surface of the wedge contacting the frame is determined by the following relations

$$f_{\mu fdizt} = -f_{\mu bdizt}, \quad i = 1, \cdots, 4 \tag{8.36}$$

$$f_{\mu fdixt} = (-1)^{i+1} f_{\mu bdizt}(\tan\gamma + \tan\phi), \quad i = 1, \cdots, 4 \tag{8.37}$$

In the same way we can derive the similar formulae for the truck 2 (see Figure 6.2).

We use the acting friction force to replace the corresponding friction forces which are calculated by the normal force timing the friction coefficient.

8.2.2 Determination of the normal forces on the surfaces of the adapters

The normal forces on the surfaces of the adapters are related to the motions of the side frames in the vertical and pitch directions and wheelsets in the vertical and roll directions. They are determined by the equation below

$$\begin{bmatrix} \mathbf{A}_{fwp} & \mathbf{M}_{fwp}\mathbf{J}_{fwp} \\ \mathbf{A}_{wwr} & \mathbf{M}_{wwr} \end{bmatrix} \begin{bmatrix} \mathbf{N}_{fwp} \\ \ddot{\mathbf{x}}_{fwwr} \end{bmatrix} = \begin{bmatrix} \mathbf{F}_{fwp} \\ \mathbf{F}_{wwr} \end{bmatrix} \tag{8.38}$$

where the entries of the matrix can be found in the appendix C.

8.2.3 The switch conditions for the stick-slip motion between frames and wheelsets

From (8.1) we can isolate the sub-system of the bolster-frame wheelsets as

$$\begin{bmatrix} \mathbf{A}_{fvy} & \mathbf{M}_{fvy} \\ \mathbf{A}_{wuvy} & \mathbf{M}_{wuvy} \end{bmatrix} \begin{bmatrix} \mathbf{N}_{fwp} \\ \ddot{\mathbf{x}}_{fvywuvy} \end{bmatrix} = \begin{bmatrix} \mathbf{F}_{fuvy} \\ \mathbf{F}_{wuvy} \end{bmatrix}. \tag{8.39}$$

For the sake of convenience the switch conditions and the corresponding acting friction forces on the surfaces of the adapters, we treat the equations of the front truck and rear truck individually.

For the front truck

$$\begin{bmatrix} \mathbf{A}_{fvyf} & \mathbf{M}_{fvyf} \\ \mathbf{A}_{wuvyf} & \mathbf{M}_{wuvyf} \end{bmatrix} \begin{bmatrix} \mathbf{N}_{fwpf} \\ \ddot{\mathbf{x}}_{fwf} \end{bmatrix} = \begin{bmatrix} \mathbf{F}_{fuvyf} \\ \mathbf{F}_{wuvyf} \end{bmatrix}. \tag{8.40}$$

and for the rear truck

$$\begin{bmatrix} \mathbf{A}_{fvyr} & \mathbf{M}_{fvyr} \\ \mathbf{A}_{wuvyr} & \mathbf{M}_{wuvyr} \end{bmatrix} \begin{bmatrix} \mathbf{N}_{fwpr} \\ \ddot{\mathbf{x}}_{fwr} \end{bmatrix} = \begin{bmatrix} \mathbf{F}_{fuvyr} \\ \mathbf{F}_{wuvyr} \end{bmatrix}. \tag{8.41}$$

The normal contact forces $\mathbf{N}_{fuvyf}, \mathbf{N}_{fuvyr}$ have been determined by the (8.38). For the slip motion the entries of the matrices $\mathbf{A}_{fvyf}$, $\mathbf{A}_{fvyr}$, $\mathbf{A}_{wuvyf}$ and $\mathbf{A}_{wuvyr}$ are only related to the kinetic friction coefficient and the system can be integrated directly. Trouble will arise while the stick motions appear between the frames and the wheelsets. In that case the friction force on that surface of the adapter neither equals the static friction force nor equals zero unless the corresponding input forces are zero. In fact the friction forces (acting friction forces) can be determined with the switch conditions.

It is strenuous work to find the all switch conditions and to calculate of the corresponding friction forces for the stick-slip motion of the sub-system of the bolster-frame wheelsets although the method is the same as that we have used in chapter 4. First we rewrite the related equations of the sub-system from chapter 7 and the kinematic constraints among the bolsters, side frames and the wheelsets in the longitudinal and lateral directions and the yaw rotation of the bolsters. Then we find all possible combinations of the stick-slip motion to get the switch conditions. The detailed description is provided in appendix D.

As a result when the stick motion of all the contact surfaces between side frame and adapters take place then the acting friction forces can be determined by the following equation.

$$\mathbf{A}^1_{b1}\mathbf{F}^1_{\mu m} = \mathbf{F}^1_m \tag{8.42}$$

where

$$\mathbf{F}^1_{\mu m} = [f_{fwx1} \quad f_{fwy1} \quad f_{fwx2} \quad f_{fwy2} \quad f_{fwx3} \quad f_{fwy3} \quad f_{fwx4} \quad f_{fwy4}]^T \tag{8.43}$$

and

$$\mathbf{A}^1_{b1} = \begin{bmatrix} a_{11} & 0 & a_{13} & 0 & a_{15} & 0 & a_{17} & 0 \\ a_{21} & 0 & a_{23} & 0 & a_{25} & 0 & a_{27} & 0 \\ a_{31} & 0 & a_{33} & 0 & a_{35} & 0 & a_{37} & 0 \\ a_{41} & 0 & a_{43} & 0 & a_{45} & 0 & a_{47} & 0 \\ 0 & a_{52} & 0 & a_{54} & 0 & a_{56} & 0 & 0 \\ 0 & a_{62} & 0 & a_{64} & 0 & 0 & 0 & a_{68} \\ 0 & a_{72} & 0 & 0 & 0 & a_{76} & 0 & a_{78} \\ 0 & 0 & 0 & a_{84} & 0 & a_{86} & 0 & a_{88} \end{bmatrix} \tag{8.44}$$

in which

$$
\begin{aligned}
a_{11} &= \frac{1}{m_w} + \frac{b_{ws}^2}{I_{wz}} + \frac{b_{bs2}^{*2}}{I_{bmf}} C\psi_{f1}, \quad a_{13} = \frac{b_{bs2}^{*2}}{I_{bmf}} C\psi_{f1}, \\
a_{15} &= \frac{1}{m_w} - \frac{b_{ws}^2}{I_{wz}} - \frac{b_{bs2}^{*2}}{I_{bmf}} C\psi_{f2}, \quad a_{17} = -\frac{b_{bs2}^{*2}}{I_{bmf}} C\psi_{f2}, \\
a_{21} &= \frac{b_{bs2}^{*2}}{I_{bmf}}, \quad a_{23} = \frac{1}{m_w} + \frac{b_{ws}^2}{I_{wz}} + \frac{b_{bs2}^{*2}}{I_{bmf}} C\psi_{f1}, \\
a_{25} &= -\frac{b_{bs2}^{*2}}{I_{bmf}} C\psi_{f2}, \quad a_{27} = \frac{1}{m_w} - \frac{b_{ws}^2}{I_{wz}} C\psi_{f2} - \frac{b_{bs2}^{*2}}{I_{bmf}} C\psi_{f2}, \\
a_{31} &= \frac{1}{m_w} - \frac{b_{ws}^2}{I_{wz}} + \frac{b_{bs2}^{*2}}{I_{bmf}} C\psi_{f1}, \quad a_{33} = \frac{b_{bs2}^{*2}}{I_{bmf}} C\psi_{f1}, \\
a_{35} &= \frac{1}{m_w} + \frac{b_{ws}^2}{I_{wz}} - \frac{b_{bs2}^{*2}}{I_{bmf}} C\psi_{f2}, \quad a_{37} = -\frac{b_{bs2}^{*2}}{I_{bmf}} C\psi_{f2}, \\
a_{41} &= \frac{b_{bs2}^{*2}}{I_{bmf}}, \quad a_{43} = \frac{1}{m_w} - \frac{b_{ws}^2}{I_{wz}} + \frac{b_{bs2}^{*2}}{I_{bmf}} C\psi_{f1}, \\
a_{45} &= -\frac{b_{bs2}^{*2}}{I_{bmf}} C\psi_{f2}, \quad a_{47} = \frac{1}{m_w} + \frac{b_{ws}^2}{I_{wz}} C\psi_{f2} - \frac{b_{bs2}^{*2}}{I_{bmf}} C\psi_{f2}
\end{aligned}
$$

$$
\begin{aligned}
a_{52} &= \frac{1}{m_w} + \frac{1}{m_f} + \frac{a_{wb}^2}{I_{fz}}, \quad a_{54} = \frac{1}{m_f} - \frac{a_{wb}^2}{I_{fz}}, \\
a_{56} &= \frac{1}{m_w}, \quad a_{62} = \frac{1}{m_f} - \frac{a_{wb}^2}{I_{fz}}, \\
a_{64} &= \frac{1}{m_w} + \frac{1}{m_f} + \frac{a_{wb}^2}{I_{fz}}, \quad a_{68} = \frac{1}{m_w}, \\
a_{72} &= \frac{1}{m_w}, \quad a_{76} = \frac{1}{m_w} + \frac{1}{m_f} + \frac{a_{wb}^2}{I_{fz}}, \\
a_{78} &= \frac{1}{m_f} - \frac{a_{wb}^2}{I_{fz}}, \quad a_{84} = \frac{1}{m_w}, \\
a_{86} &= \frac{1}{m_f} - \frac{a_{wb}^2}{I_{fz}}, \quad a_{88} = \frac{1}{m_w} + \frac{1}{m_f} + \frac{a_{wb}^2}{I_{fz}}
\end{aligned}
$$

and

$$
\mathbf{F}_m^1 = [F_{mx1} \quad F_{mx2} \quad F_{mx3} \quad F_{mx4} \quad F_{my1} \quad F_{my2} \quad F_{my3} \quad F_{my4}]^T. \tag{8.45}
$$

Then the switch condition can be expressed as a combination of (D.31)-(D.38) and

$$
\begin{aligned}
&|f_{fwx1}| \le |f_{fwx1s}|, \quad |f_{fwy1}| \le |f_{fwy1s}|, \quad |f_{fwx2}| \le |f_{fwx2s}|, \\
&|f_{fwy2}| \le |f_{fwy2s}|, \quad |f_{fwx3}| \le |f_{fwx3s}|, \quad |f_{fwy3}| \le |f_{fwy3s}|, \\
&\qquad\qquad |f_{fwx4}| \le |f_{fwx4s}|, \quad |f_{fwy4}| \le |f_{fwy4s}|
\end{aligned} \tag{8.46}
$$

where the static friction force components $f_{fwx1s}, \cdots$ are determined by the normal forces, the friction coefficient and the corresponding friction direction angles.

In the same way the switch conditions for the other bogie can be obtained as

$$\mathbf{A}_{b2}^{2}\mathbf{F}_{\mu m}^{2} = \mathbf{F}_{m}^{2} \tag{8.47}$$

where

$$\mathbf{F}_{\mu m}^{2} = [f_{fwx5} \quad f_{fwy5} \quad f_{fwx6} \quad f_{fwy6} \quad f_{fwx7} \quad f_{fwy7} \quad f_{fwx8} \quad f_{fwy8}]^{T} \tag{8.48}$$

$$\mathbf{A}_{b2}^{2} = \begin{bmatrix} b_{11} & 0 & b_{13} & 0 & b_{15} & 0 & b_{17} & 0 \\ b_{21} & 0 & b_{23} & 0 & b_{25} & 0 & b_{27} & 0 \\ b_{31} & 0 & b_{33} & 0 & b_{35} & 0 & b_{37} & 0 \\ b_{41} & 0 & b_{43} & 0 & b_{45} & 0 & b_{47} & 0 \\ 0 & b_{52} & 0 & b_{54} & 0 & b_{56} & 0 & 0 \\ 0 & b_{62} & 0 & b_{64} & 0 & 0 & 0 & b_{68} \\ 0 & b_{72} & 0 & 0 & 0 & b_{76} & 0 & b_{78} \\ 0 & 0 & 0 & b_{84} & 0 & b_{86} & 0 & b_{88} \end{bmatrix} \tag{8.49}$$

where

$$\begin{aligned}
b_{11} &= \frac{1}{m_w} + \frac{b_{ws}^2}{I_{wz}} + \frac{b_{bs2}^{*2}}{I_{bmf}} C\psi_{f3}, \quad b_{13} = \frac{b_{bs2}^{*2}}{I_{bmf}} C\psi_{f3}, \\
b_{15} &= \frac{1}{m_w} - \frac{b_{ws}^2}{I_{wz}} - \frac{b_{bs2}^{*2}}{I_{bmf}} C\psi_{f4}, \quad b_{17} = -\frac{b_{bs2}^{*2}}{I_{bmf}} C\psi_{f4}, \\
b_{21} &= \frac{b_{bs2}^{*2}}{I_{bmf}}, \quad b_{23} = \frac{1}{m_w} + \frac{b_{ws}^2}{I_{wz}} + \frac{b_{bs2}^{*2}}{I_{bmf}} C\psi_{f3}, \\
b_{25} &= -\frac{b_{bs2}^{*2}}{I_{bmf}} C\psi_{f4}, \quad b_{27} = \frac{1}{m_w} - \frac{b_{ws}^2}{I_{wz}} C\psi_{f2} - \frac{b_{bs2}^{*2}}{I_{bmf}} C\psi_{f4}, \\
b_{31} &= \frac{1}{m_w} - \frac{b_{ws}^2}{I_{wz}} + \frac{b_{bs2}^{*2}}{I_{bmf}} C\psi_{f3}, \quad b_{33} = \frac{b_{bs2}^{*2}}{I_{bmf}} C\psi_{f3}, \\
b_{35} &= \frac{1}{m_w} + \frac{b_{ws}^2}{I_{wz}} - \frac{b_{bs2}^{*2}}{I_{bmf}} C\psi_{f4}, \quad b_{37} = -\frac{b_{bs2}^{*2}}{I_{bmf}} C\psi_{f4}, \\
b_{41} &= \frac{b_{bs2}^{*2}}{I_{bmf}}, \quad b_{43} = \frac{1}{m_w} - \frac{b_{ws}^2}{I_{wz}} + \frac{b_{bs2}^{*2}}{I_{bmf}} C\psi_{f3}, \\
b_{45} &= -\frac{b_{bs2}^{*2}}{I_{bmf}} C\psi_{f4}, \quad b_{47} = \frac{1}{m_w} + \frac{b_{ws}^2}{I_{wz}} C\psi_{f4} - \frac{b_{bs2}^{*2}}{I_{bmf}} C\psi_{f4}
\end{aligned}$$

$$
\begin{aligned}
b_{52} &= \frac{1}{m_w} + \frac{1}{m_f} + \frac{a_{wb}^2}{I_{fz}}, \quad b_{54} = \frac{1}{m_f} - \frac{a_{wb}^2}{I_{fz}}, \\
b_{56} &= \frac{1}{m_w}, \quad b_{62} = \frac{1}{m_f} - \frac{a_{wb}^2}{I_{fz}}, \\
b_{64} &= \frac{1}{m_w} + \frac{1}{m_f} + \frac{a_{wb}^2}{I_{fz}}, \quad b_{68} = \frac{1}{m_w}, \\
b_{72} &= \frac{1}{m_w}, \quad b_{76} = \frac{1}{m_w} + \frac{1}{m_f} + \frac{a_{wb}^2}{I_{fz}}, \\
b_{78} &= \frac{1}{m_f} - \frac{a_{wb}^2}{I_{fz}}, \quad b_{84} = \frac{1}{m_w}, \\
b_{86} &= \frac{1}{m_f} - \frac{a_{wb}^2}{I_{fz}}, \quad b_{88} = \frac{1}{m_w} + \frac{1}{m_f} + \frac{a_{wb}^2}{I_{fz}}
\end{aligned}
$$

and

$$
\mathbf{F}_m^2 = [F_{mx5} \quad F_{mx6} \quad F_{mx7} \quad F_{mx8} \quad F_{my5} \quad F_{my6} \quad F_{my7} \quad F_{my8}]^T. \tag{8.50}
$$

So that the switch condition is a combination of (D.47)-(D.54) and

$$
\begin{array}{lll}
|f_{fwx5}| \le |f_{fwx5s}|, & |f_{fwy5}| \le |f_{fwy5s}|, & |f_{fwx6}| \le |f_{fwx6s}|, \\
|f_{fwy6}| \le |f_{fwy6s}|, & |f_{fwx7}| \le |f_{fwx7s}|, & |f_{fwy7}| \le |f_{fwy7s}|, \\
 & |f_{fwx8}| \le |f_{fwx8s}|, & |f_{fwy8}| \le |f_{fwy8s}|.
\end{array} \tag{8.51}
$$

As we have shown in chapter 4, if the acting friction forces are correctly determined for any stick motion of the system then the degrees of freedom of the system can automatically vary from one state space to another one with a different dimension. From a mathematical point of view the corresponding numerical integration method can be used without violation of the assumption of continuity.

Based on the theory we have discussed from chapter 2 to chapter 8 the program named **TruCars** has been developed for the purpose of the simulation of the motion of the three-piece-freight-truck. With the program the numerical studies can be done. We will perform the numerical investigation in the next chapter.

CHAPTER 9

The numerical investigation and the results

In this chapter we use the model of the three-piece-freight-truck which we have derived in previous chapters which is developed based on the model to investigate its dynamic performances under various conditions. We will study the hysteresis loop of the contact forces on the surfaces of the wedges under harmonic excitations from the track. The critical speed of the system will be calculated and the chaotic motion of the three-piece-freight-truck will be validated. The characteristics of the track irregularity can be described by the Power Spectral Density(PSD) but the PSD can not be used directly for the response analysis of the nonlinear dynamic system. We will derive a way to transform the PSD into a time series and then use the time series as the simulation of the rail irregularities in the lateral and vertical directions. Then the responses of the system to the track irregularity will be simulated. The comparison of the numerical results and the measured results is performed.

9.1 Discussion of the critical speed

There are two different critical speeds of vehicles on railways: The *linear critical speed* and the *nonlinear critical speed*. The line critical speed means the velocity at which the stationary solution loses its stability through a Hopf bifurcation. The linear critical speed usually gives a higher critical speed than the measured one[True, 1983-2000]. The nonlinear critical speed is the lowest speed for which a periodical motion exists and it will be determined by the bifurcation analysis. Normally the critical speed means the nonlinear critical speed in the railway vehicle system dynamics.

We know that the numerical investigation of nonlinear dynamical systems is time

consuming even for rather simple dynamic systems. Because the dynamical system of the three-piece-freight is very complicated due to the characteristics of the non-smoothness and the discontinuities and the collapse of the state space caused by the stick-slip motion originating from the two-dimensional dry friction, the time for computation of the necessary data for the bifurcation and the first return map for the purpose of a fine visualization is very long.

Figure 9.1 shows the bifurcation diagram for the determination of the critical speed. From the figure we see that the motion of the wheelset 1 changes from a stable steady motion to a periodic motion and then jumps into a chaotic motion when the speed increases. Otherwise, when decreasing from high speed to low speed then the motion changes from chaotic to steady without the periodic motion state. The linear critical speed of the three-piece-freight-truck is about 28.1 m/s and the nonlinear critical speed is about 20.5 m/s for the empty car.

In the speed range $20.5m/s$ to $26.2m/s$ we therefore find a steady as well as a chaotic attractor. In the speed range 26.2 m/s to $28.5m/s$ there exist three attractors- a steady, a periodic and a chaotic one and above $28.5m/s$ only a chaotic attractor exists. It is important to note that these results only concern the existence of attractors. Other investigations of nonlinear mechanical systems[True, 1999] have shown that the coexistence of chaotic attractors may lead to chaotic transients in the system with dangerously high amplitudes. This calls for further investigations of the dynamics of the three-piece-freight-truck model.

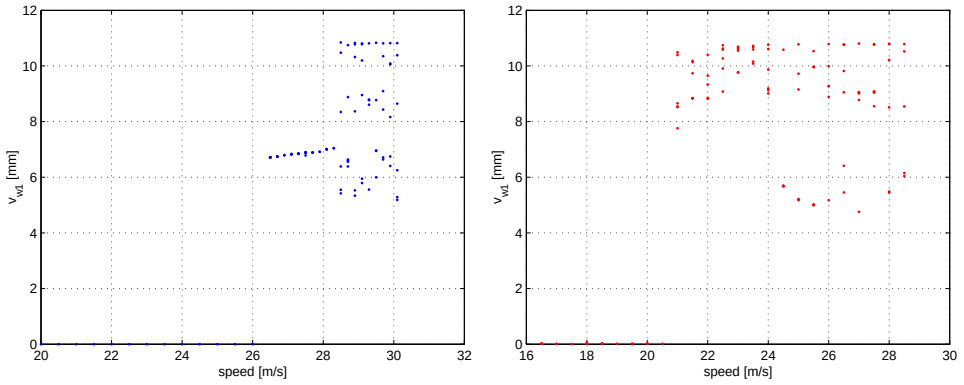

Figure 9.1: *Left: The bifurcation diagram of the three-piece-freight-truck with speed from 20 m/s to 30 m/s. Right: The bifurcation diagram of the three-piece-freight-truck with speed from 28.5 m/s to 16 m/s.*

It should be pointed out that the amplitudes of the motions of the wheelsets are not zero even at a low vehicle speed because the dry friction produces a stick-slip motion. The case is illustrated in Figure 9.2 and Figure 9.3. From the figures we know that the longitudinal displacements, u_{w1}, u_{w3} of the wheelsets 1 and 3 differ from zero. The reason is that there exists a clearance between the whleeset and the

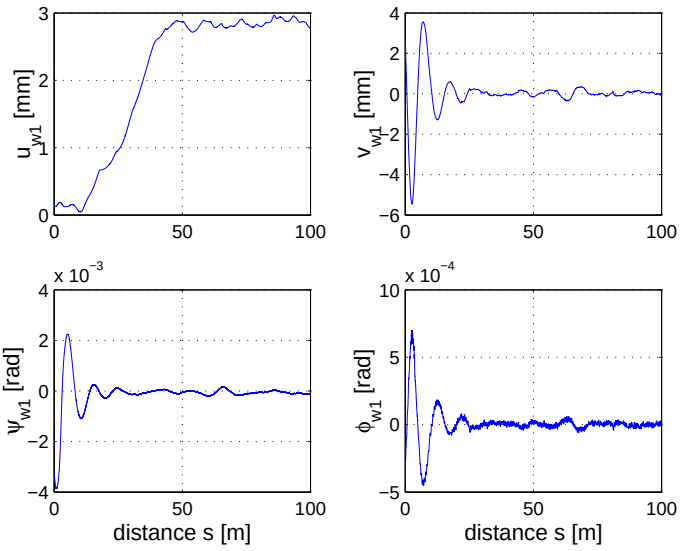

Figure 9.2: *The motions of the wheelset 1 at the vehicle speed 20 m/s*

side frame in the longitudinal direction and friction on the contact surface of the wheelset and the side frame is two-dimensional. The yaw of the wheelsets 1 and 3 differ from zero. They are not periodic motion because the motion is influenced by the stick-slip motion between the wheelset and the side frame. In the one-dimensional case, the stick-slip motion is chaotic with one-dimensional dry friction. We may say the stick-slip motion of the wheelset is chaotic too with the two-dimensional dry friction at a lower vehicle speed.

9.2 An investigation of the chaotic motion

In the study of dynamical systems the tools that are often used are: a phase space, a Poincaré map(or Lorenz first return map), the power spectra and the Lyapunov exponents. They provide information about the dynamics of the system for specific values of the parameters, e.g. the speed V in railway vehicle systems. The dynamics may also be viewed more globally over a range of parameter values, thereby allowing simultaneous comparison of periodic and chaotic behavior. The bifurcation diagram provides a summary of the essential dynamics and is therefore a useful method of acquiring this overview.

The bifurcation window from speed 28.5 m/s to 29.42 m/s is shown in the Figure 9.4. It should be noted that because of the long computer time for the complicated dynamical system the steps of the speed can not be too small. Therefore the figure is not very detailed but anyhow it still can provide information about the chaotic

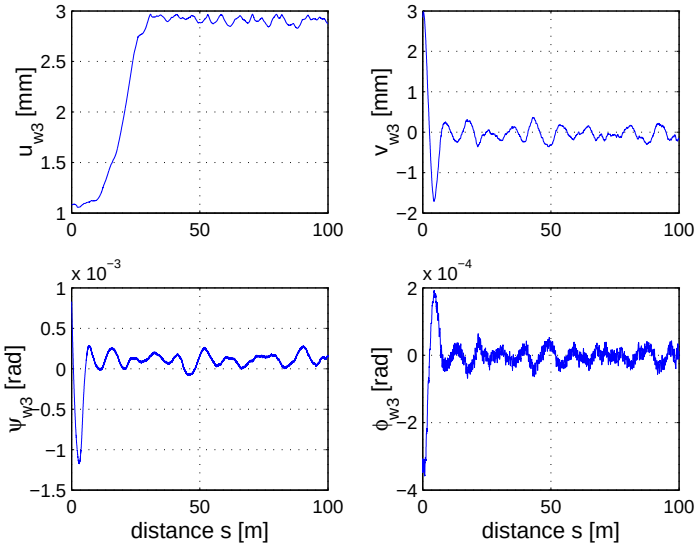

Figure 9.3: *The motions of the wheelset 3 at the vehicle speed 20 m/s*

motion. For the speed $29m/s$ the lateral displacement of the four whelssets is shown in Figure 9.5. The effects of the impacts between the side frames and the adapters and as well as the friction forces on the surfaces of the wedge and the adapters may be the main facts to make the chaotic motion special.

Here we compare the result obtained by the simulation using the present model with that obtained by NUCARS. The result comes from China Academy of Railway Sciences[Li, 2000] is shown in Figure 9.6. In that model a gondola three-piece-freight-wagon is used and some parameters are little different from the one we used in the present thesis but the model is very different. As we have seen in the previous chapters in our model the characteristics of the two-dimensional friction, stick-slip motion and the structure varying systems are included. That makes the obvious difference from the model derived with NUCARS. From the numerical results shown in Figures 9.5 and 9.6 we can find the difference of the motion between the two models. With our model, the lateral motion of the wheelset is not periodic because of the effect of the impact force of the dead-band stop and the stick-slip motion between the wheelset and the side frame with two-dimensional dry friction. The lateral motion of the wheelset from the model with NUCARS looks like a periodic motion because in that model the two-dimensional dry friction and the stick-slip motion are neglected.

The phase diagrams of the wheelsets 1 and 2 are shown in Figure 9.7.

The first return maps of the lateral displacements of wheelsets number 1 and 2 are shown in the Figure 9.8. And the first return maps of the yaw of the wheelsets 1 and 2 are shown in the Figures 9.9.

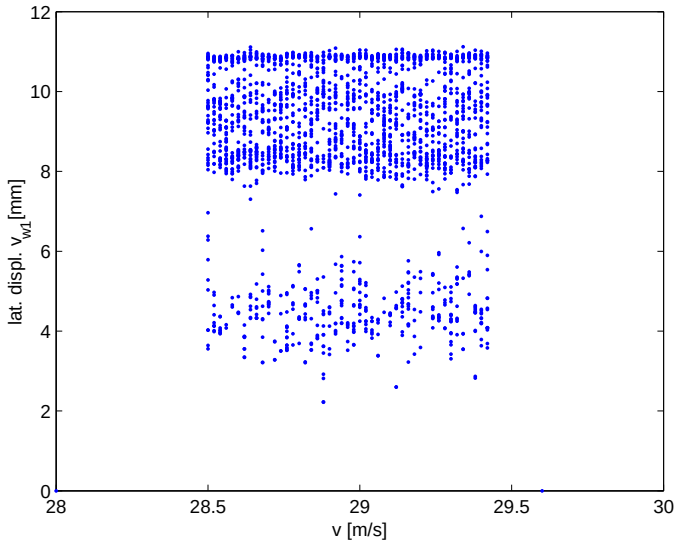

Figure 9.4: *The bifurcation diagram of the lateral motion of the wheelset 1 from the speed* $28.5m/s$ *to* $29.5m/s$.

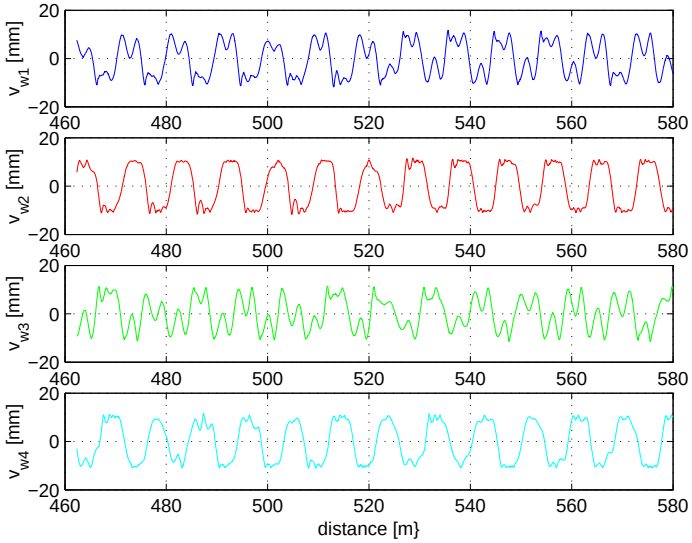

Figure 9.5: *The lateral displacements of the wheelsets with the speed* $29m/s$.

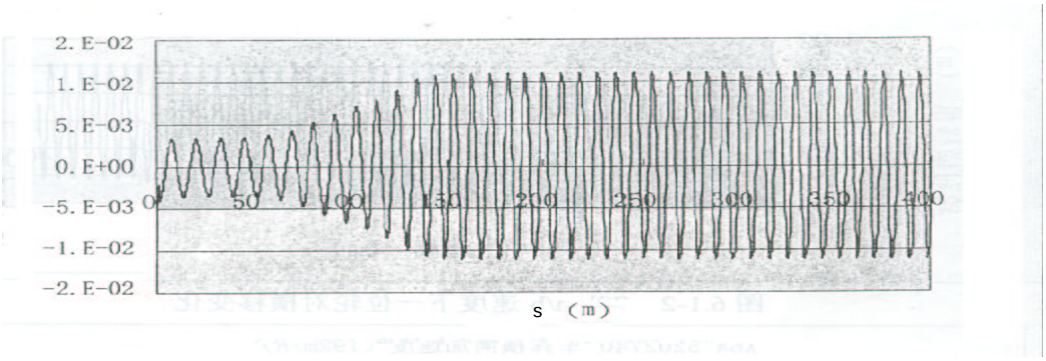

Figure 9.6: *The lateral displacements of the wheelsets with the speed* $22.778m/s$ *with NUCARS [Li, 2000]. The unit of the vertical axis is meter.*

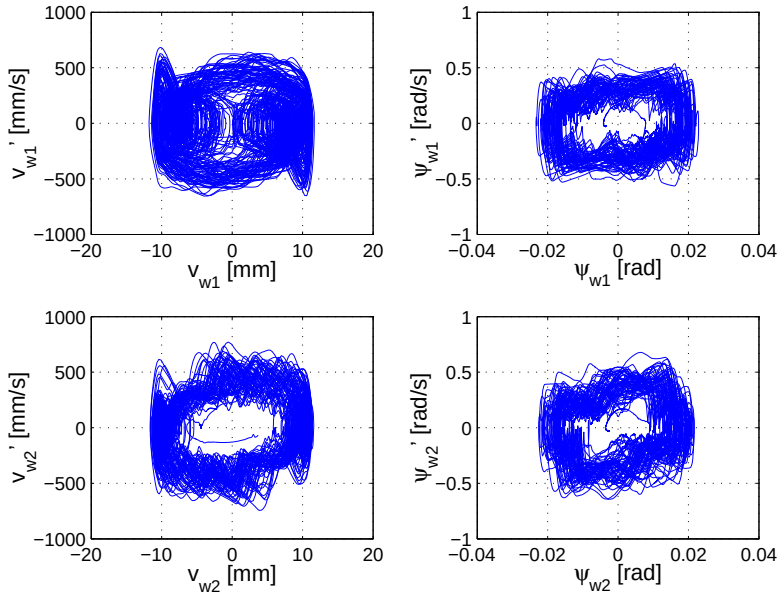

Figure 9.7: *The phase diagrams of the wheelsets 1 and 2 with the speed* $29m/s$.

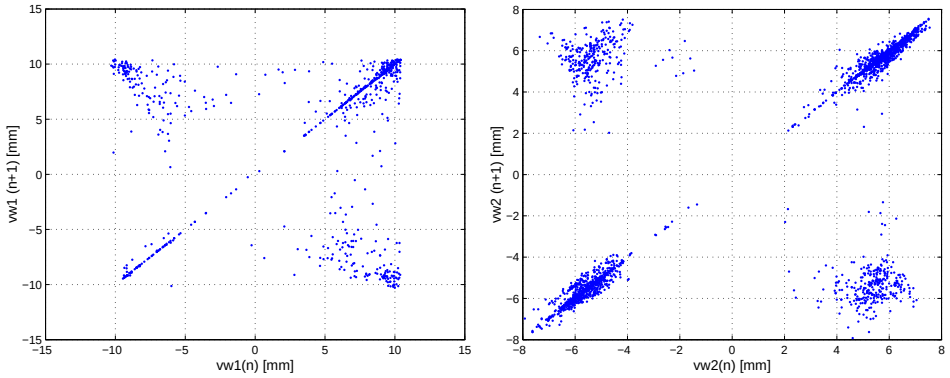

Figure 9.8: *The first return maps of the lateral displacements of wheelsets number 1 (left) and 2 (right) with the speed 29 m/s for the empty car.*

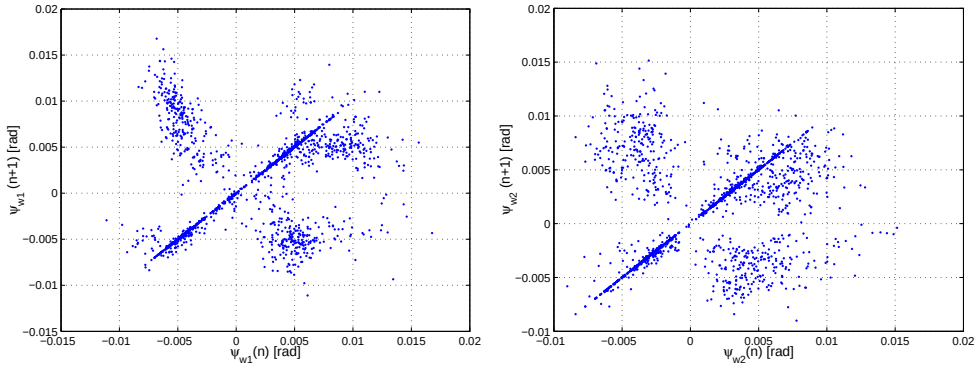

Figure 9.9: *The first return maps of the yaws of wheelsets number 1 (left) and 2 (right) with the speed 29 m/s for the empty car.*

We only have about 2000 points in the first return map. From the bifurcation diagram, the lateral displacement curves of the wheelsets, the phase diagrams and the first return maps we can definitely claim that the motion of the three-piece-freight-truck is chaotic for the running speed 29 m/s. We can also find that the chaotic motion of the three-piece-freight-truck is obviously different from the chaotic motion of the Cooperrider's passenger car model[True, 1999] since the chaotic motion is not a small perturbation on a dominating periodic motion.

9.3 The hysteresis loops of the contact forces on the surfaces of the wedges

We use the sinusoidal function as an excitation on the vertical alignment of the track. The sinusoidal function is defined by

$$ir = A_m \sin(\frac{2\pi}{L_w} s) \tag{9.1}$$

where A_m denotes the amplitude with the values 6 mm for both rails; L_w is the wave length with a value of $10m$. s stands for the running distance. The speed of the vehicle is $20m/s(72km/h)$. The friction function (1.4) is used and an empty car is considered because the possibility of the derailment of the empty car is much greater than the loaded car for the same running speed.

Figure 9.10 shows the motion of one end of the bolster relative to the corresponding side frame. Figure 9.11 shows the friction forces on the surfaces of the wedge. The upper subplot is the friction force on the surface of the wedge contacting the bolster in vertical direction; the middle and lower subplots denote the friction force on the surface of the wedge contacting the side frame in lateral and vertical directions, respectively. Because there is no lateral parasitic motion in the lateral direction of the bolster the friction force in that direction is zero as it should be. Figure 9.12 shows the hysteresis loop of the normal forces on the surfaces of the wedge. Figure 9.13 shows the normal contact force on the surface of the adapter.

The phenomenon of the hysteresis of the normal forces on the surfaces of the wedge is due to the friction forces on the surfaces of the wedge. If the friction direction angle varies discontinuously then the direction of the friction force vector changes discontinuously. Therefore the discontinuous friction forces finally cause the jump of the normal contact forces. In other words, the jump of the friction direction angle causes the jump of the normal contact forces. So the phenomenon of the hysteresis of the normal contact forces on the surfaces of the wedge appears.

If the wavelength is changed to 4 m and other parameters are unchanged then the friction forces and the normal forces on the surfaces of the wedge 1 change as shown in Figures 9.14 and 9.15. We see from Figures 9.12 and 9.15 that the amplitude of the response of the bolster in vertical direction is larger in the case of the longer wavelength(10 m) than in the case of the short wavelength(4 m).

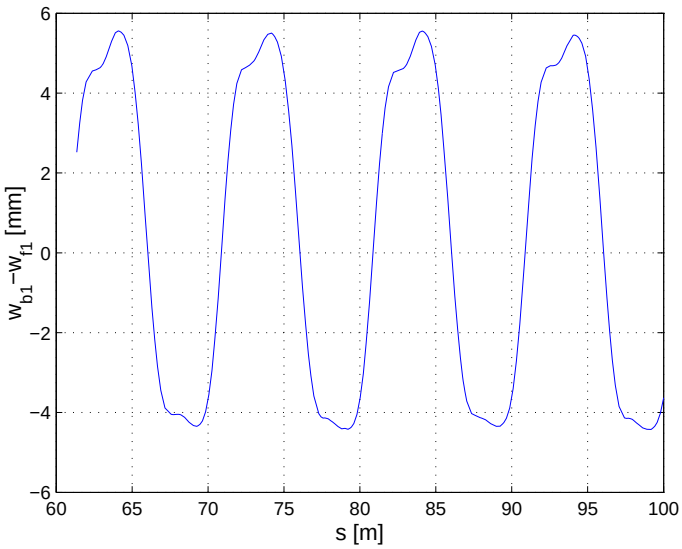

Figure 9.10: *The stick-slip motion of the front bolster in the vertical direction*

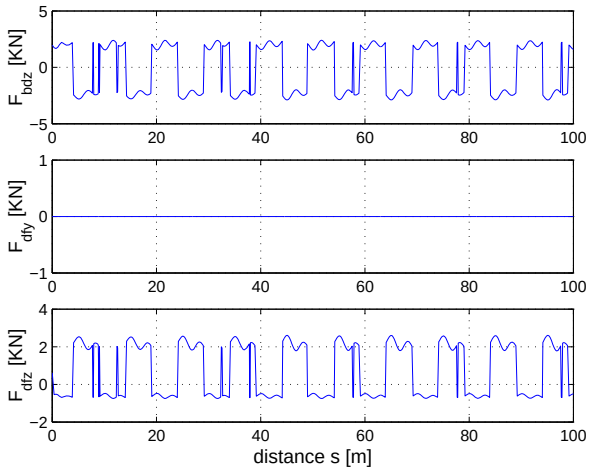

Figure 9.11: *The friction force on the surface of the wedge when the wavelength of the periodic disturbance is 10 m. The upper subplot shows the friction force between the wedge and the bolster in the vertical direction; the middle and lower subplots denote the friction force between the wedge and the frame in the lateral and vertical directions respectively.*

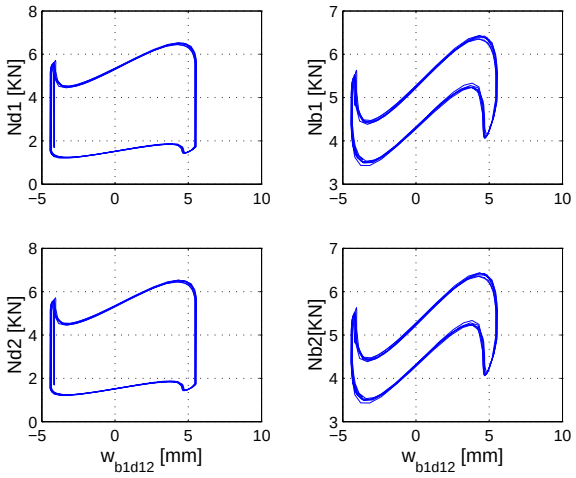

Figure 9.12: *The hysteresis loops of the normal forces on the surface of the wedges 1 and 2. The abscissa denotes the vertical displacement of the bolster and the vertical coordinate denotes the normal force. The left subplot is the normal forces on the surfaces of the wedges contacting the frame and the right subplot shows the normal forces on the surfaces of the wedges contacting the bolster.*

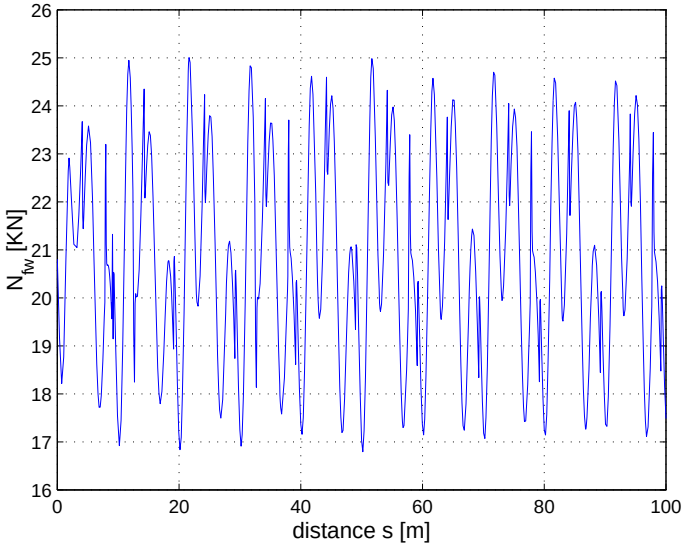

Figure 9.13: *The normal force on the surface of an adapter contacting the side frame*

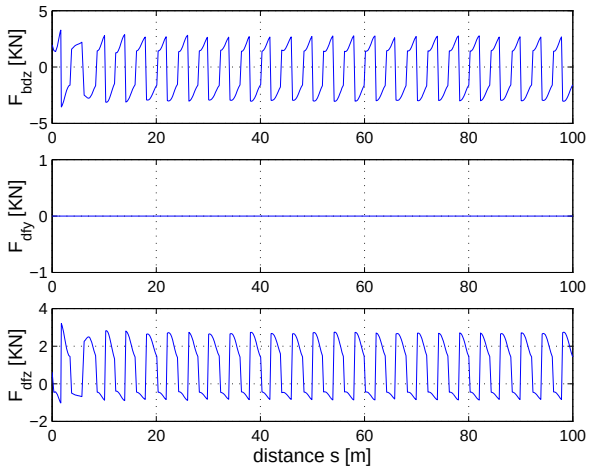

Figure 9.14: *The friction force on the surface of the wedge when the wavelength of the periodic disturbance is 4 m. The upper subplot shows the friction force between the wedge and the bolster in the vertical direction; the middle and lower subplots denote the friction force between the wedge and the frame in the lateral and vertical direction respectively.*

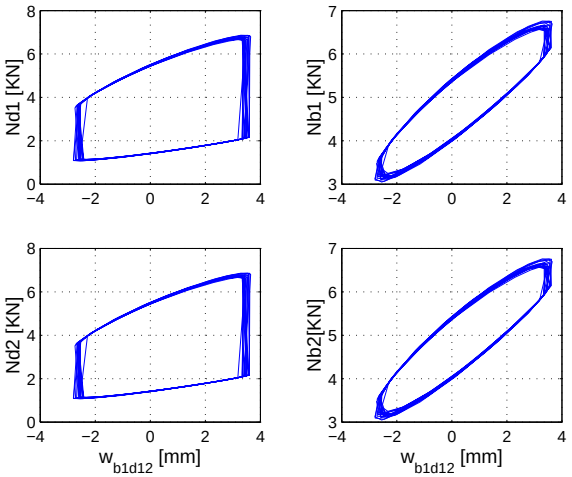

Figure 9.15: *The hysteresis loops of the normal forces on the surface of the wedges 1 and 2. The abscissa ordinate denotes the vertical displacement of the bolster and the vertical coordinate stands for the normal force. The left subplot is the normal forces on the surfaces of the wedges contacting side frame and the right subplot denote the normal forces on the surfaces of the wedges contacting the bolster.*

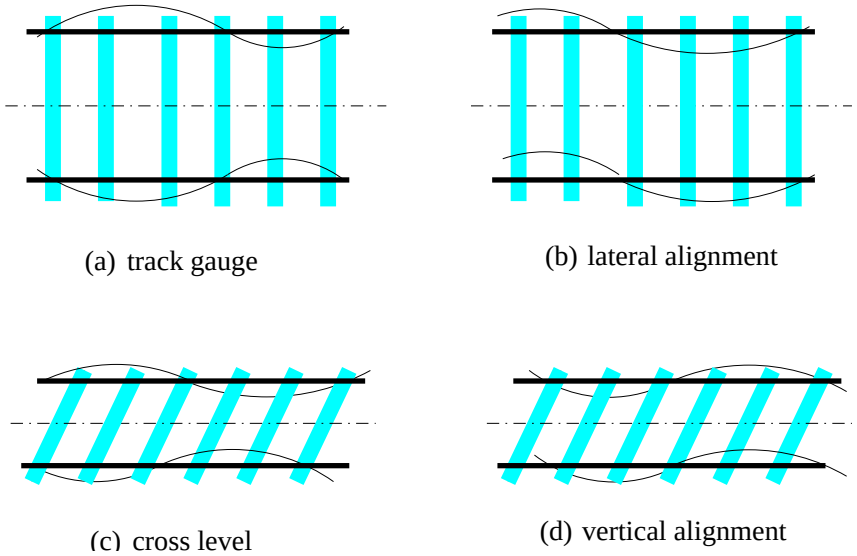

(a) track gauge (b) lateral alignment

(c) cross level (d) vertical alignment

Figure 9.16: *Definitions of track irregularities*

9.4 The responses of the system to an irregular track

9.4.1 A description of the tangent track with irregularities

The irregularities of the track geometry are defined in terms of four parameters as shown in Figure 9.16. The deviations of the track gauge, the lateral alignment, the cross level and the vertical alignment(Garg and Dukkipati, 1984) are
The gauge:

$$g = (v_l - v_r)/2. \tag{9.2}$$

The cross level:

$$cl = (w_l - w_r)/2. \tag{9.3}$$

The lateral alignment:

$$al = (v_l + v_r)/2 \tag{9.4}$$

and the vertical alignment:

$$av = (w_l + w_r)/2. \tag{9.5}$$

where v_l, v_r denotes the lateral variations of the left and right rails respectively; w_l, w_r denotes the vertical variations of the left and right rails respectively.

Table 9.1: *The parameters of the determination of the PSD*

Symbols	Units	6	5	4	3	2	1
A_v	$cm^2/rad/m$	0.0339	0.2095	0.5376	0.6816	1.0181	1.2107
A_s	$cm^2/rad/m$	0.0339	0.0762	0.3027	0.4128	1.2107	3.3634
Ω_s	rad/m	0.4380	0.8209	1.1312	0.8520	0.9308	0.6046
Ω_c	rad/m	0.8245	0.8245	0.8245	0.8245	0.8245	0.8245

Together with the half gauge b these quantities describe any type of tracks.

The power spectral density(PSD for short) of a random process provides the frequency composition of the data in terms of the spectral density of their mean square value.

The track geometry data base that represents a reasonable sample of track in the Unites States have been established for the analytical characterization of track geometry variations. There are various PSDs of the tracks provided by e.g. FRA(The Federal Railroad Administration), and the German PSD. In the present thesis the PSDs given by FRA are used and they can be modelled as following[Wang, 1994] The vertical alignment

$$S_{av}(\Omega) = \frac{kA_v\Omega_c^2}{\Omega^2(\Omega^2+\Omega_c^2)}, \quad (cm^2/rad/m). \tag{9.6}$$

The lateral alignment

$$S_{al}(\Omega) = \frac{kA_a\Omega_c^2}{\Omega^2(\Omega^2+\Omega_c^2)}, \quad (cm^2/rad/m). \tag{9.7}$$

and the track gauge and cross level

$$S_{gcl}(\Omega) = \frac{4kA_v\Omega_c^2}{(\Omega^2+\Omega_c^2)(\Omega^2+\Omega_s^2)}, \quad (cm^2/rad/m) \tag{9.8}$$

where $S(\Omega)$ denotes the relative PSDs; Ω stands for the spatial wave number (rad/m) that is related to the time frequncy f_h (Hertz) by the relation $\Omega = 2\pi f_h/V$. Other quantities are defined in the table 9.1.

9.4.2 Transformation of the Power Spectral Density(PSD) to Time series

For the nonlinear system the PSD can not be directly used as the excitations to obtain the responses because the principle of the superposition does not hold. The usual way is first to transform the PSD into time series as the excitations for the response analysis.

There may be different ways to transform the PSD into its corresponding time series. Inspired by G. Cheng[Cheng, 2000] we use the following way to do this.

We know that for a discrete time series $x_n, n = 1, ..., N$ its frequency response or spectrum can be obtained by means of the Finite Fourier Transform(FFT) [Bendat,2000][Otnes, 1972][Robinson, 1979] at the discrete frequencies

$$X_{f_k} = \Delta t \sum_{j=0}^{N-1} x_j \exp(-i(\frac{2\pi}{N})jk), \quad (k = 0, 2, \cdots, N-1) \tag{9.9}$$

where $i = \sqrt{-1}$. The modulus of the frequency spectrum, X_k is of even symmetry and the argument of the X_k is of odd symmetry about $N/2$, where $N = 2^q$ and q is selected as an integer which depends on the sampling time, the vehicle speed and the minimal wavelength.

The one-sided auto-power spectral density(PSD) is obtained from (9.9) as following:

$$S_{k1} = \frac{2\Delta t}{N}|X_k|^2, \quad (k = 1, 2, \cdots, N/2-1) \tag{9.10}$$

and the two-sided auto-power spectral density(PSD) is then

$$S_{k2} = S_{k1}/2. \tag{9.11}$$

Here the frequency interval $(0, 1/2\Delta t)$ is broken into $N/2$ parts, so that the frequency increment is

$$\Delta f = \frac{1}{N\Delta t} \tag{9.12}$$

in which the Δt denotes the sample interval and is selected to produce an adequate Nyquist frequency.

We can rewrite (9.10) as

$$S_k \frac{1}{N\Delta t} = \frac{2}{N^2}|X_k|^2, \quad (k = 1, 2, \cdots, N/2-1) \tag{9.13}$$

So that if the one-sided PSD is known a priori then the modulus of the frequency spectrum can be calculated by

$$|X_k| = \frac{N}{\sqrt{2}}\sqrt{S_k(k\Delta f)\Delta f}, \quad (k = 1, 2, \cdots, N/2-1) \tag{9.14}$$

and if the PSD is given as a two-sided power spectral density then

$$|X_k| = N\sqrt{S_k(k\Delta f)\Delta f}, \quad (k = 1, 2, \cdots, N/2-1) \tag{9.15}$$

Then the spectrum can be written as[Bendat, 2000]

$$X_k = |X_k| \exp(i\phi_k), \quad (k = 1, 2, \cdots, N/2-1) \tag{9.16}$$

where ϕ_k is assumed as uniformly distributed random numbers in the interval(0,2π).

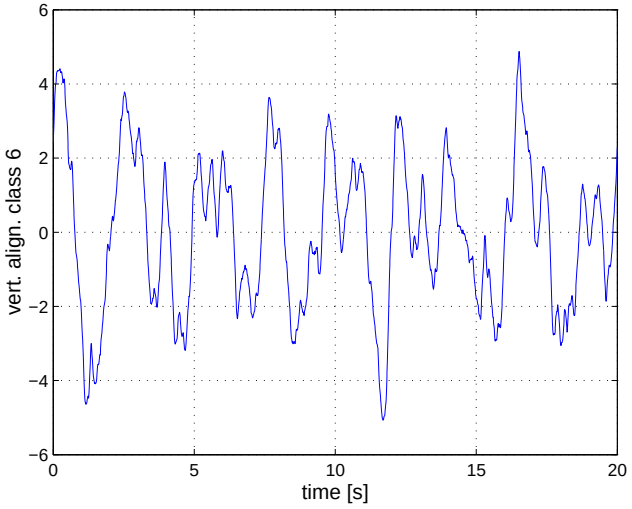

Figure 9.17: *The irregularity of the vertical alignment of a track transformed from the PSD of class 6. The unit of the vertical axis is mm.*

The numbers of the frequency spectrum X_k only contains the half integer data(k= 1,2,$\cdots$, $N/2-1$). The other half can be directly obtained using its symmetric character.

To the end, we do the inverse finite Fourier transform(IFFT) on the frequency spectrum $X(k)$ by the formula

$$x(n) = \frac{1}{N}\sum_{k=0}^{N-1} X(k) exp(\frac{i2\pi kn}{N}), \quad (n = 0, 1, 2, \cdots, N-1) \tag{9.17}$$

then the time series $x(n)$ can be obtained from the specified PSD.

The time series obtained in this way depends on the vehicle speed, V and the minimal and maximal wave length, L_{min} and L_{max}.

Figure 9.17 shows the vertical alignment of a track which is transformed from the PSD of class 6 corresponding to the speed 20 m/s. We use this time series to calculate its power spectral density (PSD) and compare it with the result by formula(9.6) and we can find that the difference is acceptable. The results are shown in Figure 9.18.

With the relations (9.2)-(9.5) the four parameters of the gauge, cross level, lateral alignment and vertical alignment can also be transformed to the geometric deviations of the profiles of the rails in the lateral and vertical directions. Figure 9.19 shows the vertical irregularities of the right rail with the PSD of class 1 to 6.

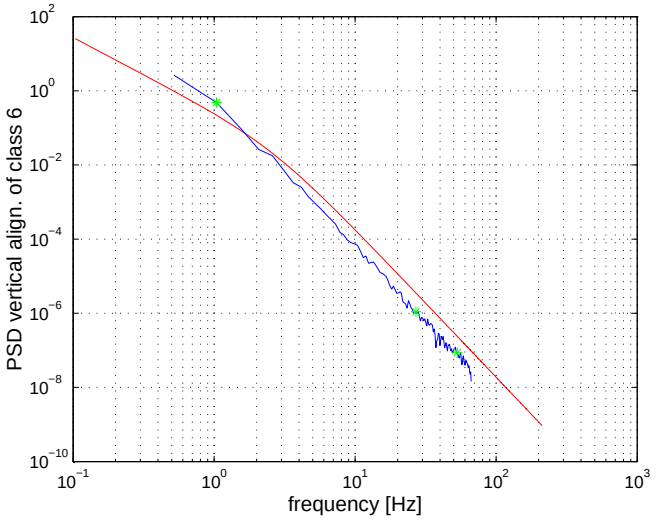

Figure 9.18: *The comparison of the theory and simulated PSD of class 6. The solid line denotes the PSD calculated by formula(9.6) and the solid line with $*$ on it is the simulated PSD.*

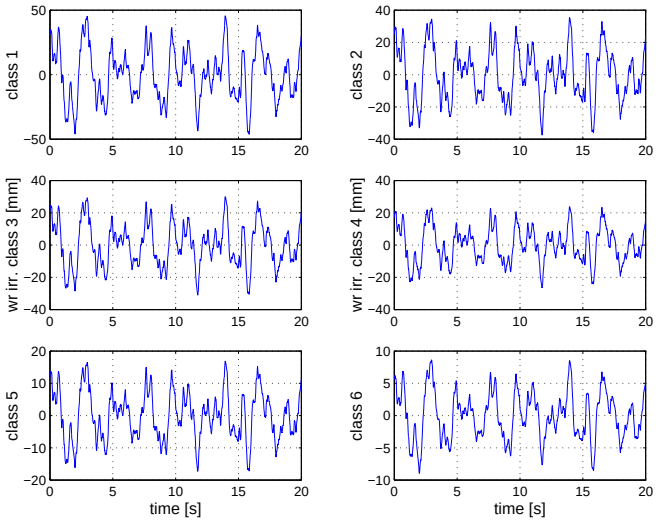

Figure 9.19: *The deviation of the profiles of the right rail in the vertical direction transformed from the PSD of class 1 to 6.*

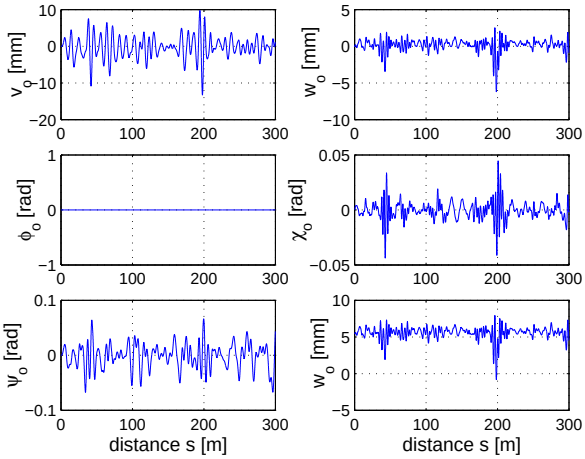

Figure 9.20: *The responses of the car body to the irregular track class 6 for the empty car. v_o, w_o, χ_o and ψ_o denote the lateral displacement, vertical displacement, roll, pitch and yaw rotations of the car body respectively.*

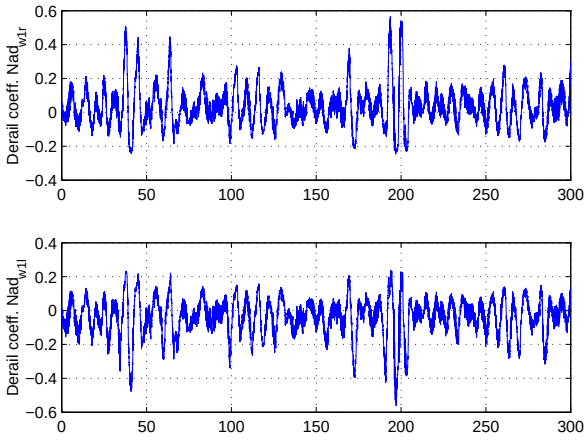

Figure 9.21: *The derailment coefficients of the right wheel/rail and the left wheel/rail of the wheelsets 1 under the excitation of the track PSD class 6 for the empty car.*

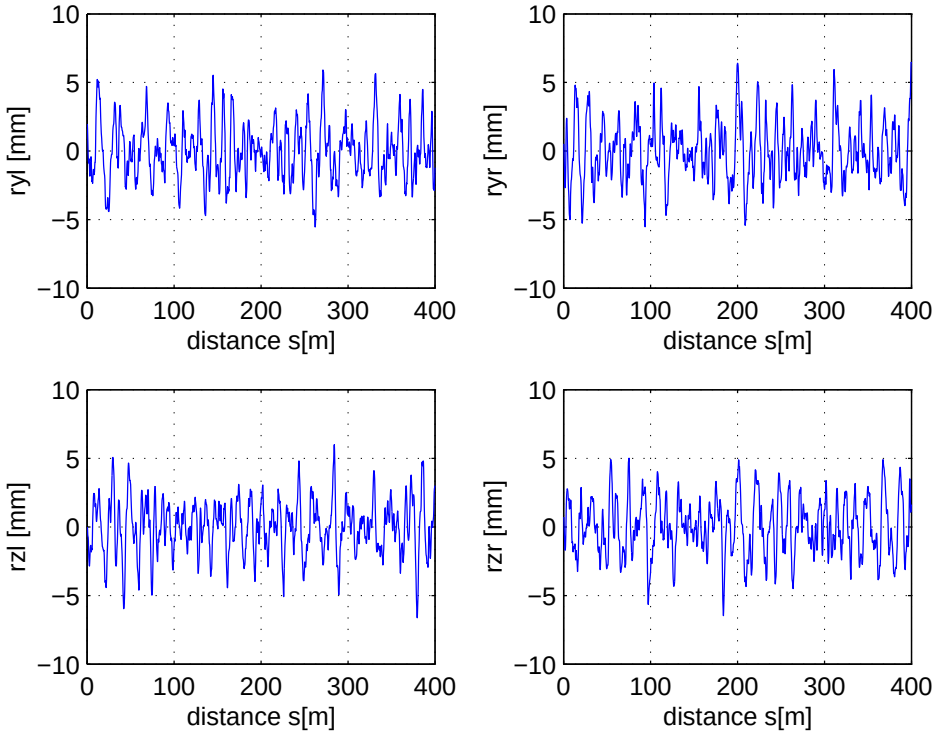

Figure 9.22: *The lateral and vertical irregularities of the rails. ryl, ryr denote the lateral deviations of the left/right rails; rzl, rzr denotes the vertical deviations of the left/right rails.*

9.4.3 The responses of the three-piece-freight-truck to the irregular track

We use the time series that we have just obtained to be the deviations of the rails in the lateral and vertical directions. The track of class 6 and the running speed 20 m/s ($72km/h$) of the vehicle are selected. The parameters of the three-piece-freight-truck are shown in appendix E.

Figure 9.20 shows the motions of the car body in the lateral, vertical displacements; roll and yaw rotations. Figure 9.21 shows the derailment coefficients, Y/Q of the right wheel/rail and the left wheel/rail of the wheelsets 1. The derailment coefficent is defined by the ratio of the lateral contact force to the vertical contact force between a wheel and a rail. An acceptable critical value of the derailment coefficient is about 0.8.

The results show that the motion of the three-piece-freight-truck is safe when the running speed is less than the nonlinear critical speed $20.5m/s$ (73.8 km/h).

In order to compare the numerical results with the measured results we next use the geometric deviations of the profiles of the rails which is transformed from the track geometry PSDs provided by the Academy of China Railway Sciences [Cheng, 2000]. Unfortunately there is no measured data of the irregular track corresponding directly to the track where the wheel/rail contact forces of the three-piece-freight-truck are measured. The lateral and vertical geometric deviations of the profiles of the left and right rails are shown in Figure 9.22. The running speed used in our simulation is $78km/h$

The measured lateral and vertical wheel/rail contact forces on the right rail are shown in Figure 9.23. The running speed of the vehicle is $78km/h$.

The numerical results of the lateral and vertical forces between the right wheel/rail are shown in Figure 9.24. We can find that the range of the lateral and vertical contact forces between the numerical and the measured results are similar. The difference between the numerical and measured results is probably due to the fact that the new truck is used in the numerical simulation but the used truck is used in the measurement.

Figure 9.25 shows the measured acceleration of the car body near the front center plate in the lateral direction. The lateral acceleration of the car body at the center plate from our simulation is shown in Figure 9.26.

In addition to the above results the other simulation results are shown in Figures 9.27-9.31. Figure 9.27 shows the tangential and normal forces on the front center plate between the car body and the bolster.

From Figure 9.28 we can find that the distribution of the normal forces on the surfaces of the wedges number 1 and 2 is asymmetrical due to the effect of the tractive effort.

Figure 9.29 shows the friction forces on the surfaces of the wedge number 1 in the lateral and vertical directions.

Figure 9.30 shows the displacements of the front wheelset. We can find that the longitudinal displacement of the wheelset is about $2mm$ so it should not be neglected

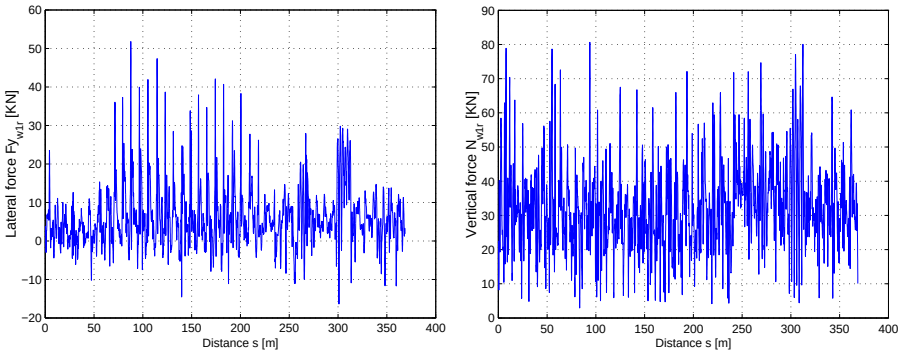

Figure 9.23: *The measured lateral and vertical forces between the right wheel/rail.*

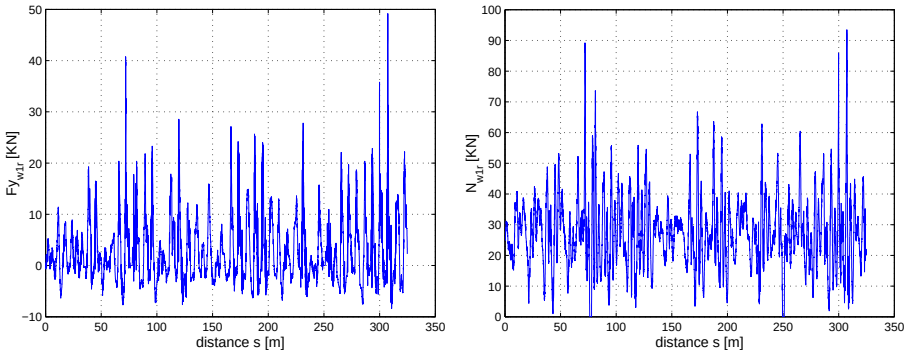

Figure 9.24: *The simulated lateral and vertical forces between the right wheel/rail.*

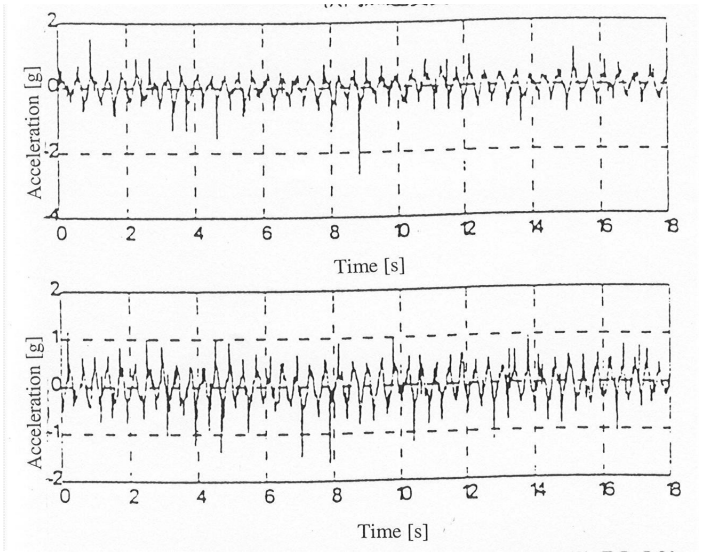

Figure 9.25: *The measured lateral acceleration of the car body near the front center plate. Upper subplot: The speed V is 75 km/h. Lower subplot: The speed V is 80 km/h.* $g = 9.81m/s^2$ *[Li, 2000]*

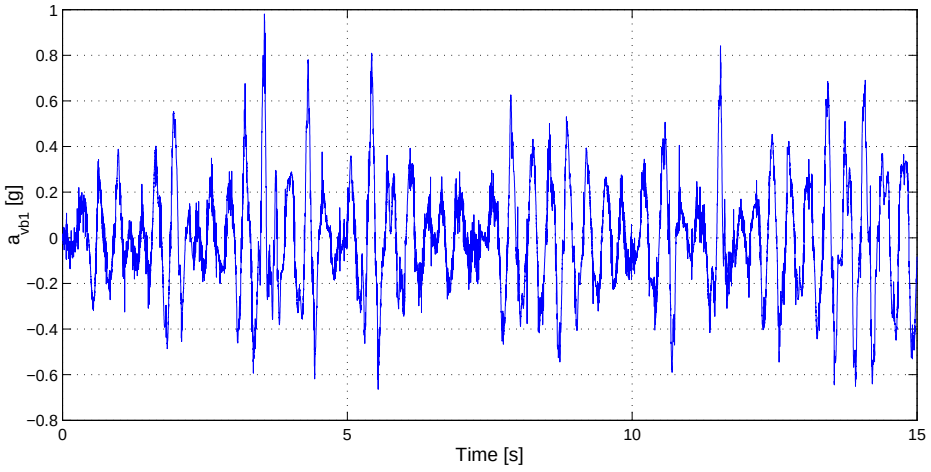

Figure 9.26: *The simulated lateral acceleration of the front center plate.* $g = 9.81m/s^2$

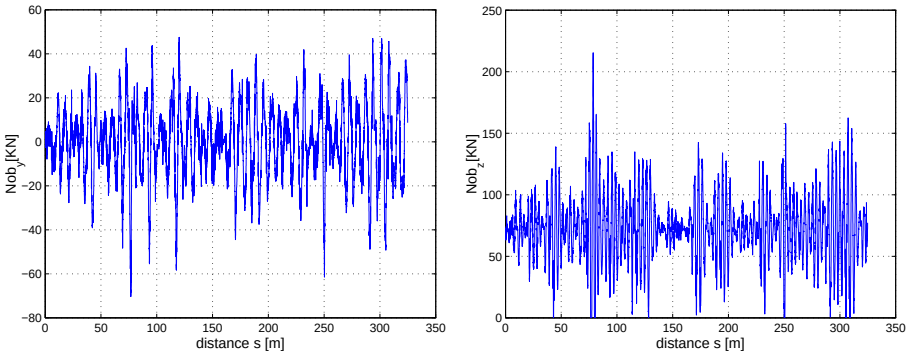

Figure 9.27: *The simulated lateral and vertical forces reacting on the front center plate.*

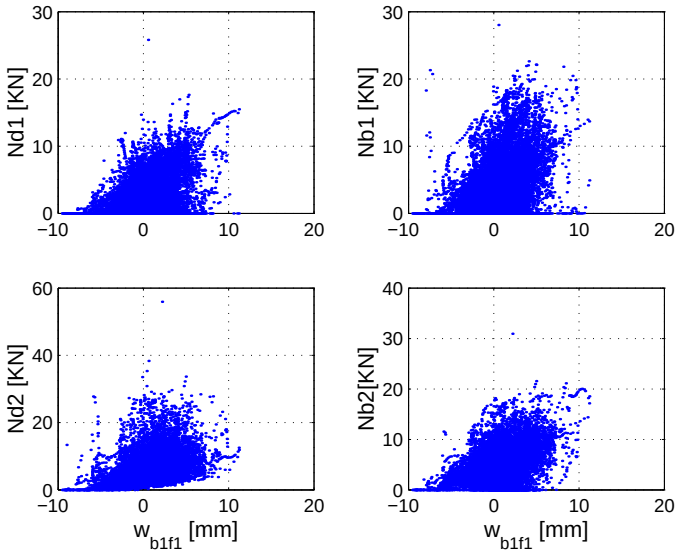

Figure 9.28: *The normal forces on the surfaces of the wedge number 1 and 2 (see Figure 6.3)*

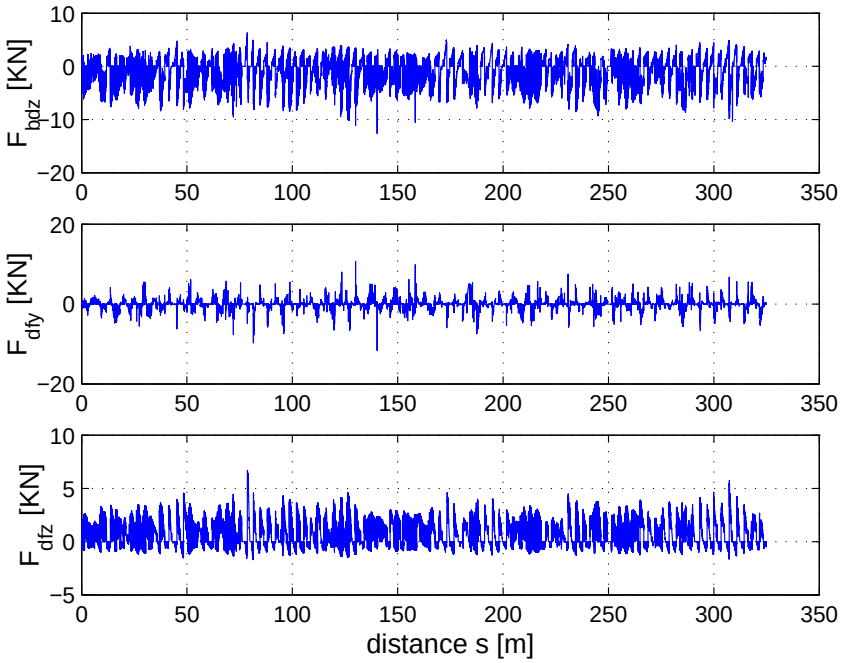

Figure 9.29: *The friction force on the surface of the wedge when the wavelength of the periodic disturbance is 4 m. The upper subplot shows the friction force on the surface of the wedge contacting the bolster in the vertical direction; the middle and lower subplots denote the friction force on the surface of the wedge contacting the frame in the lateral and vertical direction respectively*

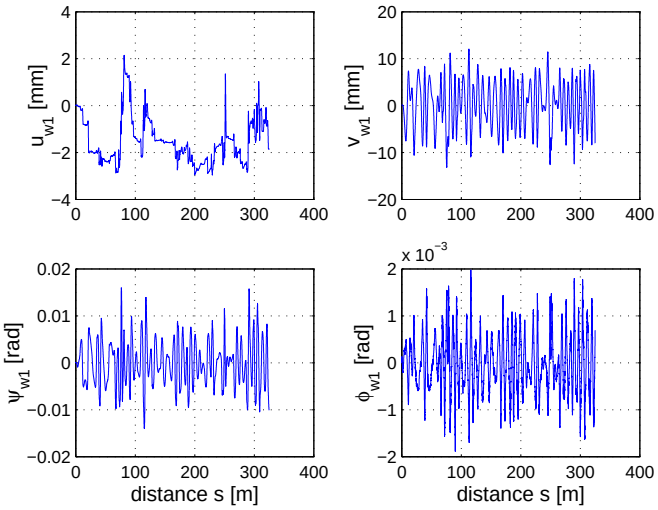

Figure 9.30: *The parasitic motion of the front wheelset.* u, v denotes the longitudinal and lateral displacements; ϕ, ψ denotes the roll and yaw rotations of the wheelset.

for the modelling of the dynamics of the three-piece-freight-truck.

Figure 9.31 then shows the derailment coefficient of the right wheel/rail of the front wheelset.

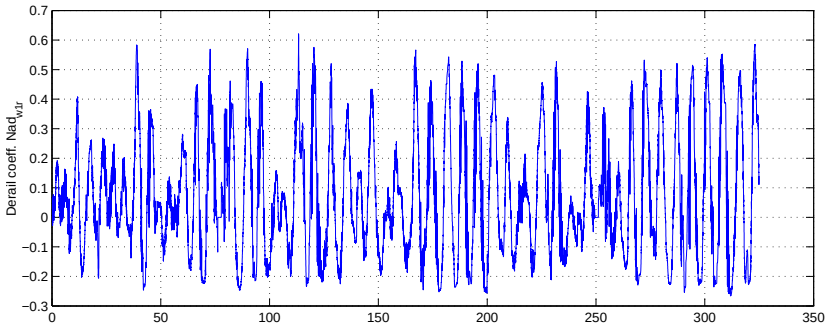

Figure 9.31: *The derailment coefficient of the right wheel/rail of the front wheelset.*

The running speed $78km/h$ $(21.67m/s)$ is higher than the nonlinear critical speed $73.8km/h(20.5m/s)$ so the motion of the three-piece-freight-truck is unsafe. The strong hunting motion of the wheelsets is clearly seen (see Figure 9.30).

CHAPTER 10

Conclusion

In this final chapter we will review in 10.1 the results which we have achieved in this thesis, and in 10.2 we will make some observations on further research.

10.1 Conclusion

The main results which have been achieved in this thesis are:

• The definition of the *friction direction angle* for the two-dimensional dry friction is described and implemented into an algorithm. It can be efficiently used to determine the components of the friction force vector in both stick and slip motion modes especially in the complex systems. It replaces the sign function used in the one-dimensional dry friction analysis.

• The stick-slip motion between two moving bodies caused by dry friction will cause a collapse of the state space of the system. If the stick motion mode is neglected then at least the number of integration steps will increase greatly because a vibration of the corresponding velocity with very high frequency will take place, which means that the problem becomes somewhat like *stiff phenomenon*, which may lead to incorrect numerical result. Therefore the stick mode should be included and the *switch conditions* must be found to treat the *structure varying systems* and the corresponding acting friction forces must be evaluated with the switch conditions.

• The switch conditions are different for various mechanical systems. For the subsystem of the bolster-wedge-frames we found two ways to treat the lateral and ver-

tical stick-slip motions respectively. All switch conditions for the sub-system of the bolster-frame-wheelsets are provided in detail.

• The degrees of freedom of the system will automatically change from one case to another one if the acting friction forces are determined correctly for the stick mode.

• The method of on line evaluation of the three-dimensional kinematic constraint parameters between wheels and rails are developed.

• The model of the three-piece-freight-truck includes the following characteristics.

★ Two-dimensional dry friction on the surfaces of the wedges as well as on the surfaces of the adapters.

★ There are 19 rigid bodies including the mass of the wedge in the railway vehicle systems with the three-piece-freight-trucks and the degrees of freedom of the system is 81.

★ The stick-slip motions of the sub-systems of the bolster-wedge-frames and the bolster-frame-wheelsets are considered.

★ The effect of the tractive effort on the vehicle on the normal contact forces on the surfaces of the wedges is included, which will cause an asymmetric distribution of the normal contact forces and the friction forces on the one pair of the wedges on the end of the bolster.

★ The dead-band stops are introduced to describe the clearances between the side frames and the adapters both in the longitudinal and lateral directions and the clearances between the car body and the side supports.

★ The anti-warp stiffness is incorporated into the description of the warping motion of the three-piece-freight-truck.

★ The elastic contact between a wheel and a rail is introduced to calculate the normal loads and the full nonlinear calculation of the creep forces.

In order to provide a fundamental method to treat the two-dimensional dry friction for the stick-slip motion analysis in chapter 2 we have introduced the conception of the friction direction angle. With the friction direction angle it is convenient to describe the stick-slip motion of the relative motion of two moving bodies in the two-dimensional case. It can also be used to analyze anisotropic friction. The theoretical and numerical studies have shown that the two-dimensional coupled oscillator can be uncoupled under certain conditions. The orbit of the responses of a two-dimensional friction oscillator will be a straight line segment, a circle or an ellipse depending on

the details of the sinusoidal excitations. In the general case, the response is a complex planar curve. For various levels of excitations, the zero-stop, one-stop, two-stops and multiple stops per cycle will appear.

In chapter 3 we use the friction direction angle to model the wedge dampers in detail. We have found that for the analysis of the relative motion of the two moving bodies with dry friction the model which only considers the slip motion does not work well because in the case of stick state the friction does not equal zero. In that case the so-called switch conditions are needed to find the acting friction forces. Some results have been obtained below.

If the bolster is only forced to move along the lateral direction, not only lateral but also vertical vibrations of a wedge will arise; and more it will induce a vertical vibration of the bolster without any excitation in the vertical direction but the amplitude of the vertical response is small compared with the lateral one.

The dynamical performance of the wedge dampers exposed to large and small excitations have been analyzed. For small amplitude excitations the motions of the wedge and the bolster are coupled. For certain large amplitudes of the exciting force or for excitation frequency in the range of the resonant frequency of the system the motions of the wedge and the bolster are separated.

In the case of coupled motion, the friction damping plays an important role to prevent resonant vibration of the bolster in vertical direction when it is exposed to a small amplitude exciting force with arbitrary frequency. If the amplitude of the exciting force becomes sufficiently large the dry friction can damp the level of the response of the system but can not damp out the resonant vibration of the system. The frequency response of the bolster in vertical direction is chaotic in nature.

For the investigation of the stick-slip motion of the system with more than two moving bodies in the presence of two-dimensional dry friction, the degrees of freedom of the system will change according to different motion states of stick or slip. We have provided a detailed description to treat the structure varying systems of this kind in chapter 4. We found that, although without rigorous mathematical verification, if the acting friction forces are correctly evaluated with the corresponding switch conditions for the stick-slip motion then the degrees of freedom of the system will vary automatically. In other words, the discontinuous system will be automatically a piecewise differentiable system.

In chapter 5 the on-line evaluation of the kinematic constraint parameters between the wheels and rails with three-dimensional contact have been developed. We have found that the yaw of wheelset influences both the kinematic constraint parameters and the penetration between the wheel and the rail. The effect can be neglected for a small value of yaw rotation of the wheelsets.

From a mathematical point of view the multibody dynamical systems with dry friction are discontinuous and a structure varying system. The three-piece-freight-truck belongs to a system of this kind. In Chapter 6, chapter 7 and chapter 8 we provide a way to model this complex system.

In chapter 9 we provided a method to transform the Power Spectral Density(PSD) into a time series. We assume that the argument of the frequency spectra is uniformly

distributed in the interval $(0, 2\pi)$ and use the relation between the PSD and the modulus of the frequency spectra to obtain the modulus. Then we use the inverse finite Fourier transform to obtain the time series. The PSDs (class 1 to 6) of tracks provided by by FRA(Federal Railroad Administration) have been transformed into the lateral and vertical geometrical deviations of the profiles of the two rails in time domain.

Through numerical investigation with the model of the three-piece-freight-truck the results have been obtained as following:

Because of the effect of the two-dimensional dry friction on the surfaces of the wedges and the surfaces of the adapters, and the effect of the impact between the side frames and the wheelsets in the longitudinal and lateral directions the motion of the wheelsets in the lateral direction is not periodic. The lateral displacements of the wheelsets from our model differ from that with NUCARS[Li,2000].

The linear critical speed of the three-piece-freight-truck is about $28.5m/s$ and the nonlinear critical speed is about $20.5m/s$. The motion of the three-piece-freight-truck is a chaotic motion for a certain speed range.

The normal loads on the wheelsets are not a periodic even though the periodic excitation from the rails is periodic.

The normal forces and the corresponding friction forces on the two surfaces of the wedge are asymmetric due to the tractive effort. It must be included in the simulation of the dynamics of the three-piece-freight-truck. The friction forces on the surfaces of the wedges can be used to evaluate the wear state of the wedge damper.

The parasitic motion of the wheelset along the longitudinal direction influences as well the creep forces as the contact state between the frame and the wheelsets. Therefore it should be included in the dynamics analysis of the three-piece-freight-truck.

In the stable motion state at low speed, the motions of the wheelsets are different from zero because of the effect of the stick-slip motion produced by the dry friction. In the present investigation the clearances between the frame and the adapter are the same for left/right sides. If they are asymmetrical then the amplitude of the lateral displacement of the wheelset in the steady motion may increase more or less.

From the bifurcation diagram, the phase diagram and the first return map of the lateral motions of the wheelsets we have concluded that the motion of the three-piece-freight-truck is chaotic motion for a running speed, for example, $29m/s$. And more the chaotic motion of the three-piece-freight-truck is obviously different from the chaotic motion of the Cooperrider's passenger car model[True, 1999] in that the chaotic motion is not a small perturbation on a periodic motion.

From a mathematical and multibody systems dynamics point of view the structure varying systems caused by the two-dimensional dry friction in the motion of the three-piece-freight-truck can not be correctly simulated with the softwares such as ADAMS/Rail, MEDYNA and NUCARS at present.

10.2 Further research

The further research should be focussed on the basic theory of stick-slip motion with two-dimensional dry friction and its application in the three-piece-freight-truck as well as in other mechanical systems.

It should be pointed out that in this thesis the stick-slip motions of the subsystems of the car body-bolster-wedges and the bolster-frame-wheelstes are treated individually without considering the coupling effects between them for their stick slip motions.

In this thesis we define the friction direction angle to describe the components of the friction force vectors on the contact surface of the two contacting bodies with two-dimensional dry friction. An alternative way may be described as following.

For the friction force force components on the contact surface of two bodies

$$\left.\begin{array}{l} F_{x\mu} = N\mu_k \frac{V_x}{V} sign(V_x) \\ F_{y\mu} = N\mu_k \frac{V_y}{V} sign(V_y) \end{array}\right\}, \quad (V_x \vee V_y \neq 0) \tag{10.1}$$

or

$$\left.\begin{array}{l} F_{x\mu} = N\mu_k \frac{F_{inx}}{F} sign(F_{inx}) \\ F_{y\mu} = N\mu_k \frac{F_{iny}}{F} sign(F_{iny}) \end{array}\right\}, \quad \begin{array}{c} (V_x \wedge V_y = 0, \\ (|F_{inx}| > |F_{y\mu s}|) \vee (|F_{yin}| > |F_{y\mu s}|)) \end{array} \tag{10.2}$$

$$\left.\begin{array}{l} F_{x\mu s} = N\mu_s \frac{V_x}{V} sign(V_x) \\ F_{y\mu s} = N\mu_s \frac{V_y}{V} sign(V_y) \end{array}\right\}, \quad (V_x \vee V_y \neq 0) \tag{10.3}$$

or

$$\left.\begin{array}{l} F_{x\mu s} = N\mu_s \frac{F_{inx}}{F} sign(F_{inx}) \\ F_{y\mu s} = N\mu_s \frac{F_{iny}}{F} sign(F_{iny}) \end{array}\right\}, \quad (V_x \wedge V_y = 0) \tag{10.4}$$

with

$$V = \sqrt{V_x^2 + V_y^2}, \quad F = \sqrt{F_{inx}^2 + F_{iny}^2}. \tag{10.5}$$

Note that if the conditions $(V_x \wedge V_y = 0)$ and $(|F_{inx}| < |F_{x\mu s}| \wedge |F_{iny}| < |F_{y\mu s}|)$ are fulfilled then the motion goes into the stick mode and the corresponding acting friction force components, $F_{x\mu t}$ and $F_{y\mu t}$ should be determined by either of the input forces in the x and y directions for the case of one moving body contacting a fixed body or by the switch conditions for the contact of two-moving bodies.

It can be imagined that it is not an efficient way to describe the friction force components for the complex system with two-dimensional dry friction. However, we recommend that a model of the dynamics of three-piece-freight-truck be derived with that method for the sake of comparison.

To find a *smart friction element* to treat the stick-slip motion for the one and two-dimensional dry friction including the *structure varying system* is no doubt a very interesting topic. It has a potential application in mechanical systems as well as in other systems.

Nonlinear dynamic performances are always interesting topics since they depend on the parameter changes. For the time limitation and the computation efficiency we have not investigated more cases of variation of the parameters. The possible existence of dangerous chaotic transients in the speed range with coexisting attractors is needed to be investigated further.

In our investigation the constant anti-warp stiffness is used. It is argued that the stability of the three-piece-freight-truck on straight track is obviously influenced by the anti-warp stiffness. The anti-warp stiffness is characterized by many factors, such as the secondary suspension, the dimension of the wedge, the friction state of the wedge surfaces, the assembly clearances between the bolster, the wedges and the side frames and the running state of the wedge dampers. How to evaluate the anti-warp stiffness is of a considerable importance for the studies of the dynamics of the three-piece-freight-truck.

In addition to the experiment for the stick-slip motions of a pair of wedge damper systems with two-dimensional dry friction, the corresponding measurements on a roller rig or on the field track are urgently needed for the purpose of the comparison with the numerical simulation results.

The present model can only be used for the motion simulations of the truck on a straight track and a straight track with irregularities. The dynamic properties of the truck on curved track is always significant for the safety of the railway vehicles. We may forecast that the clearances between the car body and the side supports will be taken up and the roll of the car body will take place when the vehicle negotiates a curved track. Therefore, the extension of the present model to the case of the vehicle negotiating curved track is wanted.

APPENDIX A

The matrix of the equation (3.64)

Here, we give each element of the matrices $\mathbf{A_s}$ which are used in (3.64). For arbitrary relative velocities $\dot{\eta}$ of a wedge and a bolster, from formulae (3.58)-(3.62) the resultant forces can be represented as:

$$F_{res} = F_l sech(\dot{\eta}\alpha) + F_h[1 - sech(\dot{\eta}\alpha)] \tag{A.1}$$

hence we have

$$\begin{aligned} F_{rx1} = {} & S_d\big\{S\theta_1 S\gamma sech(\dot{x}_d\alpha)[\mu_{sd} - \mu_{kd}] + C\gamma + \mu_{kd}S\theta_1 S\gamma\big\} - F_{kdx} \\ & + N_b\big\{S\theta_2 S\phi sech(\dot{x}_d\alpha)[\mu_{sb} - \mu_{kb}] + \mu_{kb}S\theta_2 S(\dot{x}_d\alpha) - C\phi\big\}, \end{aligned} \tag{A.2}$$

$$\begin{aligned} F_{ry1} = {} & S_d\big\{\mu_{kd}C\theta_1[sech(\dot{y}_d\alpha) - 1] - \mu_{sd}C\theta_1 sech(\dot{y}_d\alpha)\big\} + \\ & N_b\big\{\mu_{kb}cos\theta_2[1 - sech(\dot{y}_d\alpha)] + \mu_{sb}C\theta_2 sech(\dot{y}_d\alpha)\big\} - F_{kdy}, \end{aligned} \tag{A.3}$$

$$\begin{aligned} F_{rz1} = {} & S_d\big\{ - \mu_{sd}S\theta_1 C\gamma sech(\dot{z}_d\alpha) - \mu_{kd}S\theta_1 C\gamma[1 - sech(\dot{z}_d\alpha)] + S\gamma\big\} \\ & + N_b\big\{\mu_{sb}S\theta_2 C\phi sech(\dot{z}_d\alpha) + S\phi + \mu_{kb}S\theta_2 C\phi[1 - sech(\dot{z}_d\alpha)]\big\} \\ & + G_d - F_{kdz}, \end{aligned} \tag{A.4}$$

$$F_{ry2} = N_b\big\{C\theta_2 sech(\dot{y}_b\alpha)[\mu_{kb} - \mu_{sb}] - \mu_{kb}C\theta_2\big\} + S_{y2} - F_{kby}, \tag{A.5}$$

$$\begin{aligned} F_{rz2} = {} & N_b\big\{S\theta_2 C\phi sech(\dot{z}_b\alpha)[\mu_{kb} - \mu_{sb}] - S\phi - \mu_{kb}S\theta_2 C\phi\big\} \\ & + S_{z2} + G_b - F_{kbz}. \end{aligned} \tag{A.6}$$

Further simplifying yields

$$F_{rx1} = S_d a_{11} + N_b a_{12} - F_{kdx}, \tag{A.7}$$

$$F_{ry1} = S_d a_{31} + N_b a_{32} - F_{kdy}, \tag{A.8}$$

$$F_{rz1} = S_d a_{21} + N_b a_{22} + G_d - F_{kdz}, \tag{A.9}$$

$$F_{ry2} = N_b a_{42} + S_{y2} - F_{kby}, \tag{A.10}$$

$$F_{rz2} = N_b a_{52} + S_{z2} + G_b - F_{kbz} \tag{A.11}$$

hence the elements of the matrices $\mathbf{A}_s$ can be written as following.

$$a_{11} = S\theta_1 S\gamma sech(\dot{x}_d\alpha)[\mu_{sd} - \mu_{kd}] + C\gamma + \mu_{kd} S\theta_1 S\gamma, \tag{A.12}$$

$$a_{12} = S\theta_2 S\phi sech(\dot{x}_d\alpha)[\mu_{sb} - \mu_{kb}] + \mu_{kb} S\theta_2 S\phi sech(\dot{x}_d\alpha) - C\phi, \tag{A.13}$$

$$a_{21} = -\mu_{sd} S\theta_1 C\gamma sech(\dot{z}_d\alpha) - \mu_{kd} S\theta_1 C\gamma[1 - sech(\dot{z}_d\alpha)] + S\gamma, \tag{A.14}$$

$$a_{22} = \mu_{sb} S\theta_2 C\phi sech(\dot{z}_d\alpha) + S\phi + \mu_{kb} S\theta_2 C\phi[1 - sech(\dot{z}_d\alpha)], \tag{A.15}$$

$$a_{31} = \mu_{kd} C\theta_1[sech(\dot{y}_d\alpha) - 1] - \mu_{sd} C\theta_1 sech(\dot{y}_d\alpha), \tag{A.16}$$

$$a_{32} = \mu_{kb} cos\theta_2[1 - sech(\dot{y}_d\alpha)] + \mu_{sb} C\theta_2 sech(\dot{y}_d\alpha), \tag{A.17}$$

$$a_{42} = C\theta_2 sech(\dot{y}_b\alpha)[\mu_{kb} - \mu_{sb}] - \mu_{kb} C\theta_2, \tag{A.18}$$

$$a_{52} = S\theta_2 C\phi sech(\dot{z}_b\alpha)[\mu_{kb} - \mu_{sb}] - S\phi - \mu_{kb} S\theta_2 C\phi. \tag{A.19}$$

where $S\theta, C\theta, S\gamma, C\gamma, S\phi, C\phi$ denote the short expressions of the $sin\theta$, $cos\theta$, $sin\gamma$, $cos\gamma$, $sin\phi$ and $cos\phi$.

APPENDIX B

The matrices for the relations among the car body, bolsters and wedges

For the determination of the sub-system of the car body-bolster-wedges in the lateral, vertical and roll directions we have the following system from (8.1)

$$\begin{bmatrix} \mathbf{A}_{o1} & \mathbf{M}_{o1}\mathbf{J}_{o1} \\ \mathbf{A}_{d} & \mathbf{M}_{d}\mathbf{J}_{d} \\ \mathbf{A}_{bvwr} & \mathbf{M}_{bvwr} \end{bmatrix} \begin{bmatrix} \mathbf{N}_{obd} \\ \ddot{\mathbf{x}}_{odb} \end{bmatrix} = \begin{bmatrix} \mathbf{F}_{o1} \\ \mathbf{F}_{d} \\ \mathbf{F}_{bvwr} \end{bmatrix} \tag{B.1}$$

where

$$\mathbf{A}_{o1} = [\mathbf{A}_{oa} \quad \mathbf{A}_{ob}], \quad \mathbf{A}_{d} = [\mathbf{A}_{da} \quad \mathbf{A}_{db}], \quad \mathbf{A}_{bvwr} = [\mathbf{A}_{ba} \quad \mathbf{A}_{bb}], \tag{B.2}$$

$$\mathbf{N}_{odb} = [N_{oby1} \quad N_{obz1} \quad N_{oby2} \quad N_{obz2} \quad S_{d1} \quad N_{b1} \quad \cdots \quad S_{d8} \quad N_{b8}]^T \tag{B.3}$$

$$\mathbf{A}_{oa} = \begin{bmatrix} 1 & 0 & 1 & 0 \\ 0 & 1 & 0 & 1 \\ 0 & -a^*_{oc} & 0 & a^*_{oc} \\ a^*_{oc} & \mu_o\rho_o(\psi_o - \psi_{b1}) & -a^*_{oc} & \mu_o\rho_o(\psi_o - \psi_{b2}) \end{bmatrix}, \mathbf{A}_{ob} = \mathbf{0}_{4\times 16}, \tag{B.4}$$

$$\mathbf{J}_{o1} = \begin{bmatrix} \frac{1}{2} & 0 & 0 & \frac{1}{2} & 0 & 0 \\ 0 & \frac{1}{2} & 0 & 0 & \frac{1}{2} & 0 \\ 0 & \frac{1}{2} & 0 & 0 & \frac{1}{2} & 0 \\ \frac{1}{2a^*_{oc}} & 0 & 0 & -\frac{1}{2a^*_{oc}} & 0 & 0 \end{bmatrix}, \tag{B.5}$$

$$\mathbf{A}_{da} = \mathbf{0}_{16\times 4} \tag{B.6}$$

and

$$\mathbf{A}_{db} = \begin{bmatrix}
c_{11} & c_{12} & 0 & 0 & 0 & 0 & 0 & 0 \\
c_{21} & c_{22} & 0 & 0 & 0 & 0 & 0 & 0 \\
0 & 0 & c_{33} & c_{34} & 0 & 0 & 0 & 0 \\
0 & 0 & c_{43} & c_{44} & 0 & 0 & 0 & 0 \\
0 & 0 & 0 & 0 & c_{55} & c_{56} & 0 & 0 \\
0 & 0 & 0 & 0 & c_{65} & c_{66} & 0 & 0 \\
0 & 0 & 0 & 0 & 0 & 0 & c_{77} & c_{78} \\
0 & 0 & 0 & 0 & 0 & 0 & 0 & 0 \\
0 & 0 & 0 & 0 & 0 & 0 & 0 & 0 \\
0 & 0 & 0 & 0 & 0 & 0 & 0 & 0 \\
0 & 0 & 0 & 0 & 0 & 0 & 0 & 0 \\
0 & 0 & 0 & 0 & 0 & 0 & 0 & 0 \\
0 & 0 & 0 & 0 & 0 & 0 & 0 & 0 \\
0 & 0 & 0 & 0 & 0 & 0 & 0 & 0 \\
0 & 0 & 0 & 0 & 0 & 0 & 0 & 0 \\
0 & 0 & 0 & 0 & 0 & 0 & 0 & 0 \\
c_{99} & c_{910} & 0 & 0 & 0 & 0 & 0 & 0 \\
c_{109} & c_{1010} & 0 & 0 & 0 & 0 & 0 & 0 \\
0 & 0 & c_{1111} & c_{1112} & 0 & 0 & 0 & 0 \\
0 & 0 & c_{1211} & c_{1212} & 0 & 0 & 0 & 0 \\
0 & 0 & 0 & 0 & c_{1313} & c_{1314} & 0 & 0 \\
0 & 0 & 0 & 0 & c_{1413} & c_{1414} & 0 & 0 \\
0 & 0 & 0 & 0 & 0 & 0 & c_{1515} & c_{1516}
\end{bmatrix} \tag{B.7}$$

where the nonzero entries of the matrix are

$$\begin{aligned}
c_{11} &= C\gamma + \mu_d S\theta_{d1} S\gamma, \quad & c_{12} &= -C\phi + \mu_b S\theta_{b1} S\phi, \\
c_{21} &= S\gamma - \mu_d S\theta_{d1} C\gamma, \quad & c_{22} &= S\phi + \mu_b S\theta_{b1} C\phi, \\
c_{33} &= -C\gamma - \mu_d S\theta_{d2} S\gamma, \quad & c_{34} &= C\phi - \mu_b S\theta_{b2} S\phi, \\
c_{43} &= S\gamma - \mu_d S\theta_{d2} C\gamma, \quad & c_{44} &= S\phi + \mu_b S\theta_{b2} C\phi, \\
c_{55} &= C\gamma + \mu_d S\theta_{d3} S\gamma, \quad & c_{56} &= -C\phi + \mu_b S\theta_{b3} S\phi, \\
c_{65} &= S\gamma - \mu_d S\theta_{d3} C\gamma, \quad & c_{66} &= S\phi + \mu_b S\theta_{b3} C\phi, \\
c_{77} &= -C\gamma - \mu_d S\theta_{d4} S\gamma, \quad & c_{78} &= C\phi - \mu_b S\theta_{b4} S\phi, \\
c_{87} &= S\gamma - \mu_d S\theta_{d4} C\gamma, \quad & c_{88} &= S\phi + \mu_b S\theta_{b4} C\phi,
\end{aligned}$$

$$
\begin{aligned}
c_{99} &= C\gamma + \mu_d S\theta_{d5} S\gamma, \quad c_{109} = -C\phi + \mu_b S\theta_{b5} S\phi, \\
c_{109} &= S\gamma - \mu_d S\theta_{d5} C\gamma, \quad c_{1010} = S\phi + \mu_b S\theta_{b5} C\phi, \\
c_{1111} &= -C\gamma - \mu_d S\theta_{d6} S\gamma, \quad c_{1112} = C\phi - \mu_b S\theta_{b6} S\phi, \\
c_{1211} &= S\gamma - \mu_d S\theta_{d6} C\gamma, \quad c_{1212} = S\phi + \mu_b S\theta_{b6} C\phi, \\
c_{1313} &= C\gamma + \mu_d S\theta_{d7} S\gamma, \quad c_{1314} = -C\phi + \mu_b S\theta_{b7} S\phi, \\
c_{1413} &= S\gamma - \mu_d S\theta_{d7} C\gamma, \quad c_{1414} = S\phi + \mu_b S\theta_{b7} C\phi, \\
c_{1515} &= -C\gamma - \mu_d S\theta_{d8} S\gamma, \quad c_{1516} = C\phi - \mu_b S\theta_{b8} S\phi, \\
c_{1615} &= S\gamma - \mu_d S\theta_{d8} C\gamma, \quad c_{1616} = S\phi + \mu_b S\theta_{b8} C\phi,
\end{aligned}
$$

and

$$
\mathbf{J}_d = \begin{bmatrix}
0 & -S\gamma S\phi & -b^*_{bs2} S\gamma S\phi & 0 & 0 & 0 \\
0 & S\gamma S\phi & b^*_{bs2} S\gamma S\phi & 0 & 0 & 0 \\
0 & -S\gamma S\phi & -b^*_{bs2} S\gamma S\phi & 0 & 0 & 0 \\
0 & S\gamma S\phi & b^*_{bs2} S\gamma S\phi & 0 & 0 & 0 \\
0 & -S\gamma S\phi & -b^*_{bs2} S\gamma S\phi & 0 & 0 & 0 \\
0 & S\gamma S\phi & b^*_{bs2} S\gamma S\phi & 0 & 0 & 0 \\
0 & -S\gamma S\phi & -b^*_{bs2} S\gamma S\phi & 0 & 0 & 0 \\
0 & S\gamma S\phi & b^*_{bs2} S\gamma S\phi & 0 & 0 & 0 \\
0 & 0 & 0 & 0 & -S\gamma S\phi & -b^*_{bs2} S\gamma S\phi \\
0 & 0 & 0 & 0 & S\gamma S\phi & b^*_{bs2} S\gamma S\phi \\
0 & 0 & 0 & 0 & -S\gamma S\phi & -b^*_{bs2} S\gamma S\phi \\
0 & 0 & 0 & 0 & S\gamma S\phi & b^*_{bs2} S\gamma S\phi \\
0 & 0 & 0 & 0 & -S\gamma S\phi & -b^*_{bs2} S\gamma S\phi \\
0 & 0 & 0 & 0 & S\gamma S\phi & b^*_{bs2} S\gamma S\phi \\
0 & 0 & 0 & 0 & -S\gamma S\phi & -b^*_{bs2} S\gamma S\phi \\
0 & 0 & 0 & 0 & S\gamma S\phi & b^*_{bs2} S\gamma S\phi
\end{bmatrix}. \tag{B.8}
$$

The $\mathbf{A}_{ba}$ and $\mathbf{A}_{bb}$ are

$$
\mathbf{A}_{ba} = \begin{bmatrix}
-1 & 0 & 0 & 0 \\
0 & -1 & 0 & 0 \\
0 & 0 & -1 & 0 \\
0 & 0 & 0 & -1
\end{bmatrix}, \tag{B.9}
$$

$$\mathbf{A}_{bb} = \begin{bmatrix} d_{11} & 0 & d_{13} & 0 & d_{15} & 0 & d_{17} & 0 \\ 0 & d_{22} & 0 & d_{24} & 0 & d_{26} & 0 & d_{28} \\ 0 & d_{32} & 0 & d_{34} & 0 & d_{36} & 0 & d_{38} \\ 0 & 0 & 0 & 0 & 0 & 0 & 0 & 0 \\ 0 & 0 & 0 & 0 & 0 & 0 & 0 & 0 \\ 0 & 0 & 0 & 0 & 0 & 0 & 0 & 0 \\ 0 & 0 & 0 & 0 & 0 & 0 & 0 & 0 \\ 0 & 0 & 0 & 0 & 0 & 0 & 0 & 0 \\ 0 & 0 & 0 & 0 & 0 & 0 & 0 & 0 \\ d_{49} & 0 & d_{411} & 0 & d_{413} & 0 & d_{415} & 0 \\ 0 & d_{510} & 0 & d_{512} & 0 & d_{514} & 0 & d_{516} \\ 0 & d_{610} & 0 & d_{612} & 0 & d_{614} & 0 & d_{616} \end{bmatrix} \tag{B.10}$$

where the nonzero entries of the matrix are

$$\begin{aligned} d_{11} = \mu_d C\theta_{d1}, \quad d_{13} = \mu_d C\theta_{d2}, \quad d_{15} = \mu_d C\theta_{d3}, \quad d_{17} = \mu_d C\theta_{d4}, \\ d_{22} = S\phi + \mu_d S\theta_{d1} C\phi, \quad d_{24} = S\phi + \mu_d S\theta_{d2} C\phi, \\ d_{26} = S\phi + \mu_d S\theta_{d3} C\phi, \quad d_{28} = S\phi + \mu_d S\theta_{d4} C\phi, \\ d_{32} = S\phi b^*_{bs2} + \mu_b C\theta_{b1} C\phi b^*_{bs2}, \quad d_{34} = S\phi b^*_{bs2} + \mu_b C\theta_{b2} C\phi b^*_{bs2}, \\ d_{36} = S\phi b^*_{bs2} + \mu_b C\theta_{b3} C\phi b^*_{bs2}, \quad d_{38} = S\phi b^*_{bs2} + \mu_b C\theta_{b4} C\phi b^*_{bs2}, \\ d_{410} = \mu_d C\theta_{d5}, \quad d_{412} = \mu_d C\theta_{d6}, \quad d_{414} = \mu_d C\theta_{d7}, \quad d_{416} = \mu_d C\theta_{d8}, \\ d_{510} = S\phi + \mu_d S\theta_{d5} C\phi_b, \quad d_{512} = S\phi + \mu_d S\theta_{d6} C\phi_b, \\ d_{514} = S\phi + \mu_d S\theta_{d7} C\phi_b, \quad d_{516} = S\phi + \mu_d S\theta_{d8} C\phi_b, \\ d_{610} = S\phi b^*_{bs2} + \mu_b C\theta_{b5} C\phi b^*_{bs2}, \quad d_{612} = S\phi b^*_{bs2} + \mu_b C\theta_{b6} C\phi b^*_{bs2}, \\ d_{614} = S\phi b^*_{bs2} + \mu_b C\theta_{b7} C\phi b^*_{bs2}, \quad d_{616} = S\phi b^*_{bs2} + \mu_b C\theta_{b8} C\phi b^*_{bs2}, \end{aligned}$$

And $\mathbf{J}_{bvwr}$ is a 6×6 unit matrix. The mass matrices are

$$\mathbf{M}_{o1} = \begin{bmatrix} m_o & 0 & 0 & 0 \\ 0 & m_o & 0 & 0 \\ 0 & 0 & I_{oy} & 0 \\ 0 & 0 & 0 & I_{oz} \end{bmatrix}, \tag{B.11}$$

$$\mathbf{M}_d = m_d \mathbf{E} \tag{B.12}$$

where $\mathbf{E}$ is a 8×8 unit matrix.

$$\mathbf{M}_{bvwr} = \begin{bmatrix} m_b & 0 & 0 & 0 & 0 & 0 \\ 0 & m_b & 0 & 0 & 0 & 0 \\ 0 & 0 & I_{bx} & 0 & 0 & 0 \\ 0 & 0 & 0 & m_b & 0 & 0 \\ 0 & 0 & 0 & 0 & m_b & 0 \\ 0 & 0 & 0 & 0 & 0 & I_{bx} \end{bmatrix}. \tag{B.13}$$

Appendix C

The matrices for determination of the forces on the surfaces of the adapters

The normal forces on the surfaces of the adapters depend on the weights of the car body, bolsters and frames; the spring forces of the secondary suspension and the friction forces on the surfaces of the wedges, the inertia forces of the wheelsets in the vertical direction and roll rotation. From (8.1) the sub-system can be written as

$$\begin{bmatrix} \mathbf{A}_{fwp} & \mathbf{M}_{fwp}\mathbf{J}_{fwp} \\ \mathbf{A}_{wwr} & \mathbf{M}_{wwr} \end{bmatrix} \begin{bmatrix} \mathbf{N}_{fwp} \\ \ddot{\mathbf{x}}_{fwwr} \end{bmatrix} = \begin{bmatrix} \mathbf{F}_{fwp} \\ \mathbf{F}_{wwr} \end{bmatrix} \tag{C.1}$$

where

$$\mathbf{A}_{fwp} = \begin{bmatrix} -1 & -1 & 0 & 0 & 0 & 0 & 0 & 0 \\ a_{wb} & -a_{wb} & 0 & 0 & 0 & 0 & 0 & 0 \\ 0 & 0 & -1 & -1 & 0 & 0 & 0 & 0 \\ 0 & 0 & a_{wb} & -a_{wb} & 0 & 0 & 0 & 0 \\ 0 & 0 & 0 & 0 & -1 & -1 & 0 & 0 \\ 0 & 0 & 0 & 0 & a_{wb} & -a_{wb} & 0 & 0 \\ 0 & 0 & 0 & 0 & 0 & 0 & -1 & -1 \\ 0 & 0 & 0 & 0 & 0 & 0 & a_{wb} & -a_{wb} \end{bmatrix}, \tag{C.2}$$

$$\mathbf{J}_{fwp} = \begin{bmatrix} \frac{1}{2} & \frac{b_{ws}}{2} & \frac{1}{2} & \frac{b_{ws}}{2} & 0 & 0 & 0 & 0 \\ \frac{-1}{2a_{wb}} & \frac{-b_{ws}}{2a_{wb}} & \frac{1}{2a_{wb}} & \frac{b_{ws}}{2a_{wb}} & 0 & 0 & 0 & 0 \\ \frac{1}{2} & \frac{-b_{ws}}{2} & \frac{1}{2} & \frac{-b_{ws}}{2} & 0 & 0 & 0 & 0 \\ \frac{-1}{2a_{wb}} & \frac{b_{ws}}{2a_{wb}} & \frac{1}{2a_{wb}} & \frac{-b_{ws}}{2a_{wb}} & 0 & 0 & 0 & 0 \\ 0 & 0 & 0 & 0 & \frac{1}{2} & \frac{b_{ws}}{2} & \frac{1}{2} & \frac{b_{ws}}{2} \\ 0 & 0 & 0 & 0 & \frac{-1}{2a_{wb}} & \frac{-b_{ws}}{2a_{wb}} & \frac{1}{2a_{wb}} & \frac{b_{ws}}{2a_{wb}} \\ 0 & 0 & 0 & 0 & \frac{1}{2} & \frac{-b_{ws}}{2} & \frac{1}{2} & \frac{-b_{ws}}{2} \\ 0 & 0 & 0 & 0 & \frac{-1}{2a_{wb}} & \frac{b_{ws}}{2a_{wb}} & \frac{1}{2a_{wb}} & \frac{-b_{ws}}{2a_{wb}} \end{bmatrix} \tag{C.3}$$

and

$$\mathbf{A}_{wwr} = \begin{bmatrix} 1 & 0 & 1 & 0 & 0 & 0 & 0 & 0 \\ b_{ws} & 0 & -b_{ws} & 0 & 0 & 0 & 0 & 0 \\ 0 & 0 & 1 & 0 & 1 & 0 & 0 & 0 \\ 0 & 0 & b_{ws} & 0 & -b_{ws} & 0 & 0 & 0 \\ 0 & 0 & 0 & 0 & 1 & 0 & 1 & 0 \\ 0 & 0 & 0 & 0 & b_{ws} & 0 & -b_{ws} & 0 \\ 0 & 0 & 0 & 0 & 0 & 1 & 0 & 1 \\ 0 & 0 & 0 & 0 & 0 & b_{ws} & 0 & -b_{ws} \end{bmatrix} \tag{C.4}$$

and

$$\mathbf{M}_{fwp} = \mathbf{E}[m_f \quad I_{fy} \quad m_f \quad I_{fy} \quad m_f \quad I_{fy} \quad m_f \quad I_{fy}]^T, \tag{C.5}$$

$$\mathbf{M}_{wwr} = \mathbf{E}[m_w \quad I_{wx} \quad m_w \quad I_{wx} \quad m_w \quad I_{wx} \quad m_w \quad I_{wx}]^T \tag{C.6}$$

where $\mathbf{E}$ denotes a 8×8 unit matrix.

APPENDIX D

The switch conditions for the bolster-frame-wheelset subsystem

In this appendix we provide the formulations of the switch conditions for the stick-slip motion of the sub-system of the bolster-frame-wheelsets in detail.

It is not a simple work to find the all switch conditions and the calculation of the corresponding friction forces for the stick-slip motion of the sub-system of the bolster-frame-wheelsets. Here we will spend more time to discuss it in detail. The way is same as that we have used in chapter 4. First we rewrite the relative equations of the sub-system from chapter 7 as

$$m_f \ddot{v}_{f1} = \mathbf{f}_{ff1}(2) + \mathbf{f}_{sf1}(2) + f_{fwv1} + f_{fwv2}, \tag{D.1}$$

$$I_{fz}\ddot{\psi}_{f1} = a_{wb}(f_{fwv1} - f_{fwv2}) + \mathbf{f}_{sf1}(5) + M_{s\psi bf1}, \tag{D.2}$$

$$m_f \ddot{v}_{f2} = \mathbf{f}_{ff2}(2) + \mathbf{f}_{sf2}(2) + f_{fwv3} + f_{fwv4}, \tag{D.3}$$

$$I_{fz}\ddot{\psi}_{f2} = a_{wb}(f_{fwv3} - f_{fwv4}) + \mathbf{f}_{sf2}(5) + M_{s\psi bf2}, \tag{D.4}$$

$$m_w \ddot{u}_{w1} = \mathbf{f}_{sw1}(1) + \mathbf{f}_{tw1}(1) - f_{fwu1} - f_{fwu3}, \tag{D.5}$$

$$m_w \ddot{v}_{w1} = \mathbf{f}_{sw1}(2) + \mathbf{f}_{tw1}(2) + \mathbf{f}_{ctw1}(2) - f_{fwv1} - f_{fwv3}, \tag{D.6}$$

$$I_{wz}\ddot{\psi}_{w1} = b_{ws}(f_{fwu1} - f_{fwu3}) + \mathbf{f}_{sw1}(6) + \mathbf{f}_{gw1}(6) + \mathbf{f}_{tw1}(6), \tag{D.7}$$

$$m_w\ddot{u}_{w2} = \mathbf{f}_{sw2}(1) + \mathbf{f}_{tw2}(1), -f_{fwu2} - f_{fwu4}, \tag{D.8}$$

$$m_w\ddot{v}_{w2} = \mathbf{f}_{sw2}(2) + \mathbf{f}_{tw2}(2) + \mathbf{f}_{ctw2}(2) - f_{fwv2} - f_{fwv4}, \tag{D.9}$$

$$I_{wz}\ddot{\psi}_{w2} = b_{ws}(f_{fwu2} - f_{fwu4}) + \mathbf{f}_{sw2}(6) + \mathbf{f}_{gw2}(6) + \mathbf{f}_{tw2}(6), \tag{D.10}$$

$$\begin{aligned}(I^*_{bz} + 2m_f b^{*2}_{bs2})\ddot{\psi}_{b1} &= b^*_{bs2}[(f_{fwu3} + f_{fwu4})C\psi_{f2} - (f_{fwu1} + f_{fwu2})C\psi_{f1}] \\ & M_{f\psi ob1} + M_{sfw12} - M_{s\psi bf1} - M_{s\psi bf2}.\end{aligned} \tag{D.11}$$

The relative equations for the truck 2(rear truck) can be rewritten as

$$m_f\ddot{v}_{f3} = \mathbf{f}_{ff3}(2) + \mathbf{f}_{sf3}(2) + f_{fwv5} + f_{fwv6}, \tag{D.12}$$

$$I_{fz}\ddot{\psi}_{f3} = a_{wb}(f_{fwv5} - f_{fwv6}) + \mathbf{f}_{sf3}(5) + M_{s\psi bf3}, \tag{D.13}$$

$$m_f\ddot{v}_{f4} = \mathbf{f}_{ff4}(2) + \mathbf{f}_{sf4}(2) + f_{fwv7} + f_{fwv8}, \tag{D.14}$$

$$I_{fz}\ddot{\psi}_{f4} = a_{wb}(f_{fwv7} - f_{fwv8}) + \mathbf{f}_{sf4}(5) + M_{s\psi bf4}, \tag{D.15}$$

$$m_w\ddot{u}_{w3} = \mathbf{f}_{sw3}(1) + \mathbf{f}_{tw3}(1) - f_{fwu5} - f_{fwu7}, \tag{D.16}$$

$$m_w\ddot{v}_{w3} = \mathbf{f}_{sw3}(2) + \mathbf{f}_{tw3}(2) + \mathbf{f}_{ctw3}(2) - f_{fwv5} - f_{fwv7}, \tag{D.17}$$

$$I_{wz}\ddot{\psi}_{w3} = b_{ws}(f_{fwu5} - f_{fwu7}) + \mathbf{f}_{sw3}(6) + \mathbf{f}_{gw3}(6) + \mathbf{f}_{tw3}(6), \tag{D.18}$$

$$m_w\ddot{u}_{w4} = \mathbf{f}_{sw4}(1) + \mathbf{f}_{tw4}(1) - f_{fwu6} - f_{fwu8}, \tag{D.19}$$

$$m_w\ddot{v}_{w4} = \mathbf{f}_{sw4}(2) + \mathbf{f}_{tw4}(2) + \mathbf{f}_{ctw4}(2) - f_{fwv6} - f_{fwv8}, \tag{D.20}$$

$$I_{wz}\ddot{\psi}_{w4} = b_{ws}(f_{fwu6} - f_{fwu8}) + \mathbf{f}_{sw4}(6) + \mathbf{f}_{gw4}(6) + \mathbf{f}_{tw4}(6), \tag{D.21}$$

$$\begin{aligned}(I^*_{bz} + 2m_f b^{*2}_{bs2})\ddot{\psi}_{b2} &= b^*_{bs2}[(f_{fwu7} + f_{fwu8})C\psi_{f4} - (f_{fwu5} + f_{fwu6})C\psi_{f3}] \\ & M_{f\psi ob2} + M_{sfw34} - M_{s\psi bf3} - M_{s\psi bf4}.\end{aligned} \tag{D.22}$$

In the slip state, the equations (D.1)-(D.22) are independent, so that the the subsystem has 22 independent degrees of freedom. And all the friction forces assume their kinetic values for the slip motion. And then the kinematic constraints are (see chapter 6)

$$u_{f1} = -b^*_{bs2}\psi_{b1}, \tag{D.23}$$

$$u_{f2} = b^*_{bs2}\psi_{b1}, \tag{D.24}$$

$$u_{f3} = -b^*_{bs2}\psi_{b2}, \tag{D.25}$$

$$u_{f4} = b^*_{bs2}\psi_{b2}. \tag{D.26}$$

For the points on the wheelsets at the contact surfaces between the wheelsets and the side frames we have

$$u_{w1r} = u_{w1} - b_{ws}\psi_{w1}, \tag{D.27}$$

$$u_{w2r} = u_{w2} - b_{ws}\psi_{w2}, \tag{D.28}$$

$$u_{w1l} = u_{w1} + b_{ws}\psi_{w1}, \tag{D.29}$$

$$u_{w2l} = u_{w2} + b_{ws}\psi_{w2}. \tag{D.30}$$

From the above relations in the stick motion state of the wheelsets and the side frames we can deduce the following relations

$$\dot{u}_{w1} - b_{ws}\dot{\psi}_{w1} = -b^*_{bs2}\dot{\psi}_{b1}, \tag{D.31}$$

$$\dot{u}_{w2} - b_{ws}\dot{\psi}_{w2} = -b^*_{bs2}\dot{\psi}_{b1}, \tag{D.32}$$

$$\dot{u}_{w1} + b_{ws}\dot{\psi}_{w1} = b^*_{bs2}\dot{\psi}_{b1}, \tag{D.33}$$

$$\dot{u}_{w2} + b_{ws}\dot{\psi}_{w2} = b^*_{bs2}\dot{\psi}_{b1}, \tag{D.34}$$

$$\dot{v}_{w1} = \dot{v}_{f1} + a_{wb}\dot{\psi}_{f1}, \tag{D.35}$$

$$\dot{v}_{w1} = \dot{v}_{f2} + a_{wb}\dot{\psi}_{f2}, \tag{D.36}$$

$$\dot{v}_{w2} = \dot{v}_{f1} - a_{wb}\dot{\psi}_{f1}, \tag{D.37}$$

$$\dot{v}_{w2} = \dot{v}_{f2} - a_{wb}\dot{\psi}_{f2}. \tag{D.38}$$

and

$$\ddot{u}_{w1} - b_{ws}\ddot{\psi}_{w1} + b^*_{bs2}\ddot{\psi}_{b1} = 0, \tag{D.39}$$

$$\ddot{v}_{w1} - \ddot{v}_{f1} - a_{wb}\ddot{\psi}_{f1} = 0, \tag{D.40}$$

$$\ddot{u}_{w2} - b_{ws}\ddot{\psi}_{w2} + b^*_{bs2}\ddot{\psi}_{b1} = 0, \tag{D.41}$$

$$\ddot{v}_{w2} - \ddot{v}_{f1} + a_{wb}\ddot{\psi}_{f1} = 0, \tag{D.42}$$

$$\ddot{u}_{w1} + b_{ws}\ddot{\psi}_{w1} - b^*_{bs2}\ddot{\psi}_{b1} = 0, \tag{D.43}$$

$$\ddot{v}_{w1} - \ddot{v}_{f2} - a_{wb}\ddot{\psi}_{f2} = 0, \tag{D.44}$$

$$\ddot{u}_{w2} + b_{ws}\ddot{\psi}_{w2} - b^*_{bs2}\ddot{\psi}_{b1} = 0, \tag{D.45}$$

$$\ddot{v}_{w2} - \ddot{v}_{f2} + a_{wb}\ddot{\psi}_{f2} = 0. \tag{D.46}$$

In the same way the kinematic constraints for the other bogie can be written as

$$\dot{u}_{w3} - b_{ws}\dot{\psi}_{w3} + b^*_{bs2}\dot{\psi}_{b2} = 0, \tag{D.47}$$

$$\dot{v}_{w3} - \dot{v}_{f3} - a_{wb}\dot{\psi}_{f3} = 0, \tag{D.48}$$

$$\dot{u}_{w4} - b_{ws}\dot{\psi}_{w4} + b^*_{bs2}\dot{\psi}_{b2} = 0, \tag{D.49}$$

$$\dot{v}_{w4} - \dot{v}_{f3} - a_{wb}\dot{\psi}_{f3} = 0, \tag{D.50}$$

$$\dot{u}_{w3} + b_{ws}\dot{\psi}_{w3} - b^*_{bs2}\dot{\psi}_{b2} = 0, \tag{D.51}$$

$$\dot{v}_{w3} - \dot{v}_{f4} + a_{wb}\dot{\psi}_{f4} = 0, \tag{D.52}$$

$$\dot{u}_{w4} + b_{ws}\dot{\psi}_{w4} - b^*_{bs2}\ddot{\psi}_{b2} = 0, \tag{D.53}$$

$$\dot{v}_{w4} - \dot{v}_{f4} + a_{wb}\dot{\psi}_{f4} = 0. \tag{D.54}$$

and

$$\ddot{u}_{w3} - b_{ws}\ddot{\psi}_{w3} + b^*_{bs2}\ddot{\psi}_{b2} = 0, \tag{D.55}$$

$$\ddot{v}_{w3} - \ddot{v}_{f3} - a_{wb}\ddot{\psi}_{f3} = 0, \tag{D.56}$$

$$\ddot{u}_{w4} - b_{ws}\ddot{\psi}_{w4} + b^*_{bs2}\ddot{\psi}_{b2} = 0, \tag{D.57}$$

$$\ddot{v}_{w4} - \ddot{v}_{f3} - a_{wb}\ddot{\psi}_{f3} = 0, \tag{D.58}$$

$$\ddot{u}_{w3} + b_{ws}\ddot{\psi}_{w3} - b^*_{bs2}\ddot{\psi}_{b2} = 0, \tag{D.59}$$

$$\ddot{v}_{w3} - \ddot{v}_{f4} + a_{wb}\ddot{\psi}_{f4} = 0, \tag{D.60}$$

$$\ddot{u}_{w4} + b_{ws}\ddot{\psi}_{w4} - b^*_{bs2}\ddot{\psi}_{b2} = 0, \tag{D.61}$$

$$\ddot{v}_{w4} - \ddot{v}_{f4} + a_{wb}\ddot{\psi}_{f4} = 0. \tag{D.62}$$

From these kinematic constraints we can get the following conditions to form the switch conditions and to determine the acting friction forces. Combining the constraints the dynamical equations(D.1)-(D.11) become

$$\begin{aligned}
&\tfrac{1}{m_w}(-f_{fwu1} - f_{fwu3} + \mathbf{f}_{sw1}(1) + \mathbf{f}_{tw1}(1)) - \\
&\tfrac{b_{ws}}{I_{wz}}(b_{ws}(f_{fwu1} - f_{fwu3}) + \mathbf{f}_{sw1}(6) + \mathbf{f}_{gw1}(6) + \mathbf{f}_{tw1}(6)) + \\
&\tfrac{b^*_{bs2}}{I_{bmf}}(b^*_{bs2}[(f_{fwu3} + f_{fwu4})C\psi_{f2} - (f_{fwu1} + f_{fwu2})C\psi_{f1}] \\
&+ M_{f\psi ob1} + M_{sfw12} - M_{s\psi bf1} - M_{s\psi bf2}) = 0,
\end{aligned} \tag{D.63}$$

$$\begin{aligned}
&\tfrac{1}{m_w}(-f_{fwu2} - f_{fwu4} + \mathbf{f}_{sw2}(1) + \mathbf{f}_{tw2}(1)) - \\
&\tfrac{b_{ws}}{I_{wz}}(b_{ws}(f_{fwu2} - f_{fwu4}) + \mathbf{f}_{sw2}(6) + \mathbf{f}_{gw2}(6) + \mathbf{f}_{tw2}(6)) + \\
&\tfrac{b^*_{bs2}}{I_{bmf}}(b^*_{bs2}[(f_{fwu3} + f_{fwu4})C\psi_{f2} - (f_{fwu1} + f_{fwu2})C\psi_{f1}] \\
&+ M_{f\psi ob1} + M_{sfw12} - M_{s\psi bf1} - M_{s\psi bf2}) = 0,
\end{aligned} \tag{D.64}$$

$$\begin{aligned}
&\tfrac{1}{m_w}(-f_{fwu1} - f_{fwu3} + \mathbf{f}_{sw1}(1) + \mathbf{f}_{tw1}(1)) + \\
&\tfrac{b_{ws}}{I_{wz}}(b_{ws}(f_{fwu1} - f_{fwu3}) + \mathbf{f}_{sw1}(6) + \mathbf{f}_{gw1}(6) + \mathbf{f}_{tw1}(6)) - \\
&\tfrac{b^*_{bs2}}{I_{bmf}}(b^*_{bs2}[(f_{fwu3} + f_{fwu4})C\psi_{f2} - (f_{fwu1} + f_{fwu2})C\psi_{f1}] \\
&+ M_{f\psi ob1} + M_{sfw12} - M_{s\psi bf1} - M_{s\psi bf2}) = 0,
\end{aligned} \tag{D.65}$$

$$\begin{array}{l}\frac{1}{m_w}(-f_{fwu2}-f_{fwu4}+\mathbf{f}_{sw2}(1)+\mathbf{f}_{tw2}(1))+\\ \frac{b_{ws}}{I_{wz}}(b_{ws}(f_{fwu2}-f_{fwu4})+\mathbf{f}_{sw2}(6)+\mathbf{f}_{gw2}(6)+\mathbf{f}_{tw2}(6))-\\ \frac{b^*_{bs2}}{I_{bmf}}(b^*_{bs2}[(f_{fwu3}+f_{fwu4})C\psi_{f2}-(f_{fwu1}+f_{fwu2})C\psi_{f1}]\\ +M_{f\psi ob1}+M_{sfw12}-M_{s\psi bf1}-M_{s\psi bf2})=0,\end{array} \tag{D.66}$$

$$\begin{array}{l}\frac{1}{m_w}(-f_{fwv1}-f_{fwv3}+\mathbf{f}_{sw1}(2)+\mathbf{f}_{tw1}(2)+\mathbf{f}_{ctw1}(2))-\\ \frac{1}{m_f}(f_{fwv1}+f_{fwv2}+\mathbf{f}_{ff1}(2)+\mathbf{f}_{sf1}(2))-\\ \frac{a_{wb}}{I_{fz}}(a_{wb}(f_{fwv1}-f_{fwv2})+M_{s\psi bf1}+\mathbf{f}_{sf1}(5))=0,\end{array} \tag{D.67}$$

$$\begin{array}{l}\frac{1}{m_w}(-f_{fwv2}-f_{fwv4}+\mathbf{f}_{sw2}(2)+\mathbf{f}_{tw2}(2)+\mathbf{f}_{ctw2}(2))-\\ \frac{1}{m_f}(f_{fwv1}+f_{fwv2}+\mathbf{f}_{ff1}(2)+\mathbf{f}_{sf1}(2)+\\ \frac{a_{wb}}{I_{fz}}(a_{wb}(f_{fwv1}-f_{fwv2})+M_{s\psi bf1}+\mathbf{f}_{sf1}(5))=0,\end{array} \tag{D.68}$$

$$\begin{array}{l}\frac{1}{m_w}(-f_{fwv1}-f_{fwv3}+\mathbf{f}_{sw1}(2)+\mathbf{f}_{tw1}(2)+\mathbf{f}_{ctw1}(2))-\\ \frac{1}{m_f}(f_{fwv3}+f_{fwv4}+\mathbf{f}_{ff2}(2)+\mathbf{f}_{sf2}(2)-\\ \frac{a_{wb}}{I_{fz}}(a_{wb}(f_{fwv3}-f_{fwv4})+M_{s\psi bf2}+\mathbf{f}_{sf2}(5))=0,\end{array} \tag{D.69}$$

$$\begin{array}{l}\frac{1}{m_w}(-f_{fwv1}-f_{fwv3}+\mathbf{f}_{sw2}(2)+\mathbf{f}_{tw2}(2)+\mathbf{f}_{ctw2}(2))-\\ \frac{1}{m_f}(f_{fwv3}+f_{fwv4}+\mathbf{f}_{ff2}(2)+\mathbf{f}_{sf2}(2)+\\ \frac{a_{wb}}{I_{fz}}(a_{wb}(f_{fwv3}-f_{fwv4})+M_{s\psi bf2}+\mathbf{f}_{sf2}(5))=0.\end{array} \tag{D.70}$$

where the I_{bmf} stands for

$$I_{bmf}=I_{bz}+2m_f b^{*2}_{bs2}. \tag{D.71}$$

From the above equations we can reach the conclusion: While the stick motion takes place on the one contact plane then the equivalent input force must be less than or equal the corresponding equivalent static friction force component such that we have

$$|f_{\mu xs1}|\geq|F_{mx1}|,\quad |f_{\mu xs2}|\geq|F_{mx2}|,\quad |f_{\mu xs3}|\geq|F_{mx3}|,\quad |f_{\mu xs4}|\geq|F_{mx4}|, \tag{D.72}$$

$$|f_{\mu ys1}|\geq|F_{my1}|,\quad |f_{\mu ys2}|\geq|F_{my2}|,\quad |f_{\mu ys3}|\geq|F_{my3}|,\quad |f_{\mu ys4}|\geq|F_{my4}| \tag{D.73}$$

where

$$\begin{array}{rcl}f_{\mu xs1} & = & f_{fwx1s}(\frac{1}{m_w}+\frac{b^2_{ws}}{I_{wz}}+\frac{b^{*2}_{bs2}}{I_{bmf}}C\psi_{f1})+f_{fwx2s}\frac{b^{*2}_{bs2}}{I_{bmf}}C\psi_{f1}+\\ & & f_{fwx3s}(\frac{1}{m_w}-\frac{b^2_{ws}}{I_{wz}}-\frac{b^{*2}_{bs2}}{I_{bmf}}C\psi_{f2})-f_{fwx4s}\frac{b^{*2}_{bs2}}{I_{bmf}}C\psi_{f2},\end{array} \tag{D.74}$$

$$\begin{array}{rcl}F_{mx1} & = & \frac{1}{m_w}(\mathbf{f}_{sw1}(1)+\mathbf{f}_{tw1}(1))-\frac{b_{ws}}{I_{wz}}(\mathbf{f}_{sw1}(6)+\mathbf{f}_{gw1}(6)+\mathbf{f}_{tw1}(6))+\\ & & \frac{b^*_{bs2}}{I_{bmf}}(M_{f\psi ob1}+M_{sfw12}-M_{s\psi bf1}-M_{s\psi bf2}),\end{array} \tag{D.75}$$

$$f_{\mu ys1} = f_{fwy1s}(\frac{1}{m_w} + \frac{1}{m_f} + \frac{a_{wb}^2}{I_{fz}}) + f_{fwy2s}(\frac{1}{m_f} - \frac{a_{wb}^2}{I_{fz}}) + f_{fwy3s}(\frac{1}{m_w}), \tag{D.76}$$

$$F_{my1} = \frac{1}{m_w}(\mathbf{f}_{sw1}(2) + \mathbf{f}_{tw1}(2) + \mathbf{f}_{ctw1}(2)) - \frac{1}{m_f}(\mathbf{f}_{ff1}(2) + \mathbf{f}_{sf1}(2)) - \frac{a_{wb}}{I_{fz}}(M_{s\psi bf1} + \mathbf{f}_{sf1}(5)), \tag{D.77}$$

$$f_{\mu xs2} = f_{fwx1s}(\frac{b_{bs2}^{*2}}{I_{bmf}})C\psi_{f1} + f_{fwx2s}(\frac{1}{m_w} + \frac{b_{ws}^2}{I_{wz}} + \frac{b_{bs2}^{*2}}{I_{bmf}}C\psi_{f1}) + f_{fwx3s}(-\frac{b_{bs2}^{*2}}{I_{bmf}}C\psi_{f2}) + f_{fwx4s}(\frac{1}{m_w} - \frac{b_{bs2}^{*2}}{I_{wz}}C\psi_{f2} - \frac{b_{bs2}^{*2}}{I_{bmf}}C\psi_{f2}), \tag{D.78}$$

$$F_{mx2} = \frac{1}{m_w}(\mathbf{f}_{sw2}(1) + \mathbf{f}_{tw2}(1)) - \frac{b_{ws}}{I_{wz}}(\mathbf{f}_{sw2}(6) + \mathbf{f}_{gw2}(6) + \mathbf{f}_{tw2}(6)) + \frac{b_{bs2}^{*}}{I_{bmf}}(M_{f\psi ob1} + M_{sfw12} - M_{s\psi bf1} - M_{s\psi bf2}), \tag{D.79}$$

$$f_{\mu ys2} = f_{fwy1s}(\frac{1}{m_f} - \frac{a_{wb}^2}{I_{fz}}) + f_{fwy2s}(\frac{1}{m_w} + \frac{1}{m_f} + \frac{a_{wb}^2}{I_{fz}}) + f_{fwy4s}(\frac{1}{m_w}), \tag{D.80}$$

$$F_{my2} = \frac{1}{m_w}(\mathbf{f}_{sw2}(2) + \mathbf{f}_{tw2}(2) + \mathbf{f}_{ctw2}(2)) - \frac{1}{m_f}(\mathbf{f}_{ff1}(2) + \mathbf{f}_{sf1}(2)) + \frac{a_{wb}}{I_{fz}}(M_{s\psi bf1} + \mathbf{f}_{sf1}(5)), \tag{D.81}$$

$$f_{\mu xs3} = f_{fwx1s}(\frac{1}{m_w} - \frac{b_{ws}^2}{I_{wz}} + \frac{b_{bs2}^{*2}}{I_{bmf}}C\psi_{f1}) + f_{fwx2s}\frac{b_{bs2}^{*2}}{I_{bmf}}C\psi_{f1} + f_{fwx3s}(\frac{1}{m_w} + \frac{b_{ws}^2}{I_{wz}} - \frac{b_{bs2}^{*2}}{I_{bmf}}C\psi_{f2}) - f_{fwx4s}\frac{b_{bs2}^{*2}}{I_{bmf}}C\psi_{f2}, \tag{D.82}$$

$$F_{mx3} = \frac{1}{m_w}(\mathbf{f}_{sw1}(1) + \mathbf{f}_{tw1}(1)) + \frac{b_{ws}}{I_{wz}}(\mathbf{f}_{sw1}(6) + \mathbf{f}_{gw1}(6) + \mathbf{f}_{tw1}(6)) - \frac{b_{bs2}^{*}}{I_{bmf}}(M_{f\psi ob1} + M_{sfw12} - M_{s\psi bf1} - M_{s\psi bf2}), \tag{D.83}$$

$$f_{\mu ys3} = f_{fwy1s}(\frac{1}{m_w}) + f_{fwy3s}(\frac{1}{m_w} + \frac{1}{m_f} + \frac{a_{wb}^2}{I_{fz}}) + f_{fwy4s}(\frac{1}{m_f} - \frac{a_{wb}^2}{I_{fz}}), \quad \text{(D.84)}$$

$$F_{my3} = \frac{1}{m_w}(\mathbf{f}_{sw1}(2) + \mathbf{f}_{tw1}(2) + \mathbf{f}_{ctw1}(2)) - \frac{1}{m_f}(\mathbf{f}_{ff2}(2) + \mathbf{f}_{sf2}(2)) - \frac{a_{wb}}{I_{fz}}(M_{s\psi bf2} + \mathbf{f}_{sf2}(5)), \quad \text{(D.85)}$$

$$f_{\mu xs4} = f_{fwx1s}(\frac{b_{bs2}^{*2}}{I_{bmf}}) + f_{fwx2s}(\frac{1}{m_w} - \frac{b_{ws}^2}{I_{wz}} + \frac{b_{bs2}^{*2}}{I_{bmf}}C\psi_{f1}) + f_{fwx3s}(-\frac{b_{bs2}^{*2}}{I_{bmf}}C\psi_{f1}) + f_{fwx4s}(\frac{1}{m_w} + \frac{b_{bs2}^{*2}}{I_{wz}} - \frac{b_{bs2}^{*2}}{I_{bmf}}C\psi_{f2}), \quad \text{(D.86)}$$

$$F_{mx4} = \frac{1}{m_w}(\mathbf{f}_{sw2}(1) + \mathbf{f}_{tw2}(1)) + \frac{b_{ws}}{I_{wz}}(\mathbf{f}_{sw2}(6) + \mathbf{f}_{gw2}(6) + \mathbf{f}_{tw2}(6)) - \frac{b_{bs2}^*}{I_{bmf}}(M_{f\psi ob1} + M_{sfw12} - M_{s\psi bf1} - M_{s\psi bf2}), \quad \text{(D.87)}$$

$$f_{\mu ys4} = f_{fwy2s}(\frac{1}{m_w}) + f_{fwy3s}(\frac{1}{m_f} - \frac{a_{wb}^2}{I_{fz}}) + f_{fwy4s}(\frac{1}{m_w} + \frac{1}{m_f} + \frac{a_{wb}^2}{I_{fz}}), \quad \text{(D.88)}$$

$$F_{my4} = \frac{1}{m_w}(\mathbf{f}_{sw2}(2) + \mathbf{f}_{tw2}(2) + \mathbf{f}_{ctw2}(2)) - \frac{1}{m_f}(\mathbf{f}_{ff2}(2) + \mathbf{f}_{sf2}(2)) - \frac{a_{wb}}{I_{fz}}(M_{s\psi bf2} + \mathbf{f}_{sf2}(5)). \quad \text{(D.89)}$$

In the stick motion state the acting friction forces can be determined by the equations below

$$\mathbf{A}_{b1}^1 \mathbf{F}_{\mu m}^1 = \mathbf{F}_m^1 \quad \text{(D.90)}$$

where

$$\mathbf{F}_{\mu m}^1 = [f_{fwx1} \quad f_{fwy1} \quad f_{fwx2} \quad f_{fwy2} \quad f_{fwx3} \quad f_{fwy3} \quad f_{fwx4} \quad f_{fwy4}]^T \quad \text{(D.91)}$$

$$\mathbf{A}_{b1}^{1} = \begin{bmatrix} a_{11} & 0 & a_{13} & 0 & a_{15} & 0 & a_{17} & 0 \\ a_{21} & 0 & a_{23} & 0 & a_{25} & 0 & a_{27} & 0 \\ a_{31} & 0 & a_{33} & 0 & a_{35} & 0 & a_{37} & 0 \\ a_{41} & 0 & a_{43} & 0 & a_{45} & 0 & a_{47} & 0 \\ 0 & a_{52} & 0 & a_{54} & 0 & a_{56} & 0 & 0 \\ 0 & a_{62} & 0 & a_{64} & 0 & 0 & 0 & a_{68} \\ 0 & a_{72} & 0 & 0 & 0 & a_{76} & 0 & a_{78} \\ 0 & 0 & 0 & a_{84} & 0 & a_{86} & 0 & a_{88} \end{bmatrix} \tag{D.92}$$

where

$$a_{11} = \frac{1}{m_w} + \frac{b_{ws}^2}{I_{wz}} + \frac{b_{bs2}^{*2}}{I_{bmf}} C\psi_{f1}, \quad a_{13} = \frac{b_{bs2}^{*2}}{I_{bmf}} C\psi_{f1},$$

$$a_{15} = \frac{1}{m_w} - \frac{b_{ws}^2}{I_{wz}} - \frac{b_{bs2}^{*2}}{I_{bmf}} C\psi_{f2}, \quad a_{17} = -\frac{b_{bs2}^{*2}}{I_{bmf}} C\psi_{f2},$$

$$a_{21} = \frac{b_{bs2}^{*2}}{I_{bmf}}, \quad a_{23} = \frac{1}{m_w} + \frac{b_{ws}^2}{I_{wz}} + \frac{b_{bs2}^{*2}}{I_{bmf}} C\psi_{f1},$$

$$a_{25} = -\frac{b_{bs2}^{*2}}{I_{bmf}} C\psi_{f2}, \quad a_{27} = \frac{1}{m_w} - \frac{b_{ws}^2}{I_{wz}} C\psi_{f2} - \frac{b_{bs2}^{*2}}{I_{bmf}} C\psi_{f2},$$

$$a_{31} = \frac{1}{m_w} - \frac{b_{ws}^2}{I_{wz}} + \frac{b_{bs2}^{*2}}{I_{bmf}} C\psi_{f1}, \quad a_{33} = \frac{b_{bs2}^{*2}}{I_{bmf}} C\psi_{f1},$$

$$a_{35} = \frac{1}{m_w} + \frac{b_{ws}^2}{I_{wz}} - \frac{b_{bs2}^{*2}}{I_{bmf}} C\psi_{f2}, \quad a_{37} = -\frac{b_{bs2}^{*2}}{I_{bmf}} C\psi_{f2},$$

$$a_{41} = \frac{b_{bs2}^{*2}}{I_{bmf}}, \quad a_{43} = \frac{1}{m_w} - \frac{b_{ws}^2}{I_{wz}} + \frac{b_{bs}^{*2}}{I_{bmf}} C\psi_{f1},$$

$$a_{45} = -\frac{b_{bs2}^{*2}}{I_{bmf}} C\psi_{f2}, \quad a_{47} = \frac{1}{m_w} + \frac{b_{ws}^2}{I_{wz}} C\psi_{f2} - \frac{b_{bs2}^{*2}}{I_{bmf}} C\psi_{f2},$$

$$a_{52} = \frac{1}{m_w} + \frac{1}{m_f} + \frac{a_{wb}^2}{I_{fz}}, \quad a_{54} = \frac{1}{m_f} - \frac{a_{wb}^2}{I_{fz}},$$

$$a_{56} = \frac{1}{m_w}, \quad a_{62} = \frac{1}{m_f} - \frac{a_{wb}^2}{I_{fz}},$$

$$a_{64} = \frac{1}{m_w} + \frac{1}{m_f} + \frac{a_{wb}^2}{I_{fz}}, \quad a_{68} = \frac{1}{m_w},$$

$$a_{72} = \frac{1}{m_w}, \quad a_{76} = \frac{1}{m_w} + \frac{1}{m_f} + \frac{a_{wb}^2}{I_{fz}},$$

$$a_{78} = \frac{1}{m_f} - \frac{a_{wb}^2}{I_{fz}}, \quad a_{84} = \frac{1}{m_w},$$

$$a_{86} = \frac{1}{m_f} - \frac{a_{wb}^2}{I_{fz}}, \quad a_{88} = \frac{1}{m_w} + \frac{1}{m_f} + \frac{a_{wb}^2}{I_{fz}}$$

and

$$\mathbf{F}_m^1 = [F_{mx1} \quad F_{mx2} \quad F_{mx3} \quad F_{mx4} \quad F_{my1} \quad F_{my2} \quad F_{my3} \quad F_{my4}]^T. \tag{D.93}$$

In the end the switch conditions can be expressed as the combination of the (D.31)-(D.38) and

$$\begin{array}{lll} |f_{fwx1}| \leq |f_{fwx1s}|, & |f_{fwy1}| \leq |f_{fwy1s}|, & |f_{fwx2}| \leq |f_{fwx2s}|, \\ |f_{fwy2}| \leq |f_{fwy2s}|, & |f_{fwx3}| \leq |f_{fwx3s}|, & |f_{fwy3}| \leq |f_{fwy3s}|, \\ & |f_{fwx4}| \leq |f_{fwx4s}|, & |f_{fwy4}| \leq |f_{fwy4s}| \end{array} \tag{D.94}$$

where the static friction force components $f_{fwx1s}, \cdots$ are determined by the normal forces, the friction coefficient and the corresponding friction direction angles.

In the same way for the other bogie the switch conditions also can be obtained as

$$\mathbf{A}_{b2}^2 \mathbf{F}_{\mu m}^2 = \mathbf{F}_m^2 \tag{D.95}$$

where

$$\mathbf{F}_{\mu m}^2 = [f_{fwx5} \quad f_{fwy5} \quad f_{fwx6} \quad f_{fwy6} \quad f_{fwx7} \quad f_{fwy7} \quad f_{fwx8} \quad f_{fwy8}]^T, \tag{D.96}$$

$$\mathbf{A}_{b2}^2 = \begin{bmatrix} b_{11} & 0 & b_{13} & 0 & b_{15} & 0 & b_{17} & 0 \\ b_{21} & 0 & b_{23} & 0 & b_{25} & 0 & b_{27} & 0 \\ b_{31} & 0 & b_{33} & 0 & b_{35} & 0 & b_{37} & 0 \\ b_{41} & 0 & b_{43} & 0 & b_{45} & 0 & b_{47} & 0 \\ 0 & b_{52} & 0 & b_{54} & 0 & b_{56} & 0 & 0 \\ 0 & b_{62} & 0 & b_{64} & 0 & 0 & 0 & b_{68} \\ 0 & b_{72} & 0 & 0 & 0 & b_{76} & 0 & b_{78} \\ 0 & 0 & 0 & b_{84} & 0 & b_{86} & 0 & b_{88} \end{bmatrix} \tag{D.97}$$

where

$$b_{11} = \frac{1}{m_w} + \frac{b_{ws}^2}{I_{wz}} + \frac{b_{bs2}^{*2}}{I_{bmf}} C\psi_{f3}, \quad b_{13} = \frac{b_{bs2}^{*2}}{I_{bmf}} C\psi_{f3},$$
$$b_{15} = \frac{1}{m_w} - \frac{b_{ws}^2}{I_{wz}} - \frac{b_{bs2}^{*2}}{I_{bmf}} C\psi_{f4}, \quad b_{17} = -\frac{b_{bs2}^{*2}}{I_{bmf}} C\psi_{f4},$$
$$b_{21} = \frac{b_{bs2}^{*2}}{I_{bmf}}, \quad b_{23} = \frac{1}{m_w} + \frac{b_{ws}^2}{I_{wz}} + \frac{b_{bs2}^{*2}}{I_{bmf}} C\psi_{f3},$$
$$b_{25} = -\frac{b_{bs2}^{*2}}{I_{bmf}} C\psi_{f4}, \quad b_{27} = \frac{1}{m_w} - \frac{b_{ws}^2}{I_{wz}} C\psi_{f2} - \frac{b_{bs2}^{*2}}{I_{bmf}} C\psi_{f4},$$
$$b_{31} = \frac{1}{m_w} - \frac{b_{ws}^2}{I_{wz}} + \frac{b_{bs2}^{*2}}{I_{bmf}} C\psi_{f3}, \quad b_{33} = \frac{b_{bs2}^{*2}}{I_{bmf}} C\psi_{f3},$$
$$b_{35} = \frac{1}{m_w} + \frac{b_{ws}^2}{I_{wz}} - \frac{b_{bs2}^{*2}}{I_{bmf}} C\psi_{f4}, \quad b_{37} = -\frac{b_{bs2}^{*2}}{I_{bmf}} C\psi_{f4},$$
$$b_{41} = \frac{b_{bs2}^{*2}}{I_{bmf}}, \quad b_{43} = \frac{1}{m_w} - \frac{b_{ws}^2}{I_{wz}} + \frac{b_{bs2}^{*2}}{I_{bmf}} C\psi_{f3},$$
$$b_{45} = -\frac{b_{bs2}^{*2}}{I_{bmf}} C\psi_{f4}, \quad b_{47} = \frac{1}{m_w} + \frac{b_{ws}^2}{I_{wz}} C\psi_{f4} - \frac{b_{bs2}^{*2}}{I_{bmf}} C\psi_{f4},$$

$$b_{52} = \frac{1}{m_w} + \frac{1}{m_f} + \frac{a_{wb}^2}{I_{fz}}, \quad b_{54} = \frac{1}{m_f} - \frac{a_{wb}^2}{I_{fz}},$$
$$b_{56} = \frac{1}{m_w}, \quad b_{62} = \frac{1}{m_f} - \frac{a_{wb}^2}{I_{fz}},$$
$$b_{64} = \frac{1}{m_w} + \frac{1}{m_f} + \frac{a_{wb}^2}{I_{fz}}, \quad b_{68} = \frac{1}{m_w},$$
$$b_{72} = \frac{1}{m_w}, \quad b_{76} = \frac{1}{m_w} + \frac{1}{m_f} + \frac{a_{wb}^2}{I_{fz}},$$
$$b_{78} = \frac{1}{m_f} - \frac{a_{wb}^2}{I_{fz}}, \quad b_{84} = \frac{1}{m_w},$$
$$b_{86} = \frac{1}{m_f} - \frac{a_{wb}^2}{I_{fz}}, \quad b_{88} = \frac{1}{m_w} + \frac{1}{m_f} + \frac{a_{wb}^2}{I_{fz}}$$

and

$$\mathbf{F}_m^2 = [F_{mx5} \quad F_{mx6} \quad F_{mx7} \quad F_{mx8} \quad F_{my5} \quad F_{my6} \quad F_{my7} \quad F_{my8}]^T \tag{D.98}$$

where from the Eqs.(D.12)-(D.22) with Eqs.(D.47)-(D.54) we have

$$\begin{aligned} F_{mx5} \quad = \quad & \frac{1}{m_w}(\mathbf{f}_{sw3}(1) + \mathbf{f}_{tw3}(1)) - \frac{b_{ws}}{I_{wz}}(\mathbf{f}_{sw3}(6) + \mathbf{f}_{gw3}(6) + \mathbf{f}_{tw3}(6)) + \\ & \frac{b_{bs2}^*}{I_{bmf}}(M_{f\psi ob2} + M_{sfw34} - M_{s\psi bf3} - M_{s\psi bf4}), \end{aligned} \tag{D.99}$$

$$F_{my5} = \frac{1}{m_w}(\mathbf{f}_{sw3}(2) + \mathbf{f}_{tw3}(2) + \mathbf{f}_{ctw3}(2)) - \frac{1}{m_f}(\mathbf{f}_{ff3}(2) + \mathbf{f}_{sf3}(2)) - \frac{a_{wb}}{I_{fz}}(M_{s\psi bf3} + \mathbf{f}_{sf3}(5)), \quad \text{(D.100)}$$

$$F_{mx6} = \frac{1}{m_w}(\mathbf{f}_{sw4}(1) + \mathbf{f}_{tw4}(1)) - \frac{b_{ws}}{I_{wz}}(\mathbf{f}_{sw4}(6) + \mathbf{f}_{gw4}(6) + \mathbf{f}_{tw4}(6)) + \frac{b^*_{bs2}}{I_{bmf}}(M_{f\psi ob2} + M_{sfw34} - M_{s\psi bf3} - M_{s\psi bf4}), \quad \text{(D.101)}$$

$$F_{my6} = \frac{1}{m_w}(\mathbf{f}_{sw4}(2) + \mathbf{f}_{tw4}(2) + \mathbf{f}_{ctw4}(2)) - \frac{1}{m_f}(\mathbf{f}_{ff3}(2) + \mathbf{f}_{sf3}(2)) + \frac{a_{wb}}{I_{fz}}(M_{s\psi bf2} + \mathbf{f}_{sf3}(5)), \quad \text{(D.102)}$$

$$F_{mx7} = \frac{1}{m_w}(\mathbf{f}_{sw3}(1) + \mathbf{f}_{tw3}(1)) + \frac{b_{ws}}{I_{wz}}(\mathbf{f}_{sw3}(6) + \mathbf{f}_{gw3}(6) + \mathbf{f}_{tw3}(6)) - \frac{b^*_{bs2}}{I_{bmf}}(M_{f\psi ob2} + M_{sfw34} - M_{s\psi bf3} - M_{s\psi bf4}), \quad \text{(D.103)}$$

$$F_{my7} = \frac{1}{m_w}(\mathbf{f}_{sw3}(2) + \mathbf{f}_{tw3}(2) + \mathbf{f}_{ctw3}(2)) - \frac{1}{m_f}(\mathbf{f}_{ff4}(2) + \mathbf{f}_{sf4}(2)) - \frac{a_{wb}}{I_{fz}}(M_{s\psi bf4} + \mathbf{f}_{sf4}(5)), \quad \text{(D.104)}$$

$$F_{mx8} = \frac{1}{m_w}(\mathbf{f}_{sw4}(2) + \mathbf{f}_{tw4}(2) + \mathbf{f}_{ctw4}(2)) + \frac{b_{ws}}{I_{wz}}(\mathbf{f}_{sw4}(6) + \mathbf{f}_{gw4}(6) + \mathbf{f}_{tw4}(6)) - \frac{b^*_{bs2}}{I_{bmf}}(M_{f\psi ob2} + M_{sfw34} - M_{s\psi bf3} - M_{s\psi bf4}), \quad \text{(D.105)}$$

$$F_{my8} = \frac{1}{m_w}(\mathbf{f}_{sw4}(1) + \mathbf{f}_{tw4}(1)) - \frac{1}{m_f}(\mathbf{f}_{ff4}(2) + \mathbf{f}_{sf4}(2)) + \frac{a_{wb}}{I_{fz}}(M_{s\psi bf4} + \mathbf{f}_{sf4}(5)). \quad \text{(D.106)}$$

So the switch condition is a combination of the (D.47)-(D.54) and

$$\begin{array}{lll} |f_{fwx5}| \le |f_{fwx5s}|, & |f_{fwy5}| \le |f_{fwy5s}|, & |f_{fwx6}| \le |f_{fwx6s}|, \\ |f_{fwy6}| \le |f_{fwy6s}|, & |f_{fwx7}| \le |f_{fwx7s}|, & |f_{fwy7}| \le |f_{fwy7s}|, \\ & |f_{fwx8}| \le |f_{fwx8s}|, & |f_{fwy8}| \le |f_{fwy8s}|. \end{array} \quad \text{(D.107)}$$

The above switch conditions are only used for the case of all the stick motions taking place on the all four contact surfaces. If some motions between the contact surfaces are slip motions then the above switch conditions need to be modified. For example, if the slip motion takes place on the contact surface between the side frame 1 and the wheelset 1, then the acting friction forces are determined by

$$\mathbf{A}^1_{b1a}\mathbf{F}^1_{\mu ma} = \mathbf{F}^1_{ma} \tag{D.108}$$

where

$$\mathbf{F}^1_{\mu ma} = [f_{fwx2} \quad f_{fwy2} \quad f_{fwx3} \quad f_{fwy3} \quad f_{fwx4} \quad f_{fwy4}]^T, \tag{D.109}$$

$$\mathbf{A}^1_{b1} = \begin{bmatrix} a_{13} & 0 & a_{15} & 0 & a_{17} & 0 \\ a_{23} & 0 & a_{25} & 0 & a_{27} & 0 \\ a_{33} & 0 & a_{35} & 0 & a_{37} & 0 \\ a_{43} & 0 & a_{45} & 0 & a_{47} & 0 \\ 0 & a_{54} & 0 & a_{56} & 0 & 0 \\ 0 & a_{64} & 0 & 0 & 0 & a_{68} \\ 0 & 0 & 0 & a_{76} & 0 & a_{78} \\ 0 & a_{84} & 0 & a_{86} & 0 & a_{88} \end{bmatrix}, \tag{D.110}$$

$$\mathbf{F}^1_{ma} = [F_{mx1} \quad F_{mx2} \quad F_{mx3} \quad F_{mx4} \quad F_{my1} \quad F_{my2} \quad F_{my3} \quad F_{my4}]^T \tag{D.111}$$

where the $\mathbf{F}^1_{ma}$ read

$$\begin{aligned} f_{\mu xs1} &= f_{fwx2s}\frac{b^{*2}_{bs2}}{I_{bmf}}C\psi_{f1} + f_{fwx3s}(\frac{1}{m_w} - \frac{b^2_{ws}}{I_{wz}} - \frac{b^{*2}_{bs2}}{I_{bmf}}C\psi_{f2}) - \\ &\quad f_{fwx4s}\frac{b^{*2}_{bs2}}{I_{bmf}}C\psi_{f2}, \end{aligned} \tag{D.112}$$

$$\begin{aligned} F_{mx1} &= \frac{1}{m_w}(\mathbf{f}_{sw1}(1) + \mathbf{f}_{tw1}(1)) - \frac{b_{ws}}{I_{wz}}(\mathbf{f}_{sw1}(6) + \mathbf{f}_{gw1}(6) + \mathbf{f}_{tw1}(6)) + \\ &\quad \frac{b^*_{bs2}}{I_{bmf}}(M_{f\psi ob1} + M_{sfw12} - M_{s\psi bf1} - M_{s\psi bf2}) - \\ &\quad f_{fwx1}(\frac{1}{m_w} + \frac{b^2_{ws}}{I_{wz}} + \frac{b^{*2}_{bs2}}{I_{bmf}}C\psi_{f1}), \end{aligned} \tag{D.113}$$

$$f_{\mu ys1} = f_{fwy2s}(\frac{1}{m_f} - \frac{a^2_{wb}}{I_{fz}}) + f_{fwy3s}(\frac{1}{m_w}), \tag{D.114}$$

$$\begin{aligned} F_{my1} &= \frac{1}{m_w}(\mathbf{f}_{sw1}(2) + \mathbf{f}_{tw1}(2) + \mathbf{f}_{ctw1}(2)) - \frac{1}{m_f}(\mathbf{f}_{ff1}(2) + \mathbf{f}_{sf1}(2)) - \\ &\quad \frac{a_{wb}}{I_{fz}}(M_{s\psi bf1} + \mathbf{f}_{sf1}(5)) + f_{fwy1}(\frac{1}{m_w} + \frac{1}{m_f} + \frac{a^2_{wb}}{I_{fz}}), \end{aligned} \tag{D.115}$$

$$f_{\mu xs2} = f_{fwx2s}(\frac{1}{m_w} + \frac{b_{ws}^2}{I_{wz}} + \frac{b_{bs2}^{*2}}{I_{bmf}} C\psi_{f1}) + f_{fwx3s}(-\frac{b_{bs2}^{*2}}{I_{bmf}} C\psi_{f2}) + f_{fwx4s}(\frac{1}{m_w} - \frac{b_{ws2}^{*2}}{I_{wz}} C\psi_{f2} - \frac{b_{bs2}^{*2}}{I_{bmf}} C\psi_{f2}), \quad \text{(D.116)}$$

$$F_{mx2} = \frac{1}{m_w}(\mathbf{f}_{sw1}(2) + \mathbf{f}_{tw1}(2) + \mathbf{f}_{ctw1}(2)) - \frac{b_{ws}}{I_{wz}}(\mathbf{f}_{sw2}(6) + \mathbf{f}_{gw2}(6) + \mathbf{f}_{tw2}(6)) + \frac{b_{bs2}^*}{I_{bmf}}(M_{f\psi ob1} + M_{sfw12} - M_{s\psi bf1} - M_{s\psi bf2}) + f_{fwx1}(\frac{b_{bs2}^{*2}}{I_{bmf}}) C\psi_{f1}, \quad \text{(D.117)}$$

$$f_{\mu ys2} = f_{fwy2s}(\frac{1}{m_w} + \frac{1}{m_f} + \frac{a_{wb}^2}{I_{fz}}) + f_{fwy4s}(\frac{1}{m_w}), \quad \text{(D.118)}$$

$$F_{my2} = \frac{1}{m_w}(\mathbf{f}_{sw2}(2) + \mathbf{f}_{tw2}(2) + \mathbf{f}_{ctw2}(2)) - \frac{1}{m_f}(\mathbf{f}_{ff1}(2) + \mathbf{f}_{sf1}(2)) + \frac{a_{wb}}{I_{fz}}(M_{s\psi bf1} + \mathbf{f}_{sf1}(5)) + f_{fwy1}(\frac{1}{m_f} - \frac{a_{wb}^2}{I_{fz}}), \quad \text{(D.119)}$$

$$f_{\mu xs3} = +f_{fwx2s}\frac{b_{bs2}^{*2}}{I_{bmf}} C\psi_{f1} + f_{fwx3s}(\frac{1}{m_w} + \frac{b_{ws}^2}{I_{wz}} - \frac{b_{bs2}^{*2}}{I_{bmf}} C\psi_{f2}) - f_{fwx4s}\frac{b_{bs2}^{*2}}{I_{bmf}} C\psi_{f2}, \quad \text{(D.120)}$$

$$F_{mx3} = \frac{1}{m_w}(\mathbf{f}_{sw1}(1) + \mathbf{f}_{tw1}(1)) + \frac{b_{ws}}{I_{wz}}(\mathbf{f}_{sw1}(6) + \mathbf{f}_{gw1}(6) + \mathbf{f}_{tw1}(6)) - \frac{b_{bs2}^*}{I_{bmf}}(M_{f\psi ob1} + M_{sfw12} - M_{s\psi bf1} - M_{s\psi bf2}) + f_{fwx1}(\frac{1}{m_w} - \frac{b_{ws}^2}{I_{wz}} + \frac{b_{bs2}^{*2}}{I_{bmf}} C\psi_{f1}), \quad \text{(D.121)}$$

$$f_{\mu ys3} = f_{fwy3s}(\frac{1}{m_w} + \frac{1}{m_f} + \frac{a_{wb}^2}{I_{fz}}) + f_{fwy4s}(\frac{1}{m_f} - \frac{a_{wb}^2}{I_{fz}}), \quad \text{(D.122)}$$

$$F_{my3} = \frac{1}{m_w}(\mathbf{f}_{sw1}(2) + \mathbf{f}_{tw1}(2) + \mathbf{f}_{ctw1}(2)) - \frac{1}{m_f}(\mathbf{f}_{ff2}(2) + \mathbf{f}_{sf2}(2)) - \frac{a_{wb}}{I_{fz}}(M_{s\psi bf2} + \mathbf{f}_{sf2}(5)) + f_{fwy1}(\frac{1}{m_w}), \quad \text{(D.123)}$$

$$f_{\mu xs4} = f_{fwx2s}(\frac{1}{m_w} - \frac{b_{ws}^2}{I_{wz}} + \frac{b_{bs2}^{*2}}{I_{bmf}} C\psi_{f1}) + f_{fwx3s}(-\frac{b_{bs2}^{*2}}{I_{bmf}} C\psi_{f1}) + f_{fwx4s}(\frac{1}{m_w} + \frac{b_{ws}^2}{I_{wz}} - \frac{b_{bs2}^{*2}}{I_{bmf}} C\psi_{f2}), \quad \text{(D.124)}$$

$$F_{mx4} = \frac{1}{m_w}(\mathbf{f}_{sw1}(2) + \mathbf{f}_{tw1}(2) + \mathbf{f}_{ctw1}(2)) + \frac{b_{ws}}{I_{wz}}(\mathbf{f}_{sw2}(6) + \mathbf{f}_{gw2}(6) + \mathbf{f}_{tw2}(6)) - M_{f\psi ob1} + M_{sfw12} - M_{s\psi bf1} - M_{s\psi bf2}) + f_{fwx1}(\frac{b_{bs2}^{*2}}{I_{bmf}}), \quad \text{(D.125)}$$

$$f_{\mu ys4} = f_{fwy2s}(\frac{1}{m_w}) + f_{fwy3s}(\frac{1}{m_f} - \frac{a_{wb}^2}{I_{fz}}) + f_{fwy4s}(\frac{1}{m_w} + \frac{1}{m_f} + \frac{a_{wb}^2}{I_{fz}}), \quad \text{(D.126)}$$

$$F_{my4} = \frac{1}{m_w}(\mathbf{f}_{sw2}(2) + \mathbf{f}_{tw2}(2) + \mathbf{f}_{ctw2}(2)) - \frac{1}{m_f}(\mathbf{f}_{ff2}(2) + \mathbf{f}_{sf2}(2)) + \frac{a_{wb}}{I_{fz}}(M_{s\psi bf2} + \mathbf{f}_{sf2}(5)). \quad \text{(D.127)}$$

In this way we can determine the acting friction forces for all combinations of the stick-slip modes. Then the switch conditions are also determined for the stick mode by letting the acting friction forces are less than the corresponding static friction force components.

Appendix E

The parameters of the three-piece-freight-truck

Table E.1: *Parameters of the Chinese Three-Piece-Freight-Truck* C_{62}

Symbols	Name	Unit	Values
m_o	mass of car body	Kg	empty car 14600, loaded car 77000
m_b	mass of a bolster	Kg	470
m_d	mass of a wedge	Kg	8
m_f	mass of a side frame	Kg	330
m_w	mass of a wheelset	Kg	1200
I_{ox}	inertia of car body around x axis	$Kg{\cdot}m^2$	empty car 2.66×10^4, loaded car 1×10^5
I_{oy}	inertia of car body around y axis	$Kg{\cdot}m^2$	empty car 2.66×10^5, loaded car 1.2×10^6
I_{oz}	inertia of car body around z axis	$Kg{\cdot}\mathrm{m}^2$	empty car 2.84×10^5, loaded car 1.07×10^6
I_{bx}	inertia of a bolster around x axis	$Kg{\cdot}m^2$	190
I_{bz}	inertia of a bolster around z axis	$Kg{\cdot}m^2$	190
I_{fy}	inertia of a frame around x axis	$Kg{\cdot}m^2$	100
I_{fz}	inertia of a frame around z axis	$Kg{\cdot}m^2$	80

Symbols	Name	Unit	Values
I_{wx}	inertia of a wheelset around x axis	$Kg{\cdot}m^2$	740
I_{wy}	inertia of a wheelset around y axis	$Kg{\cdot}m^2$	160
I_{wz}	inertia of a wheelset around z axis	$Kg{\cdot}m^2$	740
K_{x1}	stiffnes of the band-stop between a frame and an adapter in the x direction	MN/M	55
K_{y1}	stiffness of the band-stop between a frame and an adapter in the y direction	MN/M	55
K_{x2}	stiffness of the springs of each end of a bolster in the x direction	MN/M	4.14
K_{y2}	stiffness of the springs of each end of a bolster in the y direction	MN/M	4.14
K_{z2}	stiffness of the springs of each end of a bolster in the z direction	MN/M	5.32
K_{x3}	stiffness of the springs of a wedge in the x direction	MN/M	0.6
K_{y3}	stiffness of the springs of a wedge in the y direction	MN/M	0.6
K_{z3}	stiffness of the springs of a wedge in the z direction	MN/M	0.769
K_{ob}	stiffness of the side support in the z direction	MN/M	10
$K_{\psi bf}$	anti-warp stiffness	MN/rad	1$\sim$2
μ_{sf}	static friction coefficient between a frame and an adapter		0.25-0.45
μ_{kf}	kinetic friction coefficient between a frame and an adapter		0.2-0.35
μ_{sd}	static friction coefficient between a wedge and a side frame		0.25-0.45
μ_{kd}	kinetic friction coefficient between a wedge and a side frame		0.2-0.35
μ_{sb}	static friction coefficient between a wedge and a bolster		0.25-0.45
μ_{kb}	kinetic friction coefficient between a wedge and a bolster		0.2-0.35
μ_o	friction coefficient on the surfac of the center plate		0.4

Symbols	Name	Unit	Values
b_{ws}	distance between the mass center of a wheelset to the contact point between a side frame and an adapter	m	0.97
b^*_{bs2}	distance between the mass center of a bolster to the secondary suspension	m	0.97
$2a_b$	distance between the two mass centers of the bolsters	m	8.7
$2a_{wb}$	wheelbase	m	1.75
$2a^*_{oc}$	distance between two center plates	m	8.7
b_{os}	distance between the center plate and side support	m	0.8
h_o	distance from the car body mass center to the top of track	m m	empty car 0.68, loaded car 1.3
h_b	distance from the bolster mass center to the top of track	m	0.55
h_f	distance from the frame mass center to the top of track	m	0.5
r	roll radius of a wheel	m	0.42
ρ_o	radius of a center plate	m	0.15
$2b$	gauge	m	1.435
$2b_w$	inside gauge	m	1.353
Δ_{ob}	clearance between car body and a side support	m	0.003-0.008
Δx_f	longitudinal clearance between a side frame and an adpater	m	0.003-0.006
Δy_f	lateral clearance between a side frame and an adpater	m	0.003-0.006
γ	angle of a wedge contacting a frame	deg.	2.5
ϕ	angle of a wedge contacting a bolster	deg.	45

Bibliography

[1] J. S. Bendat and A. G. Piersol(2000), Random Data, Analysis and Measurement Procedures, John Wiley and Sons.

[2] C. Bendtsen and P. G. Thomsen(1999), Numerical Solution of Defferential Algebraic Equations, IMM-REP-1999-08, ISSN 0909 6264.

[3] K. E. Brenan, S. L. Campbell and L. R. Petzold(1989), Numerical Solution of Initial-Value Problems in Differential-Algebraic Equations, North-Holland.

[4] N. Bosso, A. Gugliotta and A. Somá(2000), Simulation of a freight bogie with friction dampers, 5th ADAMS/Rail User's Conference, Haarlem, The Netherlands.

[5] Carter(1926), On the Action of a Locomotive Driving, Wheel. Proc. Royal Society, Series A, Vol. 112:151-157.

[6] G. Cheng(2000), The Analysis on Random Vibration of Vehicle/Track Coupling System, Ph.D. Dissertation(in Chinese), Southwest Jiaotong University.

[7] C. Cole and M. McCanachan(2001), Snubber Stiction in Three Piece Bogies, Proceedings of the 5th International Conference on Railway Bogies and Running Gears, Budapest, Hungary.

[8] N.K. Cooperider and *et. al.*(1976), The application of quasilinearization techniques to the prediction of nonlinear railway vehicle response. In Pacejka, H.B.(Ed.): The Dynamics of Vehicles on Roads and on Tracks. Proceedings of the IUTAM Symposium held at Delft, The Netherlands, August 1975, pp. 314-325, Amsterdam.

[9] J. P. Den Hartog(1931), Forced vibration with combined Coulomb and viscous friction, Transations of the ASME 53:107-115.

[10] A.D. De Pater(1961), The approximate determination of the hunting movement of a railway vehicle by aid of the method of Krylov and Bogoljubov. *Appl.Sci. Res.*10:205-228.

[11] A.D. De Pater(1979), The exact theory of the motion of a single wheelset moving on a purely straight track, Delft University of Technology, Laboratory for Engineering Mechanics, Report No. 648.

[12] A.D. De Pater(1981), The general theory of the motion of a single wheelset moving through a curve with constant radius and cant, Zeitschrift angewandter Mathematik und Mechanik 61:277-292.

[13] A.D. De Pater(1988), The geometrical contact between track and wheelset, *Vehicle System Dynamics* 17:127-140.

[14] A.D. De Pater(1997), The equations of motion of a simplified railway vehicle moving along a Curved track and the simulation of an uneven tangent railway track by means of a roller rig, Delft University of Technology, Laboratory for Engineering Mechanics, Report No. 1158.

[15] A.D. De Pater, P.Meijers and I.Y. Shevtsov(1999), Simulation of the motion of a railway vehicle along curved tracks, Laboratory for Engineering Mechanics, Delft University of Technology, Report No. LTM 1196.

[16] W. Duffek(1982), Contact Geometry in Wheel Rail Vehicles Contact Mechanics anf Wear of Rail/Wheel Systems, Intern. Symp. on Contact Mechanics and Wear of Rail/Wheel Systems, University of Waterloo Press.

[17] E. Eich-Soellner and C. Führer(1998), Numerical Method in Multibody Dynamics,Stuttgart.

[18] C. Esveld(1989), Modern Railway Track, Duisburg.

[19] J.R. Evans and P.J. Rogers(1998), Validation of Dynamic Simulations of Rail Vehicles with Friction Damped Y25 Bogies, *Vehicle System Dynamics Supplement* 28:219-233.

[20] B. Feeny(1992), A nonsmooth Coulomb friction oscillator, *Physica D* 59(1992), 25-38.

[21] B. Feeny and F.C.Moon(1993), Bifurcation sequences of a coulomb friction oscillator. *Nonlinear Dynamics*, 4:25-37.

[22] B. Feeny and F.C.Moon(1994), Chaos in a forced dry-friction oscillator: Experiments and numerical modeling. *Journal of Sound and Vibration*, 170(3):303-323.

[23] R. D. Fröhling, M.A. Howard and C.R. Kayser(1996), Experimental and Theoretical Investigation into Load Sensitive Damping in Three-Piece Freight Car Bogies, Proceedings of the Conference on Freight Car Truck/Bogies organised by the International Heavy Haul Association, Montreal, Canada.

[24] R.D. Fröhling(1998), The Influence of Friction Wedges on the Dynamic Performance of Three-Piece Self-steering Bogies. Proceedings of the 4th International Conference on Railway Bogies and Running Gears, Budapest, Hungary.

[25] J.F. Gardner, and J. P. Cusumano(1997), Dynamic Models of Friction Wedge Dampers, Proceedings of the 1997 ASME/IEEE Joint Railroad Conference, Boston, MA 65-69.

[26] V. K. Garg and R. V. Dukkipati(1982), Dynamics of Railway Vehicle Systems, Academic Press, New York.

[27] R.F. Harder(2000), Dynamic Modeling and Simulation of Three-Piece North American Freight Vehicle Sunspensions with Non-linear Frictional Behaviour Using ADAMS/Rail, 5th ADAMS/Rail User's Conference, Haarlem, The Netherlands.

[28] E. Hairer and G. Wanner(1991a), Solving Ordinary Differential Equations I, Stiff and Differential-Algebraic Problems, Springer.

[29] E. Hairer and G. Wanner(1991b), Solving Ordinary Differential Equations II, Stiff and Differential-Algebraic Problems, Springer-Verlag.

[30] E. J. Haug(1989), Computer Aided Kinematics and Dynamics of Mechanical Systems, Volume I: Basic Methods, Allyn and Bacon.

[31] H. Heumann(1950-1953), Grundzüge der Führung der Schienenfahrzeuge. Elektrische Bahnen.

[32] H.-K., Hong and C.-S. Liu(2000), Coulomb Friction Oscillator: Modelling and Responses to Harmonic Loads and Base Excitations, *Journal of Sound and Vibration*, 229(5):1171-1192.

[33] R.R. Huilgol(1978), Hopf-Friedrichs bifurcation and the hunting of a railway axle, *Quart. J. Appl. Sci. Res.* A.

[34] R.A. Ibrahim(1992), Friction-induced vibration, chatter, squel, and chaos, DE-Vol. 49, Friction-Induced Vibration, Chatter, Squeal, and Chaos, Edited by R.A. Ibrahim and A. Soom, ASME:107-138.

[35] H.H. Jenkins, J.E. Stephenson, G.A. Clayton, G.W. Morland and D. Lyon(1974), The Effect of Track and Vehicle Parameters on Wheel/Rail Vertical Dynamic Forces, Railway Engineering Journal.

[36] J.J. Kalker(1967), On the Rolling Contact of Two Elastic Bodies in the Presence of Dry Friction, Ph.D. Dissertation, Delft University of Technology, Delft.

[37] J.J. Kalker(1982), A Fast Algorithm for the Simplified Theory of Rolling Contact, *Vehicle System Dynamics*, 11:1-13.

[38] J.J. Kalker(1990), Three-Dimensional Elastic Bodies in Rolling Contact, Kluwer Academic Publishers.

[39] J.J. Kalker(1996), Book of Table for the Hertzian Creep Force Law, 1st ADAMS/Rail user's meeting, Utrecht, The Netherlands.

[40] Kass-Petersen(1986), Chaos in a railway bogie, *Acta Mechanica*, 61:91-107.

[41] W. Kik(1994), RSGEO and RSPROF Programs for the simulation of the Wheel-Rail or the Wheelset-Roller Kinematics, Translated by J. Litzenburger, Technical University of Denmark, 2000.

[42] J. Kisilowski and K. Knothe(1991), Advanced Railway Vehicle System Dynamics, Warsaw.

[43] Klingel(1883), Uber den Lauf Eisenbahnwagen auf gerader Bahn, Organ Fortschr. Eisenbahnwesens, Vol.38:113-123.

[44] K.Knothe and F. Böhm(1999), History of Stability of Railway and Road Vehicles, *Vehicle System Dynamics*, 31:283-323.

[45] Kragelskii(1971) Reibung und Verschleiss, VEB, Verlag Technik, Berlin.

[46] E. Kreyszig(1979), Advanced Engineering Mathematics, John Wiley and Sons, Inc..

[47] G. Li *et al* (2000), Measuremental report on the derailment of the wagons with the three-piece-freight-trucks on straint line, Research report of China Academy of Railway Sciences, No. TY 1408.

[48] T. Matsydaira(1952), Shimmy of axles with pair of wheels(in Japanese), *J. of Railway Engineering Research*, (1952):16-26.

[49] J.P. Meijaard and A.D. de Pater(1989), Railway vehicle systems dynamics and chaotic vibrations, *Int. Journal Non-Linear Mechanics*, 24:1-17.

[50] C.-H. Meng, J. Bielak and H. Griffin(1986a), The influnce of Microslip on Vibratory Response, Part I: A New Microslip Model. *Journal of Sound and Vibration*, 107(2):279-293.

[51] C.-H. Meng, H. Griffin and J. Bielak(1986b), The influence of Microslip on Vibratory Response, Part II: A Comparison with Experimental Results. *Journal of Sound and Vibration*, 107(2):295-307.

[52] C.-H. Meng and P. Chidamparam(1991), Friction Damping of Two-Dimensional Motion and its Application in Vibration Control, *Journal of Sound and Vibration*, 144(3):427-447.

[53] R. K. Otnes and L. Enochson(1972), Digital Time Series Analysis, John Wiley and Sons.

[54] J.P. Pascal and Sauvage(1991), New Method for Reducing the Multicontact Wheel/Rail Problem to One Equivalent Contact Patch, Proceedings of 12th IAVSD Symposium, Lyon,1991: 475-489.

[55] J.P. Pascal(1995), Oscillations and chaotic behaviour of unstable railway wagons over large distances. *Chaos, Solitons and Fractals*, 5(9):1725-1753.

[56] O. Polach(1999), A Fast Wheel-Rail Forces Calculation Computer Code, The Dynamics of Vehicles on Roads and on Tracks, Edited by Robert Fröhling, *Vehicle System Dynamics Supplement*, 33:728-739.

[57] F. Periard(1998), Wheel-Rail Noise Generation: Curve Squealing by Trams, Ph.D. Dissertation, Delft University of Technology.

[58] K. Popp(1992), Some Model Problems Showing Stick-Slip Motion and Chaos, DE-Vol. 49, Friction-Induced Vibration, Chatter, Squeal, and Chaos, Edited by R.A. Ibrahim and A. Soom, ASME:1-12.

[59] K. Popp(1996), *et al.*, Analysis of a Self Excited Friction Oscillator with External Excitation, Dynamics with Friction, Part I, World Scientific.

[60] E. Reithmeier(1991), Periodical Solutions of Nonlinear Dynamical Systems, Springer-Verlag.

[61] E.A. Robinson and M. T. Silvia(1978), Digital Signal Processing and Time Series Analysis, Holden-Day.

[62] G. Sauvage and J.P. Pascal(1990), Solution of the Multiple Wheel and Rail Contact Problem, *Vehicle System Dynamics*, 19:257-272.

[63] K. Y. Sanliturk and D. J. Ewins(1996), Modelling Two-Dimensional Friction Contact and its Application Using Harmonic Balance Method, *Journal of Sound and Vibration*, 193(2):511-523.

[64] S. W. Saw(1986), On the Dynamic Response of a System with Dry Friction, *Journal of Sound and Vibration*, 108(2):305-325.

[65] W. Schiehlen(1978), Generalized Constraint Forces in Ordinary Multibody Systems, Proc. 14th Yugoslav Congress on Rational and Applied Mechanics, C3-16, Jugoslavensko Drustva za Mechanika, Beograd.

[66] W. Schiehlen(1986), Technische Dynamik, Stuttgart.

[67] W. Schiehlen(1990), Multibody system handbook, Springer Verlag.

[68] R. Seydel(1988), From equilibrium to chaos, Elsevier.

[69] Z.Y. Shen, J.K. Hedrick and J.A. Elkins(1983), A comparison of alternative creep force models for rail vehicle dynamics analysis, Proc. of 8th IAVSD Symposium, Cambridge, (1983):591-605.

[70] W. Sextro(2002), Dynamical Contact Problems with Friction, Models, Methods, Experiments and Applications. Springer.

[71] A.A. Shabana(1989), Dynamics of Multibody Systems, John Wiley.

[72] E.C. Slivsgaard(1995), On the Interaction Between Wheels and Rails in Railway Dynamics, Ph.D. Dissertation, Technical University of Denmark.

[73] S. Timoshenko, D.H. Yong and W. Weaver(1974), Vibration Problems in Engineering, John Wiley and Sons.

[74] H. True and C. Kaas Petersen(1983), A bifurcation analysis of nonlinear oscillation in railway vehicles, Proc. 8th IAVSD Symposium, (1983):655-665.

[75] H. True(1993), Dynamics of a rolling wheelset. *Appl. Mech. Reviews*,46(7):438-444.

[76] H. True and Jensen(1994), Chaos and asymmetry in Railway vehicle dynamics. Periodica Polytechnica Ser. *Transp. Eng.*, 22(1):55-68.

[77] H. True(1997), Examples of chaotic motion of railroad vehicles in theory and experiment. In *Rail Transportation*, RTD Vol. 12:13-17, ASME.

[78] H. True(1999), On the Theory of Nonlinear Dynamics and its Applications in Vehicle Systems Dynamics, *Vehicle System Dynamics*, 31:393-421.

[79] H. True and R. Asmund(2002), The Dynamics of a Railway Freight Wagon Wheelset With Dry Friction Damping, *Vehicle System Dynamics*, 38:149-163.

[80] H. True(1999-2002), Personal communications and discussions.

[81] K. Wang(1984), On the Geometrical Contact between a Wheel and a Rail(in Chinese), *Journal of Southwest Jiaotong University*,1:89-98.

[82] T. Wang(1994), Vehicle System Dynamics(in Chinese), China Railway Press House, Beijing.

[83] A.K.Wickens(1965), The dynamics stability of railway vehicle wheelsets and bogies having profiled wheel. *Int. J. Solids Structures*, 1:319-341.

[84] A.K.Wickens(1975), Steering and dynamic stability of railway vehicles, *Vehicle System Dynamics*, 5:15-46.

[85] F. Xia(1996), Computer Simulation of the motion of a Wheelset with a Vehicle Body Frame, Laboratory for Engineering Mechanics, Delft University of Technology, Report No. LTM 1102.

[86] F. Xia(1998), Piecewise curve-fitting method for the measured profile, *Journal of Beijing Institute of Technology*, 7(1):62-66.

[87] F. Xia, F.S. Zhan and W.H. Zhang(2000), On the complete theory of geometrical contact between wheels and rails, *Jixie Gongcheng Xuebao/Chinese Journal of Mechanical Engineering*(in Chinese), 36(8):51-54.

[88] F. Xia(2001a), Modelling of Wedge Dampers in the Presence of Two-Dimensional Dry Friction, Proceedings of the 17th IAVSD Symposium, Copenhagen, Denmark.

[89] F. Xia(2001b), Dynamical Performances of Wedge Dampers with Two-Dimensional Dry Friction, Proceedings of the 5th International Conference on Railway Bogies and Running Gears, BUDAPEST.

[90] F. Xia(2002), Modelling of a Two-Dimensional Coulomb Friction Oscillator, accepted by *Journal of Sound and Vibvation*.

[91] J. M. Yan(1993), Vehicles on railways(in Chinese), China Railway Press House, Beijing.

[92] B. D. Yang, M. L. Chu and C. H. Meng(1998a), Stick-slip-separation analysis and Non-Linear Stiffness and Damping Characterization of Friction Contacts having Variable Normal Load, *Journal of Sound and Vibration*, 201(4):461-481.

[93] B. D. Yang and C. H. Meng(1998b), Charaterization of 3D Contact Kinematics and Prediction of Resonant and Response of Structures having 3D Frictional Constraint, *Journal of Sound and Vibration*, 217(5):909-925.

[94] B. D. Yang and C.H. Meng(2000), Periodic Response of Structures having Three-Dimensional Frictional Constraints, *Journal of Sound and Vibration*, 229(4):775-792.

[95] G. Yang(1993). Dynamic Analysis of Railway Wheelsets and Complete Vehicle Systems, Dissertation, Delft University of Technology.

[96] W. Zhai(1997), Vehicle-Track Coupling Dynamics(in Chinese), China Railway Press House, Beijing.

[97] A. Zmitrowicz(1981a), A theoretical model of anisotropic dry friction, *Wear*, 73:9-39.

[98] A. Zmitrowicz(1981b), A vibration analysis of a turbine blade system, *Int. J. Mech. Sci*, Vol.23, No.12:741-761.